Mont Terri Project

Geology, Paleohydrology, Stress Field, Hydrogeological Synthesis, Osmotic Flow
(Reprinted reports)

Berichte der Landesgeologie
Rapports du Service géologique national
Rapporti del Servizio geologico nazionale
Reports of the Swiss Geological Survey

Paul Bossart (coordinator)

Mont Terri Project

Schweizerische Eidgenossenschaft
Confédération suisse
Confederazione Svizzera
Confederaziun svizra

Federal Department of Defence,
Civil Protection and Sport DDPS

Federal Office of Topography swisstopo

Mont Terri Project

Geology, Paleohydrology, Stress Field, Hydrogeological Synthesis, Osmotic Flow
(Reprinted reports)

Berichte der Landesgeologie
Rapports du Service géologique national
Rapporti del Servizio geologico nazionale
Reports of the Swiss Geological Survey

Paul Bossart (coordinator)

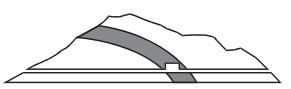

Schweizerische Eidgenossenschaft
Confédération suisse
Confederazione Svizzera
Confederaziun svizra

Federal Department of Defence,
Civil Protection and Sport DDPS

Federal Office of Topography swisstopo

Editor
Swiss Geological Survey (SGS)

Cover photo
© swisstopo

Impression
1200 copies

Order
swisstopo, CH-3084 Wabern, or e-mail to mapsales@swisstopo.ch

ISSN 1661-9285
ISBN 978-3-302-40106-5

Preface from the editor

swisstopo is pleased to present two reports which have no longer been available. Due to a demand on additional hardcopies swisstopo has decided to reprint these reports and to compile them in two miscellany volumes. The first volume deals about the geology, paleohydrology and the stress field and the second volume presents the hydrogeological synthesis and osmotic flow experiments. Both studies are domiciled to the Mont Terri anticline, where the Mont Terri rock laboratory in the Opalinus Clay is located. Both studies document the early years of the Mont Terri Project, the time span between 1996 and 2003.

The Mont Terri rock laboratory started operation in January 1996 as part of the international Mont Terri project. Research is carried out in the underground facility, which is located sideways of the Mont Terri motorway tunnel (Canton Jura, Switzerland). The aim of the project is the geological, hydrogeological, geochemical and geotechnical characterisation of clay formations, specifically the Opalinus Clay. Sixteen partners from European countries, Canada, United States and Japan now participate in the project: ANDRA, BGR, CHEVRON, CRIEPI, DOE, ENRESA, ENSI, FANC, GRS, IRSN, JAEA, NAGRA, NWMO, OBAYASHI, SCK-CEN and swisstopo.

swisstopo has acted as the operator of the rock laboratory since 2006 and is responsible for the implementation of the research programmes decided on by the partners.

swisstopo
Director Mont Terri Project
Dr. Paul Bossart

Préface de l'éditeur

swisstopo a le plaisir de vous présenter ici deux rapports aujourd'hui épuisés. En raison de la forte demande de réimpression de ces volumes, swisstopo a décidé de les compiler et de les réimprimer. Le premier volume traite de la construction des profils géologiques, des bilans paléohydrologiques et de la détermination du champ de contrainte. Le second volume, quant à lui, documente des mesures hydrogéologiques ainsi que leurs interprétations et présente un rapport sur les processus chimio-osmotiques des flux. Ces deux études traitent uniquement de la région anticlinale du Mont Terri où se situe le laboratoire souterrain du même nom niché au sein de l'argile à Opalinus. Ces études retracent les premières années du Projet Mont Terri de 1996 à 2003.

Le projet international du Mont Terri a débuté en janvier 1996 dans le laboratoire souterrain du Mont Terri, excavé en annexe de la galerie de sécurité du tunnel du même nom proche de St-Ursanne (Canton du Jura, Suisse). La caractérisation géologique, hydrogéologique, géochimique et géotechnique d'une formation argileuse, en particulier de l'Argile à Opalinus, est l'objectif principal de ce projet. Seize partenaires provenant d'Europe, de l'Amérique du nord et du Japon se sont réunis autour de ce projet. Il s'agit de l'ANDRA, BGR, CHEVRON, CRIEPI, DOE, ENRESA, FANC, GRS, IFSN, IRSN, JAEA, NAGRA, NWMO, OBAYASHI, SCK•CEN et swisstopo.

Depuis 2006, swisstopo est responsable de l'exploitation du laboratoire souterrain ainsi que de la gestion du Projet Mont Terri, et en particulier de la mise en œuvre du programme de recherche établi par les partenaires.

swisstopo
Directeur du Projet Mont Terri
Dr Paul Bossart

Vorwort des Herausgebers

swisstopo freut sich, Ihnen zwei vergriffene Berichte präsentieren zu dürfen. Weil der Bedarf nach zusätzlichen Druckexemplaren gegeben war entschied sich swisstopo, die beiden Berichte in einem Sammelband nachzudrucken. Der erste Band beinhaltet die Konstruktion von geologischen Profilen, paläohydrologischen Untersuchungen und die Ermittlung des Spannungsfeldes, und der zweite Band dokumentiert die hydrogeologischen Messungen und deren Interpretation sowie einen Bericht über chemisch-osmotische Fliessprozesse. Beide Studien beschränken sich auf das Gebiet der Mont Terri Antiklinale, worin sich das Mont Terri Felslabor im Opalinus-Ton befindet. Beide Studien dokumentieren die frühen Jahre des Mont Terri Projektes, eine Zeitspanne von 1996 bis 2003.

Das Felslabor Mont Terri besteht seit Januar 1996. Im Rahmen des internationalen Mont-Terri-Projektes wird seitlich des Mont-Terri-Autobahntunnels (Kanton Jura, Schweiz) geforscht. Das Hauptziel dieses Projektes ist die geologische, hydrogeologische, geochemische und geotechnische Charakterisierung von Tongesteinen, im speziellen des Opalinus-Tons. Heute sind 16 Partner aus Europa, Kanada, USA und Japan am Projekt beteiligt. Es sind dies ANDRA, BGR, CHEVRON, CRIEPI, DOE, ENRESA, ENSI, FANC, GRS, IRSN, JAEA, NAGRA, NWMO, OBAYASHI, SCK•CEN und swisstopo.

swisstopo ist seit 2006 der Betreiber des Felslabors Mont Terri und ist verantwortlich für die Umsetzung der von den Partnern beschlossenen Forschungsprogramme.

swisstopo
Direktor Mont Terri Project
Dr. Paul Bossart

Prefazione dell'editore

Qui di seguito swisstopo ha il piacere di presentarvi due rapporti oggi esauriti. A causa della forte domanda per una ristampa di questi volumi, swisstopo ha deciso di compilarli e di ristamparli. Il primo volume tratta della costruzione di profili geologici, dei bilanci paleoidrologici e della determinazione del campo di stress. Il secondo volume, invece, documenta delle misure idrogeologiche con la loro interpretazione e presenta un rapporto sui processi chimico-osmotici dei flussi. Questi due studi trattano unicamente della regione dell'anticlinale del Mont Terri dove si situa l'omonimo laboratorio sotterraneo scavato nell'argilla opalina. Questi studi ripercorrono i primi anni del Progetto Mont Terri dal 1996 al 2003.

Il progetto internazionale di Mont Terri è iniziato nel gennaio 1996 nel laboratorio sotterraneo di Mont Terri, scavato adiacente la galleria di sicurezza del tunnel omonimo vicino a St-Ursanne (Canton Giura, Svizzera). La caratterizzazione geologica, idrogeologica, geochimica e geotecnica di una formazione argillosa, in particolare dell'Argilla a Opalinus, è l'oggetto principale di questo progetto. Sedici partner provenienti dall'Europa, dell'America del nord e dal Giappone si sono riuniti attorno a questo progetto. Si tratta di ANDRA, BGR, CHEVRON, CRIEPI, DOE, ENRESA, FANC, GRS, IFSN, IRSN, JAEA, NAGRA, NWMO, OBAYASHI, SCK•CEN e swisstopo.

Dal 2006 swisstopo è il gestore del laboratorio sotterraneo e il responsabile del Progetto Mont Terri e in particolare, dell'attuazione del programma di ricerca stabilito dai partner.

swisstopo
Direttore del Progetto Mont Terri
Dott. Paul Bossart

Organisations involved

Project Partners

ANDRA	Agence nationale pour la gestion des déchets radioactifs, France
BGR	Bundesanstalt für Geowissenschaften und Rohstoffe, Germany
CHEVRON	Chevron Energy Technology ETC, US
CRIEPI	Central Research Institute of Electric Power Industry, Japan
DOE	U.S. Department of Energy, Office of Nuclear Energy, US
ENRESA	Empresa Nacional de Residuos Radiactivos, S.A., Spain
ENSI	Swiss Federal Nuclear Safety Inspectorate, Switzerland
FANC	The Federal Agency for Nuclear Control, Belgium
GRS	Gesellschaft für Anlagen- und Reaktorsicherheit mbH, Germany
IRSN	Institut de radioprotection et de sûreté nucléaire, France
JAEA	Japanese Atomic Energy Agency, Japan
NAGRA	National Cooperative for the Disposal of Radioactive Waste, Switzerland
NWMO	Nuclear Waste Management Organisation, Canada
OBAYASHI	Obayashi Corporation, Japan
SCK•CEN	Studiecentrum voor Kernenergie, Centre d'étude de l'énergie nucléaire, Belgium
swisstopo	Federal Office of Topography, Switzerland

Direction of the Project and Project Management

swisstopo	Federal Office of Topography

Responsible for the Mont Terri motorway tunnel system

FEDRO	Federal Roads Office, Switzerland

Authorisations

RCJU	République et Canton du Jura Département de l'Environnement et de l'Equipement

Table of Contents

Two miscellany volumes

1st Volume:
Reports of the FOWG, Geology Series, No. 4 – Bern 2003

Mont Terri Project – Geology, Paleohydrology and Stress Field of the Mont Terri Region 1–44
Paleohydrological Study on the Surroundings of the Mont Terri Rock Laboratory 45–92

2nd Volume:
Reports of the FOWG, Geology Series, No. 6 – Bern 2004

Mont Terri Project – Hydrogeological Synthesis, Osmotic Flow 1–94
An Experimental and Modelling Study of Chemico-osmotic Effects in the Opalinus Clay of Switzerland 95–126

Mont Terri Project – Geology, Paleohydrology and Stress Field of the Mont Terri Region

P. Heitzmann, J.-P. Tripet, editors

Berichte des BWG, Serie Geologie – Rapports de l'OFEG, Série Géologie – Rapporti dell'UFAEG, Serie Geologica – Reports of the FOWG, Geology Series

No. 4 – Berne 2003

Mont Terri Project – Geology, Paleohydrology and Stress Field of the Mont Terri Region

P. Heitzmann[1], J.-P. Tripet[1], editors

Berichte des BWG, Serie Geologie – Rapports de l'OFEG, Série Géologie – Rapporti dell'UFAEG, Serie Geologica – Reports of the FOWG, Geology Series

No. 4 – Berne 2003

[1]Federal Office for Water and Geology, Swiss Geological Survey, CH-3003 Berne-Ittigen

Impressum

Editor	Federal Office for Water und Geology, FOWG
Impression	1200 copies
Recommended quotation	Heitzmann, P. & Tripet, J.-P., Ed. (2003): Mont Terri Project - Geology, Paleohydrology and Stress Field of the Mont Terri Region - Reports of the Federal Office for Water and Geology (FOWG), Geology Series 4
Cover photos	DesAir (right); H. Steiger, GI (left)
Internet	This report is available as PDF file at www.swisstopo.ch
Copyright	FOWG, Berne-Ittigen, August 2003

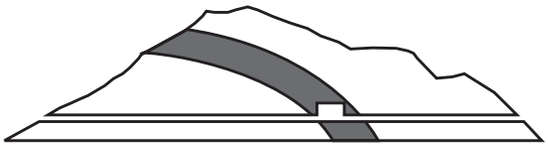

Mont Terri Project
Underground Rock Laboratory
Laboratoire souterrain

FOWG/SGS ANDRA BGR CRIEPI ENRESA GRS HSK IRSN JNC NAGRA OBAYASHI SCK•CEN

Organizations involved in the Mont Terri Project

Responsible for the Mont Terri motorway tunnel system and authorizations

RCJU	République et Canton du Jura Département de l'Environnement et de l'Equipement

Project Partners

ANDRA	Agence nationale pour la gestion des déchets radioactifs, France
BGR	Bundesanstalt für Geowissenschaften und Rohstoffe, Germany
CRIEPI	Central Research Institute of Electric Power Industry, Japan
ENRESA	Empresa Nacional de Residuos Radiactivos, S.A., Spain
FOWG/SGS	Federal Office for Water and Geology, Swiss Geological Survey
GRS	Gesellschaft für Anlagen- und Reaktorsicherheit mbH, Germany
HSK	Swiss Federal Nuclear Safety Inspectorate
IRSN	Institut de radioprotection et de sûreté nucléaire, France
JNC	Japan Nuclear Cycle Development Institute, Japan
NAGRA	National Cooperative for the Disposal of Radioactive Waste, Switzerland
OBAYASHI	Obayashi Corporation, Japan
SCK•CEN	Studiecentrum voor Kernenergie, Centre d'étude de l'énergie nucléaire, Belgium

Direction of the Project

FOWG	Federal Office for Water and Geology, Switzerland

Project Management

GI	Geotechnical Institute Ltd., St-Ursanne, Switzerland

Preface of the Editor

The first experiments of the international research project Mont Terri (St-Ursanne, Canton Jura) started in January 1996. Research is carried out in a gallery and in niches excavated from the security gallery of the Mont Terri road tunnel. The Swiss Geological Survey, a division of the Federal Office for Water and Geology (FOWG), supports hydrogeological research projects in low-permeability formations and is one of the Mont Terri partners since the beginning of the project. The aim of the project is the geological, hydrogeological, geochemical and geotechnical characterisation of a clay formation, specifically of the Opalinus Clay. Twelve partners from six different countries participate in the project. The FOWG is in charge of the project direction since July 2001 and is also responsible for the publication of the reports. For geological reasons, a repository for radioactive waste in the Mont Terri region has been ruled out.

The interpretation of the experiment results requires the knowledge of the geological conditions of the rock laboratory area. This is why the Swiss Geological Survey has ordered the realization of studies related to three topics of priority: working-out of updated geological cross-sections, paleohydrological analysis, synthesis of stress field measurements. After the publication of a general synthesis related to the initial part of the Mont Terri Project (SNHGS, Geological Report No. 23, 1999), we are pleased to present now the results of these three specific studies to a broader scientific audience. These studies have been carried out separately, for this reason they are presented here as three independent modules.

The editor would like to express his best thanks to the authors and to those who have helped with their competence and engagement to proceed with this publication. Dr. R. Burkhalter (FOWG) is gratefully acknowledged for the thorough review. We would also thank the federal and cantonal authorities for their support in the project.

The authors alone are responsible for the content of the text and the illustrations.
Further information can be found on the Internet site www.mont-terri.ch.

Préface de l'éditeur

Les premières expériences réalisées dans le cadre du projet de recherche international du Mont Terri (St-Ursanne, Canton du Jura) ont été entreprises en 1996. Les recherches sont réalisées dans une galerie et des niches excavées à partir de la galerie de sécurité du tunnel autoroutier du Mont Terri. Le Service géologique national (Office fédéral des eaux et de la géologie, OFEG) soutient l'étude des formations géologiques à faible perméabilité et collabore dès le début comme partenaire au Projet Mont Terri. L'objectif principal du projet est la caractérisation géologique, hydrogéologique, géochimique et géotechnique d'une formation argileuse, les Argiles à Opalinus. Douze partenaires de six différents pays collaborent au projet. La direction du projet est depuis juillet 2001 placée sous la responsabilité de l'OFEG, auquel incombe également la publication des rapports. Pour des raisons géologiques, il n'est pas question d'entreposer des matériaux radioactifs dans la région du Mont Terri.

L'interprétation des résultats des expériences réalisées nécessite de connaître les conditions géologiques de la région du laboratoire souterrain. Dans ce but, le Service géologique national a mandaté des études relatives à trois thèmes prioritaires : établissement de coupes géologiques actualisées, analyse paléohydrologique, synthèse des mesures du champ de contraintes. C'est avec plaisir que nous présentons ici, après une synthèse générale relative à la partie initiale du Projet Mont Terri (SHGN, Rapport géologique No 23, 1999), les résultats de ces trois études spécifiques à un large public de spécialistes. Ces études ont été réalisées séparément, c'est pourquoi elles sont présentées ici comme trois modules indépendants.

L'éditeur tient à remercier les auteurs ainsi que les personnes qui, par leur compétence et leur engagement, ont permis la réalisation de cette publication. R. Burkhalter, dr sc. (OFEG) a procédé à une lecture attentive du manuscrit. Nos remerciements s'adressent aussi aux autorités fédérales et cantonales pour leur soutien dans le projet.

Les auteurs sont seuls responsables du contenu du texte et des illustrations.
Pour toute information supplémentaire veuillez consulter le site Internet www.mont-terri.ch.

Vorwort des Herausgebers

Die ersten Experimente, die im Rahmen des internationalen Forschungsprojektes Mont Terri (St-Ursanne, Kanton Jura) durchgeführt worden sind, haben im Januar 1996 begonnen. Die Untersuchungen werden in einem erweiterten Teil des Sicherheitsstollens des Mont-Terri-Autobahntunnels durchgeführt. Die Landesgeologie im Bundesamt für Wasser und Geologie (BWG) unterstützt die hydrogeologischen Untersuchungen geringdurchlässiger geologischer Formationen und arbeitet deshalb seit Beginn als Partnerin im Mont-Terri-Projekt mit. Das Hauptziel dieses Projektes ist die geologische, hydrogeologische, geochemische und geotechnische Charakterisierung von Tongesteinen, im Speziellen des Opalinus-Tons. An dem Projekt sind zwölf Partner aus sechs Ländern beteiligt. Die Leitung des Projektes liegt seit Mitte 2001 beim BWG. Diesem obliegt auch die Veröffentlichung der Berichte. Aus geologischen Gründen ist im Mont Terri Gebiet jegliche Planung eines Endlagers für radioaktive Abfälle ausgeschlossen.

Die Interpretation der Resultate der Experimente benötigt die Kenntnis der geologischen Verhältnisse der Umgebung des Felslabors. Deshalb hat die Landesgeologie Studien in drei spezifischen Schlüsselbereichen in Auftrag gegeben: Erstellung von aktualisierten geologischen Profilen, paläohydrologischen Untersuchungen und Synthese der Stressfeld-Messungen. Es freut uns, im Rahmen der Mont-Terri-Publikationen nach der einführenden Zusammenfassung (LHG, Geologische Berichte Nr. 23, 1999) jetzt auch die Ergebnisse der drei obenerwähnten, gezielten Studien einem breiten Fachpublikum vorlegen zu können. Diese Studien sind unabhängig voneinander durchgeführt worden; darum werden sie hier als drei eigenständige Module publiziert.

Der Herausgeber möchte den Autoren und allen andern, die an diesem Band beteiligt waren, für ihren grossen Einsatz bestens danken. Dr. R. Burkhalter (BWG) sei für seine aufmerksame und konstruktive Durchsicht des Manuskriptes gedankt. Ebenfalls möchten wir den eidgenössischen und kantonalen Behörden für ihre Unterstützung im Projekt danken.

Für den Inhalt des Textes und für die Illustrationen sind die Autoren allein verantwortlich.
Weitere Informationen zum Mont Terri Projekt finden Sie unter www.mont-terri.ch.

Prefazione dell'editore

I primi studi effettuati nell'ambito del progetto di ricerca internazionale Mont Terri (St-Ursanne, Canton Giura) sono iniziati nel gennaio 1996. Le ricerche sono realizzate in un cunicolo e nelle nicchie scavate a partire dalla galleria di soccorso del tunnel autostradale del Mont Terri. Il Servizio geologico nazionale dell'Ufficio federale delle acque e della geologia (UFAEG) promuove gli studi di formazioni geologiche a bassa permeabilità, collaborando fin dall'inizio come partner del progetto Mont Terri. L'obiettivo principale del progetto è la caratterizzazione geologica, idrogeologica, geochimica e geotecnica di una particolare formazione argillosa: l'Argilla ad Opalinus. A tutt'oggi collaborano al progetto dodici partner di sei diversi paesi. Dal luglio 2001, il progetto è sotto la direzione dell'UFAEG, al quale compete anche la pubblicazione dei rapporti. La pianificazione di un deposito finale per le scorie radioattive sotto il Mont Terri è da escludere per ragioni geologiche.

L'interpretazione dei risultati delle ricerche richiede la conoscenza delle condizioni geologiche relative alla regione del laboratorio sotterraneo. Il Servizio geologico nazionale ha così dato l'incarico di effettuare studi in tre settori chiave: accertamento dei profili geologici, analisi paleoidrologiche, sintesi delle misurazioni del campo di tensione («stress field»). La pubblicazione dei relativi risultati, destinata a un largo pubblico di specialisti, rientra nell'ambito degli studi sul Mont Terri e segue la sintesi introduttiva già edita nei Rapporti geologici del SIGN, n. 23, 1999. Siccome questi ultimi tre studi sono indipendenti uno dall'altro, i risultati sono presentati in tre moduli distinti.

Ringrazio tutti gli autori, i collaboratori e le autorità cantonali e federali che, con le loro conoscenze e il loro impegno, hanno contribuito alla riuscita dell'opera. Un ringraziamento particolare va al Dr. R. Burkhalter (UFAEG) per l'attenta e costruttiva rilettura del manoscritto.

Gli autori sono gli unici responsabili del contenuto dei testi e delle illustrazioni.
Ulteriori informazioni sul progetto Mont Terri sono pubblicate all'indirizzo www.mont-terri.ch.

Federal Office for Water and Geology
The Head of the Swiss Geological Survey

Dr. Christoph Beer

Contents

Modellierung bilanzierter Profile im Gebiet Mont Terri – La Croix (Kanton Jura) 7
M. Freivogel & P. Huggenberger

Paleohydrological Study on the Surroundings of the Mont Terri Rock Laboratory 45
P. Bossart & S. Wermeille

The Stress Field in the Mont Terri Region – Data Compilation 65
P. Bossart & S. Wermeille

Modellierung bilanzierter Profile im Gebiet Mont Terri – La Croix (Kanton Jura)

M. Freivogel[1] & P. Huggenberger[1]

[1]Basel University, Geological Institute

Recommended quotation:
Freivogel, M. & Huggenberger, P. (2003): Modellierung bilanzierter Profile im Gebiet Mont Terri – La Croix (Kanton Jura). In: Heitzmann, P. & Tripet, J.-P. (Ed.): Mont Terri Project – Geology, Paleohydrology and Stress Field of the Mont Terri Region (p. 7–44). – Reports of the Federal Office for Water and Geology (FOWG), Geology Series 4.

Manuscript accepted April 15, 2002

Summary

The hydrogeology, geochemistry and rock mechanics of the Opalinus clay, a claystone formation dating from the earliest Dogger (Aalenian), have been being studied in the Mont Terri Rock Laboratory near St-Ursanne in the Canton Jura since 1996. The laboratory can be reached through the security gallery of the Mont Terri road tunnel – a part of the new A16 Transjurane motorway from Biel to Belfort – between St-Ursanne and Courgenay. The tunnel is cut through the northernmost anticline in this area of the Jura Mountains, the Mont Terri anticline. The Federal Office for Water and Geology (FOWG) runs the project with twelve international partners. The results of the study are used to estimate the possibility and safety of using in other regions similar settings in claystones as permanent disposal sites for radioactive waste.

The tectonic situation must be taken into account when synthesising experimental data in a laboratory. In the present case the pore fluids in the rock were influenced by the genesis of the anticline.

This study is focussed on two geological cross sections, one along the Mont Terri road tunnel and the other along the neighbouring La Croix railway tunnel. The profiles are modelled with a two-dimensional tectonic material balancing method. This is a suitable method to bring all the available geological data – such as drill cores, tunnel maps and geological surface maps – into context, to give a prognostic interpolation and to develop a kinematic, dynamic and geometric evolution of a deformed structure.

The idea of profile balancing is based on the assumption that the volume of rock involved in a deformation process must remain constant. In a two-dimensional case, such as a profile cross section in the direction of transport, this implies that the total area of each bed and the length of the surface of each layer must remain constant from the undeformed through to the deformed situation. A balanced profile must thus be retro-deformable, and each step of deformation of the geometry as well as all the mechanical processes involved must be geologically plausible.

It must be possible to bring the model from the original situation (smoothed section) into its present, deformed state in such a way that every step of the deformation, such as folding and faulting, and the resulting geometry is realistic. Each increment must be mathematically and physically quantifiable.

A computer application was used for the modelling. It offers fixed modules for deformation, which can be combined as wished. Instead of aiming directly for a certain solution, the geologist evolves the most plausible model in an iterative process. The user's own intuition, ideas and experience are involved in confirming or disproving original expectations.

The modelled sections of Mont Terri and La Croix give a detailed picture of the geological structure of the marginal overthrust that generates the Mont Terri anticline. Also, a step-by-step evolution of the present structure is shown. Different phases of deformation can be distinguished, some of which are associated with the folding of the Jura Mountains and others with the evolution of the Rhine graben.

A series of thirteen profiles shows the lateral evolution of the geological structures and gives a deeper insight into the regional geology.

Résumé

Depuis 1996, l'hydrogéologie, la géochimie et la géomécanique des Argiles à Opalinus - une formation argileuse datant du Dogger basal (Aalénien) - sont étudiées expérimentalement dans le laboratoire souterrain du Mont Terri, près de St-Ursanne, dans le Canton du Jura. On accède au laboratoire par la galerie de sécurité du tunnel autoroutier du Mont Terri. Situé entre St-Ursanne et Courgenay, sur un tronçon de la nouvelle autoroute Transjurane A16 qui doit relier Bienne et Belfort, le tunnel traverse le pli le plus septentrional de la chaîne du Jura, l'anticlinal du Mont Terri. Ce projet placé sous la direction de l'Office fédéral des eaux et de la géologie (OFEG) regroupe douze partenaires internationaux. Les résultats des investigations sont utilisés pour évaluer s'il est possible de stocker définitivement des déchets radioactifs dans d'autres régions, dans des roches argileuses similaires et quelle sécurité offrirait un tel dépôt final.

Il convient de placer les résultats dans leur contexte géologique, car l'évolution de l'anticlinal se répercute sur les caractéristiques des eaux interstitielles comprises dans la roche. Les conditions tectoniques doivent donc être prises en compte dans la synthèse des données expérimentales recueillies dans le laboratoire.

Deux profils géologiques sont élaborés dans le cadre de la présente étude, l'un correspondant au tunnel autoroutier du Mont Terri et l'autre au tunnel ferroviaire voisin de La Croix. Les deux coupes sont modélisées selon la méthode des profils tectoniques équilibrés en deux dimensions. Ce procédé se prête bien à l'insertion des données géologiques disponibles (descriptions de sondages, levés de tunnels, cartes géologiques de surface) dans leur contexte général, à leur interpolation aux fins de pronostics et à la description de l'évolution cinématique, dynamique et géométrique d'une structure déformée.

L'idée d'équilibrage repose sur la règle fondamentale selon laquelle le volume de la roche reste constant tout au long de sa déformation. Dans le cas bidimensionnel d'une coupe dans la direction de transport, cela signifie que la surface occupée par une couche et la longueur de son toit restent identiques entre l'état intact et l'état déformé. Il en résulte qu'on doit pouvoir «rétro-déformer» un profil équilibré en mettant en jeu des particularités géométriques et des processus mécaniques plausibles au plan géologique à chaque stade de déformation.

Le profil lissé doit être tel qu'on puisse le faire évoluer pas par pas jusqu'à l'état déformé contemporain en faisant appel à des plissements et à des décrochements réalistes. Chaque étape doit être transparente, c'est-à-dire quantifiable aux plans mathématique et physique. La modélisation recourt à une application informatique comprenant des modules prédéfinis qui peuvent être combinés ou emboîtés librement pour simuler des structures géologiques. La méthode ne vise pas à obtenir directement une solution plausible, mais à l'élaborer progressivement au cours d'un processus itératif. A chaque étape, l'opérateur géologue fait appel à son intuition, à ses idées personnelles et à l'expérience acquise pour confirmer ou rejeter progressivement les hypothèses initiales.

Appliquée aux profils du Mont Terri et de La Croix, la modélisation fournit une représentation détaillée de la structure géologique du chevauchement bordier qui forme l'anticlinal du Mont Terri. Elle expose également l'évolution qui a conduit aux structures contemporaines. On peut distinguer plusieurs phases de déformation, qui sont associées pour les unes à la formation du Fossé rhénan et pour les autres au plissement de la chaîne jurassienne.

Une série de treize profils présente l'évolution latérale des structures géologiques et fournit un aperçu plus profond de la géologie régionale.

Zusammenfassung

Im Felslabor Mont Terri bei St-Ursanne im Kanton Jura werden seit 1996 Fragestellungen zur Hydrogeologie, Geochemie und Felsmechanik einer Tonsteinformation experimentell untersucht. Es handelt sich dabei um den Opalinus-Ton aus dem untersten Dogger (Aalénien).

Das Labor ist zugänglich über den Sicherheitsstollen des Autobahntunnels Mont Terri zwischen St-Ursanne und Courgenay, einem Teil der Neubaustrecke A16 Transjurane zwischen Biel und Belfort. Der Tunnel durchfährt die regional nördlichste Falte des Juragebirges, die Mont-Terri-Antiklinale. Am Projekt sind zwölf internationale Partner unter der Leitung des Bundesamtes für Wasser und Geologie (BWG) beteiligt. Die Resultate der Untersuchungen werden verwendet, um die Machbarkeit und Sicherheit einer Endlagerung radioaktiver Abfälle andernorts in ähnlichen Tongesteinen beurteilen zu können.

Die Tektonik bildet also eine Randbedingung für die Synthese der experimentellen Daten aus dem Felslabor. So hat zum Beispiel die geologische Entwicklung der Antiklinale die Porenwässer im Gestein beeinflusst. In der vorliegenden Arbeit werden zwei geologische Profile erarbeitet. Es handelt sich um die Profilschnitte des Autobahntunnels Mont Terri und des benachbarten Eisenbahntunnels La Croix. Die Profile werden mit der Methode der zweidimensionalen tektonischen Materialbilanzierung modelliert. Diese Methode bietet sich an, die vorhandenen geologischen Daten – aus Bohrprofilen, Tunnelkartierungen, geologischen Oberflächenkartierungen etc. – in einen Kontext zu bringen, prognostisch zu interpolieren und einen kinematischen, dynamischen und geometrischen Werdegang einer deformierten Struktur zu entwickeln.

Die Idee der Bilanzierung beruht auf der Grundregel, dass sich Gesteinsvolumen bei ihrer Deformation nicht ändern. Im zweidimensionalen Fall eines Profilschnittes in Transportrichtung bedeutet dies, dass sich die Flächen der Schichtanschnitte und die Längen der Schichtoberflächen im deformierten und im undeformierten Zustand nicht unterscheiden. Ein bilanziertes Profil muss demzufolge rückdeformierbar sein, wobei bei jedem Zwischenschritt der Deformation die Geometrie und die Mechanik geologisch plausibel sein müssen.

Das ausgeglättete Profil muss Schritt für Schritt, unter Verwendung von realistischen Falten- und Bruchgeometrien, in den heutigen deformierten Zustand gebracht werden können. Jeder Zwischenschritt muss transparent, d. h. mathematisch und physikalisch quantifizierbar sein.

Die Modellierung erfolgt mit Hilfe einer Computeranwendung, die festgelegte Programmmodule anbietet. Diese Module können zur Simulation geologischer Strukturen beliebig kombiniert und verschachtelt werden. Eine plausible Lösung wird nicht direkt angestrebt, sondern in einem iterativen Prozess schrittweise erarbeitet. Der bearbeitende Geologe lässt bei jedem Schritt seine Intuition, eigene Ideen und Erfahrungen einfliessen, ursprüngliche Annahmen werden so nach und nach bestätigt oder verworfen.

Auf die Profile Mont Terri und La Croix angewendet, ergibt die Modellierung ein detailliertes Bild des geologischen Baus der Randüberschiebung, die die Mont-Terri-Antiklinale bildet. Sie stellt zudem den Weg dar, der zu den heutigen Strukturen geführt hat. Es können verschiedene Deformationsphasen unterschieden werden, die einerseits mit der Bildung des Rheintalgrabens, andererseits mit der Auffaltung des Juragebirges assoziiert sind.

In einer Serie von dreizehn Profilen wird die laterale Entwicklung der geologischen Strukturen dargestellt und ein tieferer Einblick in die regionale Geologie gegeben.

Inhalt

Zusammenfassung 9
Summary 10
Résumé 11
1 Einleitung 13
1.1 Aufgabenstellung 13
1.2 Bisherige Arbeiten im Gebiet 14
2 Methodik der Profilbilanzierung 17
2.1 Konzept 17
2.1.1 Einschränkende Faktoren und Randbedingungen 17
2.1.2 Plausibilität 18
2.2 Datenmodell und Vorgehen 19
2.2.1 Akquisition 19
2.2.2 Konstruktion 19
2.2.3 Modellierung 19
3 Geologie des Gebietes Mont Terri – La Croix, Profilmodellierung 23
3.1 Geologische Übersicht 24
3.2 Autobahntunnel Mont Terri 27
3.2.1 Akquisition 27
3.2.2 Konstruktion 27
3.2.3 Modellierung 28
3.3 Eisenbahntunnel La Croix 32
3.3.1 Akquisition 32
3.3.2 Konstruktion 32
3.3.3 Modellierung 32
3.4 Profilserie 36
3.5 Schlussfolgerungen 38
Verdankungen 40
Referenzen 41
Anhang 43

1 Einleitung

1.1 Aufgabenstellung

Im Felslabor Mont Terri bei St-Ursanne im Kanton Jura werden die hydrogeologischen, geochemischen und felsmechanischen Eigenschaften einer Tonsteinformation, des Opalinus-Tons, experimentell untersucht. Die Versuchsanlage wird von zwölf internationalen Partnern unter der Leitung des Bundesamtes für Wasser und Geologie (BWG) seit 1996 betrieben. Die aus den Experimenten resultierenden Daten vertiefen das Verständnis über Prozesse, die zur Beurteilung der Machbarkeit und Sicherheit eines Endlagers für radioaktive Abfälle in ähnlichem Gestein entscheidend sind.
Die experimentellen Untersuchungen zeigen, dass das heutige Porenwasser im Opalinus-Ton immer noch geochemische Signale zeigt, die aus der Zeit seiner Einlagerung stammen. Es handelt sich also um ursprüngliches Meerwasser. Die Kinematik der tektonischen Bewegungen der Jurafaltung und die einhergehende Erosionsgeschichte bestimmen die paläohydraulische Entwicklung des Mont Terri Felslabors. Durch die fortschreitende Erosion des Doubstales und der Mont-Terri Antiklinale findet eine Änderung der Grundwasserfliessrichtungen von Infiltration zu Exfiltration und eine Änderung der Grundwasserchemie statt (Bossart & Wermeille 2003), die also direkt von der tektonischen Geschichte abhängt.
Die Landesgeologie im BWG regte 1999 eine Neubearbeitung der Tektonik des Gebietes La Croix – Mont Terri an. Die vorliegende Arbeit, entstanden im Rahmen einer Diplomarbeit am Geologisch-Paläontologischen Institut der Universität Basel, wendet Methoden der zweidimensionalen tektonischen Materialbilanz auf zwei Profile durch die Mont-Terri-Antiklinale an. Die beiden Profilspuren sind vorgegeben durch den Autobahntunnel Mont Terri und den Eisenbahntunnel La Croix nördlich St-Ursanne. Es soll ein Modell des geologischen Untergrundes entstehen, das den Werdegang der heutigen Strukturen plausibel darlegt.
Am Mont Terri bietet sich eine Profilkonstruktion nach den Regeln der Materialbilanz an. Sie stellt eine nachvollziehbare Konstruktionsmethode dar, um Daten aus Kartierungen, Bohrungen etc. prognostisch zu interpolieren und darüber hinaus einen plausiblen kinematischen, dynamischen und geometrischen Werdegang einer geologischen Struktur zu veranschaulichen.

Im ersten Teil wird ein Überblick über die bisherigen Arbeiten im Gebiet gegeben. Anschliessend folgt im zweiten Teil ein Überblick über die Methodik, eine Diskussion der wichtigsten Annahmen und eine Beschreibung der Vorgehensweise der Modellierung. Der dritte Teil erläutert die Anwendung der beschriebenen Methoden auf zwei Profilschnitte durch die Mont-Terri-Antiklinale. Die im Modell implizierten geometrischen und kinematischen Aussagen werden in einen regionalen geologischen Kontext gestellt. Es werden Schlüsse betreffend kinematischer Entwicklung, Diskontinuitäten, Tiefenstruktur und Verkürzungsbetrag der beiden bilanzierten Profile gezogen. Weiter wird eine Serie von nicht bilanzierten Profilen gezeigt, die die tektonischen Strukturen der Mont-Terri-Antiklinale in vereinfachter Form darstellen und dadurch einen Einblick in deren laterale geometrische Entwicklung geben.

1.2 Bisherige Arbeiten im Gebiet

Im Gebiet zwischen Cornol und St-Ursanne wurden seit dem Bau des Eisenbahntunnels von La Croix um 1875 eine Reihe von geologischen Fragen untersucht. Basierend darauf existieren geologische Karten und Profile, die im Folgenden zitiert werden. In vielen Arbeiten diente das Profil des Eisenbahntunnels der Illustration der tektonischen Strukturen der Mont-Terri-Antiklinale. Die wichtigsten existierenden Profile sind in Abb. 1 zusammengestellt.

Erste Untersuchungen im Gebiet gehen zurück auf Thurmann (1832), Gressly (1853), Ducret (1874), Thurberg (1874), Koby (1889) und Rollier (1898) und deren erfolglose Suche nach Kohle und Salz. Mathey (1883) zeichnet ein erstes Profil nach seiner eigenen Kartierung des Eisenbahntunnels (Abb. 1 a), in dem er die Faltenstruktur noch nicht als Rampenantiklinale erkennt. Statt dessen wird eine sinoidale Doppelfalte angenommen, wie sie zu jener Zeit oft als Erklärung für überschobene Strukturen diente (vgl. «Glarner Doppelfalte», Heim 1878). Eine im Tunnel beobachtete Brekzienzone – in Tat und Wahrheit die durchfahrene Überschiebung – wird als breite, mit Schutt gefüllte Spalte interpretiert. Buxtorf & Lehner (1920) erkennen Brüche in der Mont-Terri-Kette, die sie als erste mit der Bildung des Rheintalgrabens assoziieren. Liniger & Wehrenfels (1926) entwerfen eine erste tektonische Kartenskizze der Umgebung von Asuel und St-Ursanne. Kelterborn (1944) erkennt den Überschiebungscharakter der Struktur und nimmt im Profilschnitt La Croix das Liegende der Ajoie als verfaltet an. Dazu kommen südfallende Brüche mit Überschiebungs- und Abschiebungscharakter (Abb. 1 b). Ein dem Schnitt Mont Terri entsprechendes Profil derselben Arbeit zeigt die Struktur ebenfalls als über eine Rampe im stark deformierten Liegenden geschobene Falte. Der nördliche Schenkel ist überkippt, die Schichten sind intern verformt und nicht zerbrochen. Ein Bruch im Keuperkern hebt die südliche Flanke gegenüber der nördlichen an (Abb. 2 a).

Im Zuge der verstärkten Suche nach nutzbaren Rohstoffen während des zweiten Weltkriegs werden die bituminösen Posidonienschiefer im Lias des Mont-Terri-Gebiets eingehend untersucht. Rickenbach (1947) publiziert Ergebnisse und eine geologische Kartenskizze des Gebiets. Von 1948 bis 1963 wird das ganze Gebiet von Blatt 1085 der Landeskarte 1 : 25 000 geologisch kartiert (Laubscher 1948, Diebold 1960, Schneider 1960, Tschopp 1960, Diebold et al. 1963, Laubscher 1963). Tschopp (1960) zeigt in einer Profilserie ein Profil entlang des Eisenbahntunnels von La Croix (Abb. 1 c). Die Mont-Terri-Antiklinale hat in jener Arbeit den Charakter einer engen Kofferfalte mit leicht eingefallenem Scheitel, die über eine Rampe auf das leicht deformierte Liegende überschoben ist und deren Südschenkel von einem steilen Bruch versetzt wird. Die Serie enthält auch ein Profil in einer Lage, die etwa dem heutigen Autobahntunnel Mont Terri entspricht (Abb. 2 b). Hier ist das Liegende wiederum gewölbt dargestellt, die Falte jedoch ist viel weniger eng, zeigt sekundäre Gewölbe und wird nur von einem steilen Bruch versetzt.

Neue Profile entstanden vor und während des Tunnelbaus der A16 Transjurane (BTN 1993, BTN 1994a, Haarpaintner & Schaeren 1997). Das Profil Mont Terri (Abb. 2 c) zeigt dort einen stark zerbrochenen Nordschenkel, dessen Schichten intern deformiert sind und fast duktil anmutende Verfaltungen aufweisen. Die Mächtigkeitszunahme des Opalinus-Tons (vgl. Kap. 3.2.3) wird durch eine Überschiebung erklärt, die bis an die Oberfläche durchschlägt. Das Profil La Croix zeigt eine verschuppte Faltenstruktur über undeformierten Schichten des Liegenden. Zu den nordvergenten Überschiebungen kommen hier steile Brüche mit wenig Versatz und eine Abschiebung im südlichen Schenkel. Die Profile am Mont Terri enthalten Information aus Bohrungen (BGA 1988, Bläsi et al. 1996, Möri et al. 1997) und zum Teil aus Tunnelkartierungen (BTN 1994a). Abb. 1 e und 2 d zeigen zum Vergleich auch die neuen, bilanzierten Profile der vorliegenden Arbeit (vgl. Kap. 3.2.3 und 3.3.3).

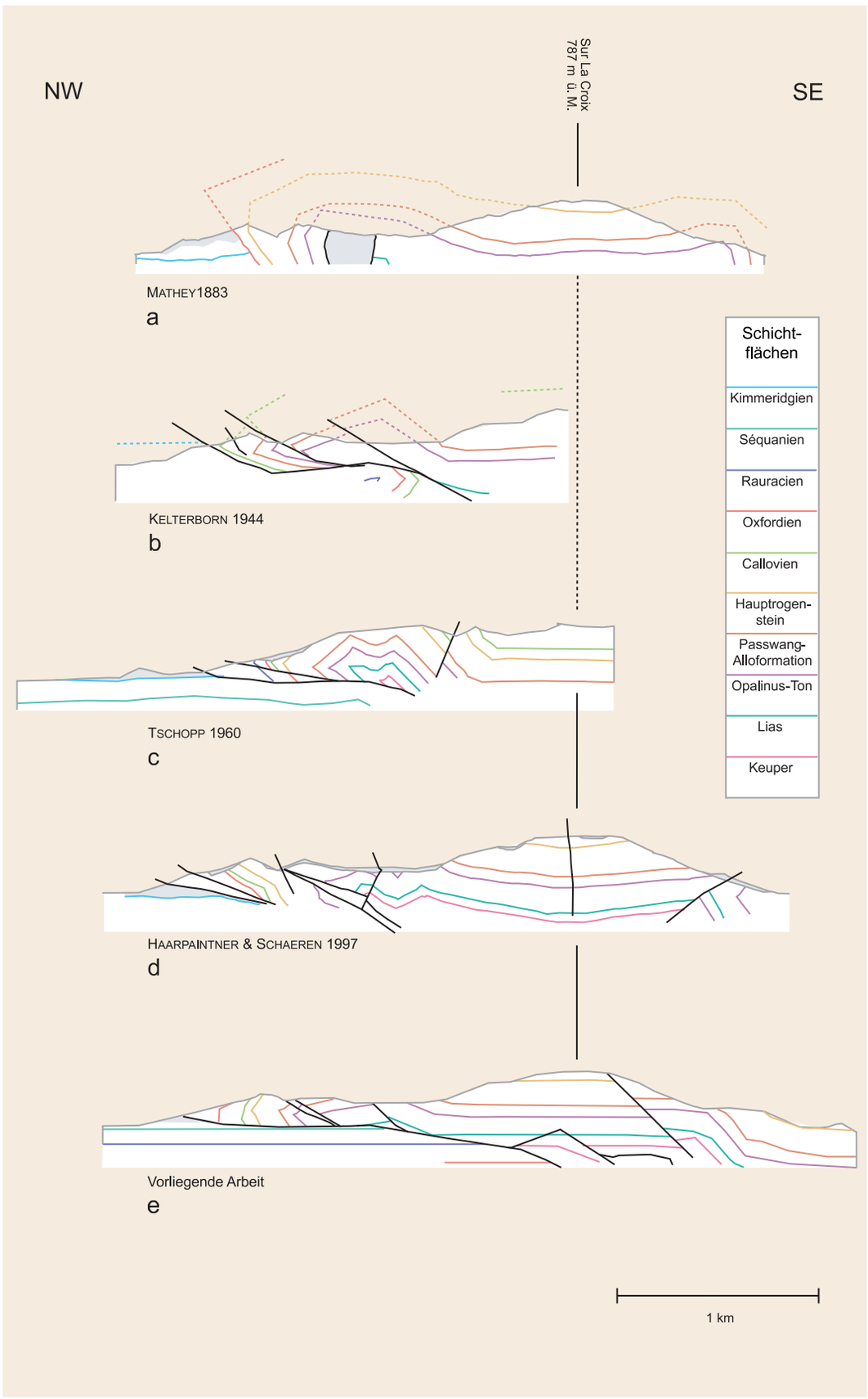

Abb. 1: Zusammenstellung der geologischen Profile entlang dem Eisenbahntunnel La Croix (vgl. Kap. 3.3.3). Abb. z.T. verändert aus den angegebenen Referenzen. Die grau gerasterten Flächen bezeichnen nicht weiter differenzierte Gesteinsmassen (tertiäre und quartäre Ablagerungen, tektonische Brekzien).

Fig. 1: Geological profiles along the La Croix railway tunnel (see chapter 3.3.3). Figure adapted from the references cited. The grey shaded areas indicate undifferentiated rocks (tertiary and quaternary sediments, tectonic breccias).

Fig. 1: Profils géologiques le long du tunnel ferroviaire de La Croix (cf. chap. 3.3.3). Figure partiellement modifiée à partir des références citées. Les surfaces grisées signalent des roches indifférenciées (sédiments tertiaires et quaternaires, brèches tectoniques).

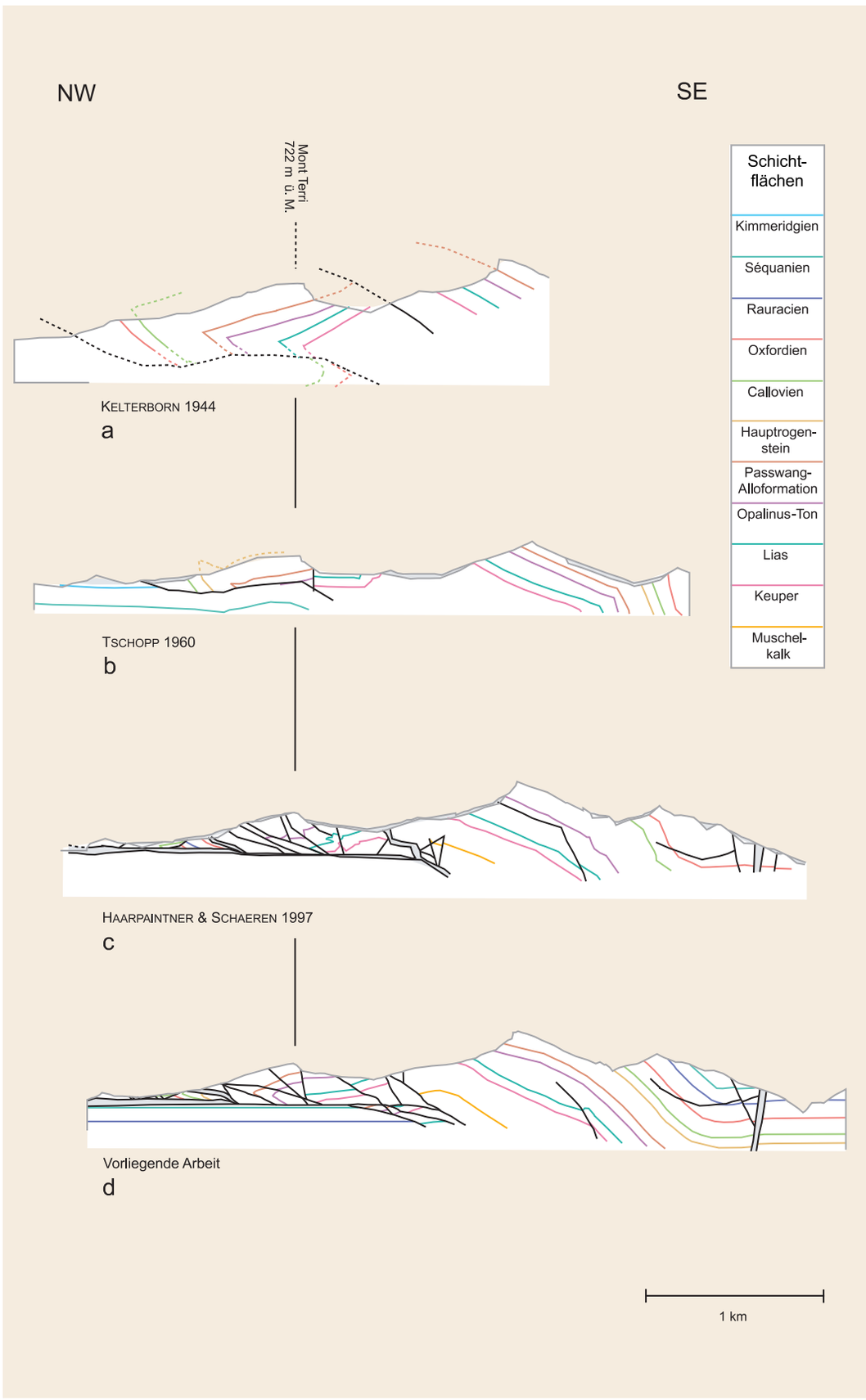

Abb. 2: Zusammenstellung der geologischen Profile nahe des Autobahntunnels Mont Terri (vgl. Kap. 3.2.3). Abb. z.T. verändert aus den angegebenen Referenzen. Die grau gerasterten Flächen bezeichnen nicht weiter differenzierte Gesteinsmassen (tertiäre und quartäre Ablagerungen, tektonische Brekzien).

Fig. 2: Geological profiles along the Mont Terri motorway tunnel (see chapter 3.2.3). Figure adapted from the references cited. The grey shaded areas indicate undifferentiated rocks (tertiary and quaternary sediments, tectonic breccias).

Fig. 2: Profils géologiques au voisinage du tunnel autoroutier du Mont Terri (cf. chap. 3.2.3). Figure partiellement modifiée à partir des références citées. Les surfaces grisées signalent des roches indifférenciées (sédiments tertiaires et quaternaires, brèches tectoniques).

2 Methodik der Profilbilanzierung

2.1 Konzept

Ein geologisches Profil dient dem Geologen als Modell, um im Feld, in Bohrungen oder Tunnelaufschlüssen gesammelte Daten zu erklären und in einen Kontext zu bringen. Die verfügbaren Daten stammen aus einer geologischen Struktur, die eine mehr oder weniger komplexe Deformationsgeschichte hinter sich hat. Die Darstellung im Profil ermöglicht es, aus zugänglichen Daten auf Strukturen zu schliessen, die nicht direkt an der Erdoberfläche sichtbar sind. Ein bilanziertes Profil dient darüber hinaus als Modell, um die Deformationsgeschichte zu erklären.
Mit der Methode der Profilbilanzierung werden Materialbilanzen erstellt. Ziel der Materialbilanz ist es, ein kinematisch und dynamisch plausibles Profil zu erreichen (vgl. Kap. 2.1.2). Es wird ein möglicher geometrischer Weg und ein möglicher mechanischer Weg vom undeformierten in den deformierten Zustand gesucht. Diese Wege müssen konsistent und plausibel sein. Die erreichte palinspastische Rekonstruktion muss plausibel sein, ebenso die einzelnen kinematischen Schritte. Zudem muss sich das Profil im deformierten Zustand in die dreidimensionale Kinematik einpassen, was eine Verbindung zum Kartenbild schafft.
Die Bilanzierung eines geologischen Profils erweitert dessen Modelleigenschaft um eine weitere Dimension; zur Aussage über den heutigen geometrischen Zustand einer Struktur kommt die Aussage über die tektonischen Vorgänge, die zu diesem Zustand geführt haben. Ein Profil, das in den einzelnen Schritten seiner kinematischen Entwicklung im Bezug auf zwei Pinlines (s. u.) keine Veränderung der Schichtlängen bzw. der Schichtflächen zeigt, ist schichtlängen- bzw. schichtflächenbilanziert. Schichtflächenbilanzierung kann auf alle Oberflächen des Schichtstapels angewendet werden oder ist auf eine besonders relevante Formationsgrenze beschränkt, das sogenannte Keybed oder den Leithorizont.
Darüberhinaus muss ein solches Profil zurückdeformierbar sein. Für den Übergang eines deformierten in einen undeformierten Zustand und zurück müssen geometrische, aber auch kinematische und dynamische Randbedingungen berücksichtigt werden.

2.1.1 Einschränkende Faktoren und Randbedingungen

Methoden der Materialbilanzierung werden vor allem in Gebieten mit spröd deformierender Tektonik angewendet, das heisst mit höchstens zwei Kilometern Überlast, sowie Tendenz zu schichtparallelem Gleiten («flexural slip»). Beides ist im Jura zu finden, wo eine mesozoische Sedimenthaut über einem kristallinen Sockel abgeschert wurde. In den kompetenten Schichten bleiben Schichtmächtigkeiten bei Verformung in erster Näherung erhalten. So kann die Massenerhaltung in Transportrichtung nicht nur auf die Flächenbilanz, sondern auf die Schichtlängenbilanz reduziert werden. Inkompetente Schichten können auch in spröd deformierendem Regime intern verfaltet werden («flexural flow») und lassen sich nur in Bezug auf die Fläche, nicht jedoch auf die Schichtlänge bilanzieren.
Die Wahl von geeigneten Rand- und Anfangsbedingungen erfordert geologisches Fingerspitzengefühl und Fachkenntnis. Die Wahl der Profilspurorientierung beispielsweise darf nicht zufällig getroffen werden, denn jede Bilanzierungstechnik setzt voraus, dass kein lateraler Transport von Material durch die Profilebene stattfindet (geschlossenes System, vgl. Laubscher 1965, Noack 1989). Folglich sollte die Profilspur wenn immer möglich in der Transportrichtung liegen, die durch einen Vektor repräsentiert wird. So kann das Gesetz der Volumenerhaltung (Goguel 1952) im zweidimensionalen Fall zum Gesetz der Flächenerhaltung reduziert werden. Zudem werden Strukturen so meist senkrecht geschnitten, wodurch Verzerrungen z. B. der Schichtmächtigkeiten entfallen.
Transportrichtungen können allerdings von Block zu Block variieren und auch im zeitlichen Ablauf der Deformation ändern, z. B. bei Flowerstrukturen, Blockrotationen (Bitterli 1992) und Änderungen der Überlast oder der Geometrie des Abscherhorizontes. Diskrete Horizontalverschiebungen oder diffuse Transferzonen, die die Profilspur durchqueren, lassen die Verkürzung im Profil in der Regel geringer erscheinen (Bitterli 1992). Ausgedehnte Drucklösungsprozesse können zu Materialumverteilungen führen (Droxler & Schär 1979, Laubscher 1979). Solche Effekte sind sehr schwierig quantifizierbar und können zu Fehlinterpretationen führen. Um eine brauchbare vektorielle Transportrichtung zu erhalten, müssen diese kinematischen Variationen über Zeit und Raum gemittelt betrachtet werden.
Die akquirierten Daten setzen fixe Randbedingungen, die durch das bilanzierte Profil erfüllt werden müssen. Dazu gehören neben Karten- und Bohrdaten auch die Lithostratigraphie mit Schichtmächtigkeiten und eventuellen Kompetenzkontrasten.
Weitere Randbedingungen stellen die Pinlines, wie sie Dahlstrom (1969) definiert: «(...) a pair of reference

lines at either end of the section in areas of no interbed slip.» Die beiden Pinlines fixieren das Profil. Sie dürfen keine Scherung erfahren und müssen immer miteinander in Bezug stehen (Abb. 3). Werden sie geschnitten, so muss der Prozess, der zum Versatz führt, alle Bedingungen der Materialbilanz erfüllen.

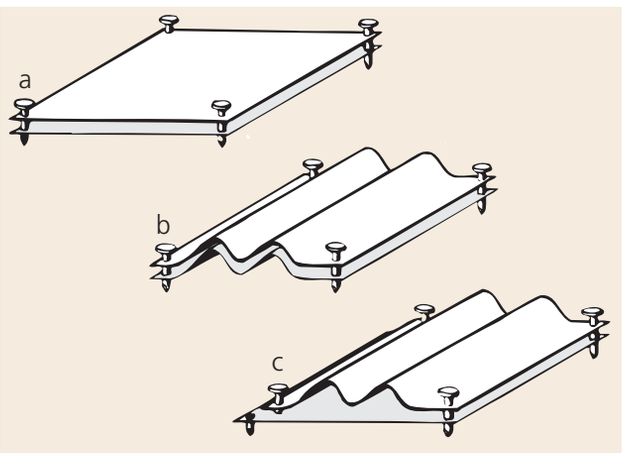

Abb. 3: Die Schichtlängenkonsistenz. Schichtlängen im undeformierten (a) und im deformierten Zustand (b) sind, auf zwei Pinlines bezogen, gleich lang. Tritt ein Bruch oder ein Décollement auf, so dass eine Pinline zerschnitten wird (c), so muss der Versatz quantifizierbar sein, um den Bezug zwischen den Pinlines zu wahren. Verändert aus Dahlstrom (1969).

Fig. 3: Layer-length consistency. The layers, measured along two pin lines, have the same length in the undeformed (a) and the deformed state (b). If a pin line is cut by a fault or a thrust (c), the dislocation must be quantifiable in order to keep track of the relation between the pin lines. Modified after Dahlstrom (1969).

Fig. 3: Cohérence dans la longueur des couches. Mesurées le long de deux «pin lines», les couches ont la même longueur à l'état non déformé (a) et à l'état déformé (b). Si une faille ou un décollement provoque la coupure d'une «pin line» (c), le déplacement doit être quantifiable, afin de conserver la relation entre les «pin lines». Modifié à partir de Dahlstrom (1969).

2.1.2 Plausibilität

Dahlstrom (1969), einer der Väter dieser Methode, prägte den Begriff der Schichtlängenbilanz (Abb. 3). Seine Definition und die von Elliot (1983) eingeführten Begriffe «viable» (realisierbar) und «admissible» (zulässig) werden von Marshak & Mitra (1988) zu einem Vorgehens- und Beurteilungskonzept erweitert (Abb. 4): Ein Profil existiert in einem deformierten und einem rückdeformierten Zustand. Ersteres muss zulässig sein, indem es realistische Falten- und Bruchgeometrien ergibt, es muss aber auch realisierbar sein, indem es in einen undeformierten Zustand überführbar ist. Letzteres muss ebenfalls zulässig sein, indem es plausible Bruchtrajektorien zeigt. Sind diese Voraussetzungen erfüllt, handelt es sich um ein bilanziertes Profil, dessen deformierter Zustand sowohl zulässig als auch realisierbar ist, und somit plausibel. Dieses Profil dient als Modell, da es eine geometrische Annäherung an die Natur darstellt. Es ist möglich, oder sogar wahrscheinlich, dass ein anderer Lösungsansatz ein in einigen Punkten unterschiedliches Profil ergibt, das ebenso plausibel ist. Eine wesentliche, wenn auch subjektive Anfangsbedingung ist die Anfangshypothese, die durch den bearbeitenden Geologen vorerst möglichst einfach gewählt und anschliessend durch die Bilanzierung untermauert oder verworfen werden muss.

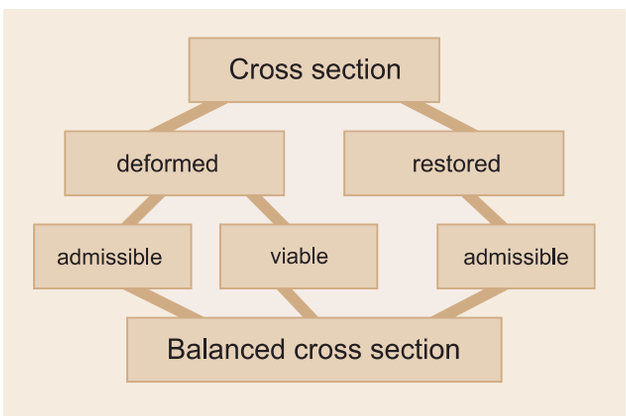

Abb. 4: Das Konzept der Profilbilanzierung nach Elliot (1983) und Marshak & Mitra (1988). Vgl. Kap. 2.1.2.

Fig. 4: The concept of profile balancing after Elliot (1983) and Marshak & Mitra (1988). See chapter 2.1.2.

Fig. 4: Le concept de profil équilibré selon Elliot (1983) et Marshak & Mitra (1988). Cf. chap. 2.1.2.

2.2 Datenmodell und Vorgehen

Die Profilbilanzierung am Computer mit dem Programm Geosec – 20™ geschieht in drei aufeinanderfolgenden Schritten: Datenakquisition, Profilkonstruktion und Modellierung. Diese Schritte sind im Datenmodell in Abb. 5 zusammengestellt.

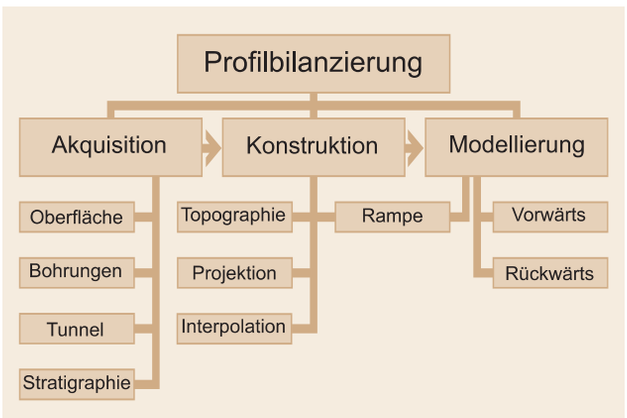

Abb. 5: Das Datenmodell des Prozesses der Profilbilanzierung. Vgl. Kap. 2.2.

Fig. 5: Data model of the profile balancing process. See chapter 2.2.

Fig. 5: Le modèle de données utilisé pour procéder à l'équilibrage des profils. Cf. chap. 2.2.

2.2.1 Akquisition

Zur Akquisition gehört das Beschaffen der Daten (Schichtgrenzen und -fallwinkel aus der Oberflächenkartierung, Schacht- und Tunnelkartierungen und Bohrungen, Schichtmächtigkeiten aus der Stratigraphie, Resultate geophysikalischer Untersuchungen etc.) und die georeferenzierte Eingabe dieser Daten in den Computer. Diese geschieht von Hand über ein Digitalisiertablett. Die Qualität des Modells hängt direkt von der Qualität und der Dichte der Daten ab. Karten- und Bohrdaten werden in Geosec – 20™ dreidimensional erfasst und enthalten Informationen wie die räumliche Lage diskreter Datenpunkte, deren stratigraphische Position, Typ (Bruch, Schichtoberfläche, Marker etc.) und die Fallwinkel. Wenn die Fallrichtung wegen Drehbewegungen des Bohrkerns nicht mehr eruiert werden kann, muss sie im Vergleich mit gesicherten (Oberflächen-)Daten interpoliert werden. Stratigraphische Daten werden in einer Abfolge von Einheiten bearbeitet, denen eine Mächtigkeit, eine seismische Geschwindigkeit und ein Wert für die Festigkeit oder Verdichtbarkeit des Gesteins zugewiesen wird. Letzterer wird für die Dekompaktion von Profilen benötigt (s. u.).

2.2.2 Konstruktion

Die Profilkonstruktion erfolgt am Bildschirm. Es muss eine Profilspur gewählt werden, die die Anfangsbedingung erfüllt, also in Transportrichtung liegt. Wie für ein klassisches geologisches Profil wird die Topografie entlang der Profilspur digitalisiert, die akquirierten Schichtfallwinkel werden projiziert, der Schichtstapel wird mit Hilfe der stratigraphischen Säule nach oben und unten extrapoliert und die Rampengeometrie sowie Brüche und Marker intuitiv festgesetzt, wo sie nicht durch Daten fixiert sind. Dann werden die zwei Pinlines definiert. An der Oberfläche entspricht das resultierende Profil bereits gut den tatsächlichen Verhältnissen, in Abhängigkeit der mit grösserer Tiefe meist abnehmenden Datendichte nimmt die Unsicherheit zu. Bruchgeometrien und Platzprobleme, wie sie etwa durch falsche Rampengeometrien entstehen, können nicht plausibel konstruiert werden. Die Tiefe des Abscherhorizonts hingegen ist oft einigermassen genau bestimmbar: Wenn der darüberliegende Schichtstapel ungestört ist und die Lage des Abscherhorizonts im Schichtstapel bekannt ist, lässt sich dessen Tiefe extrapolieren. Die Abschertiefe steht im bilanzierten Profil im Zusammenhang mit der kurvimetrischen und der volumetrischen Verkürzung (Goguel 1962, Laubscher 1965).

2.2.3 Modellierung

Die Modellierung mit Geosec – 20™ geschieht mit festgelegten Programmmodulen (s. u.) und ist iterativ, interaktiv und intuitiv. Iteration oder «trial and error», also ein schrittweises Herantasten an eine plausible Lösung, schafft erst eine Interaktionsmöglichkeit mit dem Programm. Interaktivität ermöglicht es dem bearbeitenden Geologen, bei jedem Programmschritt seine Intuition, eigene Ideen und Erfahrungen einzubringen. Die Computeranwendung übernimmt nur die Rechen- und Zeichenarbeit und weist auf mathematische Widersprüche hin. Das Programm kann nicht selbständig evaluieren und besitzt natürlich kein geologisches Fingerspitzengefühl. Die an sich sehr einfachen Programmmodule sind kombinierbar, komplizierte Sachverhalte werden aus einzelnen einfachen aufgebaut und bleiben so transparent und nachvollziehbar.
Die Modellierung kann in zwei Richtungen erfolgen. Vorwärtsmodellierung geht vom undeformierten Urzustand aus und versucht durch geeignete Kombination der Programmmodule den vorgegebenen Felddaten zu genügen. Ein solches Modell ist per se bilanziert und kinematisch plausibel. Rückwärtsmodellierung geht vom deformierten Zustand aus und hat eine Massenbilanz und Plausibilität zum Ziel. Die beiden Methoden unterscheiden sich nicht in ihrer Aussagekraft.

Die Falten- und Bruchgeometrien sollten nicht nur realistisch aussehen (vgl. Kap. 2.1.2), sondern auch mathematisch quantifizierbar sein. So kann zum Vornherein ein Katalog zu erwartender Strukturen angelegt werden, die im Einzelnen durch Module der verwendeten Computeranwendung abgedeckt werden. Eine Auswahl, die in der vorliegenden Arbeit zur Anwendung kam, ist hier zusammengestellt (aus McClay 1992 und Ramsay & Huber 1987).

- Vorlandvergente Überschiebungen (thrusts), die gerade und steil, listrisch oder als Rampe («flat – ramp – flat», Suppe 1983) angelegt sind.
- Rücküberschiebungen («backthrusts»), gemeint sind hinterlandvergente Überschiebungen.
- Abschiebungen («normal faults»), steil oder listrisch, die tektonischen Ursprungs sein können oder gravitativ als Sackung entstehen.
- Duplexe (Boyer & Elliot 1982, Mitra 1986) oder Imbrikationsstrukturen.
- Falten über Rampenüberschiebungen («fault-bend folds») nach Suppe (1983, 1985). Sie zeigen evtl. Überkippung im vorderen Schenkel.
- Falten über blinden Überschiebungen («fault propagation folds»), die evtl. Schichtmächtigkeitsveränderung durch nicht-schichtparalleles Gleiten im vorderen Schenkel (Suppe & Medwedeff 1990) und Überkippung zeigen.
- Falten über duktilen Decollements («detachment folds»). Decollements sind schichtparallele, blinde Brüche ohne Rampe nach Jamison (1987).

Analog dazu lassen sich die von Geosec – 20™ angebotenen Programmmodule auflisten (vgl. Abb. 6 a – g). Hier folgt ein Inventar aller Module und eine kurze Erklärung ihrer Funktionen und Freiheitsgrade. Die einzelnen Module können unter Verwendung verschiedener Grundparameter gestartet werden, wie Rampengeometrie, Bruchwinkel oder Versatz. Einige Module lassen auch interaktive Änderung der Parameter zu.

- Das «fault bend fold module» (FBF) dient zur Erstellung von analytischen Lösungen des Modells von Suppe (1983) für Falten über nicht-ebenen Bruchflächen. Es ist ein interaktives Modul, das die Entstehung bruchbedingter Faltengeometrien dynamisch darstellt, wenn das Hangende z. B. über eine Rampe bewegt wird (vgl. Abb. 6a). Es wird keine Deformation im Liegenden vollzogen, die Pinline des Hangenden erfährt normalerweise keine Scherung. Das Modul verwendet schichtparalleles Gleiten und ist für die Schichtlängen und -flächen bilanziert. Verwendet wird es bei extensionalen und kontraktionalen Falten über einfachen oder mehrstufigen Bruchrampen, bei Duplexen und imbrizierten Stapeln sowie bedingt bei Verhältnissen, in denen Scherung der Pinline notwendig ist.
- Die «fault propagation fold modules» (FPF) erlauben das interaktive Erstellen von Faltengeometrien über zwei verschiedenen Klassen von auslaufenden oder blinden Überschiebungen (Suppe & Medwedeff 1990). Angeboten werden:
  - Ein «single step FPF system» (Abb. 6 b), bei dem die «blinde Rampe» aus nur einem Liniensegment besteht.
  - Ein «hybrid FPF system» (Chester & Chester 1990) das die Erstellung von Falten über mehrstufigen blinden Überschiebungen erlaubt (Abb. 6 c).

  Beide Modulklassen verwenden schichtparalleles Gleiten und sind schichtlängen- und flächenbilanziert. Beide bieten Freiheitsgrade im Mächtigkeitsverhältnis der beiden Schenkel im Fall von nichtschichtparallelem Gleiten. Mit dem «single step FPF system» ist auch die Modellierung von «detachment folds» möglich (Abb. 6 d).
- Das «fault slip fold module» (FSF) wird angewendet, um progressive Deformation im Hangenden zu modellieren, wobei dieses interaktiv über einen Bruch bewegt werden kann (Abb. 6 e).
  FSF verwendet nicht schichtparalleles Gleiten, sondern vertikale oder (frei parameterisierbare) schiefe Scherung. Der Scherwinkel bestimmt die Scherrichtung im Hangenden während der Verformung. Schichtflächen bleiben erhalten, Schichtlängen in guter Näherung ebenfalls. Dazu sollte der Versatz erfahrungsgemäss nicht grösser als etwa 10 Prozent des Verkürzungsbetrages und die Bruchfläche nicht zu komplex sein. In erster Linie werden mit diesem Modul Über- und Abschiebungen modelliert.
- Das «transfer – flexural slip module» (TFS) wird verwendet, um eine Komponente durch schichtparalleles Gleiten von einem Verformungszustand in einen andern zu bringen, wobei ihre Fläche und die Länge aller zu einem Referenzhorizont parallelen Schichten erhalten bleibt. Eine Komponente ist rekursiv definiert als Körper, der von einem Mechanismus deformiert wird, der durch das TFS approximiert werden kann. Sie ist z. B. von einer Schichtfläche, einem Bruch und zwei Pinlines begrenzt (Abb. 6 f). Die Scherung kann in der Pinline auf Null fixiert werden. Dieses Modul kommt bei Vorwärts- oder Rückwärtsmodellierung in kompressivem Milieu zur Anwendung.

- Das «transfer – vertical/oblique slip module» (TVOS) entspricht dem TFS, nur dass statt schichtparallelem Gleiten vertikale oder (frei parameterisierbare) schiefe Scherung verwendet wird (Abb. 6 g). TVOS kommt vor allem bei Vorwärts- oder Rückwärtsmodellierung extensionaler Strukturen zur Anwendung.
- Das «project map data module» erlaubt, dreidimensionale Kartendaten entlang eines frei wählbaren Vektors auf die Profilebene zu projizieren.
- Das «project wells module» erlaubt, dreidimensionale Bohrdaten entlang eines frei wählbaren Vektors auf die Profilebene zu projizieren.
- Das «fault prediction module» dient zur Voraussage von Bruchgeometrien in extensionalen Bedingungen (in der vorliegenden Arbeit nicht verwendet).
- Das «compact module» kompaktiert ein deformiertes Profil um den Betrag der vertikalen Kompression durch darüberliegendes Sediment (in der vorliegenden Arbeit nicht verwendet).
- Das «decompact module» dekompaktiert ein rückdeformiertes Profil um den Betrag der vertikalen Expansion nach Entfernung einer Überlast (in der vorliegenden Arbeit nicht verwendet).
- Das «time to depth module» rechnet seismische Daten automatisch von Zeit zu Tiefe um (in der vorliegenden Arbeit nicht verwendet).
- Das «depth to time module» rechnet seismische Daten automatisch von Tiefe zu Zeit um (in der vorliegenden Arbeit nicht verwendet).

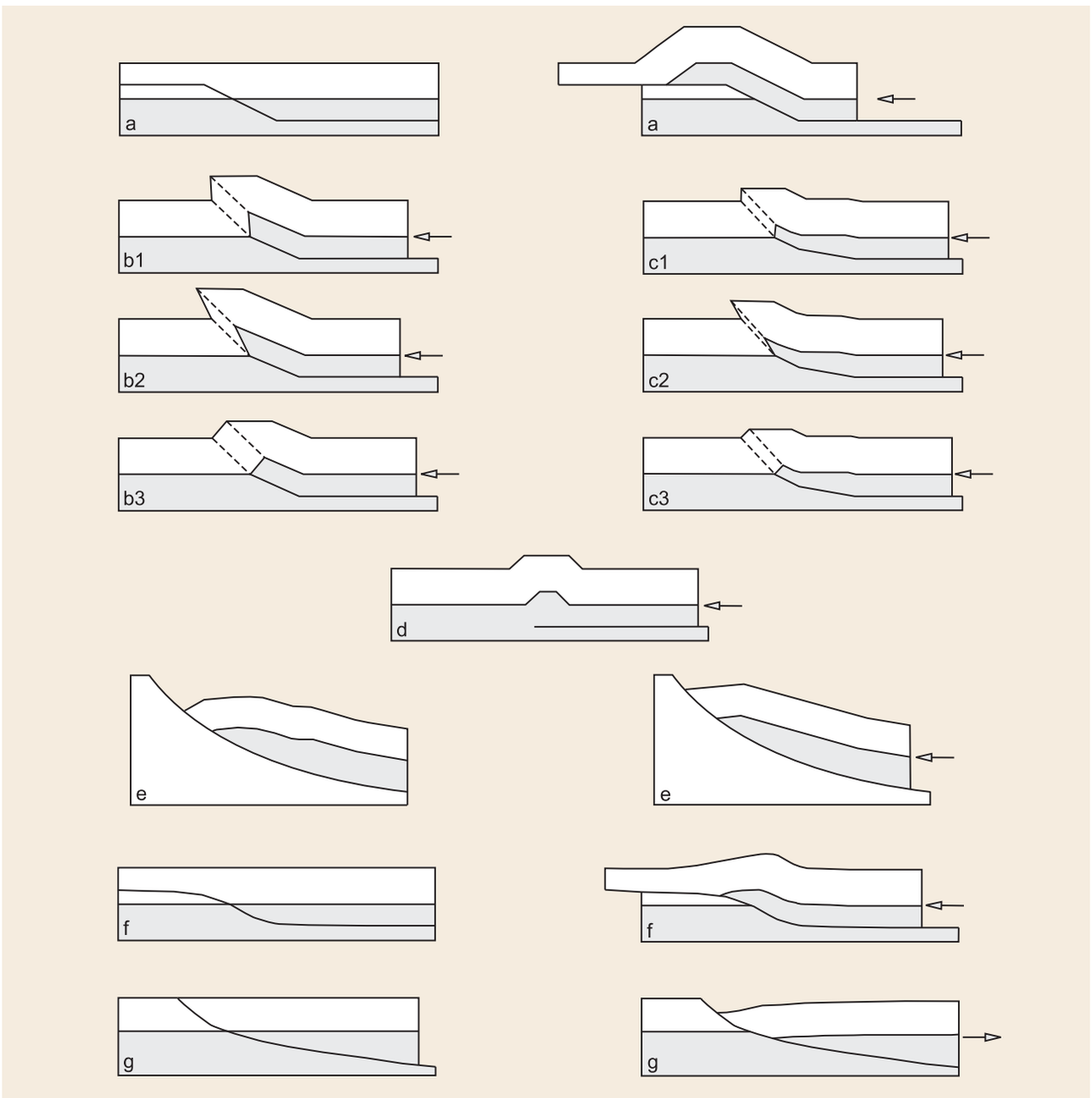

Abb. 6: Die Programmmodule von GEOSEC–20™. a) Fault bend fold module. b1) Fault propagation fold module (FPF) single step. b2) FPF single step mit Ausdünnung im vorderen Schenkel. b3) FPF single step mit Verdickung im vorderen Schenkel. c1) FPF multiple step. c2) FPF multiple step mit Ausdünnung im vorderen Schenkel. c3) FPF multiple step mit Verdickung im vorderen Schenkel. d) FPF als «detachment fold». e) Fault slip fold module mit vertikaler Scherung. f) Transfer – flexural slip module. g) Transfer – vertical/oblique slip module mit vertikaler Scherung. Vgl. Kap. 2.2.3.

Fig. 6: Program modules from GEOSEC–20™. a) Fault bend fold module. b1) Fault propagation fold module (FPF) single step. b2) FPF single step with thinning of the front limb. b3) FPF single step with thickening of the front limb. c1) FPF multiple step. c2) FPF multiple step with thinning of the front limb. c3) FPF multiple step with thickening of the front limb. d) FPF as detachment fold. e) Fault slip fold module with vertical shearing. f) Transfer – flexural slip module. g) Transfer – vertical/oblique slip module with vertical shearing. See chapter 2.2.3.

Fig. 6: Les modules du programme GEOSEC–20™. a) «Fault bend fold module»; b1) «Fault propagation fold module (FPF) single step»; b2) «FPF single step» avec amincissement du flanc antérieur; b3) «FPF single step» avec épaississement du flanc antérieur; c1) «FPF multiple step»; c2) «FPF multiple step» avec amincissement du flanc antérieur; c3) «FPF multiple step» avec épaississement du flanc antérieur; d) FPF comme «detachment fold»; e) «Fault slip fold module» avec cisaillement vertical; f) «Transfer – flexural slip module»; g) «Transfer – vertical/oblique slip module» avec cisaillement vertical. Cf. chap. 2.2.3.

3 Geologie des Gebietes Mont Terri – La Croix, Profilmodellierung

Im Folgenden wird die computergestützte Profilkonstruktion und -bilanzierung auf zwei Profilschnitte angewendet. Der Autobahntunnel Mont Terri der A16 Transjurane und der Eisenbahntunnel La Croix dienen als Profilspuren (vgl. Abb. 7). Die Modellprofile werden kinematischen und dynamischen Plausibilitätskontrollen unterzogen. Weiter werden Schlüsse über die Struktur der darunterliegenden Rampe und die geometrische und mechanische Geschichte der Überschiebung gezogen. Anhand einer Serie von nicht bilanzierten Profilen wird die laterale Entwicklung der Faltenstruktur veranschaulicht (vgl. Kap. 3.4).

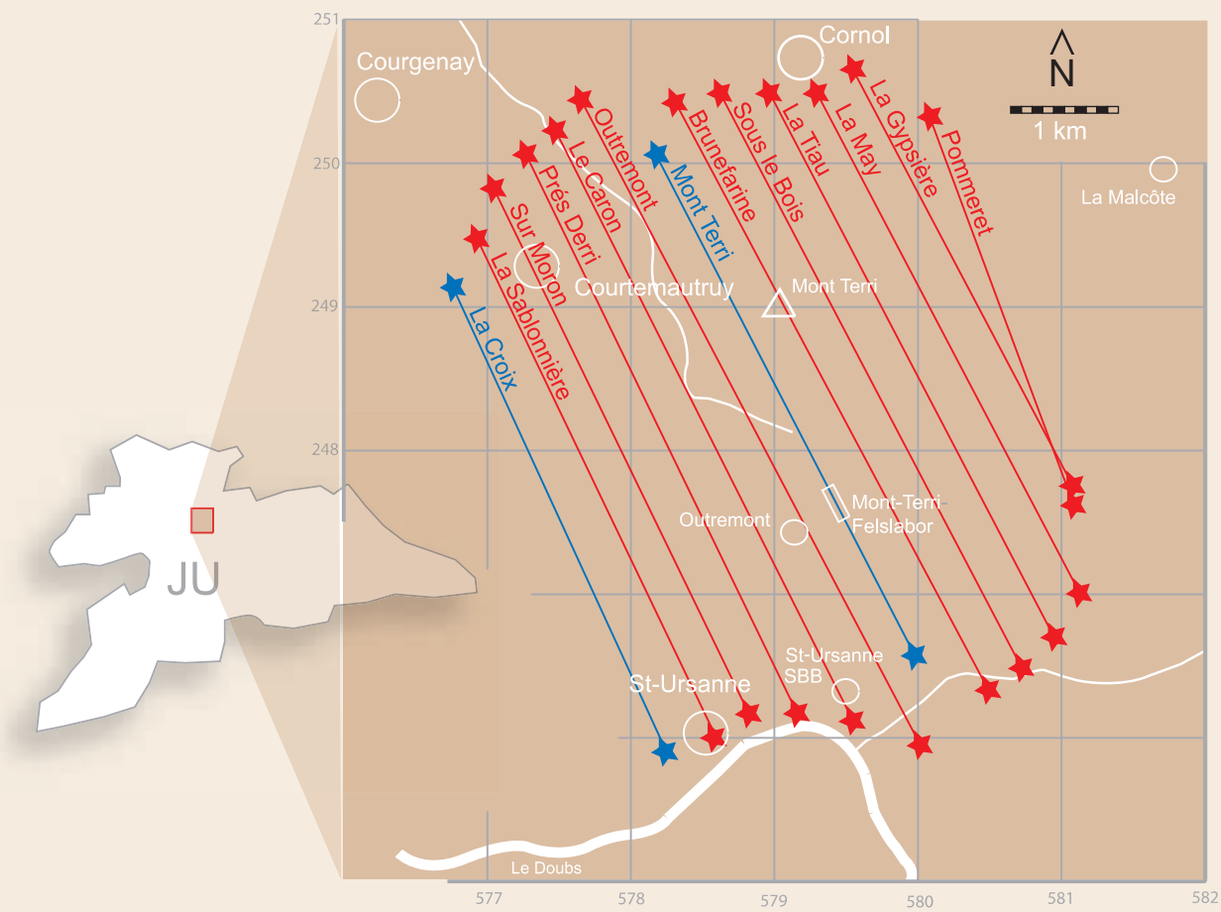

Profil	Koord. nördl. Pinline	Azimut [°]	Länge [m]	Profil	Koord. nördl. Pinline	Azimut [°]	Länge [m]
La Croix	249.135/576.135	335,4	3552	Brunefarine	250.406/578.326	332,2	4590
La Sablonnière	249.469/576.925	334,5	3844	Sous le Bois	250.478/578.624	332,2	4508
Sur Moron	249.799/577.065	334,1	4032	La Tiau	250.478/578.973	332,4	4258
Prés Derri	250.057/577.250	333,8	4330	La May	250.478/579.299	332,3	3916
Le Caron	250.221/577.459	332,9	4602	La Gypsière	250.652/579.546	332,2	3274
Outremont	250.427/577.650	332,1	5055	Pommeret	250.318/580.077	339,6	2873
Mont Terri	250.060/578.190	332,5	3930				

Abb. 7: Die Lage des Arbeitsgebietes. In blau: die Profilspuren der bilanzierten Profile. In rot: die Spuren der nicht bilanzierten Profile (vgl. Kap. 3.4 und Abb. 15). Aus der Tabelle ist die genaue Georeferenzierung der Spuren ersichtlich.

Fig. 7: Location of the study area. Blue: traces of the balanced profiles. Red: traces of the unbalanced profiles (see chapter 3.4. and fig. 15). The exact georeferencing of the traces can be seen in the table.

Fig. 7: Situation de la zone étudiée. En bleu: traces des profils équilibrés. En rouge: traces des profils non équilibrés (cf. chap. 3.4 et fig. 15). Les géoréférences précises des traces figurent dans le tableau.

3.1 Geologische Übersicht

Das bearbeitete Gebiet befindet sich im Kanton Jura zwischen St-Ursanne und Cornol und umfasst eine Fläche von ungefähr 10,5 km^2. Die genaue Lage des Gebiets ist aus Abb. 7 ersichtlich. Abb. 8 zeigt eine tektonische Übersichtsskizze der Region. Als topografische Grundlage aller akquirierten Daten dient Blatt 1085 St-Ursanne, Landeskarte der Schweiz 1 : 25 000. Alle Koordinaten werden im Schweizer Koordinatennetz referenziert.

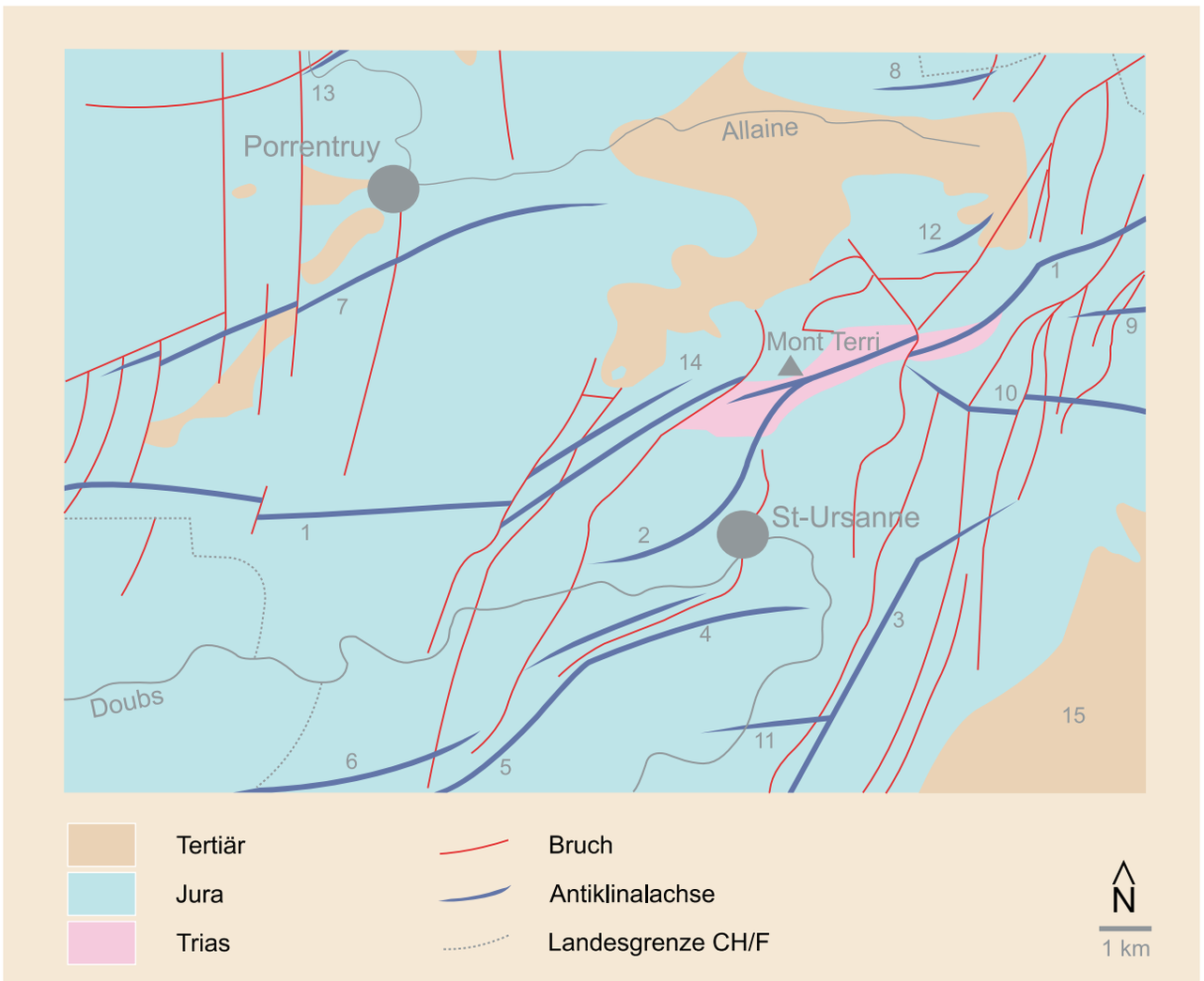

Abb. 8: Tektonische Übersicht der Region St-Ursanne – Porrentruy. 1) Mont-Terri-Antiklinale. 2) Clairmont-Antiklinale. 3) Caquerelle-Antiklinale. 4) Clos-du-Doubs-Antiklinale. 5) Spiegelberg-Antiklinale. 6) Epiquerez-Antiklinale. 7) Banné-Antiklinale. 8) Morimont-Antiklinale. 9) Movelier-Antiklinale. 10) Vorbourg-Antiklinale. 11) Nebenantiklinale von Champ de Souboz. 12) Antiklinalen im Vorland der Mont-Terri-Kette. 13) Pont-d'Able-Antiklinale. 14) Côte-de-Goule-Antiklinale. 15) Becken von Delsberg. Verändert aus Diebold et al. (1963).

Fig. 8: Tectonic overview of the region of St-Ursanne and Porrentruy. 1) Mont Terri anticline. 2) Clairmont anticline. 3) Caquerelle anticline. 4) Clos-du-Doubs anticline. 5) Spiegelberg anticline. 6) Epiquerez anticline. 7) Banné anticline. 8) Morimont anticline. 9) Movelier anticline. 10) Vorbourg anticline. 11) Secondary anticline of Champ de Souboz. 12) Anticlines in the foreland of the Mont Terri chain. 13) Pont-d'Able anticline. 14) Côte-de-Goule anticline. 15) Delsberg basin. Modified after Diebold et al. (1963).

Fig. 8: Aperçu tectonique de la région de St-Ursanne – Porrentruy. 1) Anticlinal du Mont Terri. 2) Anticlinal de Clairmont. 3) Anticlinal de la Caquerelle. 4) Anticlinal du Clos-du-Doubs. 5) Anticlinal du Spiegelberg. 6) Anticlinal d'Epiquerez. 7) Anticlinal du Banné. 8) Anticlinal de Morimont. 9) Anticlinal de Movelier. 10) Anticlinal du Vorbourg. 11) Anticlinal secondaire de Champ de Souboz. 12) Anticlinaux au front de la chaîne du Mont Terri. 13) Anticlinal du Pont-d'Able. 14) Anticlinal de la Côte-de-Goule. 15) Bassin de Delémont. Modifié à partir de Diebold et al. (1963).

Die Mont-Terri-Antiklinale ist – abgesehen von einigen Vorlandfalten in der Ajoie – die regional nördlichste Antiklinale des Faltenjuras. Die Struktur wurde mehr als 1 km über das nördlich anschliessende Tafelland der Ajoie überschoben. Die Randüberschiebung ist im Bach bei Le Caron östlich Derrière M. Terri [248.820/578.270] deutlich als geologisches Fenster aufgeschlossen, wie Kelterborn (1944) erkennt. Unter tektonisch stark beanspruchten und überkippten Gesteinen der Passwang-Alloformation findet sich dort ein flachliegender, spätiger, beiger Kimmeridgien-Kalk. Im Norden überfährt die Antiklinale autochthon auf der Tafel der Ajoie aufliegende stampische Sedimente, die Molasse alsacienne. Der Autobahntunnel Mont Terri verläuft über etwa 850 m in diesen Sedimenten knapp unter der Hauptüberschiebung.
Der Nordschenkel der Rampenantiklinale ist grösstenteils überkippt. Im Arbeitsgebiet sind Formationen von Malm bis Keuper aufgeschlossen. Der steilste Teil des Nordschenkels, durch Callovien bis Kimmeridgien gebildet, ist grossräumig auf mehreren Bruchflächen nach Norden abgeglitten, wobei auch die Definition von Abschiebungen angewandt werden könnte (vgl. Kap. 3.2.3). Der Keuper bildet eine Mulde im Kessel zwischen Les Salins und La Gypsière. Der Keuperkern ist der grösste Ausbiss triassischer Gesteine in weiter Umgebung. Südöstlich des Mont Terri [248.600/579.350] verschmälert sich der Kern auf ca. 180 m, was einerseits mit der Geländemorphologie zusammenhängt, andererseits auf eine Aufwölbung der darunterliegenden Rampe weisen könnte. Kelterborn (1944) postuliert eine ähnliche Aufwölbung unter dem Gebiet um Sur Moron westlich des Mont Terri [248.730/577.700], wobei er sie als präexistente Falte im Liegenden interpretiert, deren Achse parallel zur Achse der Mont-Terri-Antiklinale streicht. In der vorliegenden Arbeit – wie auch bei Tschopp (1960) und Haarpaintner & Schaeren (1997) – liegt das Liegende der Rampenüberschiebung immer flach. Die Verschmälerung des Kerns wird durch zwei Überschiebungen erklärt (vgl. Abb. 15 e – i).
Der Südschenkel der Antiklinale liegt normal. Es sind – abgesehen von der Mächtigkeitszunahme im Opalinus-Ton (Kap. 3.2.3) – keine Verdoppelungen festgestellt worden. Der Hauptrogenstein, der sowohl am Mont Terri als auch am gegenüberliegenden Hügelzug von La Malcôte eindrückliche Fluhen bildet, liegt im Südschenkel ca. 100 m höher als im Norden. Dies weist ebenfalls auf eine dazwischen liegende Überschiebung. Der Südschenkel geht über in die Tafel von St-Ursanne, die gegen Westen durch die Clairmont-Antiklinale von der Tafel von Ocourt getrennt wird. Gegen Osten folgt die Caquerelle-Antiklinale, die unter das Tertiärbecken von Delsberg taucht (vgl. Abb. 8). Die Brüche – es handelt sich grösstenteils um Überschiebungen – entstanden meist synkinematisch. Näheres über präexistente alttertiäre Strukturen sowie jungtertiäre Faltenjuratektonik ist in den Kapiteln über die kinematische Entwicklung der beiden bilanzierten Profile beschrieben (Kap. 3.2.3 und 3.3.3).
Vom Liegenden der Ajoie ist im Arbeitsgebiet, abgesehen vom Malmfenster bei Le Caron, nichts aufgeschlossen. Südöstlich und nordöstlich von Miécourt befinden sich Vorlandfalten, die als alttertiäre Flexuren über Brüchen angelegt sind. Des Weiteren ist die Ajoie durch rheintalische Brüche in Schollen zerlegt, wobei NNE-SSW streichende Brüche dominieren; N-S oder ENE-WSW streichende Brüche treten seltener in Erscheinung. Der Versatz der einzelnen Schollen beträgt kaum je mehr als 100 m. Die rheintalischen Brüche sind in der Randüberschiebung mitverfaltet und teils reaktiviert worden (Buxtorf & Lehner 1920, Schneider 1960).

Das schematische stratigraphische Profil in Abb. 9 unterscheidet sich von demjenigen, das im Kartierbericht von Freivogel (2001) dargestellt wird. Abb. 9 ist nach der neuesten Literatur zusammengestellt, benutzt also die aktuellen Namen der Stufen und der Lithostratigraphie. Die Kartierung hingegen wurde nach einer älterer Einteilung vorgenommen, um sie mit den andern für die Materialbilanzierung verwendeten Daten kompatibel zu machen, die nach dieser älteren Nomenklatur gegliedert wurden. Die Namen der kartierten Formationen sind ebenfalls dem Profil zu entnehmen. In den Tunnelkartierungen (BTN 1993; BTN 1994a; BTN 1994b; Allimann et al. 1998) und den Bohrungen (BGA 1988), die im Laufe des Baus des Autobahntunnels entstanden sind und als Grundlage für die vorliegende Arbeit dienen, wird der Malm unterteilt in die (im Prinzip nomenklatorisch inkorrekten) Einheiten Oxfordien, Rauracien, Séquanien und Kimmeridgien. Der so genannte «untere Dogger» (oberes Aalénien und unteres Bajocien) wird in diesen Dokumenten «Blaukalk» genannt. Dieser Ausdruck wird in der vorliegenden Arbeit durch die Passwang-Alloformation (Burkhalter 1996) ersetzt. Die verschiedenen Referenzen sind im Bildtext zu Abb. 9 zusammengestellt. Alle Mächtigkeiten (nach Laubscher 1963) sind dem stratigraphischen Profil zu entnehmen.

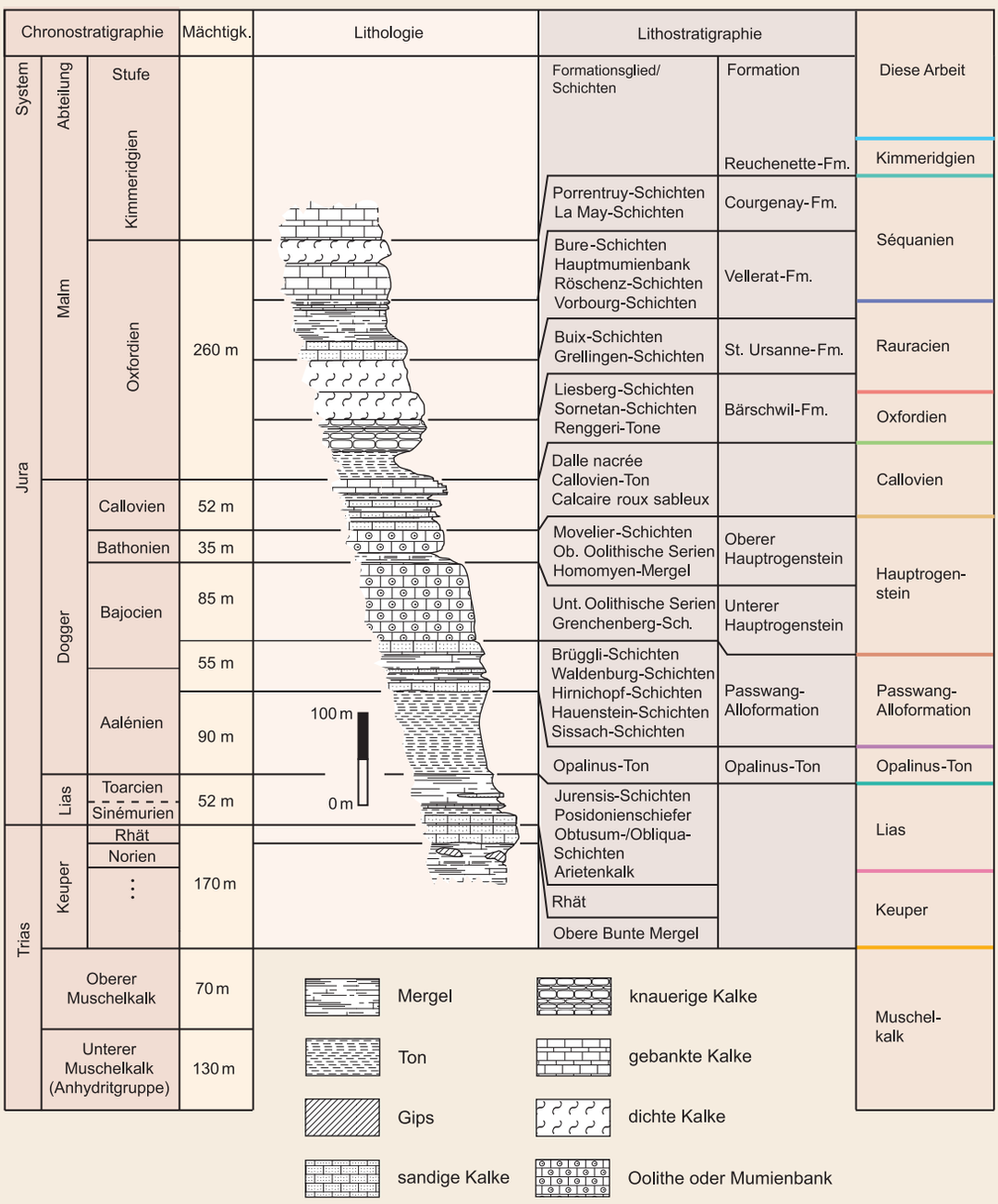

Abb. 9: Stratigraphisches Profil. Zusammengestellt aus BTN (1994a, 1994b), Burkhalter (1996), Gygi (2000) und Laubscher (1963).

Fig. 9: Stratigraphic profile. Compiled from BTN (1994a, 1994b), Burkhalter (1996), Gygi (2000) and Laubscher (1963).

Fig. 9: Profil stratigraphique. Compilation issue de BTN (1994a, 1994b), Burkhalter (1996), Gygi (2000) et Laubscher (1963).

3.2 Autobahntunnel Mont Terri

3.2.1 Akquisition

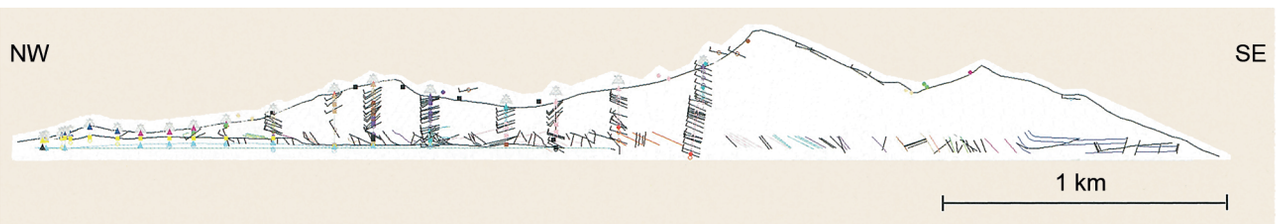

Abb. 10: Zusammenstellung der für die Bilanzierung des Profils Mont Terri verwendeten Daten. Enthalten ist die Kartierung des Tunnels (BTN 1994a) sowie Informationen aus den Bohrungen (BGA 1988) und der Oberflächenkartierung (Kohler 2000), die in die Profilebene projiziert werden. Lithologien sind farbcodiert, die Art der Oberfläche ist formcodiert, das scheinbare Einfallen ist durch Fallzeichen dargestellt. Vgl. Abb. 13.

Fig. 10: Compilation of the data used for balancing the Mont Terri profile. The map of the tunnel (BTN 1994a) is included, as well as information from drill cores (BGA 1988) and the surface mapping (Kohler 2000), which is projected onto the profile plane. Lithologies are colour coded, the surface features are shape coded, and the apparent dip is shown with dip-strike symbols. See fig. 13.

Fig. 10: Compilation des données utilisées pour équilibrer le profil du Mont Terri. Elle englobe les levés du tunnel (BTN 1994a), ainsi que des informations provenant des sondages (BGA 1988) et de la cartographie de surface (Kohler 2000), qui sont projetées dans le plan du profil. La lithologie est déterminée par un code de couleur et le type de surface par un code de forme; le pendage apparent est représenté par un signe de pendage. Cf. fig. 13.

Die Randüberschiebung ist im Profilschnitt Mont Terri dank des Tunnels sehr gut dokumentiert. Zur Verfügung stehen Tunnelkartierungen (BTN 1993; BTN 1994a; Allimann et al. 1998), Bohrungen (BGA 1988) und die geologische Karte des Arbeitsgebietes (Freivogel 2001). Eine Zusammenstellung aller im Profil Mont Terri verwendeten, bereits in die Profilebene projizierten Daten zeigt Abb. 10. Die stratigraphische Information stammt aus verschiedenen Quellen (vgl. Abb. 9). Die Mächtigkeiten der nicht aufgeschlossenen Einheiten wurden im Modellierungsprozess extrapoliert. Die stratigraphische Säule in Geosec – 20™ beinhaltet für die vorliegende Arbeit nur Formationsnamen und Mächtigkeiten (vgl. Abb. 9, rechte Kolonne). Seismische Geschwindigkeiten und Verdichtungsparameter werden nicht verwendet.

3.2.2 Konstruktion

Der erste Schritt bei der Erstellung eines bilanzierten Profils ist das Zeichnen eines klassischen Profils. Dies geschieht am Computer genau so wie es auf dem Papier geschehen würde. Als erstes wird eine Profilspur gewählt. Für die Profile dieser Arbeit sind die Spuren durch die Tunnelanlagen bereits vorgegeben. Die Tunnelführung ist nicht ganz gerade, die Projektionslinie entspricht dem «best fit». Die Tunnel wurden, um sie so kurz wie möglich zu halten, senkrecht zur Bergkette angelegt. Somit liegen sie ziemlich genau normal zur Faltenachse des Mont-Terri-Antiklinoriums. Laubscher (1972) zeigt eine zweidimensionale elastostatische Lösung für das Stressfeld des Juragebirges. Für den Mont Terri lässt sich dort ein idealisiertes Azimut der Hauptspannungsrichtung von ungefähr 338° ablesen. Die Normale auf die lokale Faltenachse hat ein Azimut von ca. 333°. Die Profilspur Mont Terri ihrerseits hat ein Azimut von 332,5°. Es wird in erster Näherung angenommen, dass beide Tunnel – Mont Terri und La Croix – in Schubrichtung der Jurafaltung liegen, die lokal durch einen idealisierten Transportrichtungsvektor festgesetzt ist (vgl. Kap. 2.1.1). Als nächstes wird die Topografie entlang der Profilspur gezeichnet, indem die Schnittpunkte mit den Höhenlinien digitalisiert werden. Dann werden die Felddaten in die Profilebene projiziert. Die Schichtgrenzen, Schichtfallen und Brüche aus den Tunnelkartierungen können für das Profil Mont Terri eins zu eins in die Profilebene digitalisiert werden. Die Oberflächen- und Bohrdaten werden entlang eines Vektors senkrecht auf die Schnittebene projiziert. Auswahlkriterium für die projizierten Daten ist in erster Linie ihre Nähe zur Profilspur. Dazu werden alle Daten aus höchstens ca. 50 m Entfernung beiderseits der Profilspur in die Schnittebene projiziert. Die einzelnen Datenpunkte werden dann subjektiv auf ihre Aussagekraft geprüft. Die verwendete Projektionsart schliesst komplexe räumliche Strukturen aus, deshalb muss für jeden Datenpunkt eine Wertung der Zuverlässigkeit vorgenommen werden. Diese beinhaltet einerseits eine Abschätzung der Datenhärte. Strukturen, die im Feld direkt beobachtet werden können, kommt somit eine grössere Signifikanz zu als interpolierten Daten. Andererseits muss auch die geologische Struktur, die den Datenpunkt umgibt, im Auge behalten werden. Ein Fallzeichen, dessen scheinbarer Fallwinkel stark vom wahren Fallwinkel abweicht, führt z. B. schon bei gerin-

ger Entfernung von der Profilspur zu Fehlern in der Projektion. Der nächste Schritt beinhaltet die Interpolation zwischen den Daten. Hier können nicht einfach Punkte miteinander verbunden werden, sondern es müssen bereits geometrische Randbedingungen eingehalten werden. Das resultierende Profil, das die Basis der Modellierung darstellt, soll im Rahmen der aufgestellten Hypothese (vgl. Kap. 2.1.2) schon möglichst plausibel sein. Dazu müssen weiterhin subjektive Wertungen und Entscheide bezüglich der Bedeutung von Strukturen getroffen werden. Dies ist vor allem bei Bruchstrukturen wichtig, da in den Bohrungen und (in geringerem Ausmass) in den Tunnelkartierungen nicht sofort ersichtlich ist, wie weitreichend oder «bedeutend» die einzelnen Strukturen sind. Abschnitte mit vielen Brüchen müssen zwangsläufig zu Bruchzonen zusammengefasst, einzelne kleinere Brüche vernachlässigt werden. Dies ist vor allem im Bereich des nördlichen Schenkels der Antiklinale der Fall, wo die Daten auf eine komplizierte Verschuppung der Gesteine hindeuten. Alle gewählten Vereinfachungen müssen im Modellierungsprozess dokumentiert bleiben, so dass sie jederzeit rückgängig gemacht werden können, falls der die geologischen Verhältnisse falsch eingeschätzt wurden.
Die Wahl der Pinlines stellt unter den örtlichen Bedingungen kein Problem dar. Im Norden ist das Profil in den undeformierten Schichten der Ajoie fixiert, bei 250.060/578.190. Im Süden steht die Pinline in der Synklinaltafel von St-Ursanne, bei 246.320/580.130.

3.2.3 Modellierung

Als Anfangshypothese des Bilanzierungsvorgangs wird eine einfache Überschiebungsrampe ohne Deformation des Liegenden angenommen. Zudem gibt es Evidenz für eine Duplexstruktur im Hangenden, da zwei Bohrungen in der Nähe des angenommenen oberen Knickpunkts der Rampe unter den triassischen Sedimenten eine Überschiebungsfläche durchfahren und darunter auf die Passwang-Alloformation stossen (BGA 1988). Die Antiklinalfalte über der Rampe zeigt, nach Extrapolation der erodierten Schichten und Rückdeformation der unten besprochenen abgeglittenen Gesteinspakete im Norden, in ihrer generellen Orientierung symmetrische Nord- und Südschenkel. Der Scheitel ist gewölbt und geht ohne Knicke in die Schenkel über. Der Nordschenkel ist durch nordvergente Brüche zerlegt und zeigt Überkippung im Kontakt mit der Überschiebungsfläche. Zwischen den nordvergenten Überschiebungen befindet sich eine rücklandvergente Abschiebungsfläche. Die Anfangshypothese sieht sie als Resultat einer Auspressung des darunterliegenden keilförmigen Gesteinspaketes, verursacht durch die Überlast, oder als durch eine späte Änderung des lokalen Spannungsfeldes reaktivierte Bruchfläche. Im Südschenkel fällt eine Verdickung im Opalinus-Ton auf, die sich genau im Bereich des Felslabors befindet. Mehrere Erklärungen können zu dieser Verdickung herangezogen werden.
Erstens könnte es sich um eine sedimentäre Mächtigkeitsschwankung handeln. Allia (1996) schliesst aus Geohistory-Analysen für die Zeit des frühen Aalénien auf eine erhöhte tektonische Subsidenz des Untergrunds, was lokale Verdickungen erklären könnte. Zweitens ist eine Deformation des Opalinus-Tons durch interne Verfaltung dieser inkompetenten Formation möglich, was zu einer Verkürzung der Schichtlänge bei gleichbleibender Schichtfläche führen würde. Drittens ist eine Überschiebung, die eine Verdoppelung der Schicht bewirkt, in Betracht zu ziehen. Diese Annahme stützt sich auf eine auf der Höhe des Labors kartierte Bruchzone.

Die Deformation soll in ihrer zeitlichen Abfolge, vom undeformierten Urzustand ausgehend, Schritt für Schritt dargestellt werden. Die einzelnen Phasen sind in Abb. 12 a – e illustriert. Die in der jeweiligen Phase noch nicht aktiven Brüche sind als vorgezeichnete Trajektorien in dunkelgrau gehalten. Zum Vergleich ist das gleiche Profil in erodiertem Zustand in Abb. 15 g enthalten. Auf die einzelnen Iterationsschritte der Modellierung soll nur eingegangen werden, wo das Ergebnis die Anfangshypothese nicht erfüllt hat.
Nach Ablagerung bleibt der Schichtstapel lange Zeit nahezu ungestört (Abb. 12 a). Erst im Alttertiär wird das Gebiet – wegen seiner Nähe zur diffusen Transferzone zwischen dem Rhein- und dem Bressegraben – in ein Bruchschollenfeld zerlegt (vgl. Kap. 3.1). Die erste Deformationsphase des Modells wird mit diesem Event erklärt. Die Rückdeformation der südvergenten Abschiebung im Nordschenkel der Antiklinale (vgl. Abb. 12 d und 12 e) nach den Kriterien der oben erwähnten Anfangshypothese ergibt Platzprobleme im abgewickelten Profil, die schwierig lösbar sind. Nach dem «error»-Prozess wird die Anfangshypothese verändert («trial»). Die erste Phase wird nun als steiler rheintalischer Bruch betrachtet, der den südlichen Teil des Profils gegenüber dem nördlichen nach unten versetzt (Abb. 12 b). Da der Bruch auch das Grundgebirge erfasst, wird auch Gestein mitbewegt, das in den nächsten Phasen zum Liegenden der Rampenüberschiebung wird, wodurch sich die Platzprobleme aufheben.
Die zweite Phase, bereits zur Jurafaltung im Miozän gehörig, erklärt die Mächtigkeitszunahme im Opalinus-Ton. Diese Verdickung schlägt stratigraphisch in die jüngsten Schichten durch. Deshalb wird die Hypothese der sedimentären Mächtigkeitsschwankung fallen gelassen. Es gibt im Südschenkel tatsächlich Evidenz für eine Aufwölbung über dem Opalinus-Ton, die in späteren Phasen passiv mitverfaltet wurde.

Die Hypothese des internen «flexural flow», bedingt durch die Inkompetenz des Opalinus-Tons, wird mit der Hypothese des Überschiebungsbruches kombiniert. Da an der Oberfläche keine Verdickung im Opalinus-Ton kartiert wurde, wird eine blinde Überschiebung angenommen, die im Opalinus-Ton endet. Es wird ein «fault propagation fold» gebildet, dessen Bruch in den Opalinus-Ton durchschlägt und das Tongestein intern verformt, d. h. verdickt (vgl. Abb. 12 c).
Im folgenden Schritt (Abb. 12 d) erfolgt die Rampenüberschiebung zusammen mit der Abscherung zweier Duplexe. Dieser Schritt ist in der Abbildung nicht bilanziert, er dient als Veranschaulichung eines Zwischenschrittes von Phase c und e.
Die Rampe ist mit ca. 22° Neigung relativ steil, dazu wird sie noch versteilt durch die Duplexe. Diese sind nötig, um das Platzproblem im Faltenkern zu lösen und den Keuper in seine heutige hohe Lage zu bringen. Die Duplexe sind nicht klassisch imbriziert, sondern als «out of sequence»-Strukturen dünn abgeschert. Im Hinterland der Antiklinale entstehen drei «out of sequence»-Brüche mit nur wenig Versatz. Die steile Bruchzone, die am Ablösepunkt der blinden Überschiebung nukleiert, enthält eine tektonische Brekzie. Ob in diesem Bereich Material quer zur Profilebene transportiert worden ist, kann nicht gesagt werden, da der entsprechende Bruch im Kartenbild aufgrund quartärer Bedeckung nicht erkennbar ist.
Die nächste Phase (Abb. 12 e) ist wiederum bilanziert. Sie zeigt die nordvergenten Überschiebungen, die den Nordschenkel zerlegen. Diese Brüche zeigen alle relativ wenig Versatz, die drei nördlichsten sogar nur so wenig, dass er aus dem Profil nicht ersichtlich wird. Auch hier findet man tektonische Brekzien, die die Vermutung nahe legen, dass möglicherweise Materialtransport durch die Profilebene hatte stattfinden können. Die im Kartenbild verifizierbaren Brüche schneiden die Profilspur nicht senkrecht, was dem Idealfall entsprechen würde, sondern in Winkeln von bis zu 30°. Angesichts der kleinen Versätze wird dieser verzerrende Faktor in der Bilanziering allerdings vernachlässigt. Die teils überkippten Schichten des Nordschenkels können mit der Programmmodulen in GEOSEC – 20™ nicht modelliert werden. Diese Schichtsequenz muss «von Hand» unter Erhaltung von Schichtflächen und -längen konstruiert werden (siehe Abb. 12, Seite 30-31).
In einer abschliessenden Phase gleiten die Gesteinsmassen des Nordschenkels gegen Norden ab. Da der grösste Teil des Nordschenkels bereits erodiert ist, ist die Datengrundlage hier sehr gering, und es gibt nur bedingt Möglichkeiten, geologische Randbedingungen zu setzen. Abb. 11 a – c zeigt eine Abfolge dieser letzten Deformationsphase, die mit den vorhandenen Daten vereinbar ist. Abb. 11 a zeigt die Detailansicht des Nordschenkels, Abb. 11 b die auf drei Flächen nach Norden abgerutschten Gesteinspakete und Abb. 11 c den heutigen, erodierten Zustand. Diese letzte Phase ist nicht bilanziert.
Der Verkürzungsbetrag im Profil Mont Terri beträgt 2140 m. Die Fläche (als «A» bezeichnet) der durch die Deformation über die ursprüngliche Lage des Referenzhorizontes gebrachten Schichten beträgt 2,46 km^2 (Referenzhorizont = Oberfläche des Kimmeridgien). Vergleiche im deformierten und undeformierten Zustand des Profils ergeben folgendes Bild: die Fläche A, die der im Hinterland «weggeschobenen» Fläche entsprechen sollte, ist um 4,5 % verkleinert. Die Längenänderung der einzelnen Schichten vom undeformierten zum deformierten Profil betragen –0,24 % (Muschelkalk), 0 % (Opalinus-Ton) und 0,75 % (Kimmeridgien). Das Profil kann angesichts der kleinen Fehler als schichtlängen- und flächenbilanziert bezeichnet werden.

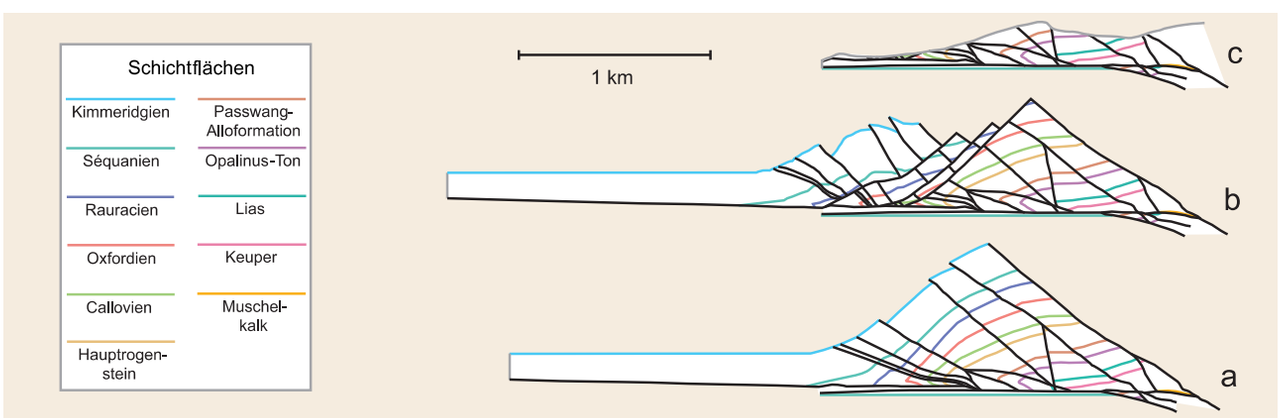

Abb. 11: Bilanzierte Detailansicht des Nordschenkels im Profil Mont Terri. Vgl. Kap. 3.2.3.

Fig. 11: Balanced detail of the northern limb in the Mont Terri profile. See chapter 3.2.3.

Fig. 11: Représentation équilibrée de détail, flanc nord du profil du Mont Terri. Cf. chap. 3.2.3.

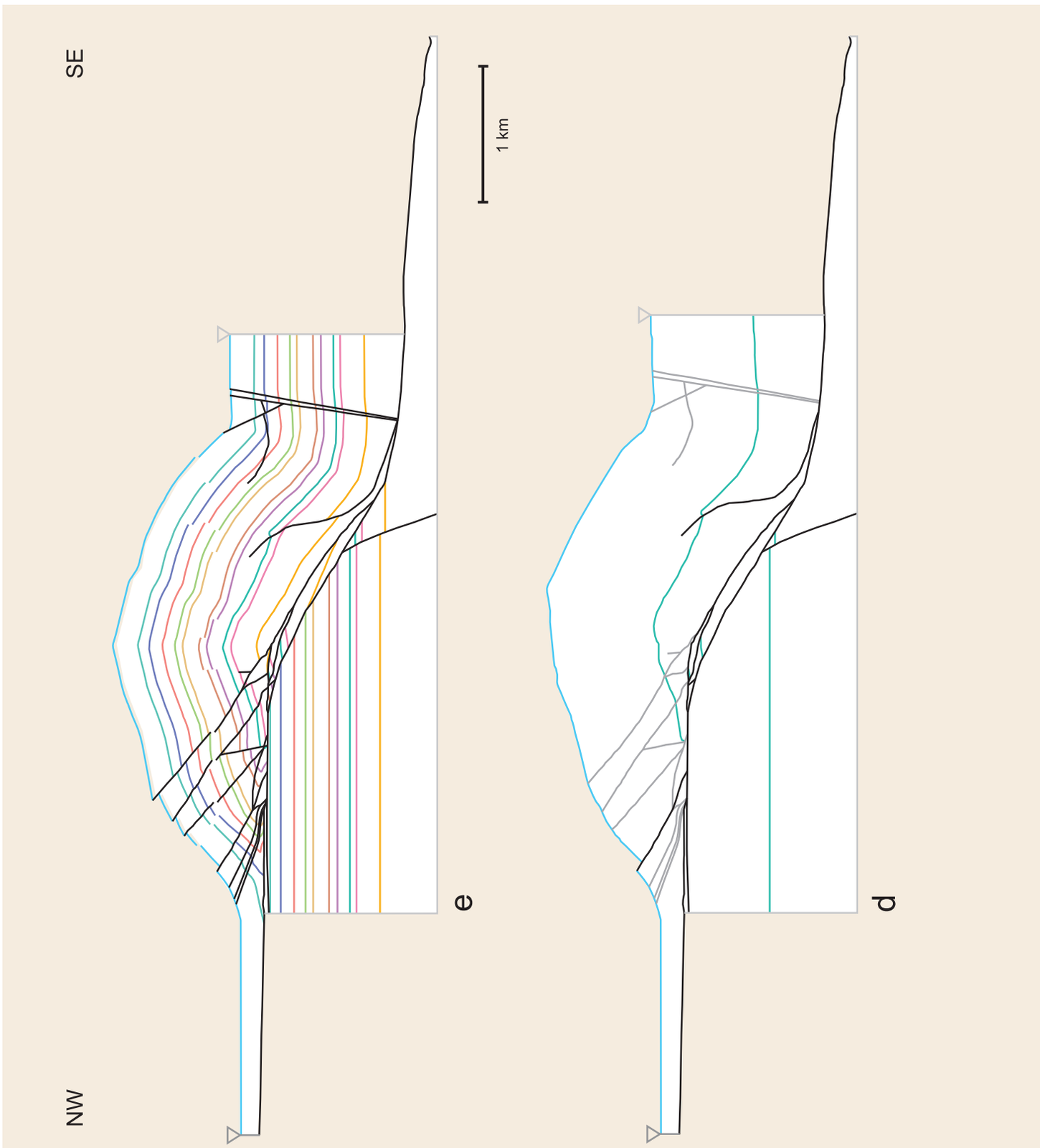

Abb. 12: Bilanzierte Abfolge des Profils Mont Terri. Vgl. Kap. 3.2.3. In Schwarz: Brüche. In Dunkelgrau: vorgezeichnete Bruchtrajektorien. In Hellgrau: Pinlines und basale Grenze des Profils.

Fig. 12: Balanced sequence in the Mont Terri profile. See chapter 3.2.3. Black: faults. Dark grey: fault trajectories. Light grey: pin lines and the basal margin of the profile.

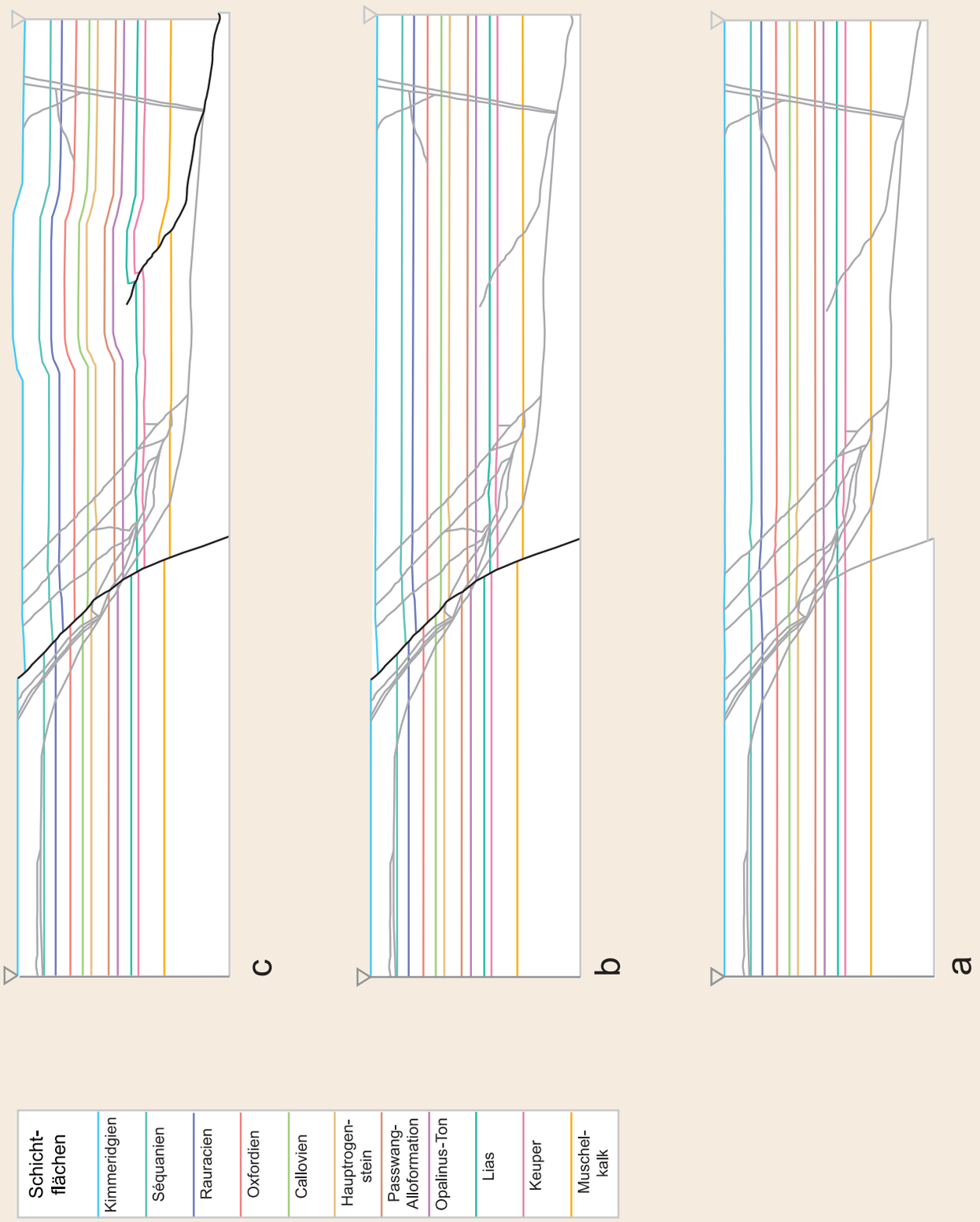

Fig. 12: Séquence équilibrée du profil du Mont Terri. Cf. chap. 3.2.3. En noir: failles. En gris foncé: tracés des failles. En gris clair: «pin lines» et limite inférieure du profil.

3.3 Eisenbahntunnel La Croix

3.3.1 Akquisition

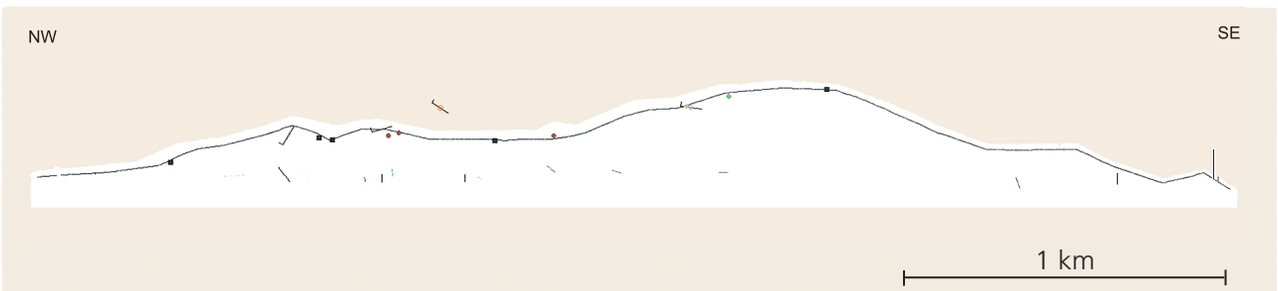

Abb. 13: Zusammenstellung der für die Bilanzierung des Profils La Croix verwendeten Daten. Enthalten ist die Tunnelkartierung (Mathey 1883) sowie Informationen aus der Oberflächenkartierung (Kohler 2000), die in die Profilebene projiziert werden. Vgl. Abb. 10.

Fig. 13: Compilation of the data used for balancing the La Croix profile. The map of the tunnel (Mathey 1883) is included, as well as information from the surface mapping (Kohler 2000), which is projected onto the profile plane. Compare to fig. 10.

Fig. 13: Compilation des données utilisées pour équilibrer le profil de La Croix. Elle englobe les levés du tunnel (Mathey 1883), ainsi que des informations provenant de la cartographie de surface (Kohler 2000), qui sont projetées dans le plan du profil. Cf. fig. 10.

Für die Modellierung des Profils entlang des Eisenbahntunnels La Croix stehen bedeutend weniger Daten als beim Autobahntunnel Mont Terri zur Verfügung. Die Datengrundlage beschränkt sich auf die geologische Kartierung von Kohler (2000) und die Tunnelkartierung von Mathey (1883), auf die das Profil a in Abb. 1 stützt. Abb. 13 zeigt die Profilebene mit dem verwendeten, bereits projizierten Datengerüst. Die stratigraphische Säule entspricht derjenigen des Profils Mont Terri.

3.3.2 Konstruktion

Auch im Fall von La Croix wird in erster Näherung angenommen, dass die Profilspur in der Richtung des Materialtransports liegt (vgl. Kap. 2.1.1 und 3.2.2). Das Azimut des Profils ist 335,4°.
Als erstes wird wiederum die Topografie erstellt, dann werden die akquirierten Daten in die Bildebene des Profils digitalisiert bzw. projiziert. Dies geschieht analog zum Ablauf der in Kapitel 3.2.2 bereits beschriebenen Konstruktion.
Die Interpolation zwischen den einzelnen Datenpunkten ist nicht unproblematisch. Aufgrund der kleinen Datenmenge ergeben sich Schwierigkeiten, die denen der Konstruktion des Profils Mont Terri entgegengesetzt sind. Es müssen nicht Strukturen zusammengefasst oder vernachlässigt werden, sondern es müssen beispielsweise Brüche festgelegt werden, die für die Konstruktion notwendig sind, die jedoch an keiner Stelle durch Daten belegt sind. Die Tunnelkartierung zeigt keinen einzigen Bruch, abgesehen von der Hauptüberschiebung, die als Brekzienzone kartiert ist (vgl. Kap. 1.2).

Die Abschiebung im Südschenkel, wie sie von Haarpaintner & Schaeren (1997) postuliert wird, konnte in der Kartierung von Kohler (2000) nicht bestätigt werden. Auch für das Profil La Croix ist die Wahl der Pinlines unkompliziert. Die nördliche steht im Tafelland der Ajoie bei 249.135/576.135, die südliche in der Tafel von St-Ursanne bei 245.900/578.240.

3.3.3 Modellierung

Die Anfangshypothese für das Profil La Croix ist die selbe wie für das Profil Mont Terri: eine Rampenüberschiebung, die aus einem Abscherhorizont im Muschelkalk nukleiert und durch Duplexe versteilt wird. Weitere belegbare Annahmen können wegen der geringen Datendichte nicht gemacht werden. Da jedoch zur Konstruktion des Profils entsprechend dem Profil Mont Terri eine rückwärtige Abschiebung im Nordschenkel benötigt wird, wird als weitere Hypothese eine rheintalische Störung angenommen, die passiv mitverfaltet wird (vgl. Kap. 3.2.3).

Das bilanzierte Profil La Croix ist in Abb. 14a–e in seinen fünf Phasen dargestellt. Analog zu Kap. 3.2.3 wird die Abfolge vom undeformierten Urzustand ausgehend erklärt.
Die ursprünglich flach liegenden Schichten (Abb. 14a) erfahren im Alttertiär eine Störung in Form eines rheintalischen Bruchs, der den Südteil des Profils gegen den Nordteil nach unten versetzt. Der Bruch zeigt einen ähnlichen scheinbaren Fallwinkel wie jener im Profil Mont Terri, der Versatz ist hier mit 120 m aber grösser. Eine nächste Phase, die analog zum Mont Terri eine

Aufwölbung durch «fault propagation folding» entstehen lässt, ist in der ursprünglichen Grundhypothese nicht enthalten, sondern hat sich im Verlauf der Bilanzierung aufgedrängt. Der «trial»-Prozess einer Rampenüberschiebung, ohne diese passiv mitüberschobene Aufwölbung, ergibt einen zu flachen Südschenkel, der sich nicht in die vorhandenen Daten einpassen lässt («error»). Eine Zwischenphase, wie sie in Abb. 14c dargestellt ist, löst dieses Problem und ergibt darüberhinaus weitere laterale Konsistenz mit dem Profil Mont Terri. Anstelle einer blinden Überschiebung muss hier ein Décollement in den Schichten des Muschelkalks angenommen werden. Dieses ergibt eine relativ enge, hohe, symmetrische Falte.
Der folgende Schritt (Abb. 14d) stellt wiederum die nicht bilanzierte Phase der Entstehung der Rampenüberschiebung und der Duplexe dar. Die im Vergleich zum Mont Terri voluminöseren Duplexe sind «out of sequence» über die Rampe geschert, versteilen diese und versetzen sie um über 500 m nach Süden.
Die Phase in Abb. 14e ist wieder bilanziert, hier werden drei steile nordvergente Überschiebungen angelegt, von denen die mittlere einen beträchtlichen Versatz von ca. 300 m aufweist. Ein so grosser Versatz in der letzten Phase wird im Profil Mont Terri nicht beobachtet, der betreffende Bruch schneidet allerdings jenes Profil nicht. Evidenz für eine letzte Phase nordvergenter Sackungen im vorderen Schenkel gibt es nicht, weder in der Tunnel- noch in der Oberflächenkartierung.
Der Nordschenkel ist teils überkippt, was abermals eine Bilanzierung «von Hand» nötig macht. Die Schichtlängen und -flächen bleiben dabei erhalten. Der Verkürzungsbetrag im Profil La Croix beträgt 1915 m, also 225 m oder 10,5% weniger als am Mont Terri.
Das lässt sich durch Entkoppelung der Profile durch Brüche erklären, die nur jeweils eines der Profile schneiden und andere Versätze zeigen. Die Fläche A, analog Kap. 3.2.3 (S. 29), beträgt 2,48 km^2, gleich viel wie am Mont Terri. Diese Tatsache hat allerdings, angesichts des Unterschiedes der Verkürzungsbeträge und der Entkoppelung der Profile, keine geologische Signifikanz.
Hingegen lässt sich eine kinematische Folgerung ziehen: zwei gleich grosse Gesteinsmassen, die über einen Referenzhorizont gehoben werden, beinhalten die gleiche potentielle Energie. Die kinetische Energie des Schubes, der zur Bildung der Antiklinale geführt hat, war also lateral über die knapp 2 km zwischen den Profilen konstant.
Die Fläche A ist im Profil La Croix nur 1,1% grösser als die im Hinterland «weggeschobene» Fläche. Die Längenänderungen einzelner Schichten betragen –3,2% (Muschelkalk), 1,7% (Opalinus-Ton) und 2,2% (Kimmeridgien). Dass der Fehler der Schichtlängen in diesem Profil etwas grösser ist als im Profil Mont Terri, erklärt sich mit der Verwendung des FSF-Moduls (vgl. Kap. 2.2.3) für die Modellierung der Überschiebungen in Abb. 14e. Da deren Gesamtversatz relativ gross ist (gegen 300 m) macht sich ein Fehler in den Schichtlängen bei Erhaltung der Schichtflächen bemerkbar.
Das Profil kann aufgrund der dennoch kleinen Fehler als schichtlängen- und flächenbilanziert betrachtet werden.

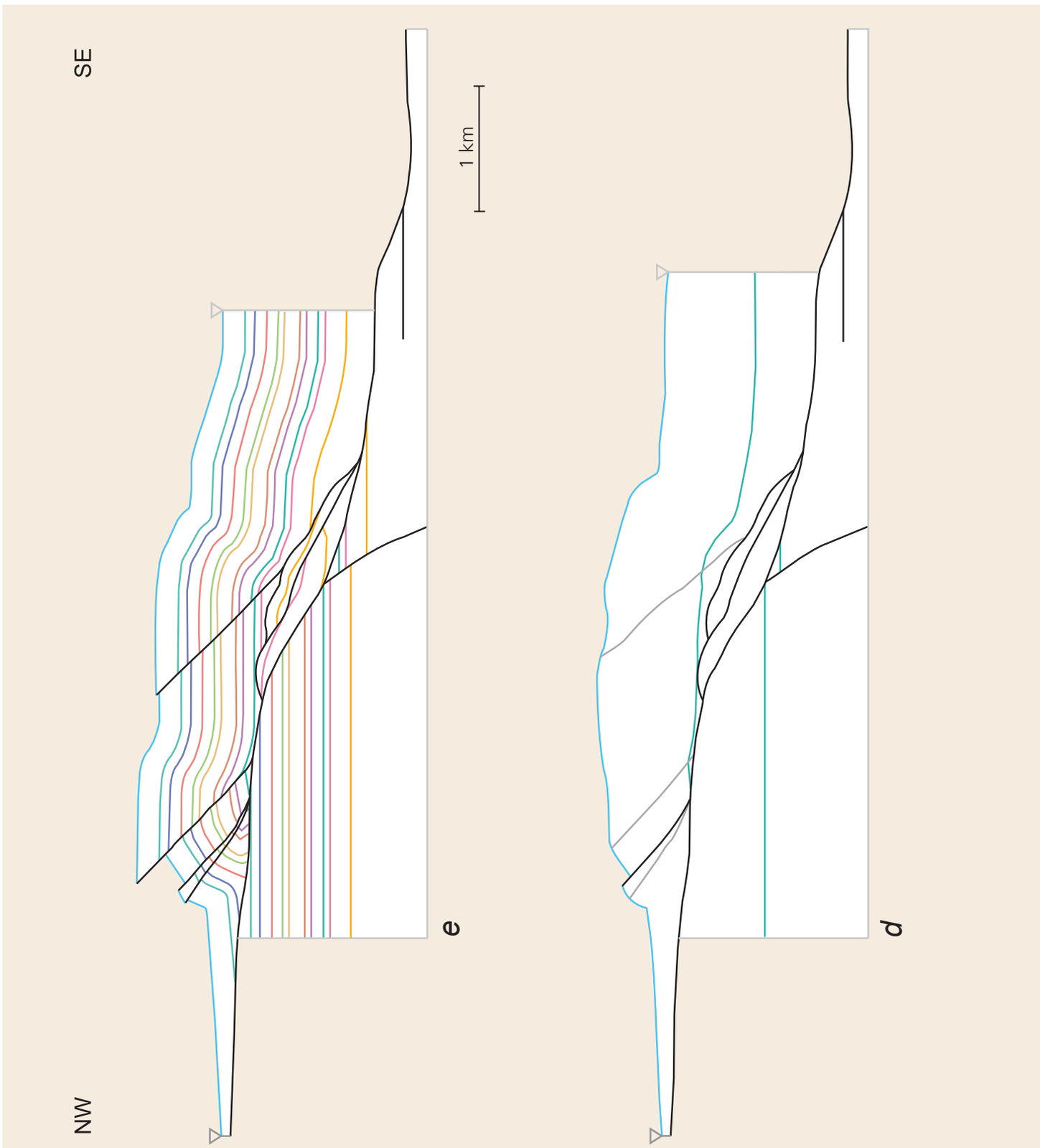

Abb. 14: Bilanzierte Abfolge des Profils La Croix. Vgl. Kap. 3.3.3. In Schwarz: Brüche. In Dunkelgrau: vorgezeichnete Bruchtrajektorien. In Hellgrau: Pinlines und basale Grenze des Profils.

Fig. 14: Balanced sequence of the La Croix profile. See chapter 3.3.3. Black: faults. Dark grey: fault trajectories. Light grey: pin lines and the basal margin of the profile.

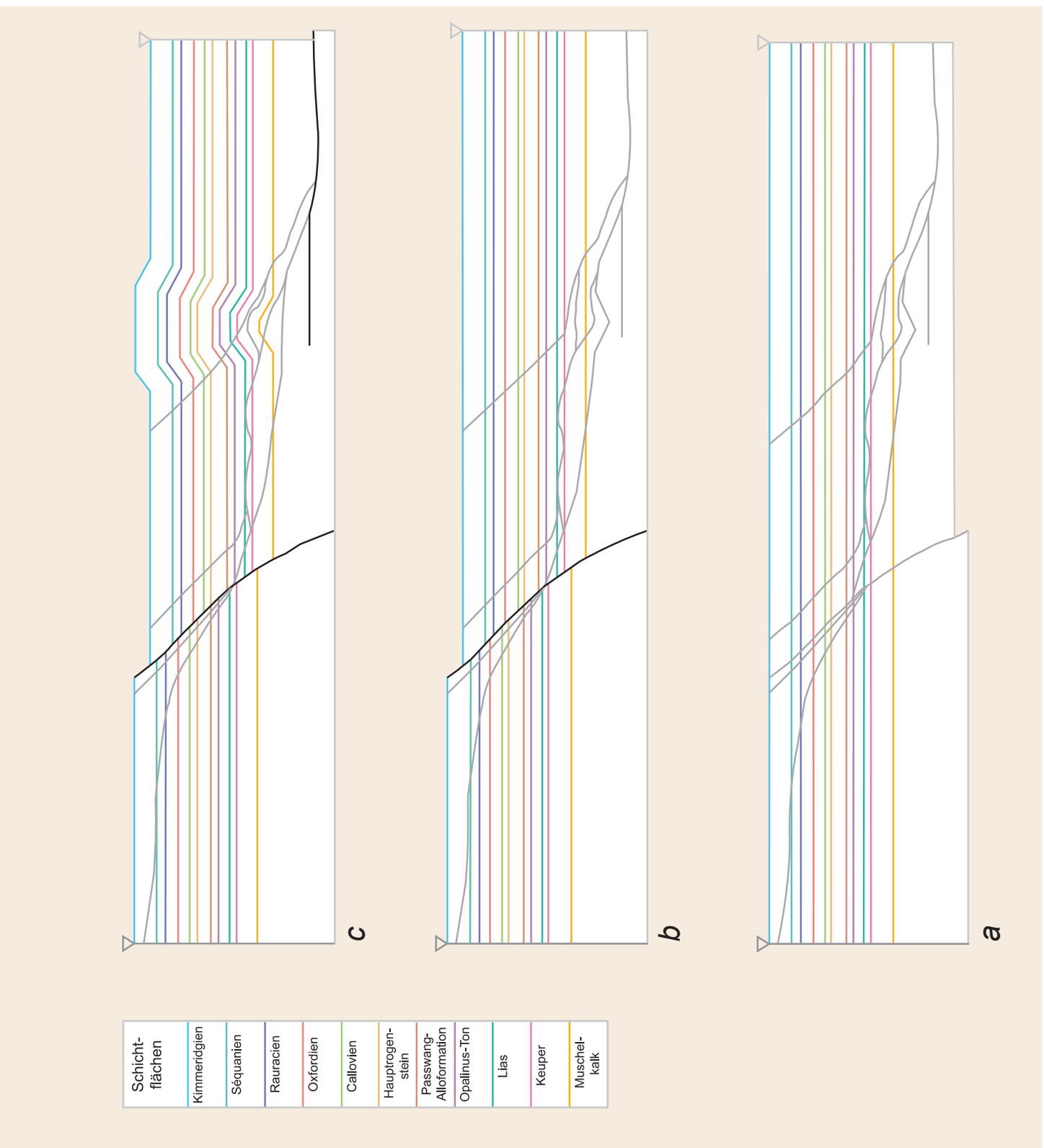

Fig. 14: Séquence équilibrée du profil de La Croix. Cf. chap. 3.3.3. En noir: failles. En gris foncé: tracé des failles. En gris clair: «pin lines» et limite inférieure du profil.

3.4 Profilserie

Zur Veranschaulichung der regionalen Geologie zeigt Abb. 15 a – m eine Serie von 13 Profilen, die im Abstand von meist 300 m durch das Arbeitsgebiet gelegt wurden. Die genaue Lage der Profilspuren geht aus Abb. 7 und der dazugehörigen Tabelle hervor.
Die Profile sind mit Ausnahme der bereits behandelten nicht bilanziert, sondern klassisch konstruiert aus dem Kartenbild (Kohler 2000, Freivogel 2001).
Aus dieser Profilserie Schlüsse über die dreidimensionale Kinematik zu ziehen, ist nur mit Vorbehalt möglich. Eine Serie von bilanzierten Profilen in nahen Abständen, zu deren Randbedingungen sich die Daten der jeweils benachbarten Profile gesellen würden, wäre zu einem brauchbaren Blockmodell umwandelbar und würden die Aussagekraft der Bilanzierung in die dritte Dimension erweitern (Bitterli 1992, Woodward et al. 1989). Sinnvoll wäre auch eine Erweiterung der Profilspuren in südliche Richtung, um die Bilanzierung über weitere Antiklinalen auszudehnen. Hier sollen trotzdem neben den rein geometrische Beobachtungen einige kinematische Konsequenzen diskutiert werden.
In den westlichen sieben Profilen fällt zunächst eine tendenzielle Verengung der Falte und Versteilung der Faltenschenkel von West nach Ost auf, mit der höchsten Faltensymmetrie im Profil g. In den nächsten drei Profilen kehrt die Tendenz um zu einer wieder weiteren, offeneren Faltenstruktur, um in den östlichsten drei Profilen zu einer kofferfaltenartigen Struktur zu wechseln. Diese Änderungen im Relief der Antiklinale könnten auf unterschiedliche Verkürzungsbeträge zurückzuführen sein. Allerdings wurden in den bilanzierten Profilen ähnliche Verkürzungsbeträge errechnet (vgl. Kap. 3.2.3 und 3.3.3). Somit bietet sich eher eine Ursache an, die in der tektonischen Struktur der Falte liegt, vor allem in der Form der Rampe und der Duplexe. Anzeichen für grössere Undulationen der Rampenüberschiebungsfläche nördlich des oberen Knickpunktes gibt es nicht.
Die Duplexstrukturen sind über die ganze Profilserie nötig, um den Faltenkern zu stopfen. Ihre in einigen Profilen angedeutete Lage ist aber hypothetisch. Auch die Geometrie des «blind fault» und dessen Auswirkungen, v. a. die Verdoppelung des Opalinus-Tons, hat ausser im Profil g keine Evidenz in Felddaten.
Der im Profil g südlich der Antiklinale einsetzende, steil nordfallende Bruch (vgl. Kap. 3.2.3) schneidet dieses und die fünf östlich folgenden Profile. Als syntektonisch entstandene Struktur ist er im gegen Osten folgenden Profil m im Nordschenkel erodiert, gegen Westen schneidet er die Profilspuren nicht.
Gemein ist den Profilen eine Tendenz zur Bildung von rückwärtigen Abschiebungen im Süden und die Zerlegung des Nordschenkels durch nordvergente Überschiebungen. Die späten Abgleitungen im Nordschenkel (vgl. Kap. 3.2.3) sind aus den vorhandenen geologischen Kartendaten nicht rekonstruierbar.
Ein interessantes Detail zeigt sich im Profil m: ein sekundäres Gewölbe im nördlichen Teil der Falte wird mit der Topographie verschnitten. Durch die erwähnte steile Bruchfläche, die hier in Nordrichtung streicht, ist diese Struktur vom Profil l abgekoppelt, das an dieser Stelle 150 m westlich verläuft.
Die Geomorphologie zeigt einen deutlichen Aufbruch der Antiklinale mit Freilegung der inkompetenten Schichten im Faltenkern. Es entstehen in den Profilen g und h sich gegenüberliegende Fluhen, die durch Abbrüche im Hauptrogenstein gebildet werden. Gegen Osten und Westen verflacht die nördliche Fluh, der Mont Terri, mit der erwähnten Öffnung der Falte. Die südliche Fluh fällt gegen Süden im «dip slope» ab. Dadurch wird ein faltenparalleles Tälchen in den inkompetenteren Schichten des Callovien und Oxfordien gebildet, südlich dessen sich ein Hügelzug aus kompetenten Malmkalken erhebt.
Im Profil h sind zwei Überschiebungsflächen für die erwähnte Verschmälerung des Keuperkernes verantwortlich (vgl. Kap. 3.1).

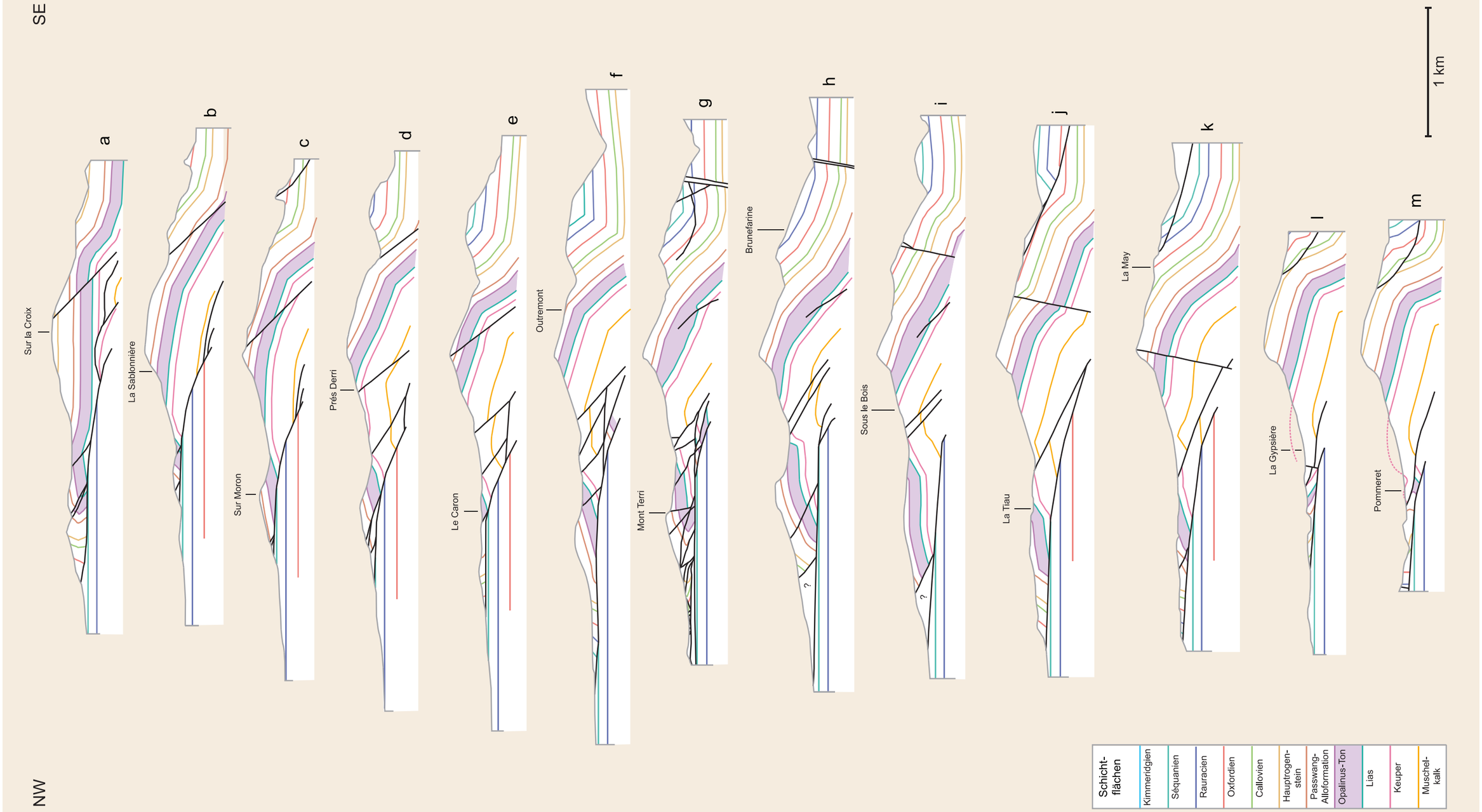

Abb. 15: Profilserie durch die Mont-Terri-Antiklinale. Vgl. Kap. 3.4. In Schwarz: Brüche. Die Profilspuren sind aus Abb. 7 ersichtlich.

Fig. 15: Series of profiles through the Mont Terri anticline. See chapter 3.4. Black: faults. The profile traces can be seen in fig. 7.

Fig. 15: Série de profils à travers l'anticlinal du Mont Terri. Cf. chap. 3.4. En noir: failles. Les traces des profils sont reportées dans la fig. 7.

3.5 Schlussfolgerungen

Während des Arbeitsprozesses der Profilbilanzierung haben sich, in Bezug auf die geologischen Verhältnisse in der Region, verschiedene Vor- und Nachteile der angewandten Methoden bemerkbar gemacht.
Ein grundlegender Vorteil liegt in der spröd deformierenden Tektonik des Juragebirges (vgl. Kap. 2.1.1), die die Methode der Materialbilanz überhaupt erst anwendbar macht. Die Pinlines sind einfach zu fixieren, da das Vorland und das direkte Hinterland der Antiklinale nicht deformiert sind. Weitere Vorteile sind die Dichte und Qualität der Datengrundlage, die laterale Konstanz der Strukturen zwischen den bearbeiteten Profilen, sowie die Flexibilität der Methodik und der Computeranwendung.
Nachteile liegen im engen regionalen Rahmen, sowohl in der zweiten als auch in der dritten Dimension. Ideal wäre eine Erweiterung der Profilspuren nach Süden, um weitere Antiklinalen zu erfassen. Die Bilanzierung weiterer Profile gegen Osten und Westen würde die Konstruktion eines dreidimensionalen bilanzierten Blockmodells erlauben (vgl. Kap. 3.4).
Da die Profilspurorientierungen durch die beiden Tunnel vorgegeben werden, hätten bei einer wesentlichen Abweichung der Transportrichtung von dieser Orientierung leicht Fehler erwachsen können. Wie aber in Kap. 3.2.2 und 3.3.2 dargelegt wird, eignet sich die Richtung der Tunnel als gemittelte Transportrichtung der Mont-Terri-Antiklinale.

Die Modellierung nach den Regeln der Materialbilanz resultiert in einer geometrischen und mechanischen Geschichte der bearbeiteten Struktur. Diese wird durch einzelne Momentaufnahmen dargestellt. Diese Resultate der Modellierung werden mittels des Vorgehens- und Beurteilungskonzeptes (Abb. 4, Kap. 2.1.2) auf ihre Plausibilität geprüft, was zu folgenden Feststellungen führt:

- Die beiden Profile sind zurückdeformierbar (vgl. Kap. 2.1).
- Sie zeigen im ausgeglätteten Zustand und in den einzelnen Schritten ihrer Deformation jeweils plausible Bruchtrajektorien für die nächste Phase (vgl. Kap. 2.1.2).
- Die deformierten Profile zeigen realistische Falten- und Bruchgeometrien (vgl. Kap. 2.1.2).
- Die Deformationsphasen gehen nahtlos ineinander über und sind transparent, d. h. sie sind aus nachvollziehbaren Programmmodulen aufgebaut (vgl. Kap. 2.2.3).
- Die beiden bilanzierten Profile sind in allen Phasen lateral konsistent und passen sich ins Kartenbild ein, sie zeigen ähnliche Verkürzungsbeträge (vgl. Kap. 2.1).
- Sie bringen die akquirierten Daten in einen geologischen Kontext (vgl. Kap. 2.1).
- Die Schichtlängen und -flächen zwischen den Pinlines ändern sich während der Deformation im Modell nicht nennenswert (vgl. Kap. 2.1).

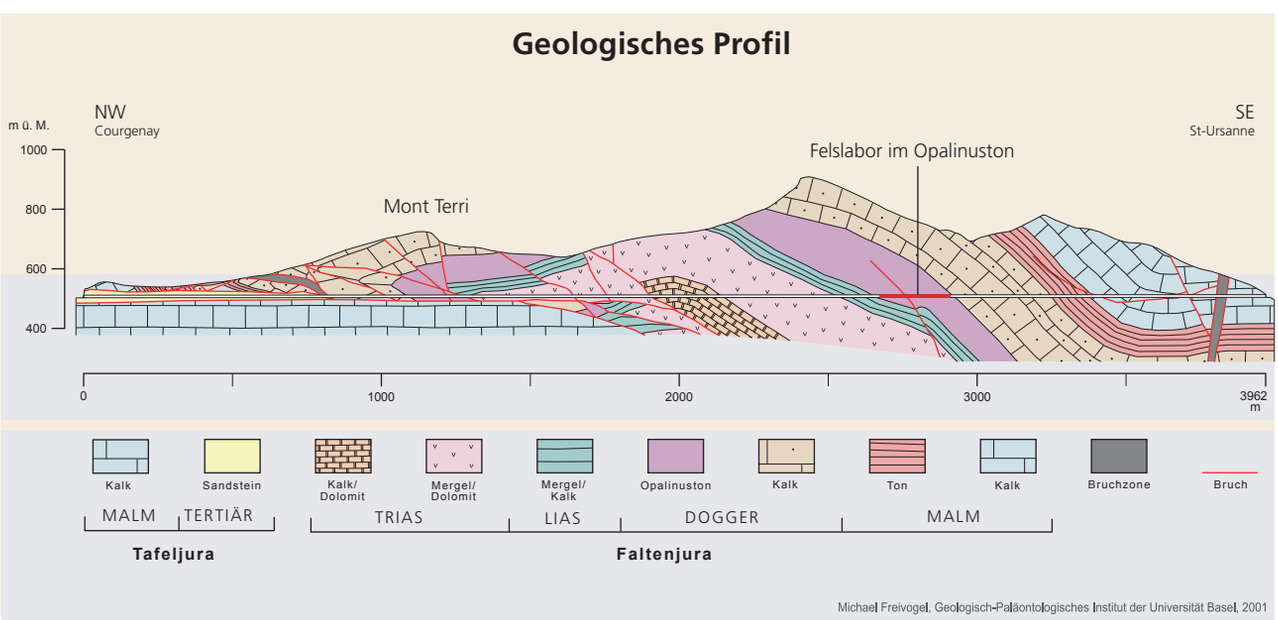

Abb. 16: Das vereinfachte geologische Profil entlang des Mont-Terri-Strassentunnels.

Fig. 16: Simplified geological profile along the Mont Terri road tunnel.

Fig. 16: Coupe géologique simplifiée le long du tunnel autoroutier du Mont Terri.

Die Profile genügen somit den Gesetzen der Materialbilanz.

Die laterale Entwicklung der Strukturen der Mont-Terri-Antiklinale wird in der Profilserie (Abb. 15) dargestellt. Sie soll nicht einer kinematischen Analyse dienen, sondern einen tieferen Einblick in die regionale Geologie geben, wie sie in Kap. 3.1 zusammengefasst wird. Eine vereinfachte Darstellung des Profils Mont Terri wird in Abb. 16 und im Anhang gezeigt. Hier sind, zur Veranschaulichung der heutigen Situation, die Lage des Tunneltrassees und des Felslabors eingezeichnet (siehe Abb. 16, Seite 38).

Einige Änderungen zum Profil c in Abb. 2 sind sofort ersichtlich, z. B. die Duplexstrukturen, der «blind fault», der die Mächtigkeitsänderung im Opalinus-Ton bewirkt, und das Vermeiden von duktil anmutenden Faltenformen. Die wesentlichen Unterschiede fallen aber nicht sofort ins Auge: die Plausibilität in Kinematik und Dynamik und die Veranschaulichung des Werdeganges der geologischen Strukturen, die ein bilanziertes Profil zu einem wertvollen Hilfsmittel bei erdwissenschaftlichen Fragestellungen machen.

Verdankungen

Die Autoren bedanken sich für die gute Zusammenarbeit mit der Landesgeologie (P. Heitzmann und J-P. Tripet) und deren finanzielle Unterstützung. Das Institut Géotechnique SA, St-Ursanne (P. Bossart), das Bureau Technique Norbert in Lausanne sowie Herr R.T. Haarpaintner haben durch ihre fachlichen Beiträge und die Daten, die sie zur Verfügung stellten, wesentlich zu dieser Arbeit beigetragen. Thomas Noack und Christian Meyer sei für die fachliche Begleitung, die Anregungen und die kritische Durchsicht des Manuskriptes recht herzlich gedankt.

Referenzen

Allia, V. (1996): Sedimentologie und Ablagerungsgeschichte des Opalinustons in der Nordschweiz. – Diss. Univ. Basel.

Allimann, M., Bagnoud, A., Becker, D., Bossart, P., Möri, A., Schürch, R. & Steiger, H. (1998): Geological Map of the Mont Terri Rock Laboratory 1 : 2 000. – Institut Géotechnique, St-Ursanne. Nicht publiziert.

Bally, A.W., Gordy, P. & Steward, G. (1966): Structure, seismic data and orogenic evolution of southern Canadian Rocky Mountains. – Bull. canad. Petroleum Geol. 14, 3376 – 3381.

BGA, Bureaux Géologiques Associés – Norbert, J. & Schindler, B. (1988): Forages de reconnaissance (Coupes détaillées 1 : 100) DMT1, TA, TB, TC, TCbis, TEN3, TEN4, TEN5, TEN6, TEN7, TEN8, TEN9, TEN10, TEN11, TRI1, TRI2, TRI3, TRI4. – Nicht publiziert.

Bitterli, T. (1992): Die Anwendung der tektonischen Materialbilanz im östlichen Faltenjura. – Diss. Univ. Basel.

Bläsi, H.R., Möri, A. & Bossart, P. (1996): Results of the Phase 1 drilling campaign, Mont Terri Project. – Mont Terri tech. Rep. TR 96 - 01, Federal Office for Water and Geology, Bern-Ittigen, Switzerland.

Bossart, P. & Wermeille, S. (2003): Paleohydrological Study on the Surroundings of the Mont Terri Rock Laboratory. In: Heitzmann, P. & Tripet, J.-P. (Ed.): Mont Terri Project – Geology, Paleohydrology and Stress Field of the Mont Terri Region (p. 45-64). – Reports of the Federal Office for Water and Geology (FOWG), Geology Series 4 .

Boyer, S.E. & Elliot, D. (1982): Thrust systems. – Bull. amer. Assoc. Petroleum Geol. 66, 1196 – 1230.

BTN, Bureau Technique Norbert, Lausanne (1993): Tunnel du Mont Terri, Profil en long géologique, prévisions – exécution, 1 : 5 000. – Nicht publiziert.

— (1994a): Tunnel du Mont Terri, Profil en long géologique et coupe horizontale, lot nord/lot sud, après exécution, 1 : 1 000. – Nicht publiziert.

— (1994b): Tunnel du Mont Terri, notice géologique, après exécution. – Nicht publiziert.

Bucher, W. (1933): The deformation of the earth's crust. – Princeton Univ. Press, Princeton, New Jersey.

Burkhalter, R.M. (1996): Die Passwang-Alloformation (unteres Aalénien bis unteres Bajocien) im zentralen und nördlichen Schweizer Jura. – Eclogae geol. Helv. 89/3, 875 – 934.

Buxtorf, A. (1916): Prognosen und Befunde beim Bau des Hauensteinbasis- und Grenchenbergtunnels und die Bedeutung der letzteren für die Geologie des Juragebirges. – Verh. natf. Ges. Basel 27, 185 – 254.

Buxtorf, A. & Lehner, E. (1920): Rheintalische Brüche in der Montterrible-Kette und im Clos du Doubs. – Eclogae geol. Helv. 16/1, 71 – 75.

Chester, J.S. & Chester, F.M. (1990): Fault-propagation folds above thrusts with constant dip. – J. struct. Geol. 12, 903 – 910.

Dahlstrom, C. (1969): Balanced cross sections. – Canad. J. Earth Sci. 6, 743 – 757.

Diebold, P. (1960): Geologie des Siegfriedblattes Ocourt (Berner Jura). – Beitr. geol. Karte Schweiz [N.F.] (111).

Diebold, P., Laubscher, H., Schneider, A. & Tschopp, R. (1963): Blatt 1085 St-Ursanne. – Geol. Atlas Schweiz 1 : 25 000, Karte 40.

Droxler, A. & Schär, J.P. (1979): Déformation cataclastique plastique lors du plissement, sous faible couverture, de strates calcaires. – Eclogae geol. Helv. 72/2, 551 – 570.

Ducret, M. (1874): Peut-on trouver de la houille à Cornol? – Actes Soc. jurass. Emul. 24, 174.

Elliot, D. (1983): The construction of balanced cross sections. – J. struct. Geol. 5, 101.

Freivogel, M. (2001): Diplomkartierung im Gebiet La Croix – Mont Terri (JU). – Diplomarb. Univ. Basel (nicht publiziert).

Geosec – 20™: © Geo-Logic Systems, New Paltz, N.Y., USA.

Gibbs, A. (1983): Balanced cross section construction from seismic sections in areas of extensional tectonics. – J. struct. Geol. 5, 153 – 160.

Goguel, J. (1952): Traité de tectonique. – Masson, Paris.

— (1962): Tectonics. – W.H. Freeman, San Francisco, London.

Gressly, A. (1853): Albâtre keupérien blanc de Montterrible. – Actes Soc. helv. Sci. nat., 40.

Gygi, R.A. (2000): Integrated stratigraphy of the Oxfordian and Kimmeridgian (late Jurassic) in northern Switzerland and adjacent southern Germany. – Denkschr. schweiz. Akad. Natw. 104.

Haarpaintner, R.T. & Schaeren, G., Bureau Technique Norbert, Lausanne (1997): Laboratoire souterrain du Mont Terri – Conditions géologiques et hydrogéologiques générales (Tunnel routier du Mont Terri, Tunnel ferroviaire de La Croix). – Mont Terri tech. Rep. TR 99-03, Federal Office for Water and Geology, Bern-Ittigen, Switzerland. Nicht publiziert.

Heim, A. (1878): Über die Stauung und Faltung der Erdrinde. – Schwabe, Basel.

Jamison, W.R. (1987): Geometric analysis of fold development in overthrust terranes. – J. struct. Geol. 9, 207 – 219.

Jones, P. & Linsser, H. (1984): Faster search for hidden geology. – Resource technol. 1, 8 – 9.

Kelterborn, P. (1944): Beobachtungen im Mont Terri - Gebiet zwischen Courgenay und Asuel (Berner Jura). – Eclogae geol. Helv. 37/2, 207 – 216.

Klingfield, R., Geiser, P. & Geiser, J. (1986): Construction of geologic cross-sections using microcomputer systems. – Geobyte 1/2, 60 – 66.

Koby, F. (1889): Peut-on trouver de la houille à Cornol? – Actes Soc. jurass. Emul. (2), 2, 239 – 252.

Kohler, J. (2000): Diplomkartierung im Gebiet des Mont Terri (JU). – Diplomarb. Univ. Basel (nicht publiziert).

Laubscher, H. (1948): Geologie des Siegfriedblattes St-Ursanne (Berner Jura). – Beitr. geol. Karte Schweiz [N.F.] 92.

— (1963): Blatt 1085 St-Ursanne. – Geol. Atlas Schweiz 1 : 25 000, Erläut. 40.

— (1965): Ein kinematisches Modell der Jurafaltung. – Eclogae geol. Helv. 58/1, 221 – 282.

— (1972): Some overall aspects of Jura dynamics. – Amer. J. Sci. 272, 293 – 304.

— (1979): Elements of Jura kinematics and dynamics. – Eclogae geol. Helv. 72/2, 467 – 483.

Liniger, H. & Wehrenfels, A. (1926): Zur Tektonik der Umgebung von Asuel und St.-Ursanne (vorläufige Mitteilung). – Eclogae geol. Helv. 20/1, 289 – 295.

Marshak, S. & Mitra, G. (1988): Basic Methods of structural geology. – Prentice Hall, New Jersey.

Mathey, F. (1883): Coupes géologiques des Tunnels du Doubs. – Verh. schweiz. natf. Ges. XXIX.

McClay, K.R. (1992): Glossary of thrust tectonic terms. In: McClay K.R. (Ed.): Thrust tectonics (p. 419 – 433). – Chapman & Hall, London.

Mitra, S. (1986): Duplex structures and imbricate thrust systems: geometry, structural position, and hydrocarbon potential. – Bull. amer. Assoc. Petroleum Geol. 70, 1087 – 1112.

Mitra, S. & Namson, J. (1989): Equal area balancing. – Amer. J. Sci. 289, 563 – 559.

Möri, A., Adler, M., Wermeille, S. & Bossart, P. (1997): Results of the Phase 2 drilling campaign. – Mont Terri tech. Rep. TR 97 – 01, Federal Office for Water and Geology, Bern-Ittigen, Switzerland.

Noack, T. (1989): Computergestützte Modellierung geologischer Strukturen im östlichen Jura; Konstruktion balancierter Profile, Gravimetrie, Refraktionsseismik. – Diss. Univ. Basel.

Ramsay, J.G. & Huber, M.I. (1987): The techniques of modern structural geology (Vol. 2). – Academic Press, London, San Diego.

Rickenbach, E. (1947): Die Vorkommen von bituminösen Schiefern. A. Die bituminösen Schiefer der Mont Terri – Antiklinale (Berner Jura). – Beitr. Geol. Schweiz, geotech. Ser. 26/1, 44 – 45.

Rollier, L. (1898): Deuxième supplément à la description géologique de la partie jurassienne de la feuille 7 de la carte géologique de la Suisse au 1 : 100 000. – Mat. carte géol. Suisse [n.s.] 8.

Schneider, A. (1960): Geologie des Siegfriedblattes Porrentruy (Berner Jura). – Beitr. geol. Karte Schweiz [N.F.] 109.

Suppe, J. (1983): Geometries and kinematics of fault bend folding. – Amer. J. Sci. 283/7, 684 –721.

— (1985): Principles of structural geology. – Prentice Hall, New Jersey.

Suppe, J. & Medwedeff, D.A. (1990): Geometry and kinematics of fault-propagation folding. – Eclogae geol. Helv. 83/3, 409 – 454.

Thurberg (1874): Kohlebohrung. – Nicht publiziert. Vgl. Kelterborn (1944), p. 208.

Thurmann, J. (1832): Essai sur les soulèvements jurassiques du Porrentruy. – Mém. Soc. Hist. nat. Strasbourg.

Tschopp, R. (1960): Geologie des Siegfriedblattes Miécourt (Berner Jura). – Beitr. geol. Karte Schweiz [N.F.] 110.

Woodward, N.B., Boyer, S.E. & Suppe, J. (1989): Balanced geological cross-sections: An essential technique in geological research and exploration. – Amer. geophys. Union, Washington, DC.

Anhang

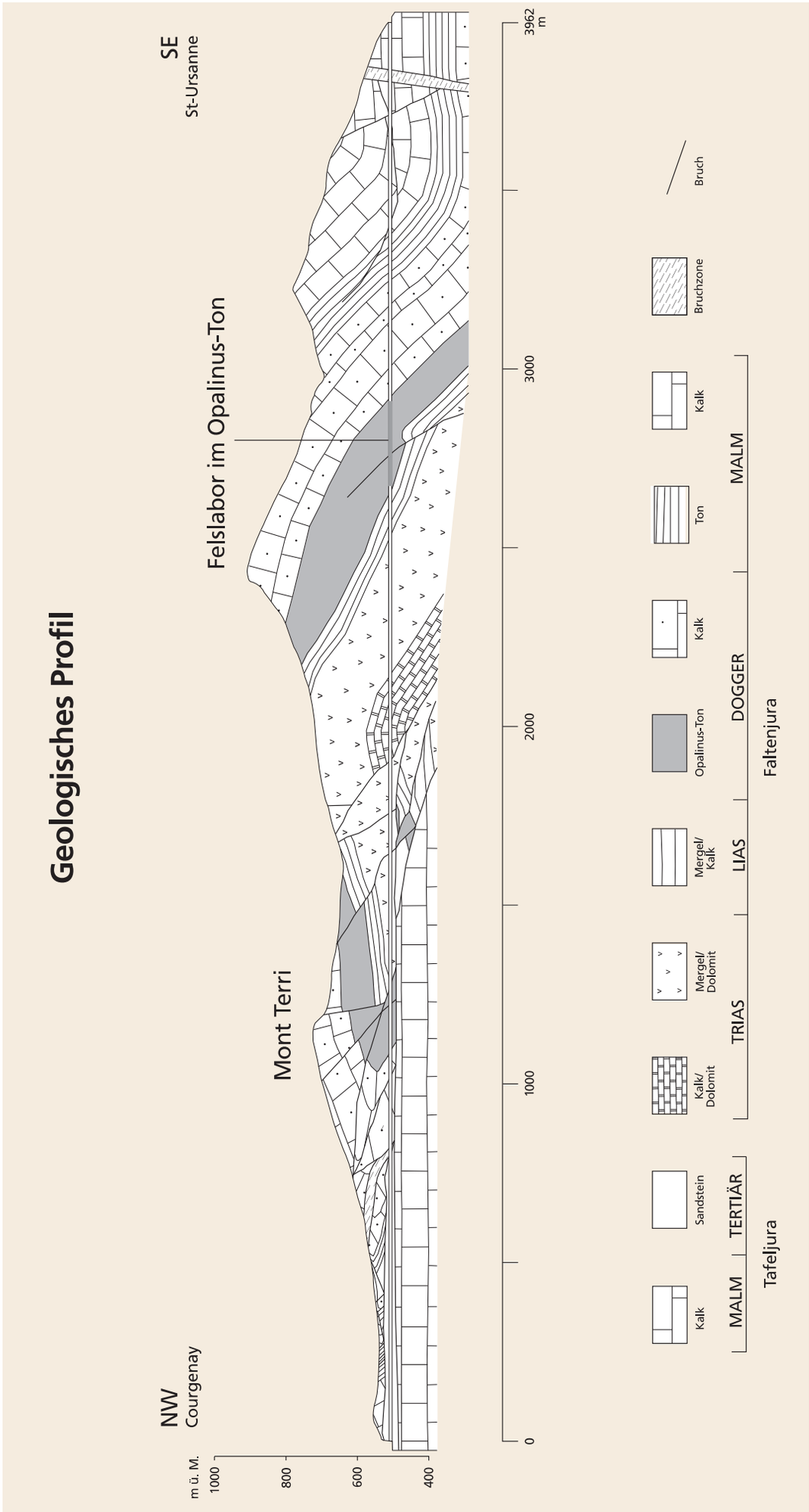

Technische Darstellung des vereinfachten geologischen Profils entlang des Mont-Terri-Strassentunnels.

Simplified geological profile along the Mont Terri road tunnel: technical illustration.

Coupe géologique simplifiée le long du tunnel autoroutier du Mont Terri: représentation technique.

Paleohydrological Study on the Surroundings of the Mont Terri Rock Laboratory

P. Bossart[1] & S. Wermeille[1]

[1]Institut Géotechnique SA, St-Ursanne

Abstract

The paleohydrological history from Oligocene to present in the area of St-Ursanne is presented in this report. This includes two erosion scenarios, one of the Doubs river and the other of the Mont Terri anticline. A sound literature review and own analyses were the basis for the paleohydrological data compilation and the interpretation. Special emphasis was placed on the impact on the Opalinus Clay in the future Mont Terri Rock Laboratory: The progressive downward erosion of the Doubs valley was responsible for the change from an infiltration system to an exfiltration system in the Opalinus Clay, and the progressive erosion of the Mont Terri anticline was affecting mainly flow and transport directions and groundwater chemistry. Time estimations are based on a number of assumptions and approximations. Thus minimum and maximum ages were estimated for both erosion scenarios.

Recommended quotation:
Bossart, P. & Wermeille, S. (2003): Paleohydrological Study on the Surroundings of the Mont Terri Rock Laboratory. In: Heitzmann, P. & Tripet, J.-P. (Ed.): Mont Terri Project – Geology, Paleohydrology and Stress Field of the Mont Terri Region (p. 45–64). – Reports of the Federal Office for Water and Geology (FOWG), Geology Series 4.

Unpublished report of March 9, 1999; updated May 3, 2002

Résumé

Le présent rapport expose l'histoire paléohydrologique des environs de St-Ursanne, pour la période qui court de l'Oligocène à l'époque contemporaine. Deux scénarios d'érosion ont fait l'objet d'études approfondies. Le premier traite de la formation de la vallée du Doubs et le second de l'érosion de l'anticlinal du Mont Terri. La base de données utilisée a notamment été élaborée à partir d'une analyse minutieuse de la littérature existante, ainsi que d'analyses originales. Les répercussions possibles sur les Argiles à Opalinus du futur laboratoire souterrain du Mont Terri ont fait l'objet d'une attention particulière: l'érosion progressive de la vallée du Doubs a occasionné le passage d'un régime d'infiltration à un régime d'exutoire, tandis que l'érosion de l'anticlinal du Mont Terri a provoqué une modification des directions d'écoulement et de transport, et un changement du chimisme des eaux souterraines. Les âges fournis dans ce rapport se basent sur diverses hypothèses et approximations. Aussi donne-t-on les âges minimaux et maximaux pour les deux scénarios d'érosion.

Zusammenfassung

Der vorliegende Bericht befasst sich mit der paläohydrologischen Geschichte in der Umgebung von St-Ursanne, und zwar in der Zeitspanne vom Oligozän bis heute. Speziell untersucht wurden zwei Erosionsszenarien. Das erste Szenario befasst sich mit der Bildung des Doubstales und das zweite mit der Erosion der Mont-Terri-Antiklinale. Die Datenbasis beruht vor allem auf einer profunden Literaturanalyse sowie eigenen Analysen. Speziell beachtet wurden dabei die möglichen Auswirkungen auf den Opalinus-Ton im zukünftigen Mont-Terri-Felslabor: Die progressive Erosion des Doubstales war verantwortlich für einen Wechsel von einem Infiltrations- zu einem Exfiltrationsregime, und die Erosion der Mont-Terri-Antiklinale verursachte eine Änderung der Fliess- und Stofftransportrichtungen sowie der Grundwasserchemie. Die im Bericht angegebenen Altersbestimmungen basieren auf einer Anzahl von Annahmen und Annäherungen. Daher sind für beide Erosionsszenarien jeweils Minimum- und Maximum-Alter angegeben.

Table of Contents

Abstract 46
Resumé 47
Zusammenfassung 47
1 Introduction 49
2 Erosion Scenario of the Doubs River 50
2.1 Overview of the regional evolution between 35 My and today 50
2.2 Erosion scenario of the Doubs river system based on literature survey 53
2.3 Erosion scenario of the Doubs river system based on own interpretation 55
3 Erosion Scenario of the Mont Terri Anticline 58
4 Discussion and Conclusion 61
Acknowledgements 62
References 63

1 Introduction

The study was initiated by the Swiss Geological Survey (SGS) with the general objective to derive an improved paleohydrological scenario for the area of the Mont Terri Rock Laboratory. A first hydrogeological, geochemical and geotechnical synthesis from field investigations of the Mont Terri Project during 1996 – 1999 is available (Thury & Bossart 1999). Further syntheses are in preparation. These reports clearly show that a reliable interpretation of the results requires often a sound analysis of the geological site conditions. Of special interest is e.g. the temporal evolution of the local hydrological system at the Mont Terri site and the erosion scenario of the St-Ursanne region. Such erosion scenarios are needed when flow and transport processes and parameters are derived from in situ tests in the Mont Terri Rock Laboratory.

The detailed objectives of this study were twofold:

- To derive the erosion scenario of the Doubs valley, including changing flow directions related to tectonic events. The hydrological impact of the Doubs valley evolution near St-Ursanne on the (future) site of the Mont Terri Rock Laboratory (infiltration and exfiltration periods in the Opalinus Clay) is of special interest.
- To derive the erosion scenario of the Mont Terri anticline. Determination of the time when the erosion level reached the top and the base of the Opalinus Clay formation is especially important for the estimation of diffusion parameters, calculated from pore water concentration profiles in the Mont Terri Rock Laboratory.

A part of this study (Chapter 2.1 and Chapter 2.2) is mainly based on a thorough literature review and intensive discussions with specialists of the Universities of Basel, Fribourg and Berne. The literature review showed that no erosion scenarios with quantitative data, such as time versus depth profiles, are available for the region of St-Ursanne. If such scenarios do exist, no relevant presentations were found by our survey. Thus, the authors made their own interpretations based on the data compiled from the literature. These data are shown in Chapter 2.3 (Erosion scenario of the Doubs river system based on own interpretation) and Chapter 3 (Erosion scenario of the Mont Terri anticline). The assumptions were formulated to be as transparent as possible. Finally it must be emphasized that no field work was carried out for this study. This study was carried out by Paul Bossart and Séverine Wermeille, from the Geotechnical Institute Ltd., and supervised by Jean-Pierre Tripet, at SGS.

2 Erosion Scenario of the Doubs River

2.1 Overview of the regional evolution between 35 My and today

The paleohydrology of the region is closely related to the paleoenvironment and the tectonic evolution; major research work has been covered within the scope of works by Buxtorf (1920), Schwab (1939), Liniger (1966), Laubscher (1948, 1961, 1962, 1963, 1987, 1992, 1998), Berger (1996), Kälin (1993, 1997), Schlüchter & Müller-Dick (1996), Gigon & Wenger (1986).
The main results are presented in a chronological table (Table 1), including periods, lithologies observed in the surroundings of St-Ursanne and of the Delémont Basin, regional surface flow directions, tectonic movements and references. The compilation of existing data is used as data base for the erosion scenario of the Doubs valley (Table 1). The individual events are chronologically presented and summarized below:

34.4 – 21.5 My (late Rupelian – early Burdigalian)

Extension and subsidence of the Rhine Graben from the Priabonian (before the Rupelian) to the late Chattian (Laubscher 1998). Formation of the Delémont Basin (see schema in Table 1) and of the Mont Terri Flexure (Laubscher 1961, 1962). Creation of N-S faults east of St-Ursanne (Laubscher 1961, 1962). Marine sediments (Lower Marine Molasse = UMM) followed by fluvial and lacustrine ones (Lower Freshwater Molasse = USM) are observed in the Delémont Basin as well as in the area of St-Ursanne and Mont Terri (Berger 1996). The site of the Mont Terri Rock Laboratory in the Opalinus Clay has had a minimum overburden of 1000 m (H.R. Bläsi, personal communication). It is assumed that the whole sedimentary pile was water saturated.

21.5 – 10.5 My (early Burdigalian – early Tortonian)

The area of St-Ursanne and Mont Terri sits on a structural high (Mont Terri Flexure, see sketch in Table 1), which is bordered to the east by east facing normal faults which mark the transition to the Delémont Basin (Laubscher 1961, 1962). Within this structural transition, two elevated domains can be distinguished; i.e. the primitive Caquerelle and Vorbourg chains (Laubscher 1948; Kälin 1993, 1997). This period represents the beginning of the erosive period of the Doubs river valley. The uplift and erosion of the Vosges and Black Forest massifs occurred between 15.1 and 12.5 My (Laubscher 1998; Kälin 1997). Sediments were transported southward, through a supposed channel located between the primitive Caquerelle and Vorbourg chains (Kälin 1993, 1997), and deposited in the Delémont Basin («Juranagelfluh» of the «Bois des Raubes» forest and «Vogesenschüttung» from Ajoie and «Bois des Raubes» forest) (Berger 1996; Kälin 1997). Lack of these sediments within the St-Ursanne and Mont Terri area is an indication for an erosive period.

10.5 – 3 My (early Tortonian – early Pliocene)

The Jura folding occurred during this period (Berger 1996). Undeformed sediments were recently found in a karst of the Vue des Alpes tunnel (NE), showing that the folding was completed by 3 My (Bolliger et al. 1993). The Mont Terri anticline, faulted during this period, began being eroded at the same time.

3 My – today (early Pliocene – Holocene)

The area of St-Ursanne and Mont Terri is still in an erosive period (Berger 1996). During the glaciation periods, the study area was free of ice (Schlüchter & Müller-Dick 1996). Figure 1 shows that during the Most Extensive Glaciation, the glacier edge was located about 8 km south of the Mont Terri Rock Laboratory.

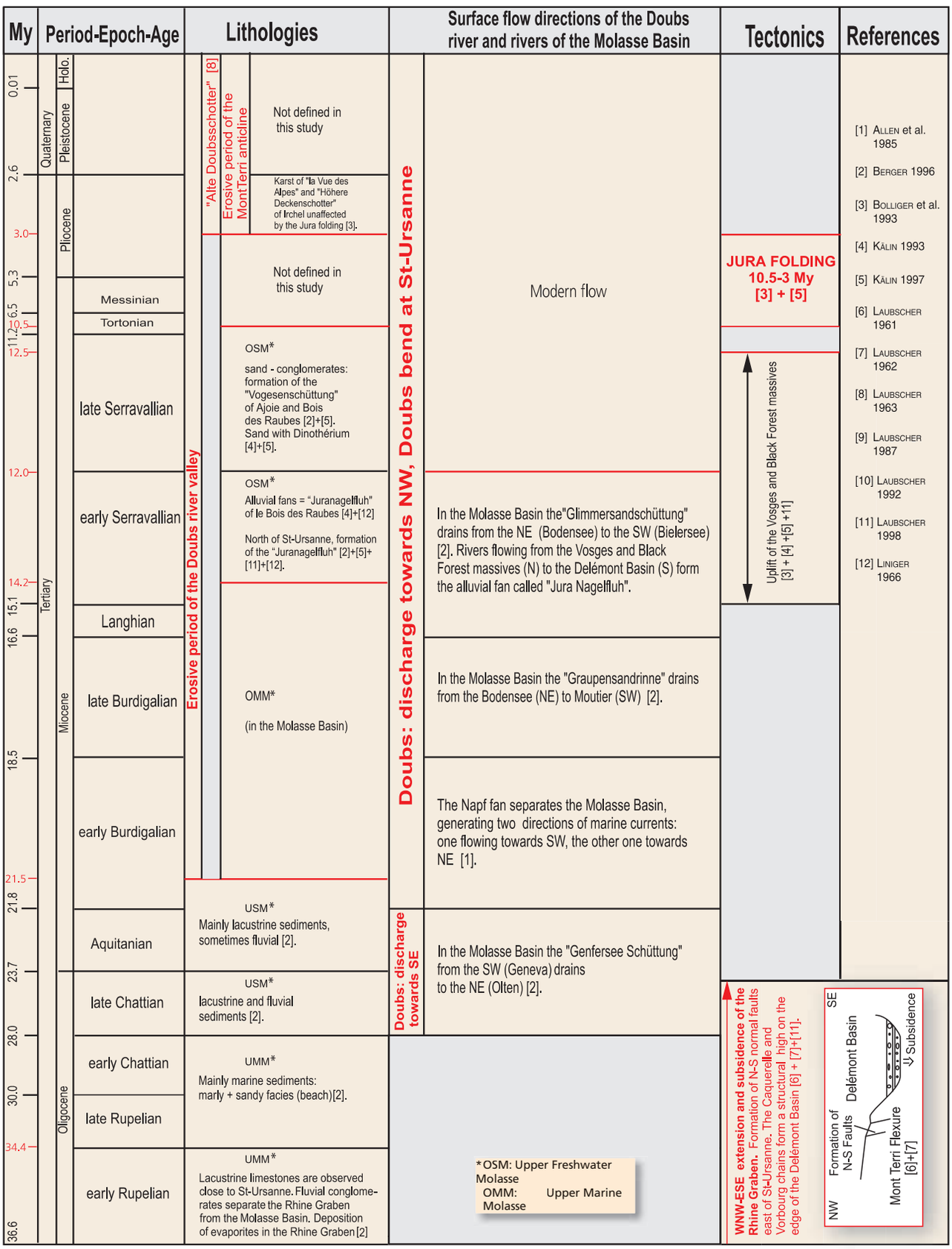

Table 1: Chronological evolution of the area of St-Ursanne. Time [My]: not to scale.

It was possible to map some rare, undated traces of old Doubs sediments (limestone gravels, «Alte Doubsschotter», Laubscher 1963). These sediments are shown in Figure 3 (red labels), where the topographic level of the sediments is plotted against their location along the Doubs river. The green labels represent loam formed by alteration and weathering of the bedrock. Again no dating is available. Schwab (1939) considered the loam deposits (green labels in Figure 3) and the «Alte Doubsschotter» (red labels) as old Doubs deposits. He distinguished 4 different terraces of the Doubs river. Laubscher (1948) confirmed only the existence of two of them, represented by limestone gravels (lower and upper terraces in red on Figure 3). Until more detailed results are available (e.g. dating of material in silt horizons), the structural evidence for two higher terraces (green labels in Figure 3) have to be denied.
Another interesting observation by Swiss speleologists concerns the rock shelter above St-Ursanne (Figure 2, Swiss coordinates 578.575/246.265). Interpreted as an old erosion level of the Doubs river (Gigon & Wenger 1986), it is located at ~500 m a.s.l. (see Figure 3). If their interpretation is correct, the rock shelter represents the oldest erosion trace of the Doubs river in the area of St-Ursanne. Its altitude is very close to that of the Mont Terri Rock Laboratory (513 m a.s.l.). It proves that the Doubs river once flowed at this level. Again no dating is available in the literature.
The authors also agree unanimously that before the Most Extensive Glaciation, 780'000 years ago (Schlüchter & Müller-Dick 1996), the level of the Doubs bed in St-Ursanne was about 35 m lower than today (Buxtorf 1920; Schwab 1939). This means that the Doubs channel has been filled with 30 – 40 m thick alluvial deposits since the most extensive glaciation (see Figure 3).

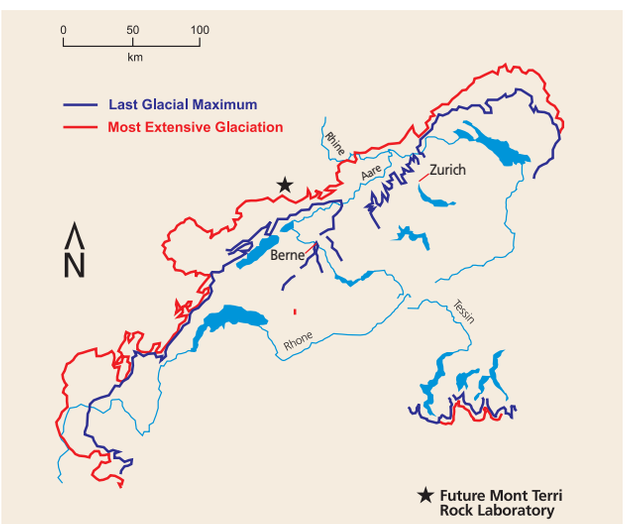

Figure 1: Extension of the Most Extensive Glaciations in Switzerland (~780'000 y before present) and the last one (28'000-14'600 y before present). After Schlüchter & Müller-Dick (1996).


Figure 2: Picture of the rock shelter above St-Ursanne at 500 m a.s.l.

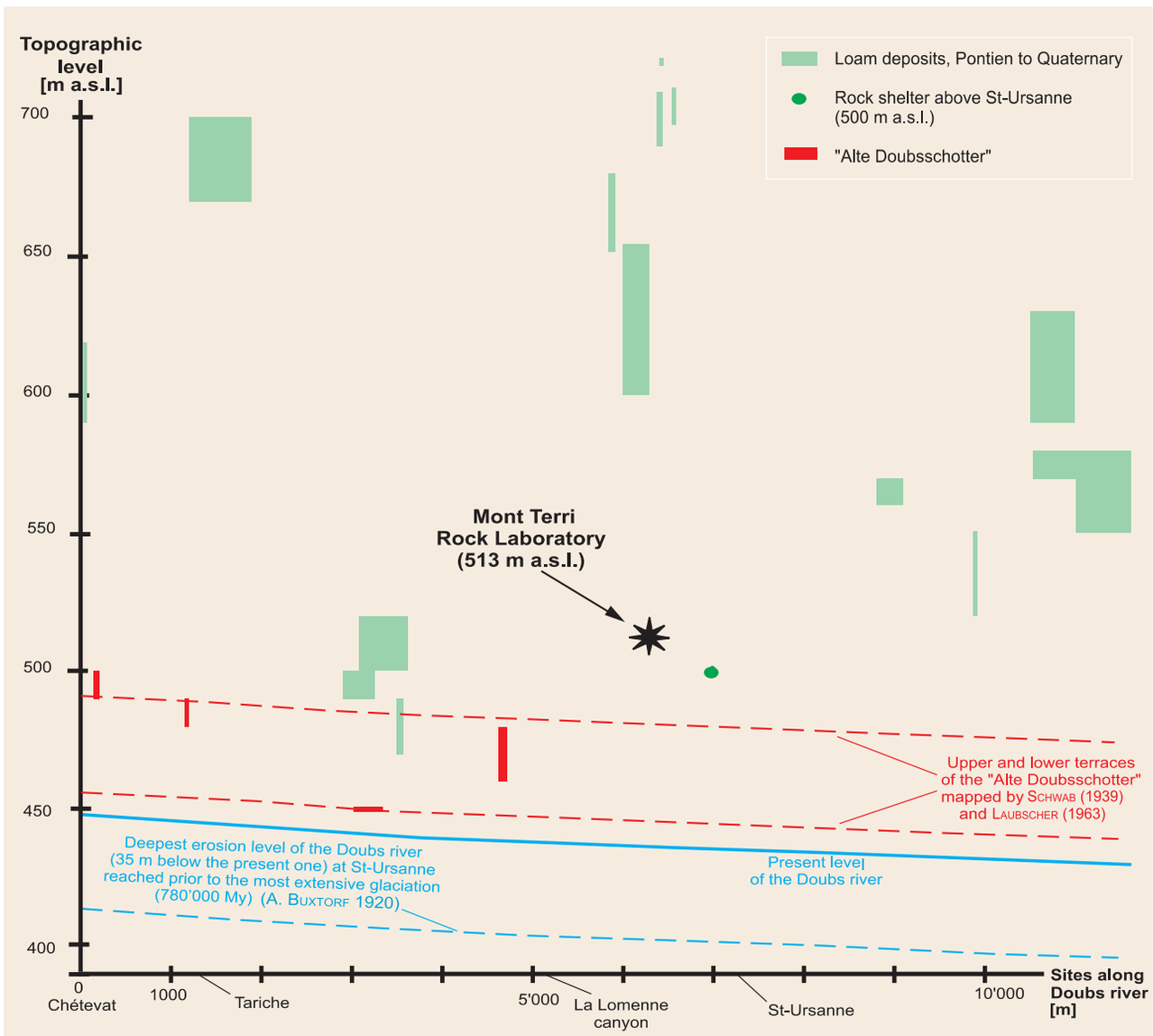

Figure 3: Erosion scenario for the St-Ursanne region (based on literature survey).

2.2 Erosion scenario of the Doubs river system based on literature survey

It seems to be evident why at present the Doubs river abruptly changes its flow direction at St-Ursanne: four anticlines (Clairmont, Mont Terri, Vorbourg and Caquerelle) build a geomorphological barrier, preventing river discharge towards north, east and south (Figure 4d). This geomorphological barrier has existed since the Jura folding (10.5–3 My). Before the Jura folding however, this barrier was not present.

The Delémont Basin started to subside by about 40 My (Laubscher 1987). Before this time (see Figure 4a), the area of St-Ursanne and Delémont was principally covered by the Lower Marine Molasse (Berger 1996). Between 40 My and 21.5 My (see Figure 4b), the Delémont Basin subsided (Laubscher 1961, 1962). Two primitive anticlines (Caquerelle and Vorbourg) were formed leaving N-S faults which can still be seen on the surface (Figure 4b and 4c, upper right corner, and Laubscher 1961, 1962). The area of St-Ursanne and Delémont is principally covered by lakes and braided river systems, which are characteristic for the time equivalents of Lower Marine Molasse (Berger 1996).

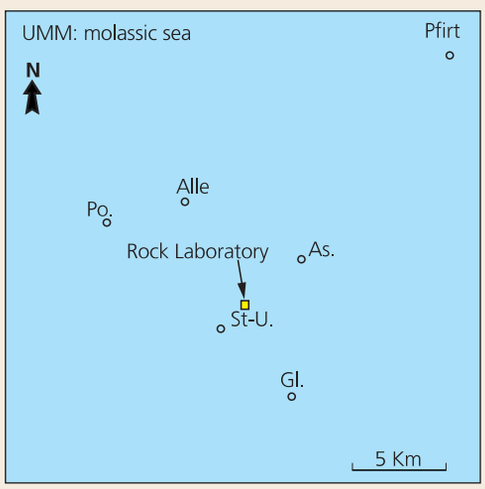

a: Before the subsidence of the Delémont Basin (40 My). The area of St-Ursanne and Delémont is covered by the UMM sea.

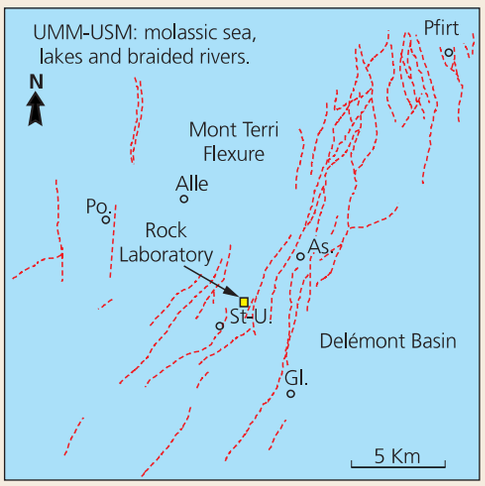

b: Between 40 and 21.5 My: Subsidence of the Delémont Basin. Formation of N-S faults east of St-Ursanne and Mont Terri Flexure. The area is covered by the UMM sea followed by lakes and braided rivers (USM).

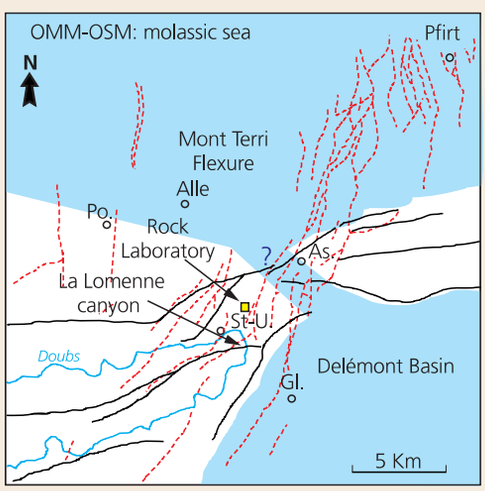

c: Between 21.5 and 10.5 My:
The Delémont Basin keeps on subsiding.The area of St-Ursanne is emerged and hydrologically separated from the Delémont Basin. Beginning of the erosive period for the Doubs valley. Formation of a primitive Doubs River.

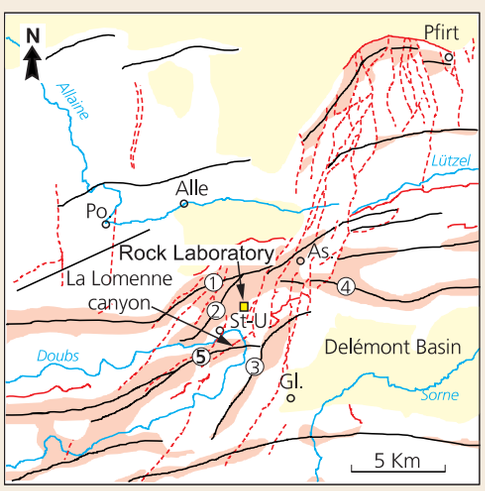

d: From 10.5 My till today:
The Jura Folding occurs between 10.5 and 3 My. Anticlines are formed. They prevent the Doubs River from flowing northwards, eastwards and southwards.

Tertiary
Malm
Dogger and other
Molasse sea
Faults
Thrusts
Anticlines

As. = Asuel
St-U. = St-Ursanne
Gl. = Glovelier
Po. = Porrentruy

OSM = Upper Freshwater Molasse
OMM = Upper Marine Molasse
USM = Lower Freshwater Molasse
UMM = Lower Marine Molasse

① Mont Terri anticline
② Clairmont anticline
③ Caquerelle anticline
④ Vorbourg anticline
⑤ Clos du Doubs anticline

Figure 4: Evolution around the future site of the Mont Terri Rock Laboratory during the last 40 My.

Between 21.5 and 10.5 My (before the Jura folding) the Delémont Basin kept subsiding (see Figure 4c). The structural high (Caquerelle and Vorbourg chains), formed by the subsidence of the Delémont Basin and the formation of the N-S faults east of St-Ursanne (Mont Terri Flexure), isolated water flows of the St-Ursanne area from the Delémont Basin. This separation was followed by different geological environments on both sides of the Mont Terri Flexure: in the Delémont Basin, alluvial sediments are deposited («Juranagelfluh» and «Vogesenschüttung») whereas in the St-Ursanne area, no such sediments are recorded in this period.
The erosion phase (e.g. Doubs river) started. Rivers in the area of St-Ursanne could no longer flow south and east. Furthermore, no traces of paleo-channels indicating a northward direction of rivers could be found in the area of Mont Terri. This is probably due to the Mont Terri Flexure: Prior to the Jura folding Mont Terri was probably slightly more elevated than St-Ursanne. We conclude that rivers in the area of St-Ursanne and Mont Terri had to flow westwards.
Furthermore, the canyon of La Lomenne (SE of St-Ursanne, see Figure 4c and Bouvier 1997) indicates that the Doubs bow at St-Ursanne was formed prior to the Jura folding due to the fact that the Doubs river is discordant to the tectonic structures: it cuts the Dogger limestones of the «Clos du Doubs» anticline. This suggests that an old river was probably active before the rising of this anticline (Schwab 1939).
During this period, the hydrological impact of the Doubs river on the future site of the Mont Terri Rock Laboratory was as follows: 21.5 My ago (beginning of the Doubs erosive period), the Opalinus Clay was covered by a rock pile of at least 1000 m thickness (Tertiary + possible Cretaceous + Malm + Dogger). Knowing that the deepest recorded erosion level of the Doubs bed in the area of St-Ursanne is located in the Oxfordian marls (Buxtorf 1920), which are stratigraphically located 240 m above the Opalinus Clay, it is supposed that the level of the Doubs bed remained, until the Jura folding, higher than the future Mont Terri Rock Laboratory. Therefore, the site of the future Mont Terri Rock Laboratory was still dominated by infiltration.
Between 10.5 and 3 My, the Jura folding greatly modified the topography in the area of St-Ursanne and Mont Terri (see Figure 4d): With the tectonic formation of the Mont Terri anticline, the site of the rock laboratory was uplifted to 513 m a.s.l.
The time at which the erosion level of the Doubs river became deeper than the level of the future Mont Terri Rock Laboratory cannot be precisely determined.
Based on data from the literature, the transfer of the hydrological system in the Opalinus Clay from an infiltration system (Doubs level higher than rock laboratory) to an exfiltration system (Doubs level lower than rock laboratory) occurred between 10.5 My (start of Jura folding) and 780'000 y (Most Extensive Glaciation).
In the following Chapter we try to estimate more precisely the time of the transfer from an infiltration to an exfiltration system at the future Mont Terri Rock Laboratory, taking into account our own ideas and interpretations.

2.3 Erosion scenario of the Doubs river system based on own interpretation

The following data from the literature were used to estimate the period when the erosion level of the Doubs bed reached the altitude (m a.s.l.) of the Mont Terri Rock Laboratory (see Figure 5):

- The Doubs channel reached its deepest level before the Most Extensive Glaciation (Buxtorf 1920), 780'000 y ago (Schlüchter & Müller-Dick 1996).
- This level is estimated at St-Ursanne at about 35 m below the present channel bottom, that is at about 400 m a.s.l. (Buxtorf 1920).
- The average level of the present Mont Terri Rock Laboratory is 513 m a.s.l.

These data are the basis for the following calculation:

Equation

$$t = \frac{dh}{Er} + C \quad [y] \text{ (equation 1)}$$

t time when the erosion level had the same height as the rock laboratory [y]

dh level difference between the Mont Terri Rock Laboratory and the deepest erosion level of the Doubs bed [m]

Er Erosion rate of the Doubs River [mm/y]

C Constant representing the time when the Doubs River bed reached its deepest level [y]

Values

dh = H2 – H1 = 113 m

H1 deepest level of the Doubs River before the Most Extensive Glaciation, at 400 m a.s.l.

H2 rock laboratory at 513 m a.s.l.

Er range: 0.05 mm/y < Er < 0.5 mm/y
(range between minimum and maximum erosion rate)

C = 780'000 y

Assumptions

- Several authors in Berger (1996) estimated the erosion rate for the molasse basin during the Mio-Pliocene. Their results are quite different depending on the region and time. The interval of erosion rate used here is an approximated range based on data published in Berger (1996).
- Equation 1 is valid for an uplift equal to zero mm/y during the last 3 My in the area of St-Ursanne. This value reflects the present situation in this region after Gugler (1991, map 5). We assume that the uplift rate was quite small. However, it is not certain that this uplift value was equal to zero during the last 3 My.
- Linear erosion rate: the effects of the glaciation on the erosion rate cannot be estimated. On one hand, the erosion rate could have been accelerated by drainage in front of the glaciers; on the other hand, it might also have been slowed during glaciation because water was retained in the glaciers. Equation 1 deals with a constant erosion rate.

Results

Two results were obtained by substituting the values into equation 1, t_{max} for a minimum erosion rate and t_{min} for a maximum erosion rate:

$t_{max} = (113\ m / 0.05 \cdot 10^{-3} m/y) + 780'000\ y = 3.04 \cdot 10^{6}\ y$

t_{max} ~3 My

$t_{min} = (113\ m / 0.5 \cdot 10^{-3}\ m/y) + 780'000\ y = 1.006 \cdot 10^{6}\ y$

t_{min} ~1 My

This estimation indicates that the Doubs River at St-Ursanne reached the level (m a.s.l.) of the future Mont Terri Rock Laboratory between 3 My and 1 My before present.
This period corresponds to a glacial period (Figure 6) called the «Schweizerische Deckenschotter» glaciations (Graf 1993).

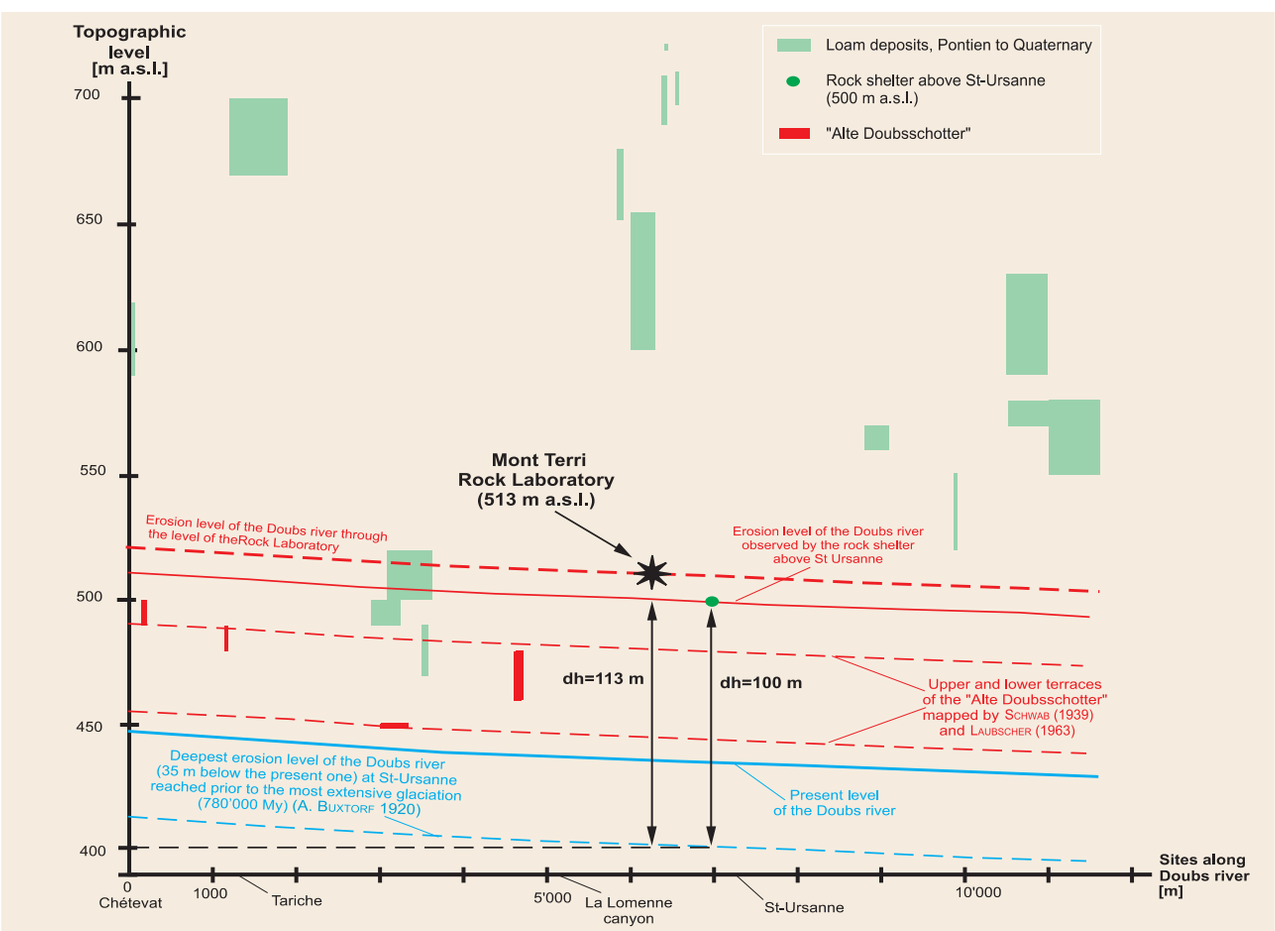

Figure 5: Erosion scenario based on own interpretation.

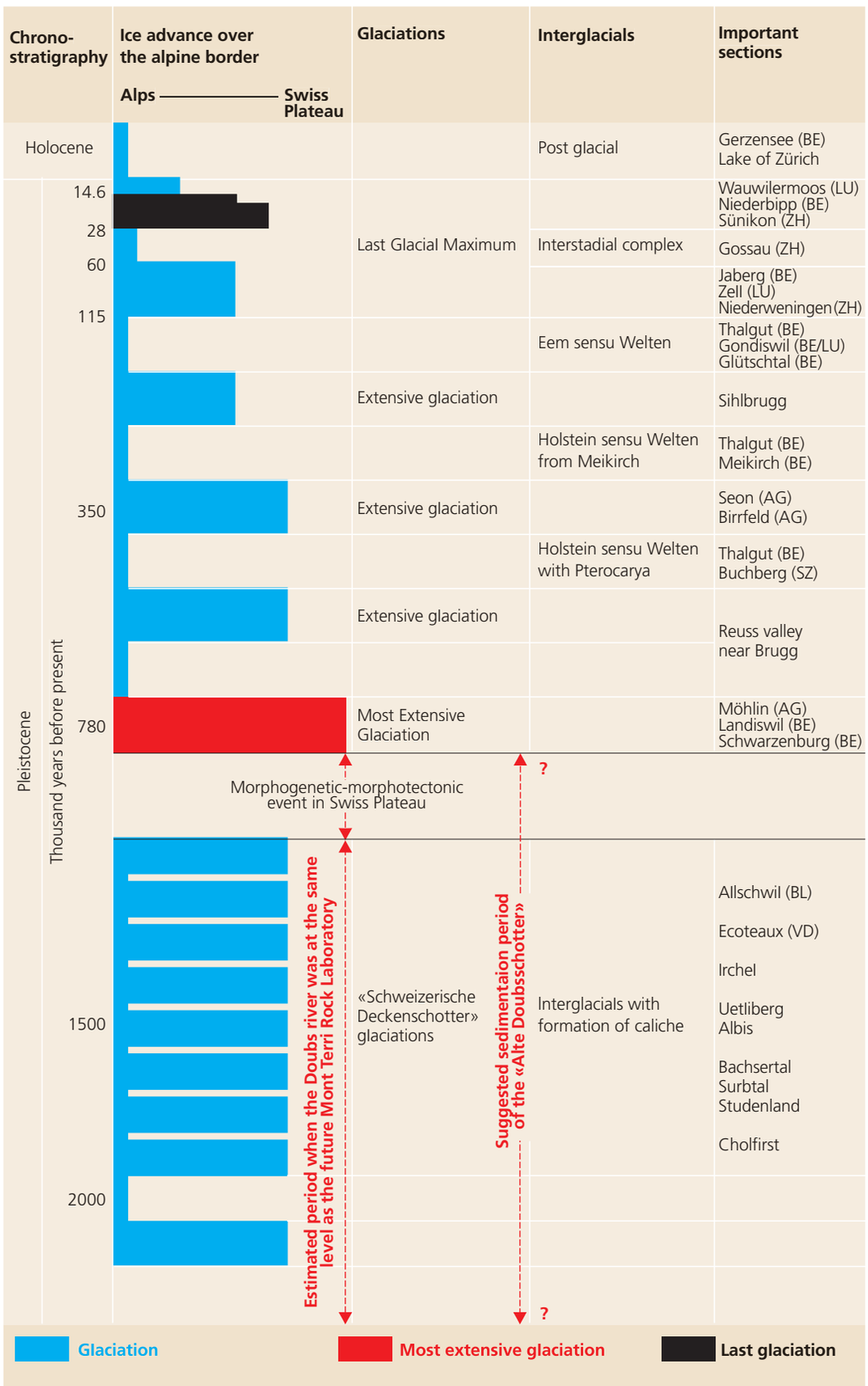

Figure 6: Dating of glacial periods in Switzerland. After Schlüchter & Müller-Dick (1996).

3 Erosion Scenario of the Mont Terri Anticline

In Chapter 2, the transition of an infiltration to an exfiltration regime in the region of the future Mont Terri Rock Laboratory is roughly dated. This change was mainly caused by the Doubs River, which was cutting down the sedimentary pile to an erosion level of more than 100 m below the future rock laboratory.
Another erosion process may have also had a great impact on the hydrological system in the Opalinus Clay. This is the erosion of the Mont Terri anticline. Furthermore, the groundwater chemistry of the whole sedimentary pile may have changed considerably when the water recharge from the surface (e.g. rain water) reached deeper lithostratigraphic units in the Mont Terri anticline.
In this context, a question of special interest is the time when the erosion level reached the karstic aquifers lying above the Opalinus Clay, and also the period when the erosion level was cutting down the Opalinus Clay in the region of the future Mont Terri Rock Laboratory.
To estimate these time periods, a similar approach was used as in the last chapter. To develop the erosion scenario of the Mont Terri anticline, the following information was needed:

- Maximum thickness of eroded strata
- Start of erosion (time)
- Present erosion level (deepest lithostratigraphic level in the Mont Terri anticline).

The method is briefly explained and the problem is solved with simple equations below.

Method

A stratigraphic pile of a certain thickness is eroded. When the erosion rate is known, the erosion times (i.e. time when erosion level reached corresponding lithostratigraphic unit) can be calculated by dividing the thickness of eroded strata by the erosion rate (see e.g. equation 4).
The maximum thickness of the stratigraphic pile above the Opalinus Clay in the area of St-Ursanne is estimated as about 1000 m (H.R. Bläsi, personal communication). The total of the thicknesses of the individual lithostratigaphic units above the Opalinus Clay and the now eroded Tertiary (and Cretaceous, if deposited at all) units gives a thickness of 820 m (without Opalinus Clay) or a thickness of 950 m (with Opalinus Clay) referred to column «Thickness» in Table 2.
The erosion rates can be calculated if the time of the erosion start is known, by simply dividing the total thickness of the eroded stratigraphic pile by the time when erosion started (see equations 2 and 3). The earliest erosion started in the Mont Terri anticline at the beginning of the Jura folding, which is 10.5 My. The latest date for beginning of erosion in the Mont Terri anticline is the end of the Jura folding at about 3 My (considering tectonics, it might well be that the Mont Terri anticline was formed at the end of the Jura folding period). Both values were included, resulting in a maximum erosion rate with start of erosion at about 3 My and a minimum erosion rate with start of erosion at about 10 My.

At present, the erosion level in the core of the Mont Terri anticline has reached the Keuper Marls of Late Triassic age. The pile of totally eroded strata results in a thickness of 1000 m (integration of thickness over all lithostratigraphic units, see Table 2).

Equations

$$Er_{max} = \frac{x_{tot}}{t_{min}} \quad \text{(equation 2)} \qquad Er_{min} = \frac{x_{tot}}{t_{max}} \quad \text{(equation 3)}$$

where

x_{tot} total thickness of eroded strata [mm]
t_{max} maximum duration of erosion [y]
t_{min} minimum duration of erosion [y]
Er_{max} maximum erosion rate [mm/y]
Er_{min} minimum erosion rate [mm/y]

$$t_1 = \frac{\sum_{i=1}^{9} x_i}{Er_{max}} \quad \text{(equation 4)} \qquad t_2 = \frac{\sum_{i=1}^{9} x_i}{Er_{min}} \quad \text{(equation 5)}$$

where

x_i thickness of lithostratighaphic unit(s), starting from top of the Keuper Marls (i = 1) through the youngest sediments, the molasse (i = 9) [mm]
i numbering of lithostratigraphic unit(s)
Er_{min} erosion rate, defined in equation 3 [mm/y]
Er_{max} erosion rate, defined in equation 2 [mm/y]
t_1 calculated minimum erosion time [y]
t_2 calculated maximum erosion time [y]

The minimum and maximum erosion times t_1 and t_2 are shown for each lithostatigraphic unit in Table 2 using units of million years (My).

Values

x_{tot} = $1 \cdot 10^6$ mm
x_i values defined in Table 2, column thickness, have to be changed into mm
i = 1,2,3....9, see Table 2, column numbering
t_{min} = $3 \cdot 10^6$ y
t_{max} = $10.5 \cdot 10^6$ y

No i	Lithostratigraphic unit	Main lithology	Stage		Thickness values [m][1]	Erosion time calculated [My][2] t_1	t_2
9	Molasse	marls, sandstones	Tertiary		~200	3.33	10.0
	Not defined in this study[3]	Not defined in this study[3]	Cretaceous				
	Twannbach Formation	limestones	Tithonian				
8	Reuchenette Formation	limestones with thin intercalations of marls	Kimmeridgian		~170	2.67	8.00
7	Courgenay Formation	limestones	Upper	Oxfordian	~230	2.10	6.30
	Vellerat Formation	marls and limestones	Middle				
	St-Ursanne Formation	limestones					
	Bärschwil Formation	shaly marls	Lower				
6	«Anceps-Athleta-Schichten» Dalle nacrée «Callovien-Ton»	marls limestones marly clay	Callovian		~30	1.33	4.00
5	Calcaire roux sableux	limestones	Bathonian		~20	1.23	3.70
4	Hauptrogenstein	(sandy) limestones			~120	1.17	3.50
3	«Lower Dogger»	(sandy) limestones	Bajocian		~50	0.77	2.30
2	**Opalinus Clay**	**shales (silty and sandy)**	**Aalenian**		**~130**	0.60	1.80
1	Jurensis Marls Posidonia Shales	marls and marly shales bituminous shales	Toarcian		~50	0.17	0.50
	Not defined in this study[3]	Not defined in this study[3]	Pliensbachian				
	Gryphaea Limestones	limestones	Sinemurian				
	Not defined in this study[3]	Not defined in this study[3]	Hettangian			recent	recent
	Keuper Marls	marls and anhydrite	Upper Triassic				

[1] Average thickness (after Laubscher, 1948; H.R. Bläsi, personal communication).

[2] Time when erosion level reached corresponding lithostratigraphic unit: t_1 is based on erosion rate of 0.3 mm/y (erosion started at end of Jura folding, 3 My); t_2 is based on erosion rate of 0.1 mm/y (erosion started at beginning of the Jura folding, 10.5 My).

[3] It is still not known whether these lithostratigraphic units and lithologies were eroded or not at all deposited.

Table 2: Erosion scenario of the Mont Terri anticline.

Assumptions

- Constant erosion rates were applied over the whole eroded thickness. No distinction was made between «soft» strata with higher erosion rates and «hard» strata with lower erosion rates.
- Erosion rates did not change with time.
- Erosion start: not precisely known. Two possibilities were studied: erosion started at 10.5 My (beginning of Jura folding) and at 3.3 My (end of Jura folding).

Results

The maximum erosion rate Er_{max} is 0.3 mm/y and the minimum erosion rate is 0.1 mm/y. The calculated erosion times for the corresponding lithostratigraphic unit(s) are shown in Table 2. Two erosion times t_1 (minimum erosion time) and t_2 (maximum erosion time) are indicated in Table 2. These erosion times are related to maximum and minimum erosion rates, respectively.

The following results were obtained for the Opalinus Clay:

- The erosion surface reached the karstic aquifers lying above the Opalinus Clay (Tripet et al., 1990) between 3.7 and 1.2 My.
- The erosion surface reached the top of Opalinus Clay between 1.8 and 0.6 My.
- The erosion surface reached the base of Opalinus Clay between 0.5 and 0.2 My.

If the means between maximum and minimum erosion times are taken, the erosion surface reached the top of the Opalinus clay at 1.2 My and the base at 0.35 My. The time difference between minimum and maximum erosion times can also be considered as the uncertainty affecting the erosion process. Then the top of the Opalinus Clay was reached at 1.2 ± 0.6 My and the base at 0.35 ± 0.15 My. These results are graphically shown in Figure 7.

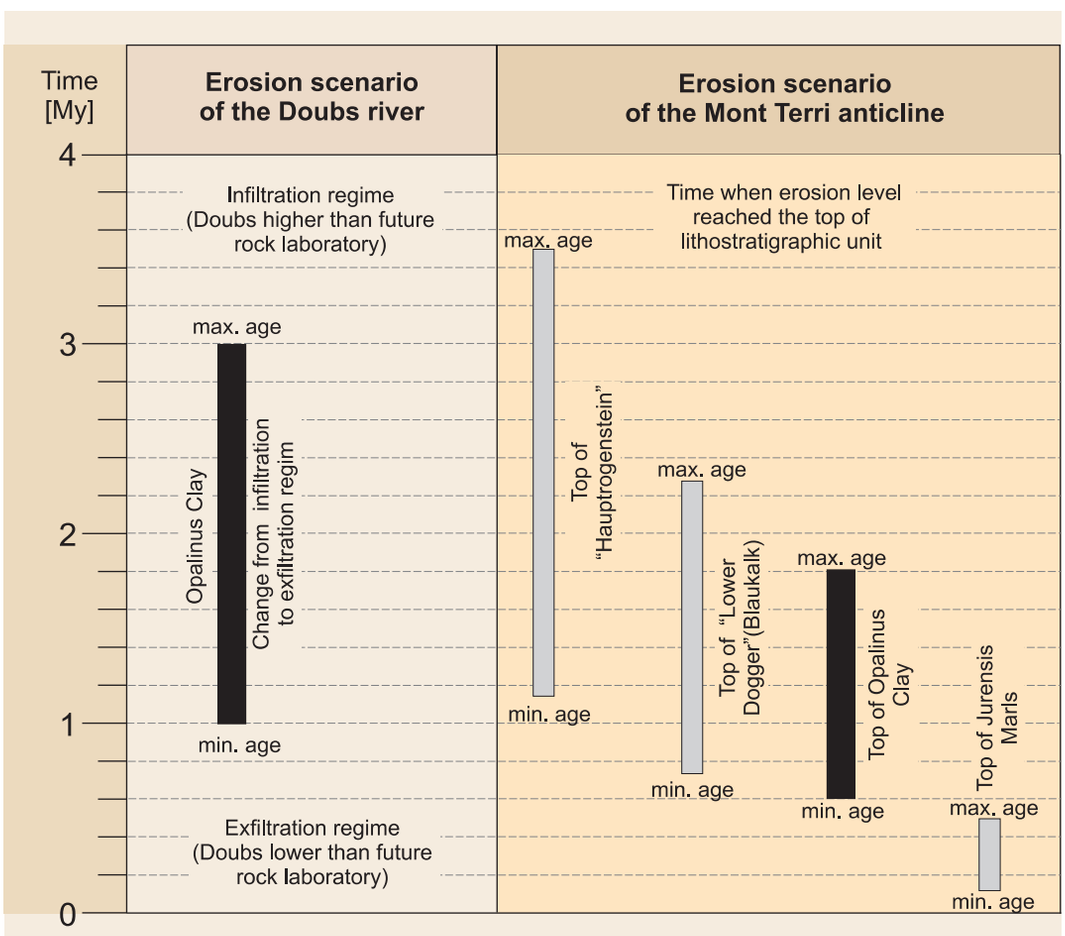

Figure 7: Results of erosion scenarios (see text for details).

4 Discussion and Conclusion

The paleohydrological impact on the future Mont Terri Rock Laboratory is mainly determined by the following two events:

- The progressive downward erosion of the Doubs valley responsible for the changing groundwater flow directions in the Opalinus Clay (from infiltration to exfiltration)
- The progressive erosion of the Mont Terri anticline, affecting flow directions and mainly groundwater chemistry.

Two erosion scenarios, one for the Doubs river valley and the other for the Mont Terri anticline, are presented. The results of these 2 scenarios are compiled in Figure 7. On the left hand side of Figure 7, the time period is shown, when the hydrological system in the Opalinus Clay of the future rock laboratory passed from an infiltration system (level of Doubs River higher than rock laboratory) to an exfiltration system (level of Doubs River lower than rock laboratory). This period could be limited to a time span between 3 and 1 My. The time difference can also be considered as uncertainty. Then the transition from an infiltration to an exfiltration system, relative to the level of the future rock laboratory, can be dated at 2 ± 1 My. On the right hand side of Figure 7, the time periods are shown, when the erosion level of the Mont Terri anticline reached the top of the Hauptrogenstein, «Lower Dogger» (both aquifers above the Opalinus Clay, the latter in contact with the Opalinus Clay), Opalinus Clay and Jurensis Marls. The erosion level reached the top of Opalinus Clay at 1.2 ± 0.6 My and its base at 0.35 ± 0.15 My.

It is important to note that these date estimations have been obtained with a certain number of assumptions and approximations. The uncertainty of the geological input data is quite high. These uncertainties include data of the poorly, or even undated, Quaternary sediments and lack of information concerning deposition of Tertiary, Cretaceous and Upper Jurassic strata. For this reason, values such as the total thickness of sedimentary pile have to be considered as first estimates. The uncertainty of both scenarios (Doubs River valley and Mont Terri anticline) was estimated by deriving or defining different erosion rates.

The results of this study, which are based on a literature survey and on our simple analytical analyses, may serve as a first base for the hydrogeological characterization around the Mont Terri Rock Laboratory. However, to improve the process of such a characterization, more work needs to be done. First, precise structural profiles, both horizontal and vertical, which are volume balanced, are needed. Secondly, the knowledge of the quaternary deposits (regional distribution, sedimentary structures, dating) around St-Ursanne has not changed since the early nineteen sixties. Such data are most important for the derivation of sound erosion scenarios. Thirdly, in-situ measurements of hydraulic potentials above and below the Opalinus Clay formation should be performed in order to determine the present regional flow field. It might be possible to reactivate the old boreholes of the Mont Terri motorway tunnel, which have been drilled from the surface towards the tunnel system. Finally, erosion scenarios could be numerically modelled, taking into account also processes such as regional uplift and non-linear erosion rates, which have been oversimplified in our study.

Acknowledgements

We would like to thank J.-P. Tripet, M. Thury and P. Heitzmann of the Federal Office for Water and Geology, who initiated this study and were open to many fruitful discussions and suggestions.
We also are grateful for valuable guidance and numerous suggestions from the following reviewers: A. Gautschi (Nagra) and C. Deguèldre (Paul Scherrer Institute) who suggested, in their first review, adding a chapter on the erosion scenario of the Mont Terri anticline. Peter Huggenberger (University of Basel, Cantonal Geologist of Basel) made numerous concrete remarks and propositions that improved the general understanding of the study.
We also thank J.-P. Berger (University of Fribourg), J.-C. Bouvier (OEPN, Canton Jura, retired) and H.-R. Bläsi (University of Berne) for their input and cordial collaboration, as well as F. Haug for the English corrections.

References

Allen, P. A., Mange-Rajetsky, M., Matter, A. & Homewood, P. (1985): Dynamic paleogeography of the open Burdigalian seaway, Swiss Molasse basin. – Eclogae geol. Helv. 78/2, 351–381.

Berger, J.-P. (1996): Cartes paléogéographiques-palinspastiques du bassin molassique suisse (Oligocène inférieur-Miocène moyen). – N. Jb. Geol. Paläont. Abh. 202/1, 1–44.

Bolliger, T., Engesser, B. & Weidmann, M. (1993): Première découverte de mammifères pliocènes dans le Jura neuchâtelois. – Eclogae geol. Helv. 86/3,1031–1068.

— (1995): Pliozäne Kleinsäuger aus den Höheren Deckenschotter des Irchels (Kt. Zürich). – Abstract geol. Soc. Switzerland, SANW-Tagung St. Gallen 1995, 36.

Bouvier, J.-C. (1997): Hydroécologie, la boucle helvético-française du Doubs. – Bull. Soc. Hist. nat. Pays de Montbéliard 1997, 167–186.

Buxtorf, A. (1920): Zur Frage der Pliozänbildungen im Nordschweizerischen Juragebirge. – Verh. natf. Ges. Basel 31, 113–132.

Diebold, P., Laubscher, H., Schneider, A. & Tschopp, R. (1963): Blatt 1085 St-Ursanne. – Geol. Atlas Schweiz 1 : 25 000, Karte 40.

Gigon, R. & Wenger, R. (1986): Inventaire spéléologique de la Suisse, II, Canton du Jura. – Comm. Spéléol. Soc. helv. Sci. nat., Porrentruy.

Gugler, E. (1991): First Order Levelling Network in Switzerland. – Rapp. sur les travaux géodésiques 87–91, Comm. géodés. suisse, ETH Zürich.

Graf, H.R. (1993): Die Deckenschotter der zentralen Nordschweiz. – Diss. ETH Zürich Nr. 10205.

Kälin, D. (1993): Stratigraphie und Säugetierfaunen der Oberen Süsswassermolasse der Nordwestschweiz. – Diss. ETH Zürich Nr. 10152.

— (1997): Litho- und Biostratigraphie der mittel- bis obermiozänen Bois des Raube-Formation (Nordwestschweiz). – Eclogae geol. Helv. 90/1, 97–114.

Laubscher, H. (1948): Geologie des Gebietes von Siegfriedblatt St-Ursanne. – Beitr. geol. Karte Schweiz [N. F.] 92.

— (1961): Die Fernschubhypothese der Jurafaltung. – Eclogae geol. Helv. 54/2, 221–282.

— (1962): Die Zweiphasenhypothese der Jurafaltung. – Eclogae geol. Helv. 55/1, 1–22.

— (1963): Blatt 1085 St-Ursanne. – Geol. Atlas Schweiz 1 : 25 000, Erläut. 40.

— (1987): Die tektonische Entwicklung der Nordschweiz. – Eclogae geol. Helv. 80/2, 287–304.

— (1992): Jura kinematics and the Molasse Bassin. – Eclogae geol. Helv. 85/3, 653–675.

— (1998): Der Ostrand des Laufenbeckens und der Knoten von Grellingen: Die verwickelte Begegnung von Rheingraben und Jura. – Eclogae geol. Helv. 91/2, 275–291.

Liniger, H. (1966): Das Plio-Altpleistozäne Flussnetz der Nordschweiz. – Regio basil. 7/2, 158–177.

Schlüchter, C. & Müller-Dick, K. (1996): Das Eiszeitalter der Schweiz. – Stiftung Landschaft und Kies, Ostermundigen.

Schwab, E. (1939): Morphologie der Freiberge (Berner Jura). – Mitt. geogr.-ethnol. Ges. Basel V, 1935–38, 1–135.

Thury, M. & Bossart, P. (1999): Mont Terri Rock Laboratory – Results of the hydrogeological, geochemical and geotechnical experiments performed in 1996 and 1997. – Geol. Rep. 23, Federal Office for Water and Geology.

Tripet, J.-P., Brechbühler, Y.-A., Haarpaintner, R.-T. & Schindler, B. (1990): Hydrogéologie des milieux à faible perméabilité: étude des marnes aaléniennes dans la galerie de reconnaissance du Mont Terri (Canton du Jura). – Bull. Soc. neuchât. Sci. nat. 113, 179–189.

The Stress Field in the Mont Terri Region Data Compilation

P. Bossart[1] & S. Wermeille[1]

[1]Institut Géotechnique SA, St-Ursanne

Abstract

A compilation of stress measurements in the Jura mountains with special emphasis to the Mont Terri Rock Laboratory is presented in this report. The Mont Terri Rock Laboratory is located in the Canton of Jura near St-Ursanne, Switzerland. Seven different methods were applied to derive qualitatively and quantitatively stress directions and magnitudes: 1) mapping or scanning of breakouts along boreholes, 2) doorstopper strain cell measurements, 3) triaxial strain cell measurements, 4) borehole slotter measurements, 5) hydraulic fracturing, 6) undercoring method and 7) rock-mechanical modelling. The interpretation of the measurements is not straightforward, especially when an anisotropic stress field together with a pronounced rock anisotropy exists, as it is the case in the Opalinus Clay.
The primary stress field could be identified in the Opalinus Clay of the Mont Terri Rock Laboratory.
The undercoring and hydraulic fracturing methods gave comparable results whereas the borehole slotter method resulted in quite unlikely stress values. Interpretation of the measurement was mainly done with rock mechanical modelling, which led to the most likely stress data set.
The obtained stress field in the Mont Terri Rock Laboratory is different from the regional stress field in the Canton of Jura. This finding is discussed and a possible interpretation is given.

Recommended quotation:
Bossart, P. & Wermeille, S. (2003): The Stress Field in the Mont Terri Region – Data Compilation. In: Heitzmann, P. & Tripet, J.-P. (Ed.): Mont Terri Project – Geology, Paleohydrology and Stress Field of the Mont Terri Region (p. 65–92). – Reports of the Federal Office for Water and Geology (FOWG), Geology Series 4.

Unpublished report of Oct. 14, 1999; updated Sept. 1, 2002

Resumé

Le présent rapport consiste en une compilation de mesures de contraintes effectuées dans la chaîne du Jura. Elles mettent l'accent sur le site du laboratoire souterrain du Mont Terri, situé près de St-Ursanne, dans le canton suisse du Jura. Sept méthodes différentes ont été appliquées pour déterminer qualitativement et quantitativement le champ de contraintes: 1) relevé des éclats de roche le long des trous de sondage; 2) mesures au moyen d'une cellule de type «doorstopper strain cell»; 3) mesures au moyen d'une cellule de type «triaxial strain cell»; 4) mesures au «borehole slotter»; 5) fracturation hydraulique; 6) sous-carottage; 7) modélisation sous l'angle de la mécanique des roches. L'interprétation des mesures est malaisée, en particulier lorsqu'un champ de contraintes anisotrope se superpose à une anisotropie marquée de la stratification, comme c'est notamment le cas dans les Argiles à Opalinus.
Il a été possible de déterminer le champ de contraintes primaire dans les Argiles à Opalinus du laboratoire souterrain du Mont Terri. Les méthodes du sous-carottage et de la fracturation hydraulique ont livré des résultats similaires, tandis que les essais au «borehole slotter» n'ont pas pu être interprétés. Le champ de contraintes le plus probable a été établi en s'appuyant sur des modèles de mécanique des roches.
Le champ de contraintes primaire identifié au voisinage du laboratoire souterrain du Mont Terri diffère du champ régional qui règne dans le Canton du Jura. Ce résultat fait l'objet d'une discussion et d'une proposition d'explication.

Zusammenfassung

Der Inhalt des vorliegenden Berichtes besteht aus einer Zusammenstellung von Stressmessungen aus dem Juragebirge unter besonderer Berücksichtigung des Felslabors Mont Terri, welches bei St-Ursanne im Kanton Jura liegt. Insgesamt kamen sieben Methoden zur qualitativen und quantitativen Bestimmung des Stressfeldes zur Anwendung. Es sind dies 1) Aufnahmen von Bohrlochrand-Ausbrüchen, 2) sogenannte «Doorstopper Strain Cell»- und 3) «Triaxial Strain Cell»-Messungen, 4) Bohrlochschlitz-Messungen, 5) die Methode des hydraulischen «Fracturings», 6) die Unterbohrmethode und 7) die felsmechanische Modellierung. Die Interpretation der Messungen ist nicht einfach, vor allem, wenn es sich wie beim Opalinus Ton um ein anisotropes Stressfeld kombiniert mit einer deutlichen Schichtungsanisotropie handelt.
Im Mont Terri Felslabor war es möglich, das primäre Stressfeld zu ermitteln. Die Unterbohrmethode und das hydraulische «Fracturing» ergaben vergleichbare Resultate, wohingegen die Bohrlochschlitz-Versuche nicht interpretierbar waren. Unter Zuhilfenahme der felsmechanischen Modellierung konnte das wahrscheinlichste Stressfeld abgeleitet werden.
Das primäre Stressfeld im Bereich des Mont-Terri-Felslabors ist mit dem regionalen Stressfeld des Kanton Juras nicht vergleichbar. Diese Resultate werden diskutiert und es wird versucht, eine mögliche Interpretation dafür zu geben.

Glossary

σ_1 maximum principal stress, magnitude in [MPa], direction in [°].

σ_2 intermediate principal stress, magnitude in [MPa], direction in [°].

σ_3 minimum principal stress, magnitude in [MPa], direction in [°].

S_H maximum horizontal stress, magnitude in [MPa], direction in [°].

S_h minimum horizontal stress, magnitude in [MPa], direction in [°].

S_V maximum vertical stress, magnitude in [MPa], direction in [°].

σ_{max} major stress (in a 2D-section), magnitude in [MPa], direction in [°].

σ_{min} minor stress (in a 2D-section), magnitude in [MPa], direction in [°].

Aspect ratio of principal stress:

The aspect ratio R is defined as the ratio of the largest to the smallest stress magnitude. Example: σ_1 = 10 MPa and σ_3 = 2 MPa, then R = 5.

Basement:

- In the sense of Nagra and Becker, «Grundgebirge»: rocks older than Triassic, including sediments of Permo-Carboniferous Trough (Becker et al. 1984; Blümling 1986; Müller et al. 1987; Becker 1989; Becker & Werner 1995; Becker 1999; Becker 2000).
- In the sense of the present report: crystalline and sedimentary rocks lying below the main overthrust (basal décollement in the Triassic evaporites).

Cover:

- In the sense of Nagra and Becker, «Deckgebirge»: sedimentary rocks younger than Permian (Becker et al. 1984; Blümling 1986; Müller et al. 1987; Becker 1989; Becker & Werner 1995; Becker 1999; Becker 2000).
- In the sense of the present report: sedimentary rocks lying above the main overthrust (basal décollement in the Triassic evaporites).

Mechanically-induced breakouts:

- Breakouts mainly influenced by the mechanical strength anisotropy of the rock. In the Opalinus Clay of the Mont Terri Rock Laboratory, the rock anisotropy is related to bedding planes.

Stress-induced breakouts:

- Breakouts mainly influenced by stress anisotropy (e.g. $\sigma_1 >> \sigma_3$).

Table of Contents

Abstract 66
Resumé 67
Zusammenfassung 67
Glossary 68
1 Introduction 70
2 Regional Stress Measurements in the Jura Mountains 71
2.1 Methods 71
2.2 Results of regional stress measurements 71
2.3 Published interpretations 74
3 Derivation of the Primary Stress Field in the Mont Terri Rock Laboratory 76
3.1 The borehole slotter technique 76
3.2 The undercoring technique 78
3.3 Hydraulic fracturing 79
3.4 Stress conditions from geological observations 80
3.4.1 Small-scale mapping of niche walls 80
3.4.2 Borehole wall mapping with a borehole camera 81
3.4.3 Mapping of breakouts by caliper logging 84
3.5 Stress conditions from rock-mechanical modelling 84
3.6 The primary stress field at Mont Terri 87
4 Conclusions and Recommendations 89
Acknowledgements 90
References 91

1 Introduction

The determination of stresses in the Mont Terri Rock Laboratory is of basic importance for several experiments dealing with the mechanical, hydraulic and chemical properties of the Opalinus Clay. Knowledge of stress directions and magnitudes is also very important when designing and constructing new galleries in the Opalinus Clay, as was done between 1989 and 1995 (security gallery and motorway tunnel) and in 1997/1998 (construction of the new gallery of the Mont Terri Rock Laboratory). Since 1996, several measurements have been carried out in the rock laboratory and many geological observations are available from which stresses within the Opalinus Clay could be derived. These measurements and observations are documented in several Technical Notes of the Mont Terri Project. When reading these Technical Notes, often it is not easy to get a comprehensive picture about the stress conditions because there are many contradictions concerning the measured stresses. One aim of this study is to compile the completed stress measurements and to identify the most reliable and likely stress data at the site of the Mont Terri Rock Laboratory. A further objective of this study is to embed these local stress findings in a regional geologic setting, in the northern Jura Mountains of Switzerland. Stress directions were derived in geological environments other than the Opalinus Clay and mainly at other depths than in the rock laboratory. These regional stresses are taken into account and compared with the ones found at the Mont Terri Rock Laboratory.

In subsequent chapters, this report displays first the present regional stress field observed in the Jura Mountains, which is also documented in the literature (Chapter 2). Then, the methods and results of stress measurements, stability observations in boreholes in the framework of the Mont Terri Project and the results of a rock-mechanical modelling study are compiled and discussed (Chapter 3). These measurements and observations result in the selection of the most likely stress data set, which represents the state of the art and should be used as reference in other experiments. Finally, conclusions and recommendations are drawn (Chapter 4).

2 Regional Stress Measurements in the Jura Mountains

Before investigating local stresses occurring in the area of the Mont Terri Rock Laboratory, it is important to have an overview of both the regional stresses occurring in the Jura Mountains and of the present tectonic situation. The question of whether the Jura still is an active thin-skinned foreland fold-and-thrust belt has to be answered. If this is the case, there should be evidence of a decoupled stress field between «basement» and «cover»[1] because of active overthrusting in the Triassic evaporite sequences.
Present regional stresses in the Jura Mountains were compiled from the literature. Becker et al. (1984), Müller et al. (1987), Becker (1989) and Becker & Werner (1995) focused their works on the determination of principal horizontal stresses (S_H, S_h) in the northern Jura Mountains and foreland. Recently, Becker (1999, 2000) published new results based on a larger number of measurements that were distributed over the entire Jura Mountains. Stress measurements from the Mont Terri Rock Laboratory are presented and discussed in detail in Chapters 3 and 4.

2.1 Methods

Five different methods were used to determine principal horizontal stresses in the Jura Mountains. The first method consists of logging breakouts along boreholes. In isotropic rocks and vertical boreholes, these breakouts may define the direction of the minimum horizontal stress (S_h). The second and third methods are the doorstopper and triaxial strain cell methods, respectively. Both methods are known as overcoring techniques (Müller et al. 1987; Becker & Werner 1995) and both techniques measure relaxation strains during and after the overcoring of a borehole. Strain release of a core sample after overcoring can be measured with the aid of strain gauge rosettes. These rosettes are attached to the borehole wall before overcoring, either at the bottom of the borehole, as in the case of the doorstopper method, or to the wall of the pilot borehole, as in the case of the triaxial cell method. The fourth is the borehole slotter method, used by Bock (1986) and Becker & Werner (1995). This method measures the strain release occurring during and after the cutting of slots into a borehole wall (technique detailed in Chapter 3.1). The fifth method is the hydraulic fracturing method (Haimson & Fairhurst 1967; Hickman & Zoback 1983; Bühler 1997 and Evans et al. 1999). This method directly measures stresses by injecting a test fluid into a borehole. The pressure is then raised until a breakdown, due to the creation of an artificial fracture, is measured. This method and its basic assumptions are described in more detail in Chapter 3.3.
The undercoring method (not used for regional derivation) was only applied in the Mont Terri Rock Laboratory and therefore not mentioned here. This method is described in more detail in Chapter 3.2.
Stress measurements were carried out in a variety of geological formations in the Jura Mountains and also at different tectonic levels. Each method used to derive stresses is complex and must also take into account other parameters such as the elastic parameters of a rock, or its anisotropy. The main published stress investigation results are presented below.

[1] The terms «basement» and «cover» are used differently in the literature. A definition is given in the glossary (sensu Nagra and Becker, sensu present report).

2.2 Results of regional stress measurements

Directions of the maximum horizontal stress (S_H), obtained with the five measurement methods, are compiled in Table 1 and in Figure 1. In Table 1, a number was assigned for each test site corresponding with Figure 1. For each site, the applied measurement method, S_H-direction, the type of lithology in which measurements were taken and references are listed in Table 1. In the column labelled S_H-direction, a B for «basement» or a C for sedimentary «cover» was added to specify whether the measurement was taken in the «basement» or in the «cover» (in the sense of Nagra and Becker, see glossary).

Results from borehole breakout observations

The borehole breakout method was used in five deep boreholes drilled by Nagra: Böttstein, Kaisten, Weiach, Riniken and Schafisheim (Becker et al. 1984; Blümling 1986 and Müller et al. 1987). Four of these five boreholes were drilled into the «basement» (in the sense of the present report, see glossary). Only one borehole, the Schafisheim borehole, was drilled from the «cover» into the «basement» (green and red in Figure 2). Thus, the Schafisheim borehole is the only borehole crossing the main overthrust (basal «décollement») which is located in the Triassic evaporites.
Figure 2 shows, for each of these five boreholes, the direction of breakouts along the holes. These breakout directions are parallel to the minimum horizontal stress (S_h) directions. The maximum horizontal stresses (S_H) are simply the directions perpendicular to S_h. In near-surface rocks (< 300 m), the general breakout direction is 140°±10°, resulting in a NE-SW trending S_H-direction except for the Schafisheim borehole, where no breakouts are available in the first 300 m. In deeper levels (> 300 m), the breakout directions vary between 25° and 70° with a mean of almost 45°, resulting in NW-

SE S_H-directions. Of special interest is the Schafisheim borehole, where a clear change in breakout direction is observed across the main overthrust. The corresponding S_H-directions change from a NNE-SSW direction (above the main overthrust) to a NW-SE direction (below the main overthrust). It is important to mention that this change in breakout directions was recorded at a depth of about 1400 m and is therefore beyond the near-surface zone.

Results from doorstopper strain cell measurements

Doorstopper measurements were applied in nine quarries: Endingen, Dielsdorf, Häfelfingen, Zunzgen, Hollwanger Hof, Kleinkems, Autechaux, La Balme and Menzenschwand (Becker et al. 1984; Müller et al. 1987; Becker & Werner 1995). These measurements were all taken in near-surface Jurassic limestones (< 10 m below surface), except in Hollwanger Hof where Triassic limestones (Upper Muschelkalk) were investigated and in Menzenschwand where the measurement was taken in granite. Results give heterogeneous S_H-directions: E-W for Endingen, NW-SE for Dielsdorf, Zunzgen, Menzenschwanden and Autechaux, NNE-SSW for Häfelfingen, NE-SW for Hollwanger Hof and La Balme, N-S for Kleinkems.

Results from triaxial strain cell measurements

Triaxial strain cell measurements were taken in four quarries and one tunnel: Trept, Schönmatt, Bintal, Krunkelbach and Sonnenberg tunnel (Müller et al. 1987; Becker & Werner 1995). Measurements at the first three locations were completed in near-surface Jurassic limestones (< 25 m below surface). In Krunkelbach, measurements were conducted in near-surface granite

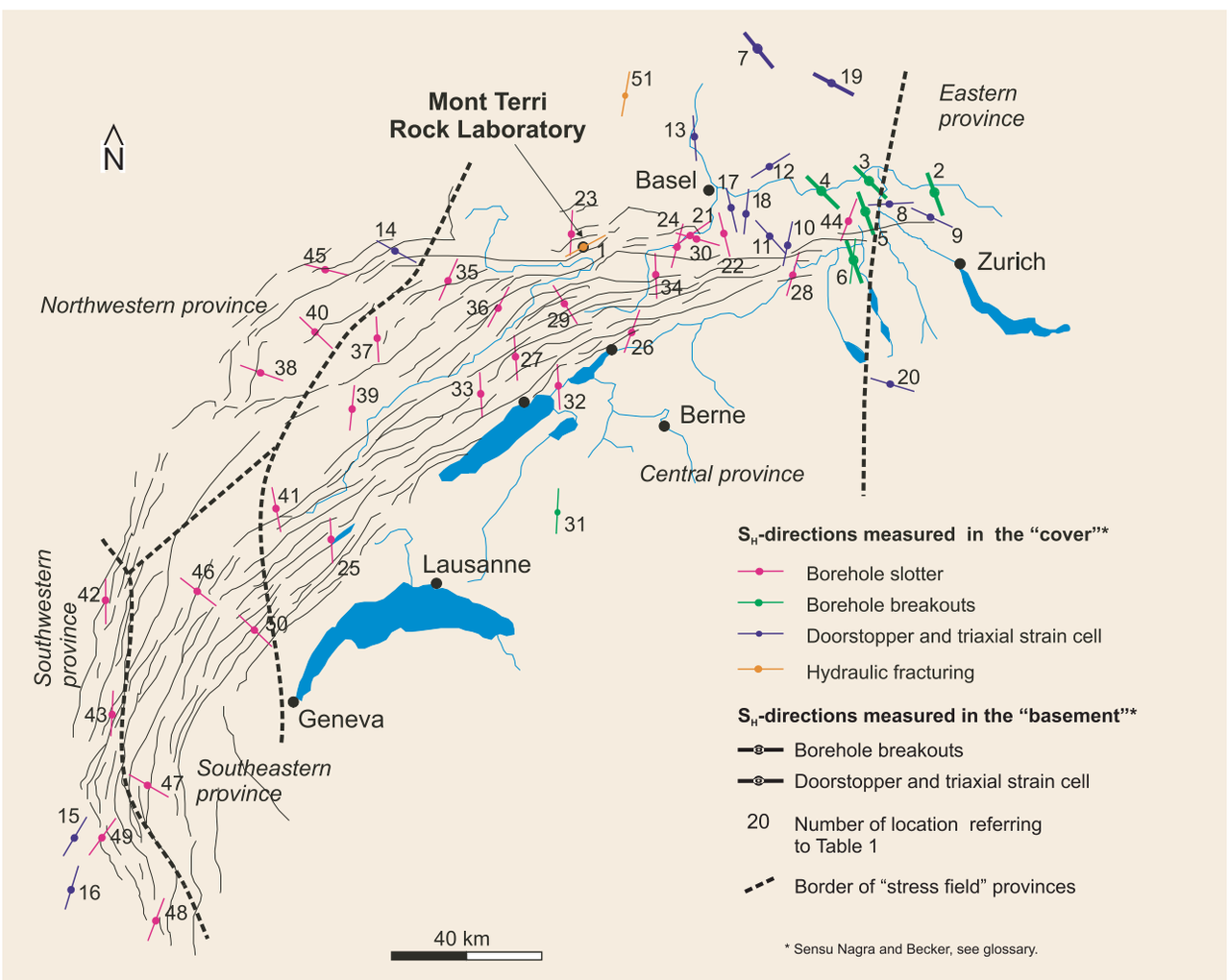

Figure 1: Recent maximum horizontal stress directions in the «basement» and the sedimentary «cover» of the Jura Mountains (sensu Nagra and Becker, see glossary). Data compiled from the literature (see also Table 1).

No	Test site	Technique	S_H-direction [°] B = «basement»* C = «cover»**	Geology	References
1	Mont Terri	Undercoring, hydraulic fracturing	C ENE- WSW	Opalinus Clay	Bigarré & Lizeur (1997) Evans et al. (1999)
2	Weiach	Borehole breakouts	B 160±10	Entire stratigraphic sequence: from sedimentary cover to crystalline	Becker et al. (1984)
3	Böttstein		B 135±10		Blümling (1986)
4	Kaisten		B 135±10		Müller et al. (1987)
5	Riniken		B 160±10		Becker (1989)
6	Schafisheim		C 7±10 B 160±10		Becker & Werner (1995)
7	Menzenschwand	Doorstopper strain cell	B ~141	Granite	Becker (2000)
8	Endingen		C 87±8	Jurassic limestones	Müller et al. (1987)
9	Dielsdorf		C 115±6	Jurassic (Oxfordian) limestones	Becker (1989) Becker & Werner (1995)
10	Häfelfingen		C 12±14	Jurassic (Bathonian) limestones	Becker et al. (1984)
11	Zunzgen		C 138±12	Jurassic (Bajocian) limestones	Blümling (1986)
12	Hollwanger Hof		C 58±31	Triassic limestones, Upper Muschelkalk	Müller et al. (1987)
13	Kleinkems		C 176±13	Jurassic (Oxfordian-Rauracian) limestones	Becker (1989) Becker & Werner (1995)
14	Autechaux	Triaxial strain cell	C 119±28	Jurassic (Oxfordian-Sequanian) limestones	Becker & Werner (1995)
15	La Balme		C 31±31	Jurassic (Bajocian) limestones	
16	Trept		C 17±22	Jurassic (Bajocian) limestones	
17	Schönmatt		C 167±2	Jurassic (Bajocian) limestones	Müller et al. (1987)
18	Bintal		C 6±31	Jurassic (Bajocian) limestones	Becker (1989) Becker & Werner (1995)
19	Krunkelbach	Borehole slotter	B ~118	Granite	Becker (2000)
20	Sonnenberg tunnel		C ~107	Sandstone	
21	Laufen 2		C 55±22	Jurassic (Oxfordian-Sequanian) limestones	Becker & Werner (1995)
22	Seewen		C 166±21	Jurassic limestones, mainly in competent Dogger and Malm formations (no detailed information available)	Becker (1999; 2000)
23	Courchavon		C 3±19		
24	Liesberg		C 15±25		
25	Le Sentier		C 177±17		
26	Vauffelin		C 20±19		
27	La Chaux-de-Fonds		C 176±16		
28	Olten		C 16±14		
29	Le Bémont		C 148±16		
30	Brislach		C 106±22		
31	Villarlod		C 3±17		
32	Cornaux		C 177±23		
33	La Chaux-du-Milieu		C 177±10		
34	Courrendlin		C 178±19		
35	Sancey-le-Long		C 24±27		
36	Maîche		C 28±21		
37	Valdahon		C 177±13		
38	Samson		C 110±15		
39	Sombacour		C 6±15		
40	Mérey-sous-Montrod		C 134±24		
41	Bief-des-Maisons		C 169±20		
42	Véria		C 180±7		
43	Villette		C 3±18		
44	Linn		C 21±10		
45	Marchaux		C 104±14		
46	Meussia		C 128±19		
47	Hauteville		C 120±25		
48	Cordon		C 21±8		
49	Villebois		C 36±12		
50	Lamoura		C 134±11	Cretaceous limestones	
51	Wittelsheim	Hydraulic fracturing	C ~10	Evaporite	Becker (2000)

*Sensu Nagra and Becker, «Grundgebirge». See glossary. **Sensu Nagra and Becker, «Deckgebirge». See glossary.

Table 1: Compilation of S_H-directions measured in the «basement» and the sedimentary «cover» of the Jura Mountains (sensu Nagra and Becker, see glossary). Based on literature survey (see references).

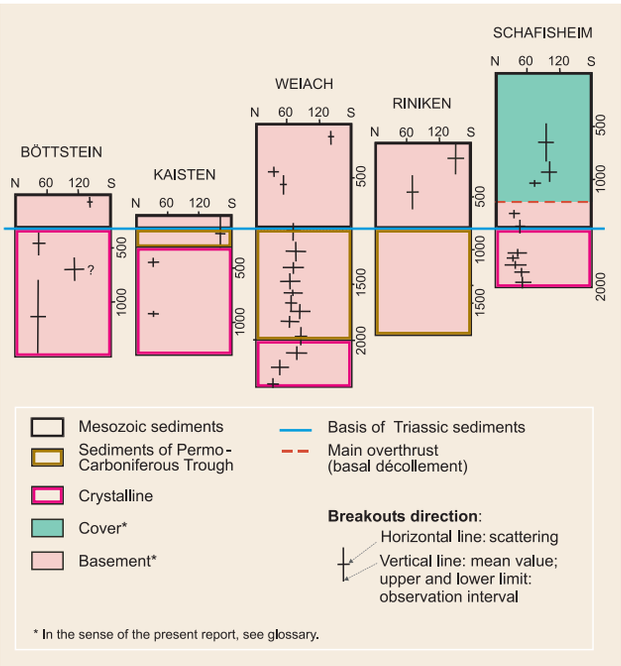

Figure 2: Average direction values of breakouts measured in five deep boreholes in the northern Jura Mountains and foreland, after Müller et al. (1987), modified. Directions in [°].

(~5 m below surface), and in the Sonnenberg tunnel, sandstones were investigated. In Trept and Bintal, S_H shows a NNE-SSW direction. In Schönmatt, a NNW-SSE S_H-direction was obtained. Both in Krunkelbach and the Sonnenberg tunnel, ESE-WNW S_H-directions were observed.

Results from borehole slotter measurements

Becker (1999, 2000) recently published new stress data obtained with the borehole slotter method. All measurements, taken in boreholes, were conducted in near-surface (<17 m) limestones (mostly Jurassic limestones, Hauptrogenstein and one in Cretaceous Limestones at Lamoura). These data cover the entire Jura Mountains (Table 1 and Figure 1). Becker (1999, 2000) recognised five stress field provinces based on similar S_H-directions (Figure 1). These are:

- A central province characterised by NNW-SSE to NNE-SSW S_H-directions. This province extends from the north of Basel to the Prealps front including the Rhine Graben and the Cantons of Basel, west part of Aargovia, Solothurn, Berne and Fribourg.
- An eastern province, showing E-W to NNW-SSE S_H-directions is located in the Canton of Zurich and north of it (Southern Germany) and in eastern Aargovia.
- A northwestern province located in France, north and south of Besançon shows similar S_H-directions as the eastern province, that is E-W to NNW-SSE.
- A small southeastern province, probably linked to the northwest province, and extending west of Geneva and further south to Aix-les-Bains is characterised by WNW-ESE to NW-SE S_H-directions.
- A small southwestern province extending from Véria to Cordon in France (i.e. from Nr. 42 to 48 in Figure 1 and Table 1). It shows NNW-SSE to NE-SW S_H-directions.

Results from hydraulic fracturing measurements

One hydraulic fracturing measurement was taken in evaporites located at Wittelsheim (Cornet & Burlet 1992; Glawe & Blümling 1997). Measurements were made in a borehole, at a depth of about 15 m below surface. S_H shows a NNE-SSW direction.

2.3 Published interpretations

The evolution and interpretation of the stress data between 1984 and 1999 is presented below. Only the major findings and interpretations of the published literature are presented.

1984 to 1988: «Decoupling of stress field»

Becker et al. (1984), Blümling (1986) and Müller et al. (1987) carried out the main interpretations of stress measurements. The changing stress field along the Schafisheim borehole is interpreted as a decoupling of the stress field above and below the main overthrust (see Figure 2). It is speculated that the main overthrust, which lies in the Triassic evaporites, is still tectonically active.

Basically, there are two hypothesis to explain observed breakouts in the logged boreholes:

1) A rotation of the stress field across the border between «basement» and «cover» (sensu Nagra and Becker, see glossary) explains the observed direction changes of borehole breakouts. This stress rotation goes hand in hand with a decoupling of the stress field across this border. Regional structures such as the Bresse depression, the upper Rhine «Graben» and the Permo-Carboniferous trough, which lie close to the investigated boreholes, disturb the local stress field and are responsible for the decoupling. Not all authors support this first hypothesis.

2) A change of the breakout mechanisms is responsible for the differently oriented borehole breakouts along the boreholes (Becker et al. 1984; Blümling 1986; Müller et al. 1987). In the near-surface rocks (< 300 m), the ratio S_H/S_h may become greater than 3, resulting in the generation of extensional cracks parallel to the S_H-direction. In deeper levels of the crust (> 300 m), the S_H/S_h ratio may become smaller and conjugate shear fractures in the S_h-direction may form in the borehole wall. Thus, near-surface breakouts have to be treated with caution when used for geological interpretations. All authors support this second hypothesis.

1989 to 1995: «Rotation of near-surface stresses»

Based on existing stress data available for the northern Jura Mountains and foreland (Becker et al. 1984; Blümling 1986; Müller et al. 1987), Becker (1989) and Becker & Werner (1995) still support the interpretation of stress decoupling between the «basement» and the «cover» (in the sense of Nagra and Becker, see glossary): fault plane solutions of earthquakes, as well as deep borehole breakouts, indicate a clear NW-SE S_H-direction within the «basement» (in the sense of Nagra and Becker, see glossary) in this region; near-surface measurements (120 doorstopper + 10 triaxial strain cell measurements) and near-surface breakouts show a stress field rotating from a N-S direction (north and east of Basel) to a NE-SW direction (north and west of Zürich). Please note that these shallow measurements and near-surface breakouts are not presented in Figure 1.
A new element of interpretation was introduced for a better understanding of the observations. This is the method of numerical modelling. Becker (1989) established a mechanical model for the detached stress field in the northern Jura Mountains and foreland. The model confirms the above mentioned hypothesis of near-surface S_H-rotation. Becker (1989) and Becker & Werner (1995) conclude that the decoupling of the stress field, observed in the northern Jura Mountains and foreland, is due to local stress concentrations produced by local geological features such as the offset of the main overthrust.

1996 to 2000: «Neotectonics»

Until 1995, stress data available for the Jura Mountains were mostly restricted to the northern Jura Mountains and foreland, where important local geological features influence the stress trajectories. New stress investigations done by Becker (1999, 2000) completely cover the Jura Mountains.
The five stress provinces (see Figure 1) recognised by Becker (1999, 2000) were compared with tectonic units (Folded Jura, Tabular Jura, Plateau Jura, Tertiary grabens, «basement»). Borders of provinces do not correspond to those of the tectonic units. This indicates that the paleostress field during the formation of the Jura thrust and fold belt (10 - 3 My), is not the same as the present stress field.
The five stress provinces were then compared to a paleostress map based on trends of fold axes and faults (Laubscher 1972), horizontal stylolites (Plessmann 1972; Meier 1984) and on calcite twins (Tschanz 1990; Hindle 1997). Good correlations were observed only in the southeastern province and within some areas of the northern Jura Mountains. The non-matching stress/paleostress directions within the other regions again support the hypothesis that the paleo- and present stress field do not coincide.
Finally, the five stress provinces (near-surface stress data) were compared to fault plane solutions of earthquakes. Stress directions observed within the «basement» generally agree with those measured in near-surface rocks.
This new interpretation no longer supports the idea of decoupling of the stress between the «basement» and the «cover» (in the sense of the present report and in the sense of Nagra and Becker, see glossary). Becker (1999, 2000) concludes that a new stage of Jura tectonics, different from the «old» thin-skinned foreland fold-and-thrust belt of the Jura Mountains, has started. The neotectonic movements include the «basement» below the main overthrust and the sedimentary «cover» above it.

3 Derivation of the Primary Stress Field in the Mont Terri Rock Laboratory

Three methods are generally applied to derive directions and magnitudes of stresses. The first method consists of measuring strains in boreholes and calculating the corresponding stresses. This method requires a model of the rock behaviour, in general assumed to be the linear elastic law. The parameters which describe this model have to be derived separately, e.g. by rock mechanical laboratory tests. The borehole slotter technique and borehole undercoring belong to this first method. The second method consists of directly measuring stresses. Hydraulic fracturing is the best-known technique for making these measurements. The third method deals with rock-mechanical modelling. A whole variety of observations and measurements can be integrated and synthesised in a conceptual model. The modelling itself tries then to simulate the system by varying e.g. the stress field. Finally a best fit of a measured and a calculated system state (e.g deformations along a borehole, convergences of tunnel wall during excavation, pore pressure changes) is obtained.
Often, geological observations like small-scale mapping of unloading fractures or breakouts along boreholes, are available. These observations are quite valuable in deriving qualitative stresses (mainly directions) and in confirming or rejecting the findings of the quantitative stress measurements.
The following sections describe the methods that have been applied in the Mont Terri Rock Laboratory to derive and measure stresses and include results and interpretations of these tests. In the IS (in situ stress) experiment, different methods of stress measurement and stress derivation in argillaceous rocks were investigated. Techniques used in the IS experiment included the borehole slotter technique, the undercoring method and hydraulic fracturing (Chapters 3.1 – 3.3). A similar description is presented for geological observations carried out in the Mont Terri Rock Laboratory. Results and interpretations of small scale mapping during the excavation of the new niches, breakouts in differently-oriented boreholes and caliper logs from the FM-B (visualisation of flow paths) and BF (borehole fluid effects) experiments are presented in Chapter 3.4. Finally, the modelling results of the mine-by test (named ED-B experiment), carried out during the construction of the new gallery, are presented (Chapter 3.5).

3.1 The borehole slotter technique

Method

The borehole slotter technique is described in Bock (1986) and is based on the principle of stress release which occurs during and after the cutting of slots into a borehole wall with a pneumatically-driven saw. A strain gauge, which is installed near these slots, measures the tangential strain of the borehole wall. The theory of linear elasticity, in particular the Kirsch equation, is applied to calculate stresses from strain measurements. The general 3D stress state is determined by 2D strain measurements carried out in three independently-oriented boreholes. Therefore, three differently-oriented boreholes were drilled into the sandy facies of the IS niche (Figures 3 and 4). Borehole BIS-B1 was drilled horizontally, roughly parallel to the bedding strike direction. Borehole BIS-B2 was oriented downward, normal to the bedding planes, and borehole BIS-B3 lies in the bedding plane but normal to its strike direction. The sandy facies was chosen because it is less elastic than the shaly one.
Dilatometer tests were carried out close to the slots in each borehole in order to determine the necessary elastic parameters.

Results

The resulting stress directions and magnitudes are listed in Table 2 (p. 86-87). Values of elastic parameters from the dilatometer tests, as well as the stress axes and magnitudes, are given by Cottour et al. (1999). The bedding anisotropy is well-reflected in the Young's modulus: values normal to bedding vary between 2'200 and 2'600 MPa (mean: 2'400 MPa), whereas values parallel to bedding are about 3 times higher and vary between 6'400 and 7'000 MPa (mean: 6'700 MPa).
The calculated maximum principal stress axis σ_1 is oriented 181/46 (southward, with a dip angle of 46°). The intermediate principal stress, σ_2, is oriented 74/16 (ENE, with a dip angle of 16°). The minimum principal stress σ_3 is oriented 330/40 (northwestwards, with a dip angle of 40°). When plotting the principal stresses in a stereonet together with the mean bedding plane orientation, it becomes clear that σ_1 and σ_2 are lying more or less in the bedding plane, whereas σ_3 is oriented normal to it. The magnitudes of σ_1 vary between 2.0 to 5.7 MPa with a best guess value of 3.1 MPa, and the values of σ_2 between 1.0 and 2.9 MPa (best guess of 1.6 MPa), whereas very low values for σ_3 have been found varying between 0.1 and 0.4 MPa (best guess of 0.15 MPa).

Mont Terri Rock Laboratory

Geological map and location of boreholes and niches

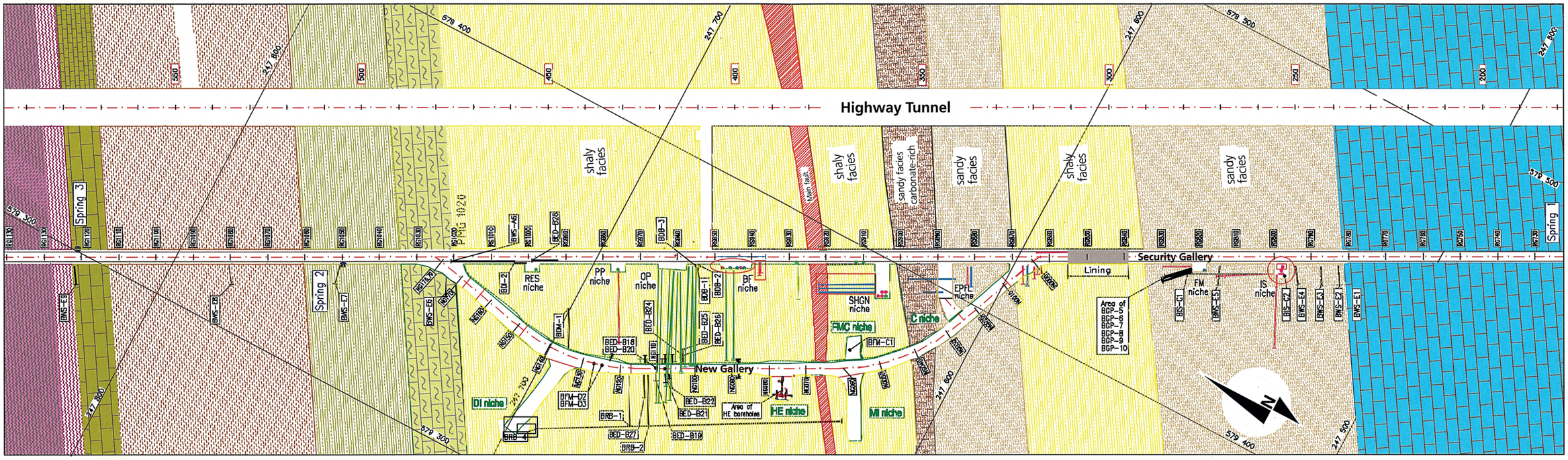

Legend:

Structures and boreholes

- Main fault
- Phase 1 boreholes
- Phase 2 boreholes
- Phase 3 boreholes
- Phase 4a boreholes

Stratigraphy

- older Triassic
- "Rhaetian" (Triassic)
- Gryphaea Limestones (Sinemurian)
- Obtusus clay + Obliana layers (Pliensbachian)
- Posidonia shales (Toarcian)
- Jurensis Marls (Toarcian)
- Opalinus Clay
  - shaly facies (Aalenian)
  - sandy facies carbonate-rich (Aalenian)
  - sandy facies (Aalenian)
- "Lower Dogger" (Aalenian - Bajocian)

Locations where stress derivations were performed

- BBF Boreholes, Caliper loggings
- BFM, BDT and BIS-A5 boreholes, Mapping of borehole breakouts
- IS niche, In situ stress experiments with borehole slotter, undercoring and hydraulic fracturing techniques

Based on:
Geological tunnel mapping 1:50 by "Bureaux Géologiques Associés, J. Norbert / B. Schindler, Delémont, 1990"
Geological niche mapping in the reconnaissance gallery by Mont Terri Consortium (1996)
Geological mapping of new gallery by Mont Terri Consortium (1997/1998)
Geological mapping during drilling campaigns by Mont Terri Consortium (1996/1999)

Institut Géotechnique, Saint-Ursanne

Date	Drew by	Attested
16.06.99	WM	Bt
05.08.99	WM	Bt
18.12.01	Ha	Bt

I:\Projekte\132\320075\7_TECHNICAL NOTES & REPORTS\TR\Tr 00-02\
\Special_Modif_CD_Bt\Figures\Figure_03.dwg

Figure 3: Geological map of the Mont Terri Rock Laboratory.

Interpretation

The stress directions derived from borehole slotting seem to be controlled by the fabric anisotropy, the bedding planes. The resulting calculated stress magnitudes are significantly lower than could be expected from the overburden pressures. There may be two reasons for these relatively low magnitudes: the Young's moduli obtained from the dilatometer tests are too low and/or the measured strains in the borehole wall cannot be explained with a linear-elastic rock material. Furthermore, the major stress release and the accompanying borehole wall deformations were almost completed when the slotter probe was introduced, thus only a small part of the elastic response could be measured, resulting in too small stresses. Finally, the too-high aspect ratio (see Glossary) of the maximum and minimum principal stresses ($\sigma_1/\sigma_3 \approx 20$) suggests that the derived stress magnitudes are not very reliable.

3.2 The undercoring technique

Method

As with the borehole slotter technique, overcoring and undercoring methods are based on measuring strains during a stress release event. In the IS experiment, only the undercoring method delivered reliable results. Thus, only the undercoring method is presented in the following. The overcoring method and results are not mentioned here. The undercoring method consists of drilling several boreholes around a future opening, such as a large diameter borehole or a small cavern. Then, strain gauges are installed at the bottom of these boreholes and the strains are recorded in the observation boreholes before, during and after the excavation work. Finally, a back-analysis procedure allows an estimation of the far-field stress pre-existing in the rock mass. The large set of strain data is statistically analysed and numerically simulated to give a best-fit solution for the stress conditions. The detailed procedure is described in Bigarré & Lizeur (1997). As with the borehole slotter technique, rock mechanical behaviour must be known (Young's modulus E, Poisson ratio ν and shear modulus G). In this case, these values were not derived from the in situ tests, but were prepared from independent rock-mechanical triaxial tests (confining pressure related to the lithostatic pressure) with the same material. These parameters cover only the elastic (non-plastic) part of an isotropic, transverse-behaving Opalinus Clay, which is the basic assumption of the method (isotropic transverse means, the parameters in the bedding plane are constant but different in a direction normal to it).
In the IS niche, a total of five boreholes (BIS-A1/A2/A3/A4 and A5) was drilled vertically downwards (Figures 3 and 4). First, four observation boreholes, A1-A4, were drilled, one in the centre and three lying in a circle with a radius of 600 mm and a distance of 120° from each other. At the bottom of these four boreholes, at a depth of 12 m, CSIRO-type Hi strain gauges were installed and connected to a permanent data acquisition system. Next, the 600 mm diameter borehole A5 was drilled in the centre of this borehole array to a depth of 13 m and the strains were recorded in the observation boreholes.

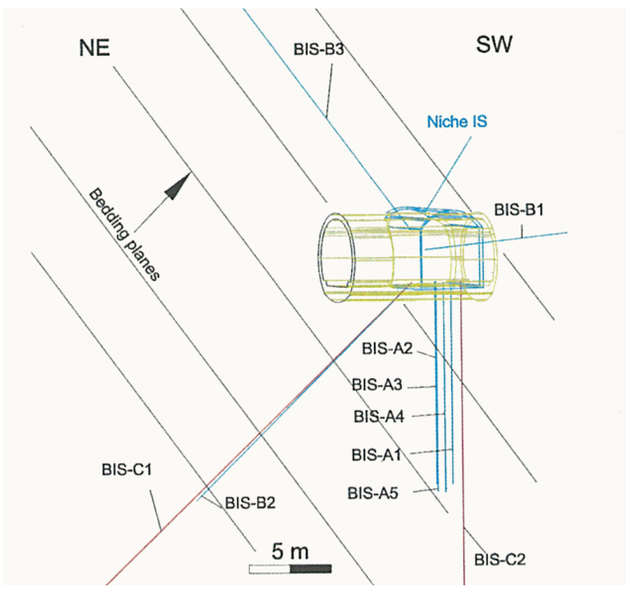

Figure 4: Location and arrangement of boreholes in the IS niche, where stress measurements were carried out.

Results

The resulting stress directions and magnitudes derived from the undercoring method are listed in Table 2 (p. 86-87). Values of elastic parameters from the rock-mechanical triaxial tests, as well as for the stress axes and magnitudes, are given by Cottour et al. (1999). As with the borehole slotter method, the bedding anisotropy is well-reflected by the Young's modulus: values normal to bedding are about 4'700 MPa and values parallel to bedding about 15'100 MPa. In addition, Young's modulus values derived from (laboratory, short-term) rock-mechanical triaxial tests are usually higher than those derived from long-term dilatometer tests. A back calculation of all measured deformations from the CSIRO strain gauges was carried out. Starting from a full data set of 144 deformations, only 68 were finally considered, resulting in the following stress field: the maximum principal stress axis, σ_1, is sub-vertical. The intermediate principal stress axis, σ_2, is sub-horizontal but about normal to the tunnel axis (50° to NE). The

minimum principal stress axis, σ_3, is sub-horizontal but subparallel to the tunnel axis (320° to NW). When plotting the principal stresses in a stereonet together with the bedding plane, it is apparent that only σ_2 lies in the bedding plane whereas the other two principal stress directions are oblique to it. The magnitudes of σ_1 vary between 6.5 and 8.0 MPa, the values of σ_2 between 4.0 and 5.5 MPa, and the values of σ_3 between 0.6 and 1.1 MPa.

Interpretation

The derived maximum principal stress fits well with the lithostatic pressure (overburden of about 250 m). The intermediate and minimum principal stresses do not coincide with the expected regional stress directions (i.e. S_H is ±N-S). This might be explained by a perturbation of the regional stress field in the fold and thrust belt of the folded Jura (the Mont Terri Rock Laboratory is located in a thrust propagation fault, the southern limb of the Mont Terri anticline). This thrust-propagated fault is limited by the main overthrust, which is located at about 500 m below the rock laboratory. Below this overthrust, the regional stress field would be acting with S_H magnitudes > S_V magnitudes. Finally, the stress magnitudes derived by the undercoring method seem to be, at least for the surroundings of the Mont Terri Rock Laboratory, more reliable than those derived from the borehole slotting technique, although the selection procedure of the deformation data sets (only 68 out of 144!) seems to be somewhat ambiguous.

3.3 Hydraulic fracturing

Method

The hydraulic fracturing method is described in Haimson & Fairhurst (1967) and later in Hickman & Zoback (1983). Unlike the borehole slotter and undercoring methods, where stresses are calculated from strain measurements, the hydraulic fracturing technique measures stresses directly. In a packed-off borehole, the pressure is progressively raised by injecting a test fluid. The evolution of the pressure is monitored until a breakdown (rapid drop in pressure), due to the creation of an artificial fracture, is measured (Figure 5). This newly-formed fracture is then subjected to a series of re-openings while re-opening pressures are measured. Theoretically, both breakdown and re-opening pressures can be directly linked to directions and magnitudes of minimum and maximum principal stresses acting perpendicular to the borehole axis. The method requires that the borehole has a circular cross section, that the rock has linear elastic and isotropic behaviour, at least in the vicinity of the test interval, and that one principal stress axis is parallel to the borehole axis. If these requirements are valid, then it can be assumed that the newly-formed fracture initiates axially, and that it propagates away from the borehole in the same plane as initiation occurs. The pressure tests are normally terminated with an impression packer survey to check the axial direction of the newly-formed fracture at least along the borehole wall.

In the Mont Terri Rock Laboratory, the hydraulic fracturing method was applied in the same geologic environment and in the same location as the borehole slotter and undercoring methods. This location corresponds to the IS niche lying in the sandy facies of the Opalinus Clay (Figure 4). Two boreholes were used: borehole BIS-C1, which is an extension of borehole BIS-B2 (borehole oriented normal to bedding, which was used for the borehole slotting tests; extension was drilled from 20 m to 31 m) and BIS-C2 which is a new vertical borehole with a length of 20 m. A total of five hydraulic fracturing tests was carried out, two in the BIS-C1 borehole and three in the BIS-C2 borehole. Each test was followed by an impression packer survey to derive the orientation of the new fracture. A detailed test description is given in Evans et al. (1999).

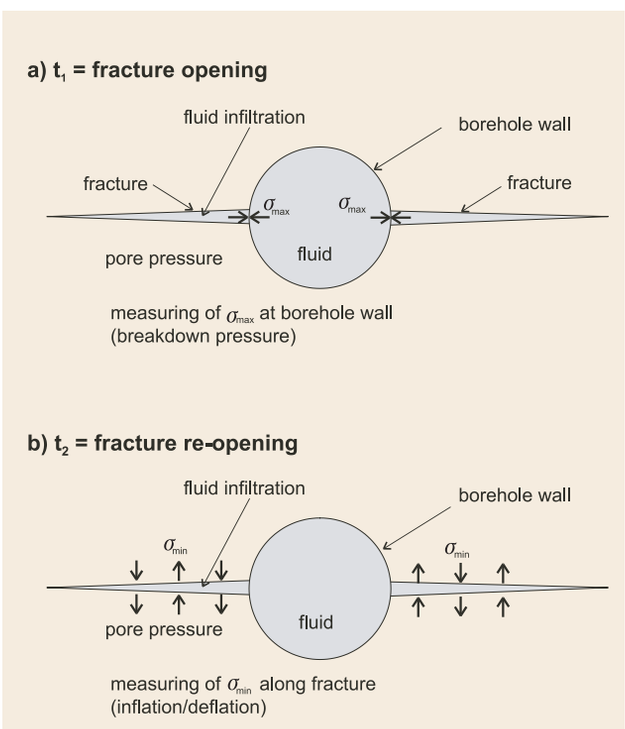

Figure 5: Hydraulic fracturing method: a) first fracture opening and b) fracture re-opening.

Results

The stress magnitude acting normal to the bedding plane was determined, which was about 4.2 MPa. It is important to mention that no newly-formed fractures which are oriented parallel to the borehole axis were observed on the impression packer. The observed new fractures were rather parallel to bedding and oblique to the borehole axis.
With a maximum principal stress σ_1 which would be sub-vertical with a magnitude of 7 MPa (similar to the overburden pressure), the minimum principal stress would be NNW-SSE, parallel to the tunnel axis, and would have a magnitude of about 3 MPa. Then, the direction of the intermediate principal stress axis tends ENE-WSW, normal to the tunnel axis. No value could be derived for its magnitude.

Interpretation

The impression packer surveys showed that no fractures parallel to the borehole axis were formed. Most of the fractures were formed in the bedding planes. The assumption of mechanical isotropy is, therefore, clearly not valid in the Opalinus Clay. These fractures are perpendicular to the borehole axis (BIS-C1) or oblique to it (BIS-C2). Thus, the principal stresses could not be directly derived from the breakdown and re-opening pressures. However, a detailed analysis of the measurements, combined with a numerical modelling analysis (Evans et al. 1999), led to the conclusion that the stress data set presented above is the most likely one, at least at the moment. Furthermore, the principal stresses derived by the hydraulic fracturing method are consistent with the stresses derived from the undercoring method, and further support the findings of the hydraulic fracturing.

3.4 Stress conditions from geological observations

Stress directions can also be determined from geological observations. New geological structures, induced by stress redistribution during and after an underground opening (excavation, borehole), give qualitative information on stress direction. They allow the confirmation or rejection of quantitative results obtained with the techniques described above.
Theoretically (Blümling 1986; Read 1996), stress-induced structures observed on a 2D-section of an isotropic rock, give the direction of the minimum stress axis σ_{min}, which is normal to the maximum one σ_{max} (Figure 6a). However, in anisotropic rocks like the Opalinus Clay, the mechanical strength anisotropy is expected to influence the formation of breakouts (Figures 6b).

In the Mont Terri Rock Laboratory, three types of geological observations were performed: small-scale mapping of niches, mapping of borehole walls with a borehole camera and mapping of borehole walls by caliper logging. The methods and results are described below.

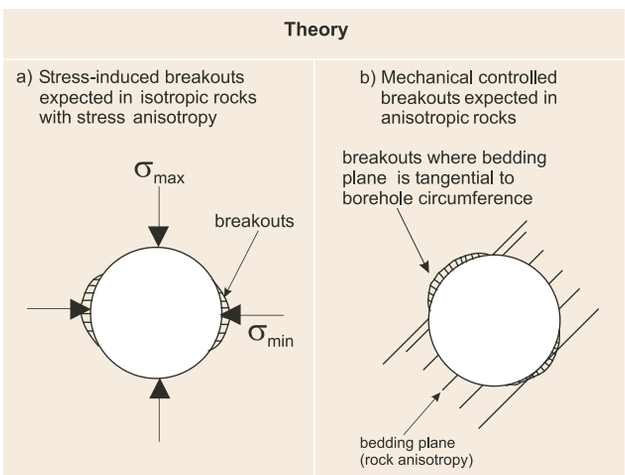

Figure 6: Borehole breakouts due to a) stress redistribution around borehole in isotropic rocks and b) anisotropic rock fabric such as the pronounced bedding planes.

3.4.1 Small-scale mapping of niche walls

Method

During and after the excavation of a gallery in the Opalinus Clay, an excavation disturbed zone (EDZ) developed in the wall of the tunnel because of the subsequent stress redistribution and the convergence of the tunnel wall. This led to the formation of an interconnected network of air-filled unloading fractures, where qualitative information on stress directions has been gained.
In the Mont Terri Rock Laboratory, small-scale mapping of unloading fractures was performed in each newly excavated niche (Bossart & Adler 1999). Results are presented below.

Results

Unloading fractures mapped in eight niches of the security gallery of the Mont Terri Rock Laboratory are schematically shown in Figure 7. They consist of steeply-inclined extension joints and shear fractures which were formed by plastic deformation in the tunnel wall due to tunnel convergence. These joints and shear fractures extend about 2 m into the rock behind the tunnel wall, whereas the first 70 cm are characterised by air-filled interconnected fractures with high hydraulic permeability. This air-filled system is further characterized by

gypsum spots, formed on fracture surfaces which result from redox processes such as transformation of pyrite into gypsum.
Fractures mapped in the eight niches of the security gallery are sketched on the block model of Figure 7. From the geometry of these fractures, the major and minimum stress axis can be derived in a 2D-section normal to the tunnel axis: the major axis (σ_{max}) is sub-vertical, whereas the minimum axis (σ_{min}) strikes horizontally ENE-WSW, normal to the tunnel axis.

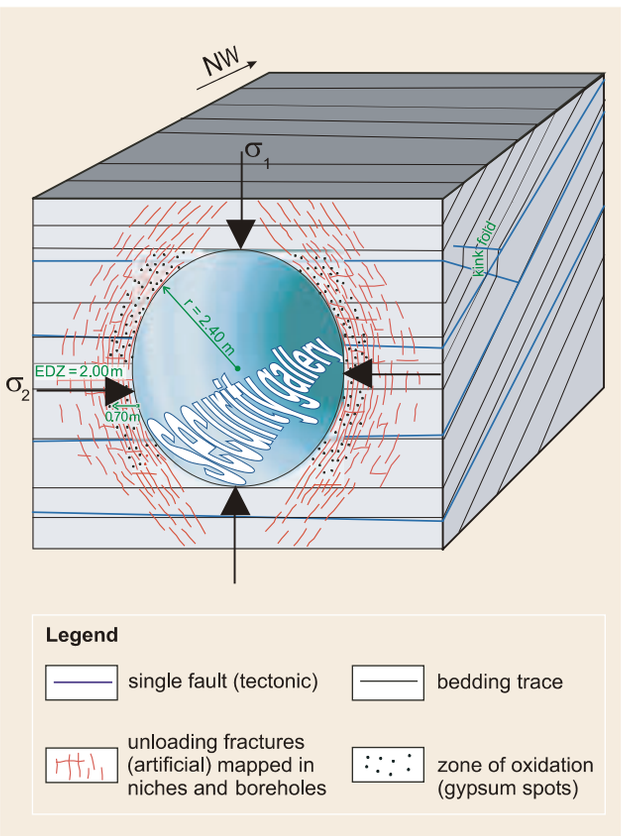

Figure 7: Block diagram presenting geometry of the excavation disturbed zone, after Bossart & Adler (1999).

Interpretation

Directions of σ_{max} (sub-vertical) and σ_{min} (horizontal, ENE-WSW), given by the small-scale mapping of unloading fractures, are consistent with those found using undercoring and hydraulic fracturing techniques, respectively σ_1 and σ_2. The method of small-scale mapping is, however, limited to 2D-studies so that only side niches could be mapped. Therefore only σ_{max} and σ_{min} could be derived, while neither σ_1 and σ_3 nor 3D-principal stress directions could be obtained. No stress magnitudes are derivable from this method.

3.4.2 Borehole wall mapping with a borehole camera

Method

A second method to derive stresses from geological observations consists of mapping structures, mainly breakouts observed along borehole walls, with a borehole camera. After mapping, it is important to analyse the geometry and orientation of breakouts in order to determine the process which induced them. In theory, breakouts can be due to:

- Stress anisotropy causing stress-induced breakouts (see Glossary and Figure 6a). In the Mont Terri Rock Laboratory, a stress anisotropy was derived by undercoring, hydrofracturing and borehole slotter experiments (see Chapters 3.2 and 3.3).
- Rock anisotropy causing mechanically-induced breakouts (see Glossary and Figure 6b). In the Mont Terri Rock Laboratory, the rock anisotropy is related to bedding planes.

In anisotropic rocks, like in the Opalinus Clay of the Mont Terri Rock Laboratory, stress-induced breakouts depend on the angle between the rock anisotropy and the stress direction. On this basis, Blümling (1986) calculated theoretical stress-induced breakouts for anisotropic rocks (Figure 8). Although this example belongs to a vertical borehole drilled in a fractured rock material (anisotropy is defined by fractures), a similar breakout geometry was also observed in boreholes of the Opalinus Clay (anisotropy defined by bedding planes), even in horizontal oriented boreholes. With the presently available data set on stress (anisotropy, directions, magnitudes of principal stresses) and rock anisotropy of the Opalinus Clay of the Mont Terri Rock Laboratory, it is possible to predict the expected direction of stress-induced breakouts (Figure 9) considering:

- Stress directions obtained with the hydraulic fracturing and undercoring methods described above: σ_1 sub-vertical, σ_2 sub-horizontal ENE-WSW oriented, σ_3 sub-horizontal NNW-SSE oriented. The magnitude of σ_1 is significantly higher than σ_3 ($\sigma_1 >> \sigma_3$) and higher than σ_2 ($\sigma_1 > \sigma_2$).
- Rock anisotropy (bedding planes): azimuth and dip angle are around 160/45.

To simplify the description of breakout directions, sections normal to the borehole axis have been defined as follows (see Figure 10): in horizontal boreholes, the «top» of the borehole section is defined as 0°, and its «bottom» as 180°; in vertical boreholes, north is defined as 0° and south as 180° (see Figure 10). In this way, in a borehole horizontally drilled in a WSW-ENE direction (perpendicular to the security gallery), breakouts observed

at 90° and 270° have a NNW-SSE direction. Stress-induced breakouts expected in the Opalinus Clay are shown in Figure 9 for three preferential borehole directions:

- Boreholes parallel to bedding and perpendicular to the security gallery. The angle between σ_1 and the rock anisotropy (bedding) is about 45°. After Blümling, 1986 (Figure 8c), stress-induced breakouts are expected around 90° and 270°.
- Sub-horizontal boreholes parallel to the security gallery. The angle between σ_1 and the rock anisotropy is 90°. After Blümling 1986 (Figure 8 e + f), four zones showing stress-induced breakouts are expected around 45°, 135°, 225° and 315°.
- Vertical boreholes drilled downwards. The angle between S_H (in this case identical to σ_2) and the rock anisotropy is 0°. After Blümling 1986 (Figure 8a), four zones showing stress-induced breakouts are expected around 50–60°, 140–150°, 230–240° and 320–330°.

In the Mont Terri Rock Laboratory, observed breakouts which fit the expected stress-induced breakouts of Figure 9 are considered as breakouts due to stress redistribution, whereas breakouts which do not fit with the expected stress-induced breakouts but show clear relations with bedding planes (e.g. bedding plane is tangential to circumference of borehole) are interpreted as mechanically-induced breakouts controlled by the strong rock anisotropy.

In the Mont Terri Rock Laboratory, walls of eight boreholes, each oriented in one of the three previous different directions, were mapped by the authors. Boreholes BFM-B4, BFM-B5, BFM-B6, BFM-B7 and BFM-B8 were horizontally drilled (for location see Figure 3), perpendicular to the axis of the security gallery and parallel to the bedding plane (ENE-WSW). They all have a depth of about 4 m. Boreholes BDT-1 and BDT-4 were drilled sub-horizontally and parallel to the security gallery (NNW-SSE). Although they were both drilled between 1996 and 1997 to a depth of 14 m, the present observation depth is shorter than 4 m because of borehole closure. Borehole BIS-A5, with a diameter of 600 mm, was vertically drilled downwards to about 13 m (BIS-A5 is the borehole used for the undercoring experiment, see Chapter 3.2). The comparison between effective breakouts mapped in the Opalinus Clay and expected stress-induced breakouts reveals interesting results.

Results

Results of borehole wall mapping with a borehole camera are shown in Figure 10 on 2D-sections normal to the borehole axis. In horizontal boreholes drilled parallel to bedding (Figure 10), three breakout directions were observed: the most frequent breakouts are localised at 135° and 315° (grey zones). They occur strictly where the bedding is tangential to the borehole circumference. These breakouts do not fit with the breakouts in Figure 9 and are thus related to mechanical breakouts

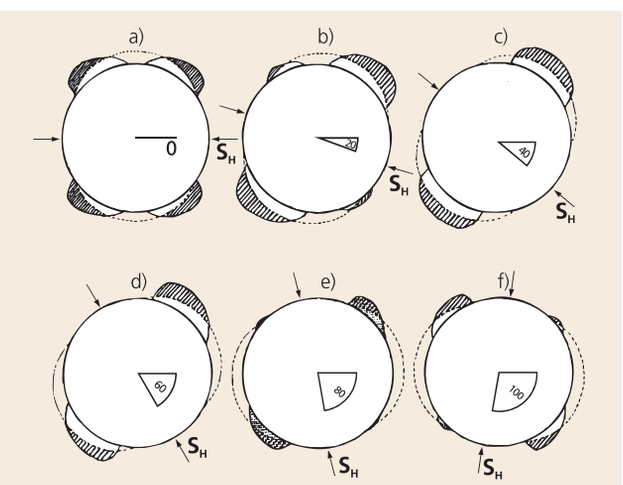

Figure 8: Calculated theoretical stress-induced breakouts for anisotropic rocks like the Opalinus Clay, in a vertical borehole (after Blümling 1986). Hatched zones represent stress-induced breakouts expected in anisotropic rocks. Dashed lines represent stress-induced breakouts expected in isotropic rocks. Angle between the stress anisotropy (S_H-direction) and the material anisotropy (locations of reduced strength in the rock, e.g. a preferential direction of fractures or bedding planes) varies between 0° and 100°.

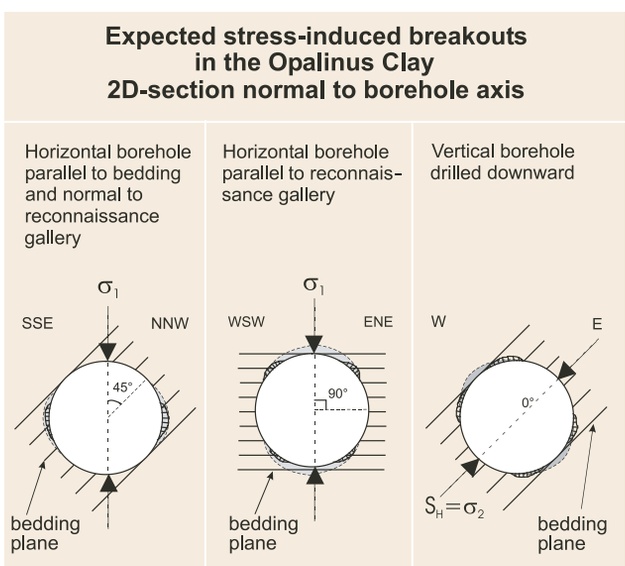

Figure 9: Expected stress-induced breakouts observed in the Opalinus Clay of the Mont Terri Rock Laboratory for three different borehole directions. Hatched zones represent stress-induced breakouts expected in anisotropic rocks. The grey zones represent stress-induced breakouts expected both in isotropic and anisotropic rocks.

due to clear strength anisotropy of the Opalinus Clay. The second set of breakout directions, less frequent and pronounced than the first one, is located at 90° and 270° (hatched zones). These breakouts fit well with the expected stress-induced breakouts (see Figure 9). Therefore, they are related to the stress anisotropy. The third type of breakout is observed on the «top» of borehole sections (0°) and only in the first metre from the borehole mouth. These breakouts seem to be directly related to the steeply-inclined unloading fractures of the excavation disturbed zone (superposition of excavation disturbed zone and borehole disturbed zone). In sub-horizontal boreholes, drilled parallel to the security gallery, three directions of breakouts were observed (Figure 10). The first two are located at 45° – 225° and 135° – 315° (hatched zones). Fitting well with the expected stress-induced breakouts (Figure 9), they are related to the stress anisotropy. The third type of breakout is observed on the «top» of borehole sections (0°) and only in the first metre from the borehole mouth (as for boreholes drilled parallel to bedding). These breakouts are also related to the excavation disturbed zone. In the vertical borehole drilled downwards, breakout zones were mapped around 160° and 340° (grey and hatched zones). In this case, breakouts reflect both the mechanical strength anisotropy and the stress anisotropy.

To summarise, three types of breakout were observed.

- Mechanically-induced breakouts, observed where the bedding is tangential to the borehole circumference, and which are related to the mechanical strength anisotropy of the Opalinus Clay. Statistically, they constitute about 75% of the breakouts.
- Stress-induced breakouts related to the stress anisotropy of the Opalinus Clay.
- Breakouts influenced by steeply-inclined unloading fractures of the excavation disturbed zone (EDZ). They are restricted to the first metre in the gallery wall.

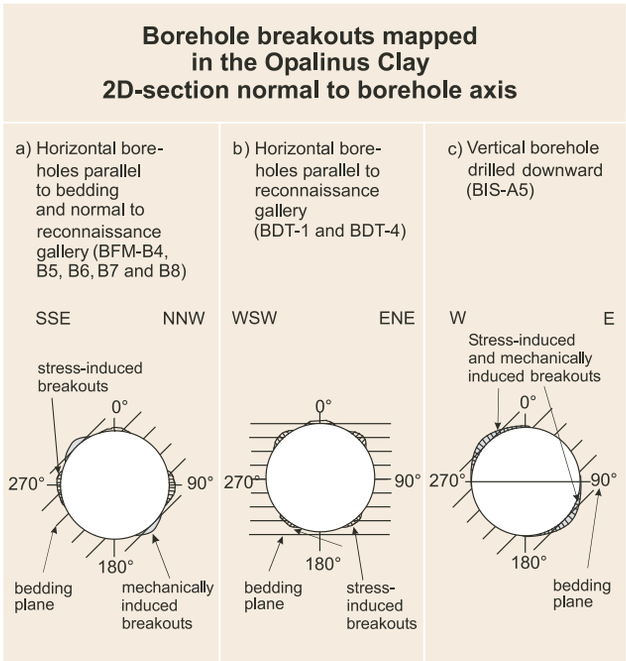

Figure 10: Borehole breakouts mapped in the Opalinus Clay. Hatched zones represent stress-induced breakouts, whereas grey zones represent mechanically-induced breakouts: a) horizontal borehole parallel to bedding strike and normal to tunnel axis, b) horizontal borehole parallel to tunnel axis, c) vertical, downwards directed borehole.

Interpretation

Breakouts induced by three different factors were observed in the Opalinus Clay of the Mont Terri Rock Laboratory: mechanically-induced breakouts (mechanical strength anisotropy), stress-induced breakouts and breakouts influenced by fractures of the excavation disturbed zone. Mechanically-induced breakouts are much more frequent (75% of observed breakouts) than stress-induced breakouts.

The method to derive stress directions from borehole breakouts is mainly bound to 2D-observations (plane normal to borehole axis) and should be used with caution. Without supplementary information, it cannot be used to determine stress directions. It is, however, a good qualitative method to confirm or reject findings of quantitative stress measurements obtained with other techniques such as undercoring, hydraulic fracturing and borehole slotter methods.

Stress-induced breakouts observed in the Opalinus Clay of the Mont Terri Rock Laboratory confirm the sub-vertical direction of σ_1 found with hydraulic fracturing and undercoring methods. The two other stress axes, σ_2 and σ_3, are oriented sub-horizontally. The most plausible direction for σ_3 is an orientation parallel to the gallery (NNW-SSE). Then σ_2 lies normal to the gallery.

For a better interpretation of stress-induced breakouts in the Opalinus Clay of the Mont Terri Rock Laboratory, observation of the borehole breakouts should be made just after drilling in differently directed boreholes. Of special interest are horizontal boreholes drilled within the bedding plane towards WSW-ENE. In these boreholes, breakouts due to mechanical strength anisotropy are expected to be observed, where bedding is tangent to the borehole circumference. These locations do not coincide with the expected locations of stress-induced breakouts. Therefore, the identification of mechanically or stress-induced breakouts can best be done in boreholes drilled parallel to bedding strike. The situation is different in vertical boreholes, where no stress direction can be clearly derived because the effect of mechanical strength anisotropy overlaps that of the stress anisotropy.

3.4.3 Mapping of breakouts by caliper logging

Method

A second way to localise stress-induced breakouts is to perform oriented caliper logging. This method consists of measuring the geometry of a borehole with a four-arm caliper instrument. The four arms are arranged in an orthogonal position. Before starting the measurements, arm 1 is oriented towards magnetic north. Starting usually from the bottom of the borehole, the rotating caliper instrument is slowly pulled out and the diameter of the borehole is scanned.
In the Mont Terri Rock Laboratory, caliper logs were performed in the BF experiment where the stability of boreholes, containing different borehole fluids, was observed over extended time periods. Three boreholes were vertically drilled in the BF niche (see Figure 3). Both unoriented and oriented caliper logs were made (Möri & Bossart 1996; Möri et al. 1997; Möri et al. 1998). Some selected results of caliper logs are presented below.

Results

Figure 11 shows the caliper log of BBF-2, a borehole initially filled with deionised water that developed large breakouts (swelling capacity is high in a borehole containing deionised water). The first two columns represent for each arm the radius of the BBF-2 borehole measured the 14.08.98. The three columns on the right are a compilation of diameter measurements (arm 1 & 3 and 2 & 4) realised at different dates (29.02.96, 15.04.97, 15.05.98, 14.08.98). Note in each column the parallelism between curves.
The third column of Figure 11 shows the direction of arm 1 during the last logging (0 – 360°). Note its stabilisation between 4 and 10 m. BIP logging (borehole imaging processing) performed by CORE Ltd. (USA) in 1998 showed that the borehole geometry (section) had been deformed from a circle to a wedge shape, preventing arms from turning. Arm 1 was trapped in the wedge showing an average direction of N70°E. The bigger caliper undulations (breakouts) are located along the arms 2 & 4 axes which are located at 90° from arm 1, that is NNW-SSE. In summary (see Table 2), all the caliper logs of BBF-1, BBF-2 and BBF-3 give a general NW-SE direction for breakouts (Albert et al., 1998).

Interpretation

The derivation of stress directions by caliper logging in fluid-filled boreholes has to be treated with caution. The softening of the borehole wall may guide subsequent caliper logs and even provoke breakouts. Each time during caliper logging in BBF boreholes, the 4 caliper arms were trapped in the same paths and grooved the paths deeper and deeper. Furthermore, the previous chapter (3.4.2, Borehole wall mapping with a borehole camera) showed that breakouts mapped in vertical boreholes of the Opalinus Clay should not be used to derive stress directions because the effect of the rock anisotropy overlaps that of the stress anisotropy. Thus, no valuable information on stress direction is derivable from caliper logging performed in the Opalinus Clay. Vertical boreholes should be used with caution when deriving stresses from borehole breakouts.

3.5 Stress conditions from rock-mechanical modelling

Method

The excavation of the new gallery of the Mont Terri Rock Laboratory in 1997/1998 was monitored in about 12 boreholes, which were drilled from the security gallery into the target area of the new gallery (see Figure 3, Phase 3 boreholes). These boreholes were instrumented to measure deformations and pore pressures before, during and after the excavation of the new gallery, hence the response to excavation could be fully tracked. Additionally, convergence measurements in the new gallery were carried out at different times after completion of the excavation.
The elastic response of each equipped location was calculated with the boundary element code EXAMINE 3D (Martin & Lanyon 2003). The idea was to find an initial stress tensor which fits the measured and calculated deformations and convergences during the subsequent excavation of the new gallery and which was also able to simulate the secondary stress field around the new galleries (stress re-distributions). Also integrated in this modelling are observations from borehole breakouts and the changing pore water pressures during excavation.
EXAMINE 3D is a code taking only the elastic deformations into account. The plastic deformations were not considered. However, the calulations with EXAMINE 3D demonstrated that it is possible to distinguish between elastic and plastic deformations during the excavations.

Results

The main result is an initial stress tensor, which can be used to model the system behaviour during the excavation of the new gallery. This stress tensor, recommended by Martin & Lanyon (2003) is the following: the maximum principal stress axis, σ_1, is sub-vertical oriented (azimuth of 210° and dip of 70°) and its magnitude varies between 6 and 7 MPa. The intermediate principal stress axis, σ_2, lies subparallel to the tunnel axis (azi-

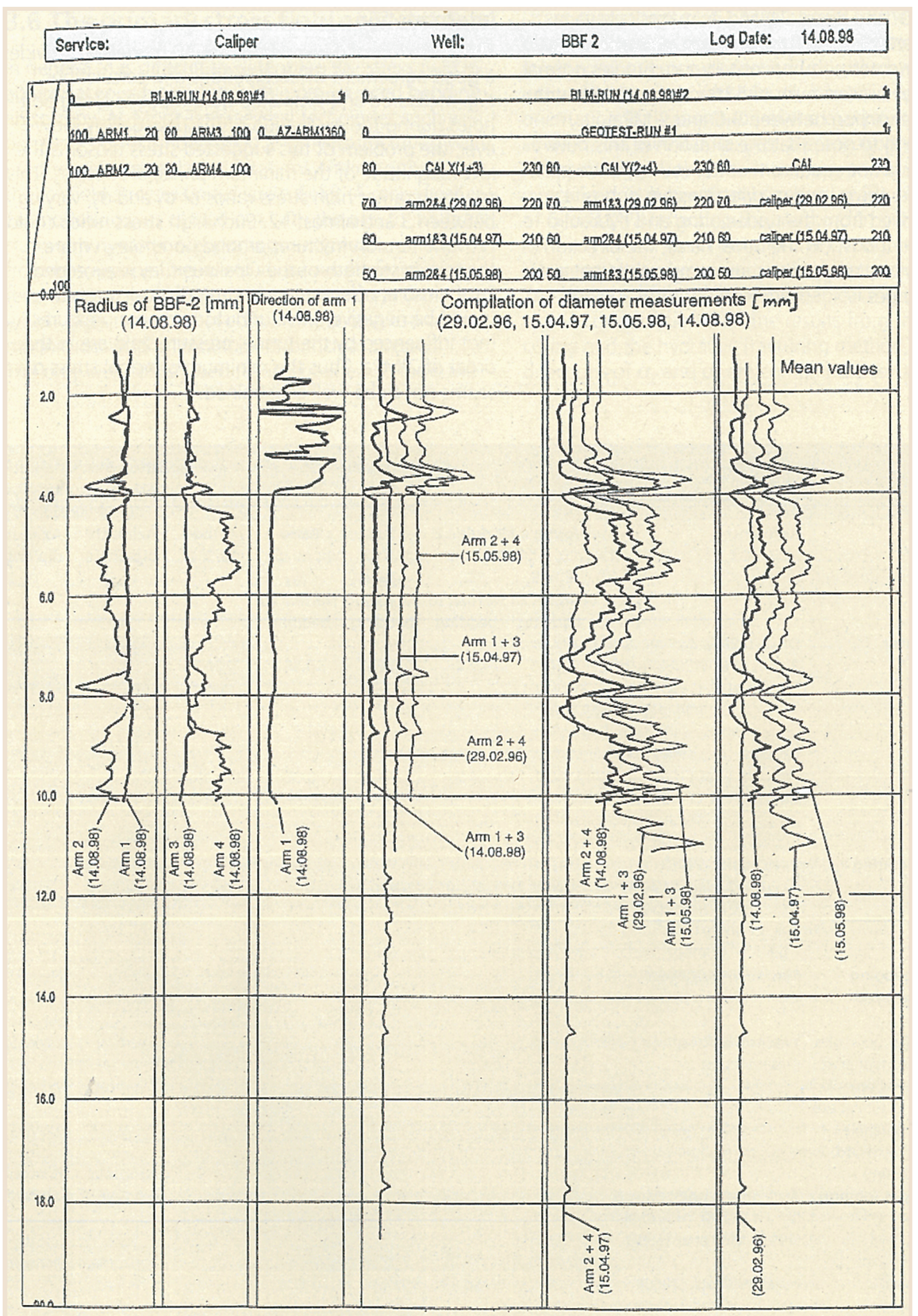

Figure 11: Caliper logs in the fluid-filled borehole BBF-2, niche BF – facsimile of field record (for location see Figure 3).

muth of 320° and dip of 7°) and its magnitude varies between 4 and 5 MPa. The minimum principal stress axis, σ_3, is oriented sub-horizontally too, but lies normal to the tunnel axis (azimuth of 52° and dip of 18°) with a magnitude varying between 0.6 and 2 MPa.
It is interesting to note that the direction of this new stress tensor is not equal to that derived from the previous methods: the σ_2 and σ_3 directions are opposite to those derived from the undercoring and hydraulic fracturing methods. On the other hand, the direction of σ_1 and the stress magnitudes are comparable and are in the same ranges.

Interpretation

The stress tensor derived from the 3D modelling provides a good agreement of observations and calculations, e.g. measured and simulated deformations along boreholes during the excavation of the new gallery. However, the problem of this suggested stress tensor is the low magnitude of the minimum principal stress σ_3. This results in rather high stress ratios of σ_1 and σ_3, varying between 3 and almost 12. Such high stress ratios could provoke tension fractures around boreholes, where the tensile strength of the Opalinus Clay is exceeded. Furthermore, effective minimum principal stresses would be negative, since undisturbed pore pressures (not influenced by the tunnel pressure sink) are in the order of 2 MPa. Thus the minimum principal stress σ_3 seems not to be well constrained.

		Elastic parameters					Stress Axis Orientations derived from breakouts (2-dimensional)		
Method	**Reference**	**Young's Modulus E [GPa]**		**Poisson's Ratio ν**		**Method (E, ν)**	**Azimuth/ dip angle σ_{max}**	**Azimuth/ dip angle σ_{min}**	
		$E_2 = E_3$ Parallel to bedding	**E_1 Normal to bedding**	**$\nu_{12} = \nu_{13}$ Parallel to bedding**	**ν_{23} Normal to bedding**				
Borehole slotter	Bühler (1997) Rummel et al. (1998a, b, c) Cottour et al. (1999)	6.7	2.4	0.35	0.35	Dilatometer			
Undercoring	Bigarré & Lizeur (1997) Hommand et al. (1997) Cottour et al. (1999)	15.1	4.7	0.12	0.36	Laboratory tests			
Hydraulic fracturing	Evans et al. (1999) Hickman & Zoback (1983) Haimson & Fairhurst (1967) Bühler (1997)								
Small scale mapping of newly excavated side niches	Bossart & Adler (1999)						Sub -vertical	Normal to tunnel axis. Subhorizontal	
Mapping borehole breakouts Horizontal boreholes normal to tunnel axis	Wermeille & Bossart, present report						Vertical	NNW-SSE	
Mapping borehole breakouts Horizontal boreholes parallel to tunnel axis							Vertical	WSW-ENE	
Mapping borehole breakouts Vertical borehole drilled downward (60 cm diam.)							WSW-ENE Sub-horizontal	NNW-SSE Sub-horizontal	
Oriented caliper logging	Albert et al. (1998), Möri & Bossart (1996), Möri et al. (1997), Möri et al. (1998)						SW-NE Sub-horizontal	NW-SE Sub-horizontal	
Rock mechanical modelling	Martin & Lanyon (2003)								

Table 2: Compilation of available stress measurements and modelling performed in the Opalinus Clay of the Mont Terri Rock Laboratory.

3.6 The primary stress field at Mont Terri

In general, it is difficult to determine the stress field in an argillaceous formation with a pronounced bedding anisotropy. At Mont Terri, several techniques such as borehole slotter, undercoring and hydrofracturing were used to determine the orientations and magnitudes of the far-field stresses (initial stress field). A rock-mechanical modelling was carried out with the aim to integrate static and dynamic observations and measurements from in-situ experiments. All these results from in situ tests and the modelling are now compiled in Table 2, which gives mainly an overview of the best estimates of magnitudes and orientations of principal stresses.
The only well constrained result obtained so far is the stress component of 4.2 MPa normal to the bedding planes. This stress component, which is not a principal stress component, was derived using the hydrofracturing technique. Also satisfactorily constrained is the orientation and magnitude of the maximum principal stress σ_1. All methods (except the borehole slotter method) suggest that the maximum principal stress direction σ_1 is subvertically oriented, with magnitudes of 6 to 8 MPa reflecting the overburden pressure. Less constrained are the orientations and magnitudes of the intermediate and minimum principal stresses σ_2 and σ_3. The findings from the rock mechanical modelling are e.g. in contradiction with the results from the undercoring and the hydraulic fracturing method, when the directions of σ_2 and σ_3 are compared (see Table 1 and

	Magnitudes and Orientations of Principal Stresses (3-dimensional)						
	σ_1 [MPa]	**σ_2 [MPa]**	**σ_3 [MPa]**	**Azimuth/ dip angle σ_1** [...°/...°]	**Azimuth/ dip angle σ_2** [...°/...°]	**Azimuth/ dip angle σ_3** [...°/...°]	**Remarks** Opalinus Clay behaves as a transverse isotropic rock. Values of elasticity modules in the bedding plane are identical (E_2=E_3), but not equal to the value normal to bedding plane (E_1). The same is true for the Poisson Ratio values.
	3.1	1.6	0.15	181/46	74/16	330/40	• Linear elastic material • Anisotropy is **not** considered • Dry boreholes • Stresses are calculated • σ_1 and σ_2 in bedding plane
	6.5 – 8.0	4.0 – 5.5	0.6 – 1.1	Sub-vertical	50° to NE (± normall to tunnel axis) Sub-horizontal	320° to NW (± parallel to tunnel axis) Sub-horizontal	• Linear elastic material • Anisotropy **is** considered • Dry boreholes • Stresses are calculated • Same result as hydraulic fracturing
	7.0	3 < σ_2 <7 σ normal to bedding = 4.2	3	Sub-vertical	WSW-ENE (normal to tunnel axis) Sub-horizontal	NNW-SSE (parallel to tunnel axis) Sub-horizontal	• Assumes linear elastic material (not valid at Mont Terri) • Borehole filled with fluid • Stresses are measured • Hydrofrac parallel to borehole axis **not** observed • Always fracturing parallel bedding
							• Method mainly bound to a 2D-case.
							• This method is bound to 2D-case.
							• Stress-induced breakouts in horizontal boreholes and can be often distinguished from mechanically breakouts.
							• Stress induced breakouts are difficult to distinguish from mechanically induced breakouts in vertical boreholes.
							Breakouts obtained from vertical boreholes should be used with caution to derive stress directions. Mechanical breakouts (e.g. bedding parallel slip) are difficult to distinguish from stress-induced breakouts.
	6 – 7	4 – 5	0.6 – 2	210/70	320/07	52/18	Elastic modelling with EXAMINE 3D, taking into account deformation measurements in boreholes and tunnel convergences of the ED-B mine-by test.

Figure 1). On the other hand, all methods suggest a rather low σ_3-magnitude, indicating a value less than 2 MPa. Pore pressures, which are not influenced by the tunnel sink, are also in the order of 2 MPa. This would results in an effective minimum principal stress σ_3' which is negative, indicating a tensile stress field at Mont Terri. So far, there are no observations and measurements supporting such an initial tensile stress field at Mont Terri. Thus it is not recommended to use an initial stress tensor with a σ_3-magnitude less than the pore pressure.

Finally, taking into account all the results of the modelling exercise and part of undercoring and hydraulic fracturing method, we recommend the following stress data set to be used as an initial stress tensor:

σ_1: **Magnitude range of 6-7 MPa, Azimuth 210°, dip 70°,**

σ_2: **Magnitude range of 4-5 MPa, Azimuth 320°, dip 10° (~parallel to tunnel),**

σ_3**: Magnitude range of 2-3 MPa, Azimuth 50°, dip 20° (~normal to tunnel).**

When taking into account the observations of the mapping of newly excavated side niches and the observed borehole breakouts, together with the undercoring and hydraulic fracturing method, then the following stress directions are recommended (please note that borehole breakouts don't reveal stress magnitudes):

σ_1**: vertically directed,**

σ_2**: horizontal, SW-NE directed (~normal to tunnel),**

σ_3**: horizontal, NW-SE directed (~parallel to tunnel).**

Thus the azimuths and dips of σ_2 and σ_3 of the initial stress tensor may be exchanged. It seems that the magnitudes of the stress tensor are better constrained than its directions.

With this initial stress tensor, the altered (secondary) stress field around the underground openings in the Mont Terri Rock Laboratory can be estimated using analytical solutions or numerical models. In the new NW-SE directed gallery, the tangential stresses are highest in the tunnel walls exceeding the peak strength of the Opalinus Clay (triaxial laboratory tests suggest a Mohr-Coulomb envelope with an effective cohesion c_z' of 2.2 MPa and an effective angle of internal friction φ_z' of 25° [Bock 2001]), leading to an excavation disturbed zone as described in Figure 7. At the ceiling and floor of the tunnel, reactivation of the bedding planes was observed, with indication of shear movements on the planes. This is explained by the lower compressive strengths of the bedding planes (c_z' = 1 MPa and φ_z' = 23° [Bock 2001]).

Due to the high mechanical anisotropy of the Opalinus Clay, which is mainly defined by the bedding planes, borehole breakouts should be used with caution to derive stress directions, e.g. minimum and maximum directions in a 2D-section. The borehole breakouts indicate rather mechanical strength anisotropy than stress anisotropy. On the other hand, some cases exist where breakouts along the borehole wall could be clearly related to the minimum stress direction. Good candidates for such observations are boreholes drilled in a horizontal direction (the plane normal to the borehole axis contains σ_1 leading to high aspect ratios with σ_3 or σ_2. Thus the most prominent stress-induced borehole breakouts are expected to be observed in such boreholes). However, such a distinction of stress-induced or mechanically-induced breakouts is only meaningful if the stress directions are already known, at least in rocks containing a pronounced fabric anisotropy such as the Opalinus Clay.

4 Conclusions and Recommendations

- A whole variety of stress measurements derived by different methods in different formations and tectonic units and which were sampled at different depths are available in the Jura Mountains. These data were compiled in this report, but a common interpretation of these data is not available yet and different ideas of different authors exist (e.g. use of near-surface data for regional geological interpretation). A nice and rather clear example originates from the Schafisheim borehole drilled by Nagra in north of Switzerland, where a decoupling of the stress field across the main overthrust in the Triassic evaporites could be demonstrated. The present-day stress field is not a simple one, especially as far as its directions are concerned. Five stress provinces with diverging directions describe in the best way the present stress field in the Jura Mountains.
- Although principal stresses were not directly measurable in the Opalinus Clay of the Mont Terri Rock Laboratory, even by the hydraulic fracturing method, a most likely stress data set could be derived and is now available. Directions and magnitudes of the principal stresses are:
  σ_1: Magnitude range of 6–7 MPa, sub-vertically directed with an azimuth of 210° and dip of 70°.
  σ_2: Magnitude range of 4–5 MPa, sub-horizontally directed with an azimuth of 320° and dip of 10°. This intermediate principal stress is oriented sub-parallel to the main galleries and tunnels at Mont Terri.
  σ_3: Magnitude range of 2–3 MPa, sub-horizontally directed with an azimuth of 50° and dip of 20°. This minimum principal stress is oriented more or less normal to the main galleries and tunnels at Mont Terri.
  The magnitudes of these principal stresses are better constrained than the corresponding directions, especially those of σ_2 and σ_3. These intermediate and minor stress directions are not definite and may be also exchanged.
- The local stress field in the Opalinus Clay of the Mont Terri Rock Laboratory, which lies in the southern limb of the Mont Terri anticline, does not coincide with the expected regional stress field. The local maximum principal stress is sub-vertically oriented and doesn't coincide with the expected regional NW-SE directed principal stress direction. One possible reason could be that the main overthrust, which is located below the Mont Terri Rock Laboratory in the Triassic evaporites, acts as a decoupling horizon.
- The method to derive stress directions from borehole breakouts in the Opalinus Clay should be used with caution. About ¾ of these structures could be attributed to mechanical strength anisotropy and only ¼ may be linked to real stress anisotropy and redistribution of stresses. This ratio of three may be even higher in the shaly facies of the Opalinus Clay, where the fabric anisotropy is more strongly developed than in the sandy facies.
- Small-scale mapping of unloading fractures in the excavation disturbed zone, in newly-excavated niches and galleries, could be used to trace the stress re-distribution around these openings and thus to derive principal stress directions. This method is mainly bound to a 2D-case. 3D-principal stress directions are difficult to obtain. No stress magnitudes are derivable from small-scale mappings.
- It is recommended to use stress derivation methods that take plastic deformations in the Opalinus Clay into account (e.g. plastic deformations in the borehole wall during and just after drilling). Furthermore, the hydraulic fracturing method should be repeated in the shaly facies, but with a hydrocarbon based fracturing fluid. Such a fluid avoids swelling and fracture impressions would be possible.
- To better interpret borehole breakouts in the Opalinus Clay (is it an effect of mechanical strength isotropy or a matter of stress anisotropy and stress re-distribution? What is the role of the air humidity?), observations of such deformations should be made in systematically drilled and differently directed boreholes: e.g. two boreholes lying in the bedding plane (one of which is parallel to bedding strike and the other normal to the strike direction) and one borehole normal to the bedding plane. The temporal evolution and propagation of breakouts could be studied by drilling different sets of boreholes at different times, and by exhibiting these boreholes to different tunnel climates (e.g. ventilated and non-ventilated boreholes). Measurements and observations should be carried out with a BIP (Borehole Imaging Processing) camera, where breakouts are identifiable, mapped and oriented. Measurements (borehole wall mapping) should be carried out immediately after drilling and repeated regularly in order to distinguish between stress induced and fabric induced breakouts. Caliper logs should not be used anymore because they mechanically affect the smooth borehole wall during logging.

- Rock-mechanical modelling should be continued and intensified, using also codes where inelastic material laws are implemented and thus plastic deformations can be handled. Furthermore, effective stress concepts should be introduced, where e.g. also pore pressure changes during an excavation are considered (hydro-mechanical coupling). Finally, future modelling studies should consider different tunnel climates and water contents of the surrounding rock, since rock-mechanical properties of Opalinus Clay are largely dependant on the saturation state of the rock.

Acknowledgements

We would like to thank J.-P. Tripet, M. Thury and P. Heitzmann of the Federal Office for Water and Geology who initiated this study and were open to many fruitful discussions and suggestions.
We also are grateful for valuable guidance and numerous suggestions from the following reviewers: C. Bauer (ANDRA), W.H. Müller (NAGRA), J.-P. Tripet (FOWG) and P. Heitzmann (FOWG). We would like to thank A. Becker (Institute of Geophysics, ETHZ) for his precious informations and efficient collaboration. We also thank H. Steiger from the site support of the Mont Terri Rock Laboratory, who gave us a hand during the mapping of borehole breakouts with the video camera. Last but not least we would like to thank B. Pearson and F. Haug who made all the English corrections.

References

Albert, W., Lux, K.N., Stump, U. & Kaufmann, A. (1998): BF experiment: Oriented caliper logging and spectral gamma ray logging in boreholes BBF.1/2/3. – Mont Terri tech. Note TN 98-59 (internal report), Federal Office for Water and Geology, Bern-Ittigen, Switzerland.

Becker, A., Blümling, P. & Müller W.H. (1984): Rezentes Spannungsfeld in der zentralen Nordschweiz. – Nagra tech. Ber. NTB 84-37.

Becker, A. (1989): Detached neotectonic stress field in the northern Jura Mountains, Switzerland. – Geol. Rdsch. 78/2, 459–475.

Becker, A. & Werner, D. (1995): Neotectonic state of stress in the Jura Mountains. – Geodinamica Acta 8/2, 99–111.

Becker, A. (1999): In situ stress data from the Jura Mountains. New results and interpretation. – Terra Nova 11/1, 9–15.

— (2000): The Jura Mountains. An active foreland fold-and-thrust belt? – Tectonophysics, 321, 381 – 406.

Bigarré, P. & Lizeur, A. (1997): In situ stress measurements (IS-A): results of the in situ experiment, calculation of the stress. – Mont Terri tech. Note TN 97-14 (internal report), Federal Office for Water and Geology, Bern-Ittigen, Switzerland.

Blümling, P. (1986): In situ Spannungsmessung in Tiefbohrungen mit Hilfe von Bohrlochrandausbrüchen und die Spannungsverteilung in der Kruste Mitteleuropas und Australiens. – Diss. Fak. Physik Univ. Karlsruhe.

Bock, H. (1986): In situ validation of the borehole slotting stressmeter. – Proc. int. Symp. on Rock Stresses, Stockholm, 261–270.

Bock, H. (2001): Rock Mechanics Analyses and Synthesis (RA experiment): Data Report on Rock Mechanics. – Mont Terri tech. Rep. TR 2000-02, Federal Office for Water and Geology, Bern-Ittigen, Switzerland.

Bossart, P. & Adler, M. (1999): Tectonic and Artificial Fractures. In: Thury, M. & Bossart, P.: Mont Terri Rock Laboratory – Results of the hydrogeological, geochemical and geotechnical experiments performed in 1996 and 1997 (p. 19-26). – Geol. Rep. 23, Federal Office for Water and Geology.

Bühler, C. (1997): Borehole slotter experiment (IS-B): results of short-term dilatometer measurements. – Mont Terri tech. Note TN 97-16 (internal report), Federal Office for Water and Geology, Bern-Ittigen, Switzerland.

Cornet, F.H. & Burlet, D. (1992): Stress field determination in France by hydraulic test in boreholes. – J. geophys. Res. 97/B8, 11829–11849.

Cottour, P., Bigarré, P., Camus, P., Bauer-plaindoux, C. & Blümling, P. (1999): Evaluation of In Situ Stresses: Comparison of Techniques. In: Thury, M. & Bossart, P.: Mont Terri Rock Laboratory – Results of the hydrogeological, geochemical and geotechnical experiments performed in 1996 and 1997 (p. 160-170). – Geol. Rep. 23, Federal Office for Water and Geology.

Deichmann, N. (1990): Seismizität der Nordschweiz 1987–1989, und Auswertung der Erdbebenserien von Günsberg, Läufelgingen und Zeglingen. – Nagra tech. Ber. NTB 90.

Evans, K., Piedevache, M. & Portmann F. (1999): Hydrofracture stress test in boreholes BIS-C1 and CIS-C2. – Mont Terri tech. Note TN 99-55 (internal report), Federal Office for Water and Geology, Bern-Ittigen, Switzerland.

Glawe, U. & Blümling, P. (1997): Felsmechanische Daten, in situ Spannungen und Berechnungen für den Standort Wellenberg. – Felsbau 15/6, 440–447.

Haimson, B.C. & Fairhurst, C. (1967): Initiation and extension of hydraulic fractures in rocks. – Soc. Petrol. Eng. J. September, 310–318.

Hickman, S. & Zoback M.D. (1983): The interpretation of hydraulic fracturing pressure-time data for in situ stress determination. In: Hydraulic fracturing stress measurements. – National Academy Press, Washington, 44–54.

Hindle, D. (1997): Quantifying stresses and strains from the Jura Arc, and their usefulness in choosing a deformation model for the region. – Ph.D. Thesis, Univ. Neuchâtel.

Hommand, F., Gaire, P., Bigarré, P. & Cottour, P. (1997): In situ stress measurement IS-A: Results of laboratory tests (mechanical characterization of OPA samples from Mont Terri). – Mont Terri tech. Note TN 97-13 (internal report), Federal Office for Water and Geology, Bern-Ittigen, Switzerland.

Laubscher, H. (1972): Some overall aspects of Jura dynamics. – Amer. J. Sci. 272, 293–304.

Martin, C.D. & Lanyon, G.W. (2003): EDZ in Clay Shale: Mont Terri. – Mont Terri tech. Report (in preparation). Federal Office for Water and Geology, Bern-Ittigen, Switzerland.

Meier, D. (1984): Zur Tektonik des schweizerischen Tafel- und Faltenjura (regionale und lokale Strukturen, Kluftgenese, Bruch- und Faltentektonik, Drucklösung). – Clausthaler geowiss. Diss. 14.

Möri, A. & Bossart, P. (1996): Results of Phase 1 drilling campaign. – Mont Terri tech. Rep. TR 96-01, Federal Office for Water and Geology, Bern-Ittigen, Switzerland.

Möri, A., Adler, M., Wermeille, S. & Bossart, P. (1997): Results of the Phase 2 drilling campaign. – Mont Terri tech. Rep. TR 97-01, Federal Office for Water and Geology, Bern-Ittigen, Switzerland.

Möri, A., Cabal, P., Bossart, P., Adler, M. & Wermeille, S. (1998): Results of Phase 3 drilling campaign. – Mont Terri tech. Rep. TR 98-01, Federal Office for Water and Geology, Bern-Ittigen, Switzerland.

Müller, W.H., Blümling, P., Becker, A. & Clauss, B. (1987): Die Entkopplung des tektonischen Spannungsfeldes an der Jura-Überschiebung. – Eclogae geol. Helv. 80/2, 473–489.

Plessmann, W. (1972): Horizontal-Stylolithen im französisch-schweizerischen Tafel- und Faltenjura und ihre Einpassung in den regionalen Rahmen. – Geol. Rdsch. 61, 332–347.

Read, R.S. (1996): Characterizing excavation damage in highly-stress granite at AECL's Underground Research Laboratory. – International conference on deep geological disposal of radioactive waste, EDZ Workshop, 20 September 1996. Canadian Nuclear Society, 35–46.

Rummel, F., Hettkamp, Th. & Weber, U. (1998 a): Gasfrac self-healing experiment: Rock mechanical laboratory test on Opalinus Clay core samples. – Mont Terri tech. Note TN 98-18 (internal report), Federal Office for Water and Geology, Bern-Ittigen, Switzerland.

— (1998 b): Laboratory experiments for the determination of deformation mechanisms and a constitutive law for time dependent deformation behaviour of the Opalinus Clay (Phase 3). – Mont Terri tech. Note TN 98-35 (internal report), Federal Office for Water and Geology, Bern-Ittigen, Switzerland.

— (1998 c): DM experiment: Laboratory experiment for the determination of deformation mechanisms and a constitutive law for time dependent deformation behaviour of the Opalinus Clay (Phase 3). – Mont Terri tech. Note TN 98-55 (internal report), Federal Office for Water and Geology, Bern-Ittigen, Switzerland.

Thury, M. & Bossart, P. (1999): Mont Terri Rock Laboratory – Results of the hydrogeological, geochemical and geotechnical experiments performed in 1996 and 1997. – Geol. Rep. 23, Federal Office for Water and Geology.

Tschanz, X. (1990): Analyse de la déformation du Jura central entre Neuchâtel (Suisse) et Besançon (France). – Eclogae geol. Helv. 83/3, 543–558.

Werner, D. & Becker, A. (1996): Ermittlung von Gebirgsspannungen in der Schweiz und deren Interpretation. – Felsbau 14/3, 154–156.

Mont Terri Project – Hydrogeological Synthesis, Osmotic Flow

Berichte des BWG, Serie Geologie – Rapports de l'OFEG, Série Géologie – Rapporti dell'UFAEG, Serie Geologia – Reports of the FOWG, Geology Series

No. 6 – Bern 2004

Mont Terri Project – Hydrogeological Synthesis, Osmotic Flow

P. Heitzmann (editor)

Berichte des BWG, Serie Geologie – Rapports de l'OFEG, Série Géologie – Rapporti dell'UFAEG, Serie Geologia – Reports of the FOWG, Geology Series

No. 6 – Bern 2004

Contents

Synthesis of Hydrogeological Investigations at the Mont Terri Site (Phases 1 to 5)

P. Marschall, J. Croisé, L. Schlickenrieder, J.-Y. Boisson, P. Vogel & S. Yamamoto 7

An Experimental and Modelling Study of Chemico-osmotic Effects in the Opalinus Clay of Switzerland

D.J. Noy, S.T. Horseman, J.F. Harrington, P. Bossart & H.R. Fisch 95

Impressum

Editor	Federal Office for Water and Geology, FOWG
Recommended quotation	Heitzmann, P., editor (2004): Mont Terri Project – Hydrogeological Synthesis, Osmotic Flow. Reports of the Federal Office for Water and Geology (FOWG), Geology Series No. 6.
	For individual articles:
Marschall, P. et al. (2004):	Synthesis of Hydrogeological Investigations at the Mont Terri site (Phases 1 to 5). In: Heitzmann, P. (Ed.): Mont Terri Project – Hydrogeological Synthesis, Osmotic Flow (p. 7–92). – Reports of the Federal Office for Water and Geology (FOWG), Geology Series No. 6.
Noy, D. J. et al. (2004):	An Experimental and Modelling Study of Chemico-osmotic Effects in the Opalinus Clay of Switzerland. In: Heitzmann, P. (Ed.): Mont Terri Project – Hydrogeological Synthesis, Osmotic Flow (p. 95–126). – Reports of the Federal Office for Water and Geology (FOWG), Geology Series No. 6.
Cover photos	© Nagra, © Comet
Internet	This report is available as PDF file at www.swisstopo.ch

Organizations involved in the Mont Terri Project

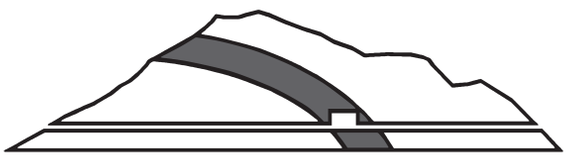

Mont Terri Project
Underground Rock Laboratory
Laboratoire souterrain

FOWG/SGS ANDRA BGR CRIEPI ENRESA GRS HSK IRSN JNC NAGRA OBAYASHI SCK•CEN

Responsible for the Mont Terri motorway tunnel system and authorizations

RCJU
République et Canton du Jura
Département de l'Environnement et de l'Equipement

Project Partners

ANDRA
Agence nationale pour la gestion des déchets radioactifs, France

BGR
Bundesanstalt für Geowissenschaften und Rohstoffe, Germany

CRIEPI
Central Research Institute of Electric Power Industry, Japan

ENRESA
Empresa Nacional de Residuos Radiactivos, S.A., Spain

FOWG/SGS
Federal Office for Water and Geology, Swiss Geological Survey

GRS
Gesellschaft für Anlagen- und Reaktorsicherheit mbH, Germany

HSK
Swiss Federal Nuclear Safety Inspectorate

IRSN
Institut de radioprotection et de sûreté nucléaire, France

JNC
Japan Nuclear Cycle Development Institute, Japan

NAGRA
National Cooperative for the Disposal of Radioactive Waste, Switzerland

OBAYASHI
Obayashi Corporation, Japan

SCK·CEN
Studiecentrum voor Kernenergie, Centre d'étude de l'énergie nucléaire, Belgium

Direction of the Project

FOWG
Federal Office for Water and Geology, Switzerland

Project Management

GI
Geotechnical Institute Ltd., St-Ursanne, Switzerland

List of authors

Hydrogeological Synthesis: List of authors

J.-Y. Boisson
I.R.S.N. / D.E.S. / S.E.S.I.D.
Bat. UIS / pièce 224
60–68 Avenue du Général Leclerc BP n°17
F-92 262 Fontenay-aux-Roses Cedex France
jean-yves.boisson@irsn.fr

J. Croisé
Colenco Power Engineering AG
Täfernstrasse 26
CH-5405 Baden, Switzerland
jean.croise@colenco.ch

P. Marschall
Nagra
Hardstrasse 73
CH-5430 Wettingen, Switzerland
paul.marschall@nagra.ch

L. Schlickenrieder
Colenco Power Engineering AG
Täfernstrasse 26
CH-5405 Baden, Switzerland
liane.schlickenrieder@colenco.ch

P. Vogel
BGR
Stilleweg 2
CH-30655 Hannover, Germany
p.vogel@bgr.de

S. Yamamoto
Obayashi Corporation
Shinagawa Intercity Tower B, 2-15-2 Konan,
Minatoku,
Tokyo 108-8502, Japan
yamamoto.shuichi@obayashi.co.jp

Editor

Peter Heitzmann
Federal Office for Water and Geology
Swiss Geological Survey
CH-3003 Bern
Switzerland
peter.heitzmann@bwg.admin.ch

Osmotic Flow: List of authors

P. Bossart
Geotechnisches Institut AG
Gartenstr. 13
CH-3007 Bern, Switzerland
paul.bossart@geo-online.com

H.R. Fisch
Solexperts AG
Schulstrasse 5
CH-8603 Schwerzenbach, Switzerland

J.F. Harrington
British Geological Survey
Kingsley Dunham Centre
Keyworth
Nottingham
NG12 5GG
United Kingdom

St.T. Horseman
British Geological Survey
Kingsley Dunham Centre
Keyworth
Nottingham
NG12 5GG
United Kingdom

D.J. Noy
British Geological Survey
Kingsley Dunham Centre
Keyworth
Nottingham
NG12 5GG
United Kingdom

Preface of the Editor

The international research project Mont Terri (St-Ursanne, Canton Jura) started in January 1996. Research is carried out in a gallery and in niches excavated from the security gallery of the Mont Terri road tunnel. The aim of the project is the geological, hydrogeological, geochemical and geotechnical characterisation of a clay formation, specifically of the Opalinus Clay. Twelve partners from six different countries participate today in the project. The Swiss Geological Survey, a division of the Federal Office for Water and Geology (FOWG), supports hydrogeological research projects in low-permeability formations and is one of the Mont Terri partners since the beginning of the project. The FOWG is in charge of the project direction since July 2001 and is also responsible for the publication of the reports. For geological reasons, a repository for radioactive waste in the Mont Terri region has been ruled out.

After the completion of different experiments in the field of hydrogeology during phases 1 to 5, the results obtained were compiled in an extensive synthesis. Following the publication of a general synthesis (SNHGS, Geological Report No. 23, 1999), the geological description of the Mont Terri region (Reports of the FOWG, Geology Series No. 4, 2003) and the geochemical synthesis (Reports of the FOWG, Geology Series No. 5, 2003), we are pleased to present now the hydrogeological synthesis and a special report on osmotic flow to a broader scientific audience. The editor would like to express his best thanks to the authors and all others contributing to this volume for their special effort. We would also like to thank the Mont Terri Partners for their excellent collaboration and the federal and cantonal authorities for their support in the project. Dr. P. Heitzmann (FOWG) is gratefully acknowledged for the edition of this report.

The authors alone are responsible for the content of the text and the illustrations.

Further information can be found on the Internet site www.mont-terri.ch.

Préface de l'éditeur

Depuis 1996, des expériences dans le cadre du projet de recherche international du Mont Terri (St-Ursanne, Canton du Jura) sont réalisées dans une galerie et des niches excavées à partir de la galerie de sécurité du tunnel autoroutier du Mont Terri. L'objectif principal du projet est la caractérisation géologique, hydrogéologique, géochimique et géotechnique d'une formation argileuse, les Argiles à Opalinus. Douze partenaires de six différents pays collaborent aujourd'hui au projet. Le Service géologique national (Office fédéral des eaux et de la géologie, OFEG) soutient l'étude des formations géologiques à faible perméabilité et collabore dès le début comme partenaire au Projet Mont Terri. La direction du projet est depuis juillet 2001 placée sous la responsabilité de l'OFEG, auquel incombe également la publication des rapports. Pour des raisons géologiques, il n'est pas question d'entreposer des matériaux radioactifs dans la région du Mont Terri.

Après l'achèvement des différentes expériences hydrogéologiques des phases 1 à 5, les résultats obtenus ont été mis en valeur sous la forme d'une vaste synthèse. C'est un plaisir de présenter ici à un large public de spécialistes cette synthèse hydrogéologique, accompagnée d'un rapport spécial sur le flux osmotique, après la publication d'une première synthèse générale (SHGN, Rapport géologique No 23, 1999), la description géologique de la région du Mont Terri (Rapports de l'OFEG, Série géologie No 4, 2003) et la synthèse géochimique (Rapports de l'OFEG, Série géologie No 5, 2003). L'éditeur tient à remercier les auteurs ainsi que les personnes qui, par leur compétence et leur engagement, ont permis la réalisation de cette synthèse. Nos remerciements s'adressent aussi à nos partenaires du Projet Mont Terri pour leur précieuse collaboration et aux autorités fédérales et cantonales pour leur soutien dans le projet. P. Heitzmann, dr.sc.nat. (OFEG) est remercié du suivi de l'édition du rapport.

Les auteurs sont seuls responsables du contenu du texte et des illustrations.

Pour toute information supplémentaire, veuillez consulter le site Internet www.mont-terri.ch.

Vorwort des Herausgebers

Seit 1996 werden im Rahmen des internationalen Forschungsprojektes Mont Terri (St-Ursanne, Kanton Jura) in einem erweiterten Teil des Sicherheitsstollens des Mont-Terri-Autobahntunnels Untersuchungen durchgeführt. Das Hauptziel dieses Projektes ist die geologische, hydrogeologische, geochemische und geotechnische Charakterisierung von Tongesteinen, im Speziellen des Opalinus-Tons; heute sind zwölf Partner aus sechs Ländern daran beteiligt. Die Landesgeologie im Bundesamt für Wasser und Geologie (BWG) unterstützt die hydrogeologischen Untersuchungen geringdurchlässiger geologischer Formationen und arbeitet deshalb von Beginn an als Partnerin im Mont-Terri-Projekt mit. Die Leitung des Projektes liegt seit Mitte 2001 beim BWG. Dieses ist auch für die Veröffentlichung der Berichte verantwortlich. Aus geologischen Gründen ist im Mont-Terri-Gebiet jegliche Planung eines Endlagers für radioaktive Abfälle ausgeschlossen.

Nach der Durchführung verschiedener hydrogeologischer Experimente während der Phasen 1 bis 5 sind deren Ergebnisse zu einer umfassenden Synthese verarbeitet worden. Es freut uns, im Rahmen der Mont-Terri-Publikationen nach der einführenden Zusammenfassung (LHG, Geologische Berichte Nr. 23, 1999), der geologischen und hydrologischen Beschreibung des Mont-Terri-Gebietes (Berichte des BWG, Serie Geologie Nr. 4, 2003) und der Geochemie-Synthese (Berichte des BWG, Serie Geologie Nr. 5, 2003) jetzt auch die hydrogeologische Synthese sowie den Spezialbericht über Osmose einem breiten Fachpublikum vorlegen zu können. Das BWG als Herausgeber möchte den Autoren und allen andern, die an diesem Band beteiligt waren, für ihren grossen Einsatz bestens danken. Ebenfalls danken möchten wir unseren Mont-Terri-Partnern für die wertvolle Zusammenarbeit sowie den eidgenössischen und kantonalen Behörden für ihre Unterstützung im Projekt. Dr. P. Heitzmann sei für die Begleitung der Herausgabe gedankt.

Für den Inhalt des Textes und die Illustrationen sind die Autoren allein verantwortlich.

Weitere Informationen zum Mont-Terri-Projekt finden Sie unter www.mont-terri.ch.

Prefazione dell'editore

Dal gennaio 1996, ricerche effettuate nell'ambito del progetto di ricerca internazionale Mont Terri (St-Ursanne, Canton Giura) sono realizzate in un cunicolo e nelle nicchie scavate a partire dalla galleria di soccorso del tunnel autostradale del Mont Terri. L'obiettivo principale del progetto è la caratterizzazione geologica, idrogeologica, geochimica e geotecnica di una particolare formazione argillosa: l'Argilla ad Opalinus. A tutt'oggi collaborano al progetto dodici partner di sei diverse nazioni. Il Servizio geologico nazionale dell'Ufficio federale delle acque e della geologia (UFAEG) promuove gli studi di formazioni geologiche a bassa permeabilità, collaborando fin dall'inizio come partner del progetto Mont Terri. Dal luglio 2001, il progetto è sotto la direzione dell'UFAEG, al quale compete anche la pubblicazione dei rapporti. La pianificazione di un deposito finale per le scorie radioattive sotto il Mont Terri è da escludere per ragioni geologiche.

Dopo aver concluso diverse ricerche idrogeologiche durante le fasi da 1 a 5, i risultati sono stati presentati in un'ampia sintesi. La sintesi e il rapporto speciale sul flusso osmotico, destinati a un largo pubblico di specialisti, fanno seguito alla sintesi introduttiva (SIGN, Rapporti geologici, n. 23, 1999), alla descrizione geologica della regione (Rapporti dell'UFAEG, Serie geologia n. 4, 2003) e alla sintesi geochimica (Rapporti dell'UFAEG, Serie geologia n. 5, 2003). Ringrazio tutti gli autori e le persone che, con le loro conoscenze e il loro impegno, hanno contribuito alla riuscita dell'opera. I ringraziamenti vanno estesi anche ai partner del Mont Terri e alle autorità cantonali e federali per la preziosa collaborazione e il sostegno al progetto. Un ringraziamento particolare va al Dr. P. Heitzmann (UFAEG) per l'edizione del rapporto.

Gli autori sono gli unici responsabili del contenuto dei testi e delle illustrazioni.

Ulteriori informazioni sono pubblicate all'indirizzo www.mont-terri.ch.

Federal Office for Water and Geology
The Head of the Swiss Geological Survey

Dr. Christoph Beer

Synthesis of Hydrogeological Investigations at Mont Terri Site (Phases 1 to 5)

P. Marschall, J. Croisé, L. Schlickenrieder, J.-Y. Boisson, P. Vogel & S. Yamamoto

Recommended quotation:
Marschall, P. et al. (2004): Synthesis of Hydrogeological Investigations at the Mont Terri Site (Phases 1 to 5).
In: Heitzmann, P. (Ed): Mont Terri Project – Hydrogeological Synthesis, Osmotic Flow (p. 7–92). – Reports of the Federal Office for Water and Geology (FOWG), Geology Series No. 6.

Abstract

The Mont Terri project has provided the opportunity to assess hydrogeological testing procedures in the clay-rich Opalinus Clay formation and to shed light on the hydrogeological setting of the Mont Terri region of Northern Switzerland. The hydrogeologically relevant field methodologies applied, data analyses performed and results obtained from experiments conducted in the Mont Terri rock laboratory in the years 1996 to 2000 served as a data base for the three objectives of this synthesis:

– Assessment of the achievements of the hydrogeological investigations both in terms of *development of investigation techniques* and in terms of geoscientific *data analysis.*
– Development of a *conceptual model of groundwater flow* at the Mont Terri site.
– Development of a *conceptual model of gas migration mechanisms* in the Opalinus Clay.

The intended audience of this report includes readers with a hydrogeological background, in general, and an interest in the hydrodynamics of clay-rich formations, in particular. The introduction to the Mont Terri rock laboratory and its geological environment is brief. However, comprehensive literature on the Mont Terri project is referenced.

Various types of hydraulic long-term monitoring systems, e.g. classical inflatable multipacker systems, PP system and minipacker piezometers, were tested in the rock laboratory and evaluated with special focus on their applicability in clay-rich formations. Design criteria were established which prove particularly useful for investigations in Opalinus Clay, such as the minimisation of the effective volume of the observation interval and the appropriate selection of the materials for the downhole equipment to prevent corrosion and to allow for representative porewater sampling.

The results from the hydraulic packer testing were assessed for possible clay-specific artifacts which could be introduced as a consequence of drilling techniques and testing methodologies. The experiments demonstrated that chemico-osmotic effects may influence the transmissivity of the formation zone immediately beyond the borehole wall. The effect is minor, however, and does not significantly affect the formation-property estimates.

A preliminary conceptual hydrogeological model of the Mont Terri site was developed. The hydrogeological units of main concern for the underground laboratory and its vicinity are the karstified "Lower Dogger" aquifer and the Opalinus Clay formation, a highly efficient flow barrier. The hydraulic significance of the Jurensis Marls and Posidonia Shales to the North has not been established very well. The main fault, which intersects the rock laboratory, does not affect the barrier function of the Opalinus Clay. The hydraulic conductivity of the Opalinus Clay generally shows low spatial variability and lies in the range of 2×10^{-14} – 2×10^{-12} m/s. The expected range of specific storage is 2×10^{-7} – 3×10^{-5} 1/m. The primary driving force for porewater flow in the Opalinus Clay at the Mont Terri site is gravity: the long-term observations of hydraulic head depict a clear cone of depression towards the gallery system. Also, the "Lower Dogger" aquifer to the South represents a sort of constant pressure boundary for the hydraulic system.

An assessment of the gas transport mechanisms with results from laboratory and in-situ experiments showed evidence of both non-dilatant and dilatant gas transport. The observed gas entry pressure for the Opalinus Clay was generally low (< 1 MPa). Enhancement of gas permeability was observed at elevated gas injection pressures (2–3 MPa), suggesting that gas flow is entailed by microscopic pathway dilation processes. Hydrofrac experiments exhibited frac pressures of 9 MPa and refrac pressures in the order of 4–5 MPa.

Acknowledgements

The authors would like to thank Prof. G. de Marsily (Laboratoire Geologie Appliquée, Université Pierre et Marie Curie, Paris / France), Dr. P. Bossart (Mont Terri Project, St. Ursanne / Switzerland) and Dr. M. Thury (Mont Terri Project and Nagra, Wettingen/Switzerland) for inspiring discussions and for valuable review comments on this manuscript. Their contributions to the facts and interpretations greatly improved the overall value of the report and are gratefully acknowledged.

Contents

Abstract 9
Acknowledgments 10
List of Contents 11
List of Tables 12
List of Figures 13

1 Introduction 15
1.1 The Mont Terri project: Phases 1 to 5 15
1.2 Scope and objectives 17
1.3 Report organisation 17

2 Hydrogeological Site Investigations in Phases 1 to 5 18
2.1 Geological setting 18
2.2 Program overview 18
2.3 Experiments of hydrogeological relevance 20

3 Developments in Hydrogeological Investigation Techniques and Data Analysis 23
3.1 Particular issues of interest 23
3.2 Suitability assessment of hydrogeologically relevant data 23
3.3 Developments in long-term monitoring systems for pore pressure and water sampling 24
3.3.1 Problems related to the clay-rich environment 24
3.3.2 Equipment portraits 24
3.3.3 Equipment performance 27
3.3.4 Concluding remarks 28
3.4 Impact of drilling technique on packer test results 29

4 Conceptual Model of Groundwater Flow at the Mont Terri Site 31
4.1 Introduction 31
4.2 General outline of the synthesis approach 31
4.3 Hydrogeological data base from Phases 1 to 4 32
4.3.1 Packertests 32
4.3.2 Permeameter tests 35
4.4 Assessment of coupled processes 37
4.4.1 Threshold gradient 37
4.4.2 Osmosis 41
4.4.3 Coupled hydro-mechanical processes 43
4.5 Groundwater flow at different scales 49
4.5.1 Site scale (10^1 – $>10^3$ m) 50
4.5.2 The scale of tunnel investigations (10^{-1} – 10^1 m) 53
4.5.3 The scale of core mapping (10^{-3} – 10^{-1} m) 55
4.5.4 The sub-millimeter scale 55
4.6 Pore pressure distribution at the Mont Terri site 58
4.6.1 Data base 58
4.6.2 Interpretation of the pore pressure distribution in the Opalinus Clay formation 61
4.6.3 Simple assessment of the galleries' drainage effects with numerical simulations 62
4.7 Evaluation of current hydrogeological site understanding 66

5 Gas Migration Mechanisms in the Opalinus Clay 67
5.1 Introduction 67
5.2 Conceptual approaches of gas migration in clay formations 67
5.3 Quality assurance of gas related experiments 69
5.4 Modelling of gas related experiments 71
5.4.1 Two-phase flow modelling of the gas threshold pressure test in BGP-4 71
5.4.2 Hydro-mechanical modelling of the BGS-2 gas injection experiment Objectives 73
5.4.3 Long-term gas injection tests 76
5.4.4 Hydrofrac an gasfrac experiments 76
5.5 Evaluation of achievements 79
5.5.1 Two phase flow modelling of the gas threshold pressure test in BGP-4 Objectives 79
5.5.2 Hydro mechanical modelling of the BGS-2 gas injection experiment Objectives 82

6 Summary and Conclusions 86
6.1 Summary of achievements 86
6.2 Unresolved issues and outlook 87

7 References 88
Mont Terri technical Notes 89

List of Tables

Table 1.1: Organisations involved in the Mont Terri project 16
Table 2.1: Main contributing experiments to the hydrogeological investigations at the Mont Terri site 19
Table 3.1: Summary of the suitability assessment with resulting suitability typing. 24
Table 3.2: Summary of the results from the final hydraulic test sequence after fluid replacement with Pearson water in boreholes BDB-1, BDB-2 and BDB-3 35
Table 4.1: Overview of the relevant packer test results in the Opalinus Clay formation at the Mont Terri rock laboratory 35
Table 4.2: Summary of results from the permeameter tests and structural investigations. 36
Table 4.3: Range of validity of Darcy's law and threshold gradient estimates. 41
Table 4.4: Hydrogeological classification of the lithostratigraphic units in the Mont Terri region (after Thury & Bossart 1999). 52
Table 4.5: Ranges of hydraulic properties in the 3 facies of the Opalinus Clay. 55
Table 4.6: Mineralogy of the clay-rich shaly facies of the Opalinus Clay at Mont Terri after Mazurek (2001). 56
Table 4.7: Microstructural properties of the Opalinus Clay at Mont Terri after Nagra 2002 57
Table 5.1: Overview of potential gas migration mechanisms. 57
Table 5.2: Summary of the quality review of the field and laboratory methods. 70
Table 5.3:Summary of the quality review of the data analysis of gas tests performed in Phases 1 to 5 71
Table 5.4: Two-phase flow parameters as derived from laboratory experiments on core samples of the Opalinus Clay from the Mont Terri rock laboratory. 72
Table 5.5: Two-phase flow parameters as derived from gas threshold pressure tests at the Mont Terri rock laboratory. 74
Table 5.6: Hydraulic fracturing experiment in interval I2.2 of borehole BGS-2: stages of the complex test sequence. 78

List of Figures

Figure 1.1: Location map of the Mont Terri Rock Laboratory (Thury & Bossart eds. 1999) 15
Figure 1.2: Overview of the organisational structure and distribution of responsibilities for the Mont Terri project as of July 2001 16
Figure 2.1: (a) View toward the North, with St-Ursanne in the foreground and Mont Terri in the center with the red arrow indicating the southern entrance of the motorway tunnel. (b) 3D view of the Mont Terri rock laboratory..... 18
Figure 2.2: 3D view of the Mont Terri site showing niches and boreholes of relevance for the synthesis of hydrogeological investigations..... 22
Figure 3.1: Piezometer systems tested in Phases 1 to 4 of the Mont Terri research program..... 26
Figure 3.2: Pressures recorded with inflatable packers and mechanical minipacker piezometers during the interference test of the GP experiment/Phases 1 and 2 27
Figure 3.3: Pressures recorded with inflatable p ackers and PP equipment in the GP experiment/ Phases 3 and 4..... 28
Figure 3.4: Map view and cross-section of the set-up for the systematic investigation of the impact of the drilling technique and the chemical composition of the test fluids on packer test results..... 30
Figure 4.1: Baseline simulation of pressure response in BGP-1 33
Figure 4.2: Baseline simulation of pressure change and derivative during BGP-1 – R12 constant-rate injection test 33
Figure 4.3: Uncertainty analysis of BGP-1 hydraulic conductivity and specific storage estimates 34
Figure 4.4: Schematic configuration of the BGS permeameter after Harrington et al. 2001..... 36
Figure 4.5: Permeameter test conducted in the OP experiment..... 38
Figure 4.6: Simulation of a sequence of rate injection and head injection tests in BGP-4 as part of the GP experiment 39
Figure 4.7: Simulation of the crosshole response in BGP-3/I1 to a sequence of rate injection and head injection tests in BGP-4 40
Figure 4.8: Pressures recorded in borehole BOP-1 ... 42
Figure 4.9: Schematic diagram showing Total Dissolved Solids vs. Distance along the Mont Terri reconnaissance gallery..... 43
Figure 4.10: Interference test in the FM niche with a water-injection test in BGP-6: test configuration with the four boreholes..... 45
Figure 4.11: Inverse modelling of the packer test conducted in BGP-6 47
Figure 4.12: Hydro-mechanical modelling of the interference test in BGP-6 – simulated interval pressures..... 49
Figure 4.13: Hydraulically relevant structural and stratigraphic elements at various scales of observation..... 50
Figure 4.14: (a) Simplified geological cross-section through the Mont Terri anticline along the motorway tunnel, showing the location of the Mont Terri rock laboratory (Thury & Bossart 1999) and (b) simplified map of the Mont Terri anticline 51
Figure 4.15: Chloride profiles as an indirect evidence for groundwater flow conditions in the Opalinus Clay and in the adjacent stratigraphic formations 53
Figure 4.16: The scale of tunnel investigations (10^{-1} – 10^{1} m) 54
Figure 4.17: Small scale mapping of structural features in the BF niche of the reconnaissance gallery 55
Figure 4.18: Photographic documentation of drillcores and classification of lithological/structural features.
Figure 4.19: Visualisation of the microstructure of Opalinus Clay by SEM 57
Figure 4.20: Determination of equivalent pore radii by Hg porosimetry and nitrogen desorption 57
Figure 4.21: Cross-section through the Mont Terri site with piezometric levels..... 58
Figure 4.22: Pressure monitoring from mid 1997 to early 1999 59
Figure 4.23: The pressure transients in the period from July 1999 to June 2000 61
Figure 4.24: Compilation of pressure observations in boreholes of the Mont Terri rock laboratory on 30.06.2000 62
Figure 4.25: Compilation of pressure observations gathered in boreholes at the Mont Terri rock laboratory on 30.06.2000 63
Figure 4.26: Vertical configuration and 2D finite element mesh used to simulate the pressure head 64
Figure 4.27: Simulation of the distribution of pressure head 64
Figure 4.28: Comparison of pressure observations and the results of the numerical simulation with $K = 1\times10^{-13}$ m/s and $S_s = 1\times10^{-6}$ 1/m..... 65
Figure 5.1: Schematic view of the isostatic cell and sample assembly for the Opalinus Clay samples as part of the GP experiment 72
Figure 5.2: Photographs of the BED-C5/7 sample taken right after the gas injection test..... 73
Figure 5.3: Diagnostic analysis of gas threshold pressure test in interval I4.2 of borehole BGP-4 74
Figure 5.4: Long-term gas injection experiment in the GP-A/GS site 75
Figure 5.5: Sequence of hydrofrac and re-frac events

in test interval I2.2 of borehole BGS-2..... 77
Figure 5.6: Hydraulic response in interval I1.2 of borehole BGS-1 to the hydrofrac and re-frac events in test interval I2.2 of borehole BGS-2..... 78
Figure 5.7: Modelling of the extended gas threshold pressure test in interval I4.2 of borehole BGP-4 with a two-phase flow simulator..... 81
Figure 5.8: Modelling of the gas test sequence in BGS-2/I2 with TOUGH2..... 83
Figure 5.9:Coupled 3D hydro-mechanical simulation: Pressure history in BGS-2/I2, BGS-1/I2 and BGS-2/I3, and FIM data in boreholes BGS-3 and BGS-4 84

1 Introduction

1.1 The Mont Terri project: Phases 1 to 5

The Mont Terri project was called to life in 1995. The common interest of the founding organisations concerned argillaceous formations as potential host rocks for repositories of radioactive waste. The hub of the international research project is the Mont Terri rock laboratory in the Mont Terri motorway tunnel in northwestern Switzerland (Figure 1.1). Its testing ground is the Opalinus Clay, a Mesozoic shale formation.
The organisational structure of the Mont Terri project is sketched out in Figure 1.2. The Director of the Mont Terri project is a member of the Swiss Geological Survey of the Federal Office for Water and Geology (FOWG/SGS). Delegates of the FOWG/SGS as well as of the remaining partner organisations form the program committee which is responsible for the definition of annual research programs (see Table 1.1) and budgets. This way each project partner may bring forward its own experiment proposals or express interest to participate in others. Incidentally, the annual research periods are referred to as Phases which generally span from the beginning of July of one year to the end of June of the following year.
The FOWG/SGS submits the annual research programs to the République et Canton Jura for authorisation. Once the research program for a Phase has been authorised it is the responsibility of the project manager (represented by Geotechnical Institute Ltd of St-Ursanne), to implement it in the laboratory. Each experiment is assigned a principal investigator who is one of the delegates representing the participating project partners for that particular experiment. The principal investigator, together with the experiment delegates and the project manager, ascertains that the scientific goals of the experiment are achieved. In particular, the technical performance of field work and laboratory tests as well as the quality assurance of the project documentation, are their key concerns. Complementary, the project management draws responsible for the on-site coordination of the field work, the book keeping and the distribution of reports. The work is then carried out by a series of contractors of which currently there are about 23 universities and national research institutes plus more than 30 companies from six European countries and Japan.
The research program conducted at the Mont Terri rock laboratory is rather comprehensive. The overall aim, to broaden the geoscientific data base as a prerequisite for comprehensive understanding of the barrier function of argillaceous formations, calls upon the full spectrum of geosciences. It may best be summarised with the following objectives:

- Evaluation of investigation techniques particularly suitable to a low permeability clay-rich medium
- Characterisation of the Opalinus Clay formation in terms of its geological, hydrogeological, geochemical and mechanical properties
- Characterisation of changes in the argillaceous host rock environment as induced by gallery excavation, by exposure to a heat source and by chemically aggressive fluids
- Evaluation of suitable techniques for repository construction, waste emplacement and gallery sealing in the Opalinus Clay

The activities of Phases 1 to 4 of the Mont Terri project were occupied predominantly by the compilation of a broad basis of geoscientific data in a fairly short period of time, rather than at conducting elaborate data analyses and integrated interpretations. At the end of Phase 4 a new type of scientific projects was implemented specifically for the interdisciplinary interpretation of data acquired to that point in time: "Geo-

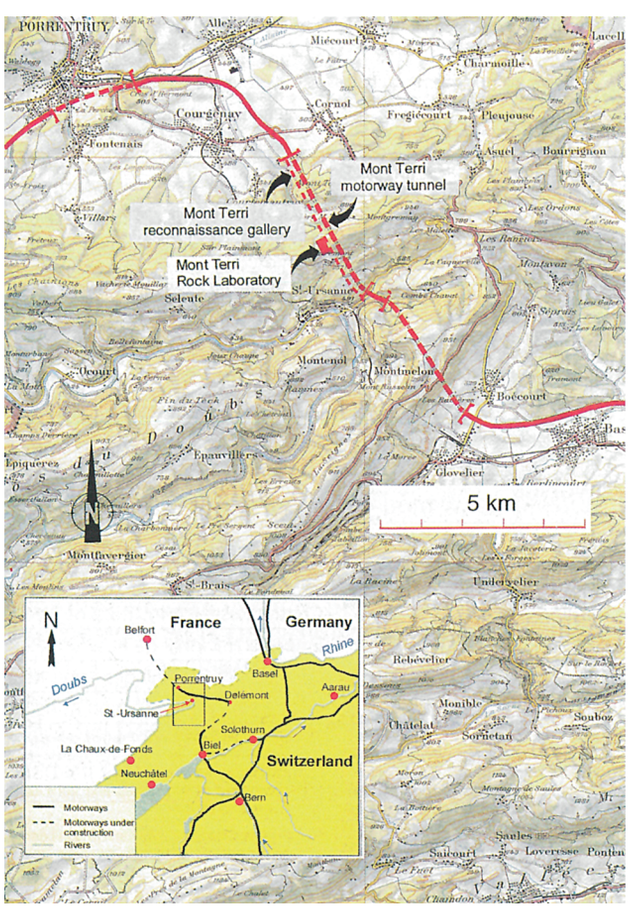

Figure 1.1: Location map of the Mont Terri Rock Laboratory (Thury & Bossart eds. 1999). Published with the permission of swisstopo (BA046450).

chemical Modelling" (GM), "Rock Mechanical Analyses" (RA) and "Hydrogeological Analyses" (HA). This report is part of the HA project and summarises the interpretation and synthesis of the hydrogeological data base from Phases 1 to 5. Project partners are BGR, IRSN, Nagra and Obayashi Corporation.

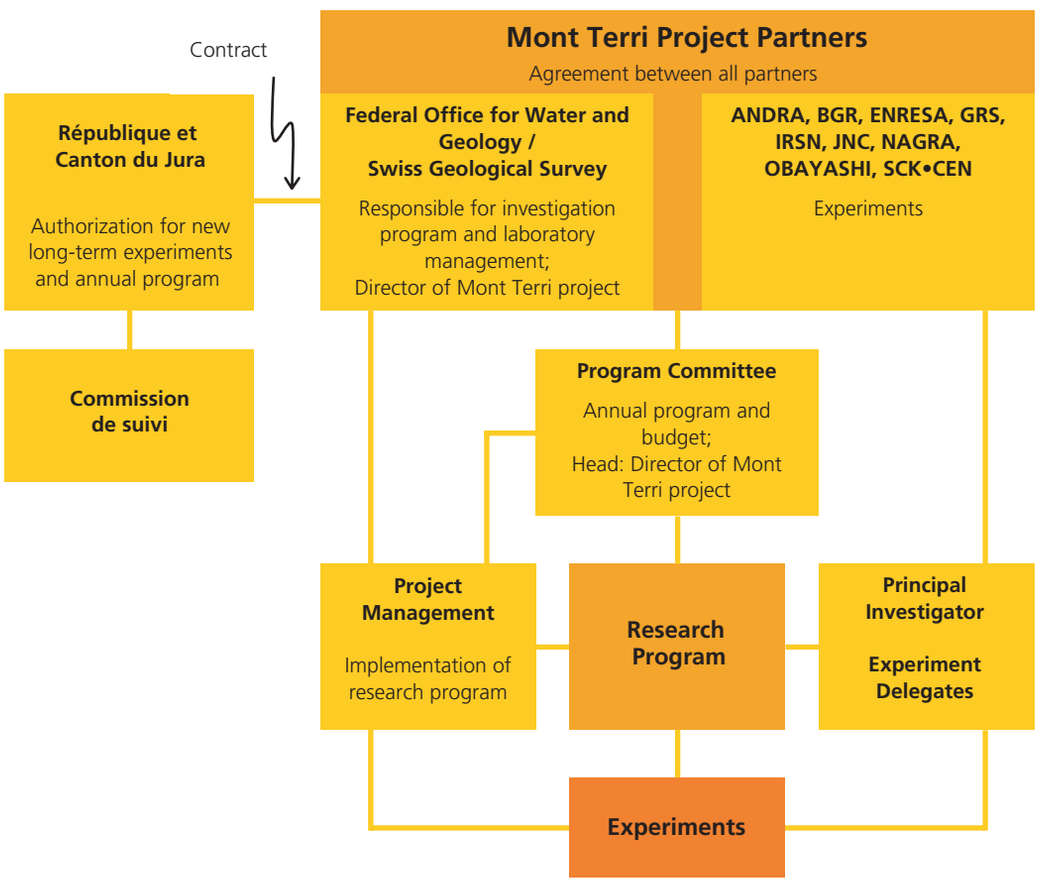

Figure 1.2: Overview of the organisational structure and distribution of responsibilities for the Mont Terri project as of July 2001 (after www.forumvera.ch Bulletin 03/01).

Project Partners

FOWG/SGS	Federal Office for Water and Geology/Swiss Geological Survey (Director of the Mont Terri project)	Switzerland
ANDRA	Agence nationale pour la gestion des déchets radioactifs	France
BGR	Bundesanstalt für Geowissenschaften und Rohstoffe	Germany
CRIEPI*)	Central Research Institute of Electric Power Industry	Japan
ENRESA	Empresa Nacional de Residuos Radiactivos, S.A.	Spain
GRS	Gesellschaft für Anlagen- und Reaktorsicherheit mbH	Germany
IRSN	Institut de radioprotection et de sûreté nucléaire	France
JNC	Japan Nuclear Cycle Development Institute	Japan
NAGRA	National Cooperative for the Disposal of Radioactive Waste	Switzerland
OBAYASHI	Obayashi Corporation	Japan
SCK·CEN	Studiecentrum voor Kernenergie, Centre d'étude de l'energie nucléaire	Belgium

Project Management

GI	Geotechnical Institute Ltd., St-Ursanne	Switzerland

Table 1.1: Organisations involved in the Mont Terri project (*) joined in July 2002).

1.2 Scope and objectives

The early Phases of the Mont Terri project emphasised data collection in the field and initial analysis. Integrated approaches to the interpretation of field results had been assigned low priority. Consequently, many of the field and laboratory investigations were documented in a series of Mont Terri Technical Notes without a well-defined level of quality assurance. It was left to the different experimental teams to specify their quality requirements for the contractors' reports. Eventually, at the end of Phase 4 the project partners agreed to implement a new type of scientific projects. These were to stress the synergetic interpretation of the data compiled since the beginnings of the project for the interests of specific disciplines. The experiments initiated for this purpose in the realm of the Mont Terri research program are Geochemical Modelling and Synthesis (GM; Pearson et al. 2003), Rock Mechanical Analyses (RA; Bock 2001, 2002) and Hydrogeological Analyses (HA).
This report is one of the products of the HA experiment. The project partners participating in this experiment have been BGR (Germany), IRSN (France), Nagra (Switzerland) and Obayashi Corporation (Japan). The report's purpose is to provide a synthesis of the hydrogeological investigations conducted at the Mont Terri site in the course of project Phases 1 through 5, i.e. from the project's beginnings in 1996 to mid 2000. The approach chosen to attain this goal divides the synthesis into three subtasks:

- To assess the achievements of the hydrogeological investigations both in terms of *development of investigation techniques* and in terms of geoscientific *data analysis* in low permeability argillaceous formations
- To establish a *conceptual model of groundwater flow* at the site
- To establish a *conceptual model of gas migration mechanisms in Opalinus Clay*

The concluding efforts are dedicated to an assessment of the current level of overall conceptual understanding of groundwater flow at the site, as well as to open issues requiring further attention.
The intended readership of this report includes scientists actively involved in the experimental work at the Mont Terri laboratory and, more generally, hydrogeologists working with shaly aquitards. The synthesis may be of interest particularly to scientists and engineers engaged in projects related to the geological disposal of radioactive waste. For an account of the larger scope and context of the Mont Terri project, the reader is referred to, for example, Thury & Bossart eds. (1999). This report does not cover the complex hydromechanical processes observed in the excavation disturbed zone (cf. Martin & Lanyon 2004), nor those in the unsaturated zone.

1.3 Report organisation

The opening chapter 1 provides general organisational background on the Mont Terri project, outlines the overall goals and motivation of the project, and introduces the objectives for this synthesis of hydrogeological investigations. Beyond that, the report essentially follows the objectives as stated above.
Chapter 2 is an introduction to the hydrogeological site investigations conducted in Phases 1 through 5. It sets the stage for the subsequent chapters with a short outline of the infrastructure of the underground rock laboratory and a brief review of the experiments of relevance for the synthesis of hydrogeological investigations overall.
Chapter 3 then provides a more detailed look of the hydrogeologically relevant investigations with an assessment of three specific aspects: (i) the suitability of hydrogeologically relevant data for consideration in the synthesis; (ii) recent developments in long-term monitoring methodologies for in-situ pore pressures; and (iii) the reliability of packer test results.
Chapter 4 establishes a conceptual model of groundwater flow for the Mont Terri site. The regional extent of the site scale is in the order of several kilometers. More detailed relevant scales addressed in the model are those generally covered in tunnel investigations, in core mapping and in small experimental or microscopic work. These are characterised in terms of groundwater flow mechanisms and site specific hydraulic parameters. The final section discusses the current perception of the distribution of pore water pressure at the site.
Chapter 5 is devoted to gas migration mechanisms in the Opalinus Clay. Relevant mechanisms are assessed, experimental work on gas migration is reviewed and information on the two-phase flow properties of the Opalinus Clay is compiled.
The final chapter summarises the key findings of the synthesis and points out some unresolved issues with an outlook on developments to be expected in the project's future.

2 Hydrogeological Site Investigations in Phases 1 to 5

2.1 Geological setting

There are two main structural domains of the Jura mountains in Switzerland: the Tabular Jura and the Folded Jura. Rocks in the Jura mountains are of Triassic to early Cretaceous age and were deposited mostly in marine environments with generally uniform subsidence. They comprise limestones, evaporitic rocks, and marls/shales. Mont Terri, situated near the town of St-Ursanne (Figure 2.1a) is the northernmost of a series of anticlines of the Folded Jura, and has been overthrust at least 1 km north-westwards over the Tabular Jura. In its total length, the anticline is 50 km along strike and, at Mont Terri, is an asymmetrical dome-shaped fold. Folding took place during the Late Miocene to Pliocene, about 10 to 2 Ma ago.
Rocks of Middle Jurassic to Triassic age (i.e. Dogger to Keuper) are exposed on the present surface of Mont Terri (cf. also Figure 4.14). The formation of interest, the Opalinus Clay, is of Lower Aalenian age (Dogger α, 180 to 178 Ma). In northern Switzerland it forms an 80 to 160 m thick sequence of claystone and marl with intercalated sandy and calcareous layers and lenses. In the Mont Terri underground laboratory, the Opalinus Clay is met at a present overburden of 250 to 320 m. The past overburden is estimated to at least 1000 m. The formation dips from 20 to 60° to the southeast and intersects the reconnaissance gallery for a 243 m long section (Figure 4.14a). It is underlain by the Toarcian Jurensis marl (Lias ζ) and overlain by the so-called Lower Dogger (Lower Bajocian/Upper Aalenian, elsewhere called Murchisonae-Concava Beds, Dogger α, or Blaukalk). Between the Muschelkalk aquifer below and the Malm aquifer above, the shale succession from Keuper/Lias to Dogger forms a 300 to 450 m thick sequence of low to very low permeability rocks. The Opalinus Clay can be considered to have water-saturated pore space but practically no water circulation. The overlying Malm formation represents a regional karstic aquifer (e.g. Hauptrogenstein), whereas the underlying Liassic marls and limestones (e.g. Gryphaea Limestones) are only weakly karstified with local water inflows. This very brief description of the geological and hydrogeological setting of the laboratory has been taken from Thury & Bossart eds. (1999), however, in depth discussions will follow in sections 4.5 to 4.7. Notably, an excellent summary of the geology of the Mont Terri site is given in Pearson et al. (2003).

2.2 Program overview

The Mont Terri underground laboratory is located in northwestern Switzerland near the town of St-Ursanne (Figure 2.1a). The laboratory is positioned in the reconnaissance gallery for one of the tunnels of the A16 Transjurane" motorway. Constructed in 1989, the reconnaissance gallery meanwhile has taken on the function of an escape route, i.e. a safety gallery for the motorists. In order to keep the gallery clear of obstructions, the experimental set-ups of the laboratory and the majority of the drilling activity were placed in eight niches especially excavated for this purpose in 1996. All experiments are carried out within the bounds of the Opalinus Clay.
An expansion of the Mont Terri research program prompted the excavation of the roughly 230 m long "new gallery" in the winter of 1997/98. It, too, lies in the Opalinus Clay and the additionally introduced experiments were again set up in niches. Figure 2.1b shows a schematic of the layout of the Mont Terri rock laboratory.

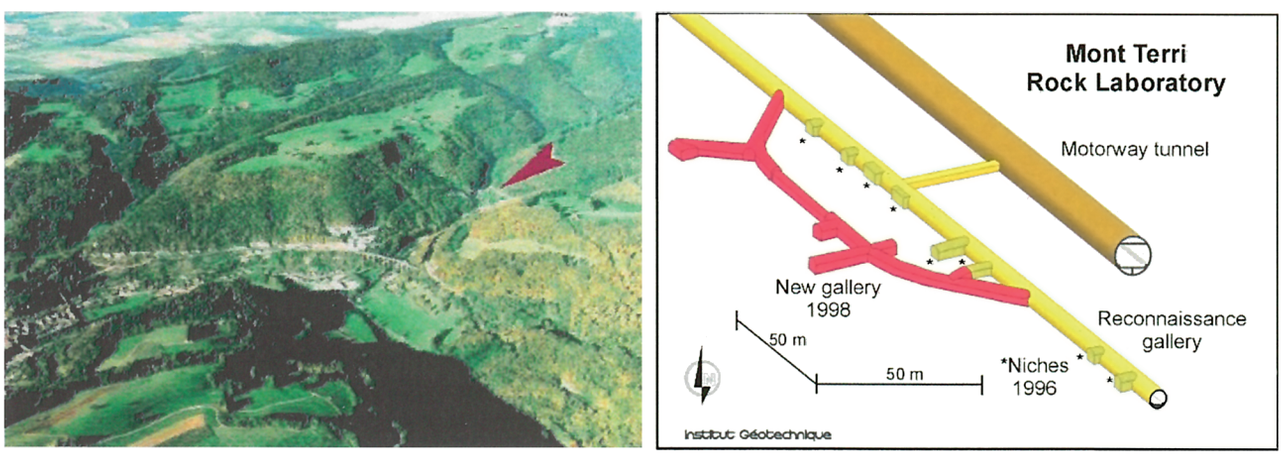

Figure 2.1: (left) View toward the North, with St-Ursanne in the foreground and Mont Terri in the center with the red arrow indicating the southern entrance of the motorway tunnel. (right) 3D view of the Mont Terri Rock laboratory.

The initial set of experiments was run in Phases 1 and 2 between January, 1996 and June, 1997. Hydraulic tests were parts of various experiments designed – at the early stage – primarily to test drilling and measuring techniques in view of the particular challenges posed by the clay-rich mineralogy of the Opalinus Clay formation. From Phase 3 onward, the main focus of the hydrogeologically relevant experiments clearly shifted toward the hydraulic characterisation of the site, i.e. the gathering of representative data. An overview of these experiments is provided in Table 2.1. The experiments' names are an implication of the fact that the investigation approaches and the principal topics of interest have been various. Whereas experiments like the Hydraulic and Gas Permeability experiment (GP), the Pore Pressure experiment (PP), the Deep Borehole Simulation experiment (DB) and one component of the Flow Mechanism experiment (FM-C) have concentrated on hydraulic packer testing mostly in the undisturbed Opalinus Clay, the ED-A and ED-B experiments were concerned with comparable testing methods but aimed at the excavation disturbed zone. The Gasfrac Self-Healing experiment (GS) and part of GP were devoted mostly to gas testing. The Borehole Fluids Effects (BF) and FM-A experiments shared fluid logging as a common investigation method. The Evaporation Logging experiment (FM-D) was established mainly to test new tools while the Groundwater Sampling experiment (WS-A) was set up primarily for fluid sampling. The Osmotic Pressure experiment (OP) served the analysis of osmotic effects.

Experiment	**Hydrogeological relevance**	**Most pertinent Technical Notes**[1)]	**Phases / Years**[2)]
GP	In-situ hydraulic and gas tests for the determination of the hydraulic and two-phase flow parameters; permeameter tests	96-18, 96-26, 96-27, 97-28, 98-24, 98-25, 99-05, 99-06, 99-07	1 – 5 1996 – 2000
GP-A/GS	Long-term gas injection test/Gasfrac self-healing	2000-06, 2000-07, 2000-10, 2000-11, 2000-12, 2000-13	1 – 6 1996 – 2001
PP	Measurement of the porewater pressure	97-01, 97-02, 97-03	1 – 3 1996 – 1998
DB	Deep borehole hydraulic testing	98-62	4 – 5 1998 – 2000
DT	Drilling techniques (hydraulic test)	96-20	1 – 2 1996 – 1997
BF	Borehole fluid effect	96-05, 96-11, 97-07, 97-36, 98-40, 99-33 (97-29)	1 – 7 1996 – 2002
FM-A	Flow mechanism: fluid logging (& ion-selective logging)		1 – 2 1996 – 1997
WS-A	In-situ groundwater sampling	98-48	1 – 7 1996 – 2002
OP	Hydraulic flow and osmotic pressure	97-39	1 – 6 1996 – 2001
ED-A	EDZ hydraulic and pneumatic tests	97-32	1 – 3 1996 – 1998
ED-B	EDZ porewater pressure monitoring	98-58	4 – 5 1998 – 2000
n.a.	Hydrodynamic characterisation in laboratory	97-38	3 1997
FM-C	Flow mechanism: tracer test (hydraulic testing)	99-49	1 – 7 1996 – 2002
FM-D	Evaporation measurements on tunnel wall and in borehole	96-30, 98-11	3 – 6 1997 – 2001
n.a.	Hydraulic head measurements associated with tunnel excavation	99-22	previous to Mont Terri project

[1)] for complete references please refer to chapter 7

[2)] from Thury & Bossart (1999) and annual work programs

Table 2.1: Main contributing experiments to the hydrogeological investigations at the Mont Terri site with a selection of associated technical notes and an indication of the timeframe within the research program (Note: Some experiments have extended beyond Phase 5. However, only those references are listed which were available by mid 2000).

2.3 Experiments of hydrogeological relevance

It would be beyond the scope of this report to provide detailed descriptions of all relevant experiments. Suffice it then to give a brief overview of the methodology, or at least pertinent parts thereof, for the experiments listed in Table 2.1. For niches and borehole locations, please refer to Figure 2.2.

The GP experiment encompasses hydraulic tests and gas threshold pressure tests in order to investigate single and two-phase flow processes in the Opalinus Clay. The hydraulic tests, including constant rate and constant head injection and pulse tests, have been carried out with various packer configurations in a series of boreholes drilled explicitly for this purpose. The main purpose of the experiments was (i) to investigate the governing flow mechanisms in the Opalinus Clay (possible deviations from Darcy's law), (ii) to determine flow models (flow geometry, coupled processes) and (iii) to estimate representative hydraulic parameters (and two-phase flow parameters).

Attempts have been made to monitor cross-hole pressure responses and responses in intervals located above the test interval, as well as geomechanical reactions to the hydraulic testing. The gas threshold pressure tests have been performed solely in borehole BGP-4. All hydraulic and gas tests have been analysed quantitatively and in detail for formation parameters like hydraulic conductivity, formation storage and gas entry pressure as well as for matrix pressure.

As an independent part of the GP experiment, GP-A is treated in combination with the GS experiment. The hydraulic fracturing tests with hydraulic and gas testing components were conducted in boreholes BGS-1 and BGS-2 and concluded in quantitative estimates of transmissivity for the water phase and of compressibility of the intact formation prior to fracturing. Long-term gas tests are expected to result in two-phase flow properties. Deformations were observed in BGS-3 and BGS-4 in response to hydraulic testing in the adjacent boreholes.

The aim of the PP experiment has been the development and validation of a methodology to measure porewater pressure in formations with very low hydraulic conductivity and free water content. The design of the multi-packer system was to avoid leakage from the test interval, and to minimise the annulus volume and the equipment compressibility in the test section. The very stiff mechanical packers were tested in-situ for their sealing capacity before first pressure build-up measurements were recorded in two test intervals in the Opalinus Clay. The experience gained in the Mol rock laboratory of SCK•CEN concerning PP measurements helped to adequately design the PP equipment for Mont Terri.

The DB experiment was part of the preparation work for the deep borehole project at Benken. Its main concern is the optimisation of the packer testing methodology. Boreholes BDB-1, BDB-2 and BDB-3 at Mont Terri were to simulate the borehole and testing conditions in terms of effects due to different drilling muds and of expected responses to hydraulic testing. The tests included pulse injection, constant head injection and slug withdrawal.

The drilling technique (DT) experiment consisted of three boreholes, BDT-1 to 3 which were all drilled with different fluids. Drilling with compressed air resulted in the most stable boreholes and highest drillcore quality. Of interest to the hydrogeological synthesis are the hydraulic tests performed in three intervals in BDT-2: pulse injection, constant head injection, constant head withdrawal and long-term constant rate injection. The series of tests and the analysis of their observations resulted in transmissivity and corresponding hydraulic conductivity values.

The BF and FM-A experiments are treated in combination for the purpose of the hydrogeological analysis as they share a common investigation method, the fluid logging. In essence, fluid logging entails continuous measurements of electrical conductivity and temperature in a borehole. Ideally, the profiles are then analysed for the location of advective formation water influx as well as the inflow rate and salinity of the formation fluid. Logging took place in numerous boreholes and the records were analysed and interpreted to various degrees. A special type of fluid logging, the ion-selective logging was applied in borehole BGP-4. As a form of hydrochemical logging it is applied to monitor long-term interaction of the borehole fluid with the borehole walls and allows at least for qualitative interpretations of hydraulically relevant processes.

In the course of the WS-A experiment it was possible for the first time to collect formation water of the Opalinus Clay. The observed, temporally variable water inflow into isolated sections of the three boreholes BWS-A1, BWS-A2 and BWS-A3 provided input for estimates of hydraulic conductivity as well as valuable information for the geochemical characterisation of the pore water.

The osmotic properties and effects have been studied in various laboratory and field experiments (OP-experiment). Of particular interest in the current context are the laboratory experiments on hydraulic osmotic flow. The block samples were taken from the shaly facies in the FM-C and SHGN niches. Included in the experiments are the derivation of estimates of hydraulic properties like hydraulic conductivity and specific stor-

age and, in particular, osmotic permeability and osmotic efficiency both under steady-state and transient conditions. In-situ experiments have been carried out using fluids with different chemical potentials, i.e. different salinities. The observed pressure changes served to evaluate the osmotic efficiency of the clay membrane.
The ED-A experiment involves hydraulic and pneumatic tests in the excavation disturbed zone (EDZ). The Modular Mini-Packer System was used in boreholes BED-A1, BED-A3 and BED-A5 for short and long-term constant head testing. The hydraulic conductivity values determined from these tests should provide information on the lateral reaches of the EDZ from the tunnel wall, i.e. could contribute to the definition of the boundary conditions for the conceptual site model.
The ED-B experiment is also associated mostly with the excavation disturbed zone. The main component of the experiment was the monitoring of pressure changes in five horizontal boreholes between the two galleries with various packer configurations before, during and after the excavation of a central section of the new gallery. Some of the intervals are located at a sufficient distance from both galleries to provide estimates on the pore pressure of the undisturbed rock. In other words, given the low hydraulic diffusivity of the Opalinus Clay, it is very likely that these testing intervals are influenced very little by the drainage effect of the tunnel, at least at early observation times.
Laboratory tests have augmented the available information regarding the hydraulic characteristics of the Opalinus Clay. Most notable reference for the current purposes is TN 97-38 which describes tests carried out on a set of samples from the shaly facies with the intention of obtaining the permeability of the natural rock.
The FM-C experiment is focussed on the study of transport mechanisms in the main fault. Hydraulic tests were performed in two intervals in borehole BFM-C1: constant head injection, pressure recovery and pulse injection in the main fault, and pulse injection in the shaly facies. The tests were analysed quantitatively for values of transmissivity and hydraulic conductivity.
The evaporation measurements of the FM-D experiment were conducted in two different set-ups. At first, evapometers were installed on the tunnel wall to check the applicability of the equipment. The results warranted the second experiment, this time in borehole BFM-D1. In simple terms, a probe was driven through an isolated and ventilated test interval, recording humidity and temperature. An attempt was also made to evaluate the suction force acting on the borehole wall using a tensiometer and a psychrometer. The evaporation logging successfully located points of high evaporation. The quantitative back analyses resulted in first estimates of hydraulic conductivity and storage coefficient.
Hydraulic head measurements recorded before and during the excavation of the reconnaissance gallery and motorway tunnel in piezometers along the tunnel traverse are not part of the experiments conducted at the Mont Terri laboratory but constitute an important source of information and as such are noteworthy in the given context.

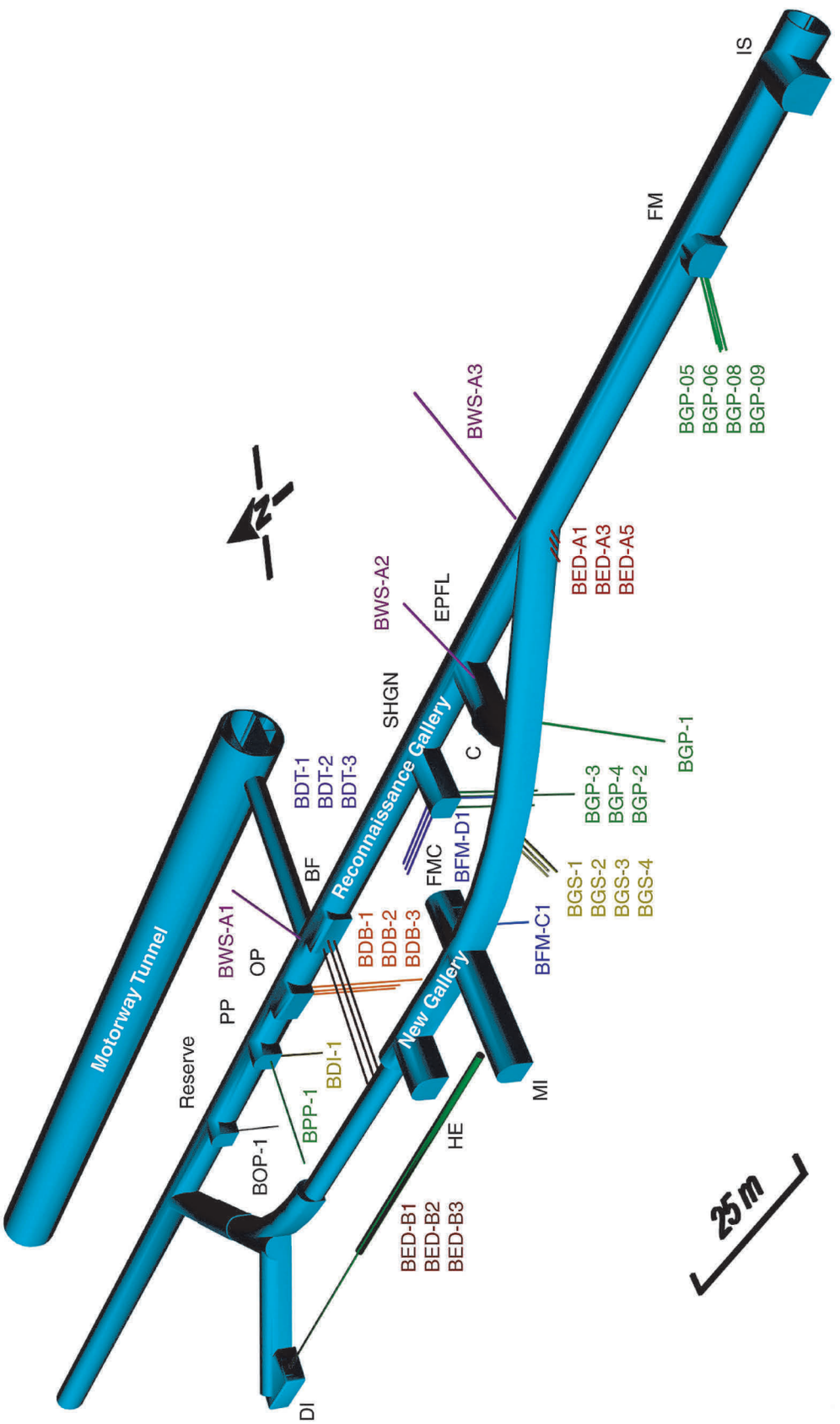

Figure 2.2: 3D view of the Mont Terri site showing niches and boreholes of relevance for the synthesis of hydrogeological investigations.

3 Developments in Hydrogeological Investigation Techniques and Data Analysis

3.1 Particular issues of interest

The above overview of experiments which were conducted at least in part in Phases 1 to 5 and which bear relevance for the hydrogeological synthesis, sheds light on the first of three subtasks of the hydrogeological synthesis for the Mont Terri site. To re-iterate from chapter 1.2, the subtask concerns an assessment of the achievements of the hydrogeological investigations both in terms of the development of *investigation techniques* and in terms of geoscientific *data analysis* in low permeability argillaceous formations. The achievements from these generic objectives need to be examined for their site-specific components before they may enter the conceptual model of groundwater flow at the Mont Terri site. The particular issues of interest for this task are:

– An assessment of the suitability of hydrogeological information acquired as a result of the contributing experiments in Phases 1 to 5 (see Table 2.1).
– An assessment of the achievements in the development of methodologies for field observations and for the analysis of long-term monitoring of pore pressures.
– An assessment of the impact of the drilling technique and testing fluid on the reliability of packer test results from argillaceous formations.

These issues are each treated separately and in detail in the following sections.

3.2 Suitability assessment of hydrogeologically relevant data

From 1996 to 1999 the Mont Terri project saw the execution of many experiments for a variety of different purposes as defined by the various experiment teams. The organisations' motivation for participation was manifold: training staff members in field investigations, development of site characterisation tools suitable for argillaceous formations, and – last, but not least – compiling a geoscientific data base for the Opalinus Clay at the Mont Terri site. The concequence is a wealth of observations, measurements and analytical results. However, the level of quality assurance achieved for the execution, analysis and documentation of the individual tests is rather non-uniform. A core aspect of the early stage of the HA project was, therefore, the establishment of a well-balanced and reliable hydrogeological information base using a thorough suitability assessment (TN 2000-22A).
With the intention to extract the maximum possible amount of information from the available information pool for integration into the Mont Terri conceptual site model (chapter 4), the HA project team looked clearly beyond the group of experiments specifically designated for the hydrogeological characterisation of the undisturbed Opalinus Clay. A key element of the suitability assessment is, therefore, the scanning of Technical Notes for potentially relevant quantitative and qualitative information and the subsequent assessment of the selected information for its suitability to contribute to the conceptual site model.
The objective of the suitability assessment is, first, to filter out hydraulically relevant information and, second, to assign suitability types to the pertinent information. In an attempt to minimise the bias and to warrant the uniform treatment of all information, the assessment process is designed as a pre-defined and traceable procedure equally applicable to all experiments. The rigorous assessment procedure developed for this purpose consists of the following elements:

i) Definition of *suitability criteria*, i.e. "What are the deliverables required to build the conceptual site model?"
ii) Definition of *assessment criteria*, i.e. "Which experimental aspects shall be checked in the assessment?"
iii) Definition of *suitability levels*, i.e. "How suitable are the data for integration into the Mont Terri site model?"
iv) Evaluation of each individual experiment according to the general definitions i), ii) and iii)

The final products of the assessment process are the *suitability levels* assigned to the reviewed information. They are defined as follows:

T1 The available results are either unreliable or inconclusive with respect to the hydrogeological characterisation of the Opalinus Clay.
T2 The experiment or an individual part thereof provides reliable qualitative results which are suitable for integration into the hydrogeological synthesis.
T3 The experiment or an individual part thereof provides reliable quantitative results which are suitable for integration into the hydrogeological synthesis with appropriate uncertainty ranges.

In cases where information is classified as either T2 or T3, additional analyses and interpretation might be desirable, for example with revised conceptual assumptions, more elaborate tools and methodologies, or sensitivity and uncertainty analyses. This type of recommendation is indicated with an asterisk: T2* and T3*, respectively.

Experiment: Investigation method considered	Testing suitable?	Sufficient documentation? Data sensible?	Adequate data analysis performed?	Suitability type
GP: Hydraulic testing	yes	yes	yes	T3 / T3*
GP-A / GS: Hydraulic & gas testing	yes	yes	yes	T3
PP: Porewater pressure testing	yes	yes	yes	T3
DB: Hydraulic testing	yes	yes	yes	T3 / T3*
DT: Hydraulic testing	yes	yes	yes	T2
FM-A & BF: Fluid logging	yes	yes	yes	T2
FM-A: Ion-selective logging	no	—	—	T1
WS-A: In-situ groundwater sampling	yes	yes	T2	
OP: Hydraulic & osmotic flow	yes	yes	yes	T3
ED-A: Hydraulic testing	no	—	—	T1
ED-B: Porewater pressure testing	yes	yes	no	T3*
n.a.: Hydrodynamic characterisation	yes	yes	yes	T3
FM-C: Hydraulic testing	yes	yes	yes	T3
FM-D: Evaporation logging	no	—	—	T1
n.a.: Hydraulic head measurements	yes	yes	yes	T2

The authors would like to express unambiguously that the assessment scheme applied here is not to be mistaken for a judgement of the equipment's design and general applicability, the workmanship involved in field testing, the know-how introduced into the analysis and interpretation of the raw data, etc.! Instead, it is our attempt to organise the massive amounts of information available according to the suitability for the specific purposes of this report.

Table 3.1: Summary of the suitability assessment with resulting suitability typing.

The experiments presented in Table 2.1 were assessed individually for their suitability in contributing to the hydrogeological characterisation of the Opalinus Clay at the Mont Terri site. The assessment process followed step by step the above described methodology. The results are summarised in Table 3.1 and, incidentally, include practically the entire data base employed in chapter 4. The reader interested in the detailed reasoning and information used in the assessment process for individual tests and experiments is referred to TN 2000-22A. The level of comprehension and quality of the data base attained through the suitability assessment leads to the recommendation of implementing the procedure again in future phases.

3.3 Developments in long-term monitoring systems for pore pressure and water sampling

3.3.1 Problems related to the clay-rich environment

The particular conditions prevalent in argillaceous rock formations turn the monitoring of pore pressure and the long-term monitoring of groundwater chemistry through sampling into non-trivial problems. Several potentials act on the water in the pore space of argillaceous rocks. Horseman et al. (1996) provide a comprehensive review of these potentials: in addition to the usual pressure and gravitational potential known from typical granular porous media, potentials also found in saturated clays are those due to chemical osmosis and adsorption. The rock's geomechanical behavior causes borehole closure effects due to stress re-distribution and generally associated poor borehole stability. Another source of uncertainty is due to chemical interactions between the rock and the fluid used to flush the observation interval. If the chemical composition of the flushing fluid is not adapted to the porewater chemistry, long-term equilibration processes may bias pressure observations, for example, through the occurrence of chemico-osmotic swelling of clay particles. Some of the factors which may prove to be advantageous for the design of long-term monitoring systems, therefore, are:

- the minimisation of the effective volume of the observation interval
- the introduction of mechanical support along the entire observation interval to prevent borehole collapse (e.g. with a porous screen filter)
- the connection of flow lines at both the top and bottom ends of the observation intervals to allow for a complete flushing
- the appropriate selection of the materials such as stainless steel, teflon or PEEK for the downhole equipment to prevent corrosion and to foster undisturbed porewater sampling.

3.3.2 Equipment portraits

In the early phases of the Mont Terri project (Phases 1 and 2), the development and testing of long-term monitoring systems was an important goal. Particularly the PP experiment focussed on developing a system for long-term monitoring of pore pressure and long-term water sampling (cf. Thury & Bossart 1999).
In total, three different types of long-term monitoring systems were applied in the investigation Phases 1 to 4 (Figure 3.1):

– classical inflatable packer systems
– newly developed PP systems
– mini-packer piezometers

More recently, a new PP-type system was developed in Phase 5 as part of the Heater Experiment (TN 2000-01). It is not considered any further in the context of the HA project because comprehensive information for cross-comparison of the new piezometer with the other systems was not yet available at the end of Phase 5.
The selection of one or the other type of long-term monitoring equipment is governed by a variety of issues. Foremost of all are the specific requirements and objectives of an individual experiment. For example, a principal interest in water sampling may favour a different system than a primary interest in pore pressure observations. Other aspects are costs involved, the expected pore pressure limits, the anticipated depth of emplacement for the system, its retrievability, etc. For the HA project the main concern of the assessment of the various equipment systems is their suitability for long-term pore pressure monitoring. The following equipment portraits, therefore, focus on this concern.

Classical inflatable packer system

Many of the Mont Terri boreholes, among these BGS-1, BGS-2, BGP-1, BGP-4 and BGP-5, were equipped with inflatable double or triple packer systems. They served the hydraulic characterisation of the formation with packer testing or long-term monitoring. The packers have a diameter of typically 80–85 mm and a sealing length of 0.5 m or rather 1.0 m. The set-up of a triple packer system is illustrated in Figure 3.1a, at center. The packers are inflated with water through hydraulic lines. The stability of the packer pressure is controlled by manometers at the surface. The length of the testing or observation interval ranges from several decimeters to more than 10 m. The interval volume can be minimised by inserting dummies. The achievable packer pressures were tested systematically in Phases 1 and 2 of the GP experiment (TN 96-27, TN 97-28). The tests indicated that packer pressures of more than 40 bars could hardly be maintained for prolonged periods. At such elevated packer pressures, frequent re-injection of water was required to stabilise the pressure. This resulted in considerable increases of the packer volume and in changes of the interval volumes.

PP system

The PP system was developed in Phases 1 and 2 (1996/1997) in the PP experiment (TN 97-01). PP systems were installed in the boreholes BPP-1, BDI-1, BED-B1, BED-B2, BED-B3 and BGP-6. The system as installed in borehole BPP-1 is an assemblage of a multipacker system with four packers and two sintered steel filters. The multipacker system consists of two double packer systems, each with a hydraulic and a mechanical packer (Figure 3.1b). A modified, simpler PP system consists only of the stiff mechanical packers and no hydraulic packers. Such systems were used after the PP experiment. It should be noted that PP-systems and mechanical packer systems are "lost" systems which cannot be retrieved. The classical packer systems (including MMPS) are systems which may be de-installed, provided the borehole stability conditions allow for it. The intent for using a double packer system was to inject resin between the hydraulic and the mechanical packers to obtain long-term sealing. The sintered steel element represents the observation interval. This tube has an outer diameter which is only a few millimeters smaller than the borehole diameter. Synthetic porewater can be circulated through this porous steel or porous poly-ethylene filter. The interval lengths were typically in the range of 20–100 cm.

Mechanical minipacker piezometers

As part of the GP experiment in Phase 2 (TN 96-27), low cost minipacker systems were designed to observe pore pressures in the small-diameter boreholes BGP-2 and BGP-3. Mechanical packers with a sealing length of 20 cm and a nominal diameter of 32 mm were installed at depths of 7.5 m and 8.9 m, respectively (Figure 3.1a). The observation intervals extended from these packers to the bottoms of the boreholes. However, before the mechanical packers were set, the observation intervals were filled with a coarse sand to avoid further borehole collapse and to minimise the interval volume. Each of the observation intervals was connected to equipment outside of the borehole with a pressure monitoring line and a flow line.

(a)

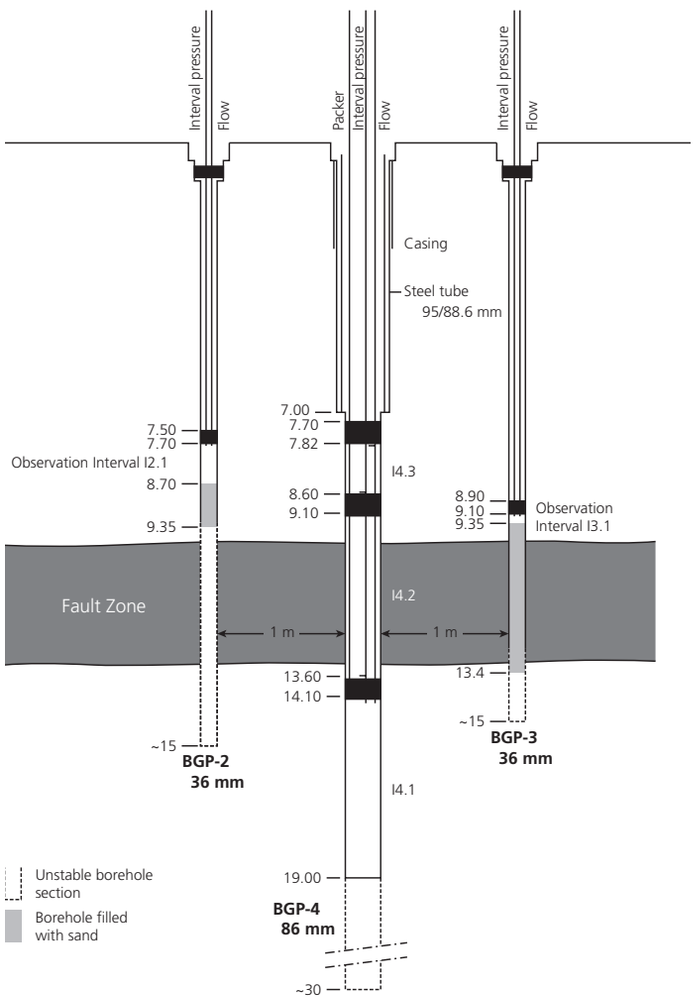

Figure 3.1: Piezometer systems tested in Phases 1 to 4 of the Mont Terri research program: (a) classical inflatable triple packer system in borehole BGP-4 and mechanical minipacker systems in BGP-2 and BGP-3 as applied in the GP experiment / Phase 2 (TN 96-27) and (b) PP system developed in the PP experiment / Phases 1 and 2 (TN 97-01 & TN 97-02).

(b)

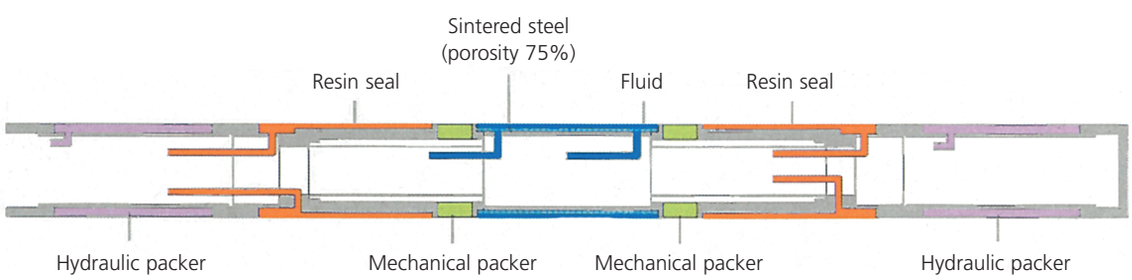

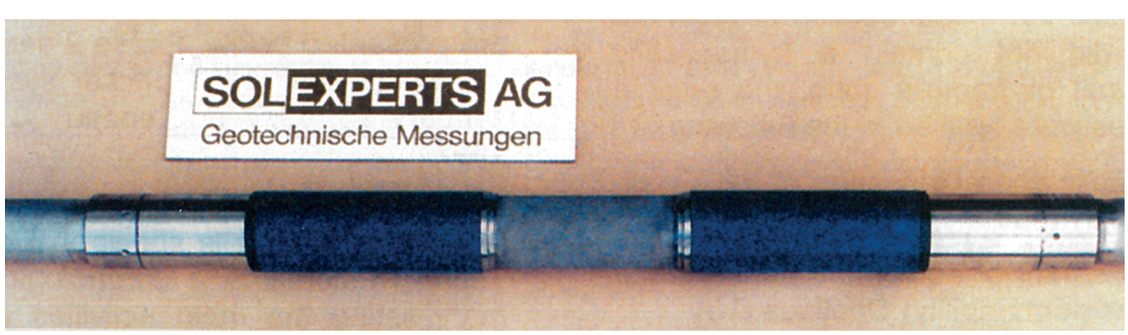

3.3.3 Equipment performance

An assessment of the equipment's performance was, in most cases, a by-product of the experiments rather than a separately defined task. As a result, the assessments are of limited scope and detail. Nevertheless, sufficient information is available to comment particularly on the following aspects:

– the performance with respect to the ease of emplacement in the borehole, proper sealing of the observation interval, equipment failure and other potential mechanical problems
– the homogeneity of pore pressure records from different systems

These aspects are discussed here in form of two cross-comparisons between systems. For the comparison of the absolute values of the pore pressure observations one must remember that a certain degree of difference is to be expected due to the different distances between the observation intervals and the galleries.

Classical inflatable packer versus mechanical minipacker piezometer

As part of GP / Phase 2, a comparison of pore pressure measurements was carried out between the classical inflatable triple packer system and the mechanical minipacker piezometer. One of the experiments is an interference test: a hydrotest sequence was conducted in test interval I4.2 in the main fault of borehole BGP-4 with pressure observations in boreholes BGP-2 and BGP-3 (see Figure 3.1a). The distances between the I4.2 in BGP-4 and the observation intervals were 1 m each. The mechanical minipacker piezometers were used for the observation intervals because of their low-budget maintenance while inflatable packers were used for the test interval because they are relatively easily recoverable and have a movable injection system. Figure 3.2 shows the crosshole pressure reactions monitored in interval I2.1 of BGP-2 and in interval I3.1 of BGP-3. Consistent pore pressures are evident in BGP-3: during the PSR phase prior to the hydraulic test sequence, the pore pressure in BGP-3 is quite similar to the pressure measured in I4.2 of BGP-4 (350 – 400 kPa). Subsequently, clear responses are observed for each test event, indicating that the minipacker piezometer works well.
The interval pressure recorded by the mini-piezometer in BGP-2 is less consistent with the aforementioned observations. Pressures increase from -65 kPa to +25 kPa which corresponds to a water level of 6.5 m below ground and 2.5 m above ground, respectively. This is due to the unsaturated conditions prevailing in the observation interval of BGP-2, which obscure the crosshole response. Therefore, care has to be taken when building this type of mini-piezometer to achieve full water saturation within the interval.
In summary, the experience from the GP experiment

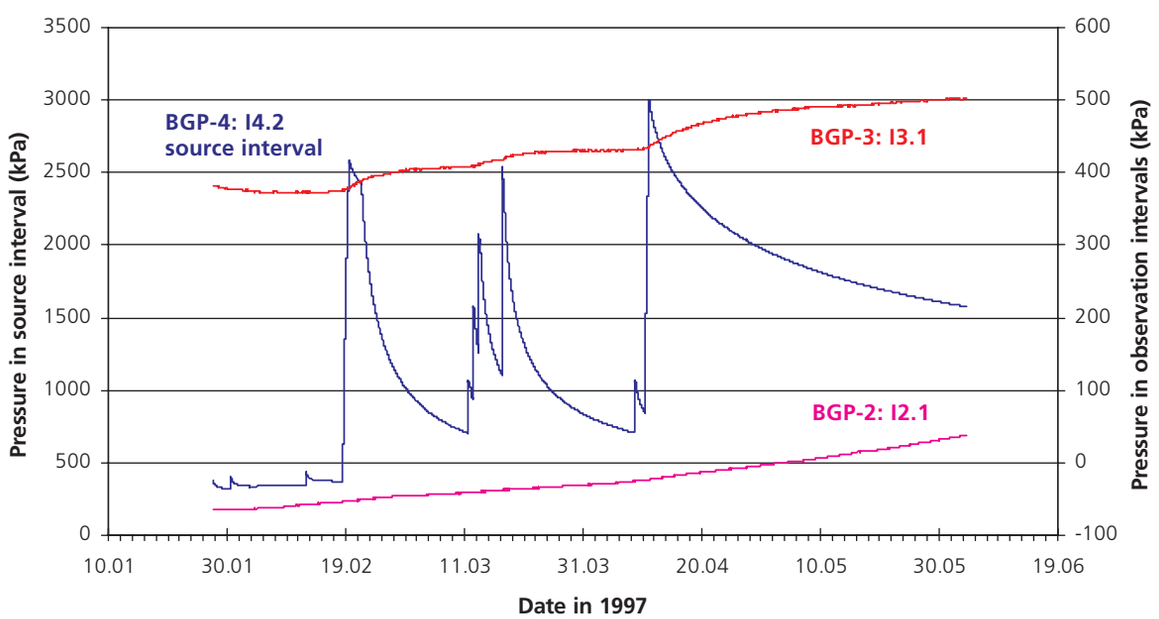

Figure 3.2: Pressures recorded with inflatable packers and mechanical minipacker piezometers during the interference test of the GP experiment / Phases 1 and 2: Pore pressure observations in intervals I2.1 of BGP-2 and I3.1 of BGP-3 in response to a hydrotest sequence in source interval I4.2 of BGP-4.

has proven the minipacker piezometer to be a low-budget system for long-term monitoring of pore pressure which works reasonably well when properly installed. These systems are also easy to install in sub-vertical boreholes of up to 10 m length. Sealing sections of more than 50 cm are favourable. The mechanical minipackers are suitable for low pore pressures of less than 500 kPa; higher pore pressures require inflatable minipackers. Sealing of the borehole section above the packer seat with resin or bentonite may improve the long-term performance of the minipacker piezometer.

Classical inflatable packer versus PP system

In Phases 3 and 4 (1998/1999) of the GP experiment, a PP system with three monitoring intervals and an inflatable triple packer system was installed in boreholes BGP-5 and BGP-6 in the FM niche. The niche lies in the sandy facies and the boreholes' orientation is roughly perpendicular to bedding. The inclined boreholes were drilled parallel to each other. The distance between the boreholes was less than 1 m. The observation intervals isolated with the conventional packer system were intervals I5.1, I5.2 and I5.3 of BGP-5 with their mid-points located at 9.3 m, 8.0 m and 6.6 m from borehole mouth, respectively. The test and observation intervals isolated with the PP system were intervals I6.1, I6.2 and I6.3 of BGP-6 with their mid-points located at 10.1 m, 7.9 m and 5.5 m from borehole mouth, respectively. Figure 3.3 shows the pressure records in all observation intervals during a hydrotest in interval BGP-6/I2. Prior to testing, some of the corresponding observation intervals exhibit comparable pore pressures (BGP5/I2: 256 kPa, BGP-6/I2: 315 kPa). During the hydrotest sequence, the responses in the observation intervals are extremely weak. Merely the pressure curves for I6.1 and I6.3 of BGP-6, and I5.1 of BGP-5 show sizeable changes.
Nevertheless, the long-term monitoring of pore pressures in boreholes BGP-5 and BGP-6 shows that pore pressure measurements from the PP system and the inflatable packer system are consistent to each other. The PP system is appropriate for continuous monitoring of pore pressures and for water sampling. The inflatable packer equipment is a removable system which is well-suited for site characterisation purposes, but was also shown to be appropriate for long-term monitoring of pore pressures.

3.3.4 Concluding remarks

Inflatable packers are most favourable for site characterisation purposes where the following features and flexibilities are advantageous: removable packer seats, borehole screening, water injection at high pressures, variable packer length etc. The PP system is very suitable for water sampling and long-term monitoring.

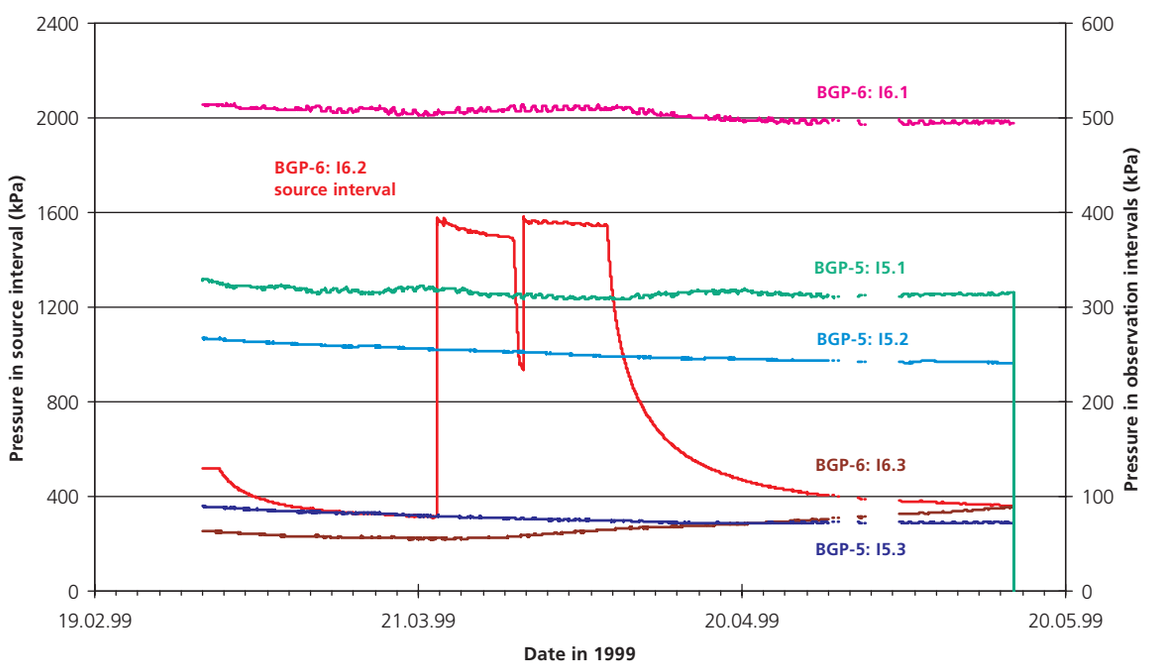

Figure 3.3: Pressures recorded with inflatable packers and PP equipment in the GP experiment / Phases 3 and 4: Pore pressure in the BGP-5 and BGP-6 observation intervals in response to a hydrotest sequence in source interval I6.2 of BGP-6.

Because of its mechanical packers, some flexibility is lost, however, as the tightness of the interval cannot be controlled with the pressure levels applied in the packers. Therefore, it relies heavily on the quality of the resin sealing. The low-budget minipacker piezometers are most appropriate for observation purposes, at low pressures and for rather shallow emplacements in the borehole. Pore pressure monitoring in the excavation disturbed zone is a typical application for the minipacker systems.

3.4 Impact of drilling technique on packer test results

Considerable technical challenges were faced in hydraulic testing of the Opalinus Clay formation at Mont Terri due to the poor borehole stability and the low hydraulic conductivity. The DB experiment was initiated to assess possible distortions of packer test results by effects of the drilling methodology and by impacts of the drilling and test fluids (TN 98-62). Three vertical boreholes were drilled in close proximity of each other in the shaly facies in the OP niche (Figure 3.4). Borehole BDB-1 was drilled with air and BDB-2 and BDB-3 were drilled with a silicate/polymer mud and a potassium-chloride/polymer mud, respectively. Immediately after drilling, the boreholes were equipped with double packer systems. An initial hydraulic testing campaign was performed in BDB-2 and BDB-3 with the drilling mud. Subsequently, the drilling fluids in all three boreholes were replaced by Pearson water, i.e. a synthetic porewater designed to minimise swelling effects, and the test sequence was repeated in the second testing campaign with the intention of analysing the impact of the testing fluid on the results. Typical test sequences were a succession of initial pressure recovery, pulse injection and constant head injection events sometimes followed by a slug withdrawal and a prolonged pressure recovery. After termination of the second campaign, pore pressure was monitored in the boreholes for more than a month. Finally, the third hydraulic testing campaign was done to assess possible changes in hydraulic parameters due to long-term processes in the boreholes such as borehole closure, swelling or osmotic flow.

Table 3.2 presents the results of the first and second hydraulic testing campaigns. Values of hydraulic conductivity are given in terms of inner zone and outer zone, i.e. analogous to radial shells around the boreholes. The outer zone corresponds to the properties of the undisturbed rock. Significant differences between the inner and outer zone conductivities were not observed. It must be stated that the specific storage values are not the result of interference testing but of single-hole analysis and that they are, therefore, poorly constrained. In summary, the following conclusions were drawn from the DB experiment:

– A comparison of the tests conducted in the three boreholes revealed no relevant differences between the first and second testing campaigns conducted before and after the fluid exchange.
– The most consistent test responses and analysis results were achieved in borehole BDB-2, drilled with silicate/polymer mud, followed by borehole BDB-3, drilled with KCl/polymer mud.
– The only relevant inexplicable test responses were recorded in borehole BDB-1. In this borehole, the

Test interval	**Inner zone hydraulic conductivity K_1 [m/s]**		**Outer zone hydraulic conductivity K_2 [m/s]**		**Specific Storage S_s [1/m]**	
	before	**after fluid exchange**	**before**	**after fluid exchange**	**before**	**after fluid exchange**
BDB-1 I1.1 9.9-15.1 m fbm	-	1.2×10^{-12}	-	3.8×10^{-13}	-	3.8×10^{-6}
BDB-1 I1.2 3.0-9.1 m fbm	-	3.3×10^{-13}	-	1.2×10^{-13}	-	8.2×10^{-6}
BDB-2 I2.1 10.5-20 m fbm	2.1×10^{-13}	2.1×10^{-13}	4.2×10^{-14}	3.2×10^{-14}	9.5×10^{-6}	7.4×10^{-6}
BDB-2 I2.2 4.5-9.7 m fbm	3.8×10^{-13}	3.8×10^{-13}	1.3×10^{-13}	1.3×10^{-13}	1.3×10^{-5}	9.6×10^{-6}
BDB-3 I3.1 9.3-16.4 m fbm	2.8×10^{-13}	2.8×10^{-13}	9.9×10^{-14}	9.9×10^{-14}	7.0×10^{-6}	5.6×10^{-6}
BDB-3 I3.2 3.0-8.5 m fbm	1.8×10^{-12}	1.5×10^{-12}	9.1×10^{-13}	9.1×10^{-13}	7.3×10^{-6}	1.8×10^{-6}

Table 3.2: Summary of the results from the final hydraulic test sequence after fluid replacement with Pearson water in boreholes BDB-1, BDB-2 and BDB-3. Test interpretation based on a finite skin flow model, i.e. inner zone/outer zone.

long-term monitoring phase demonstrates inexplicable changes in slope and roll-over. It would be feasible that this was caused by two-phase flow phenomena induced by air drilling.

– The testing conditions encountered in the Mont Terri Opalinus Clay, neither fluid-rock interaction nor osmosis have significant impact on the transmissivity determination.
– The diagnostic plot comparison between the second and third testing campaigns conducted before and after long-term monitoring showed a slight increase of the near borehole transmissivity by less than half an order of magnitude. It is, however, not clear whether this effect is due to the approximately one month long exposure of the test intervals to synthetic porewater, or to stress redistribution.

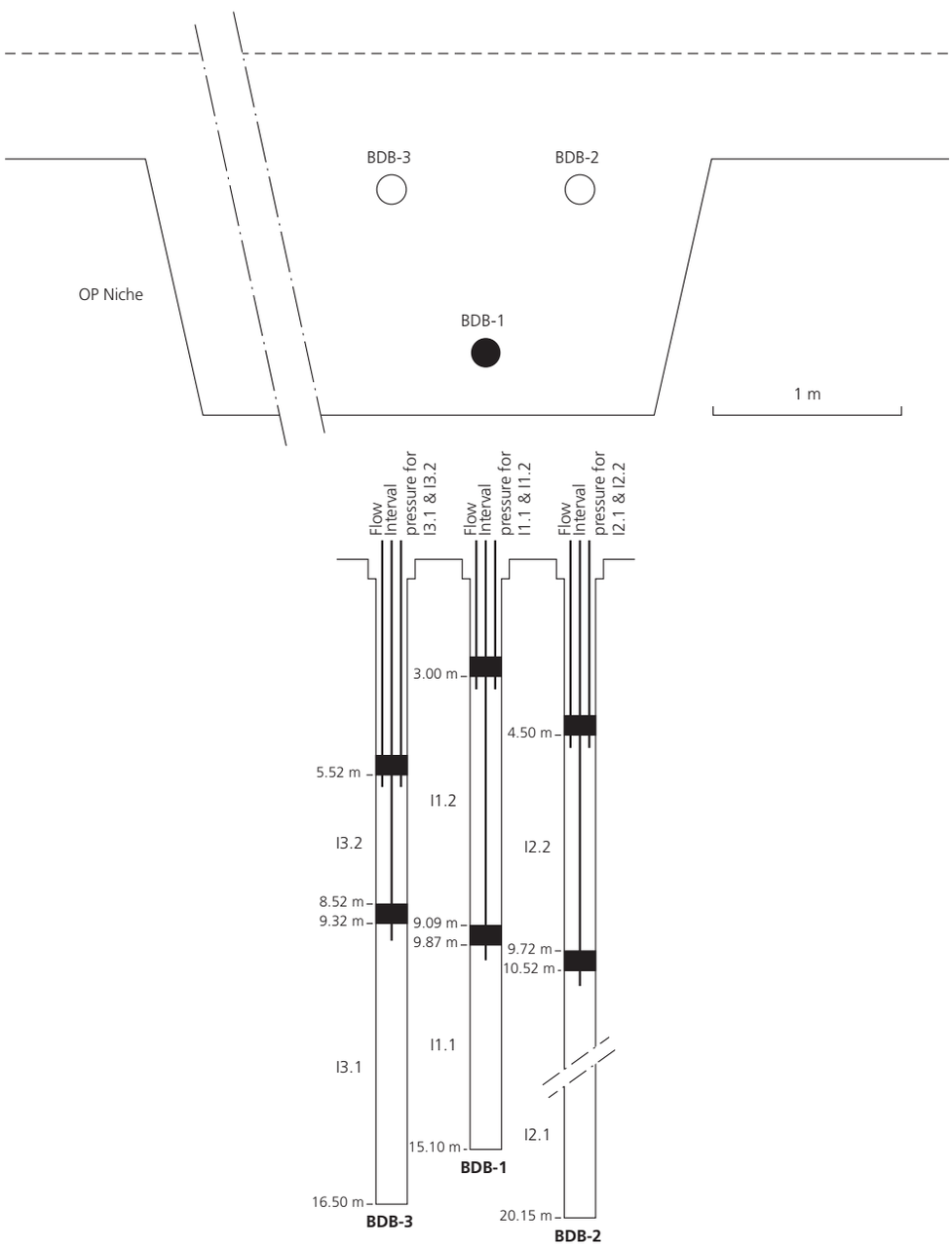

Figure 3.4: Map view and cross-section of the set-up for the systematic investigation of the impact of the drilling technique and the chemical composition of the test fluids on packer test results. The three boreholes BDB-1, BDB-2 and BDB-3 were drilled with air, silicate/polymer mud and potassium-chloride/polymer mud, respectively. Synthetic porewater was used for hydraulic testing.

4 Conceptual Model of Groundwater Flow at the Mont Terri Site

4.1 Introduction

The conceptual model of groundwater flow at the Mont Terri site is based on the accomplishments from Phases 1 to 5, that is from 1996 to 2000, of the Mont Terri research program. The data base is made up of those results of hydrogeological field and laboratory investigations, which have passed the suitability assessment described in chapter 3.2. Furthermore, various geological and geochemical data sets are used, which have been quality assured as part of Nagra's Geosynthesis Project (Nagra 2002). In the process of deriving the conceptual model, the hydrogeological data base is analysed in the context of the given hydrogeological setting, the relevant groundwater flow mechanisms are highlighted, and the different scales of groundwater flow are reviewed. Representative hydraulic properties of the undisturbed Opalinus Clay are assigned to the relevant scales of groundwater flow. Finally, the current level of understanding of the hydraulic head distribution in the Opalinus Clay and the adjacent stratigraphic formations is discussed. The rock properties of interest are: hydraulic conductivity, anisotropy factor, flow threshold gradients (limits of applicability of Darcy's law), specific storage and conceptual hydro-mechanical models (in particular porosity-permeability relationships).
This report covers neither the complex hydro-mechanical processes observed in the excavation disturbed zone (cf. Martin & Lanyon 2004), nor those in the unsaturated zone. Still, the tunnel nearfield forms the inner boundary of the local-scale hydrogeological model and is therefore important for the HA project. Furthermore, as the Opalinus Clay is known to be an overconsolidated clay-rich shale formation (Thury & Bossart 1999), its geomechanical properties and in-situ stress conditions are expected to play a vital role in the groundwater flow systems (Bock 2002). The integration of such information will be the topic of future Phases of the HA project.

4.2 General outline of the synthesis approach

In the context of common hydrogeological applications like the management of groundwater resources, tight claystone formations are treated as aquicludes, assuming that porewater is not mobile at ambient conditions as diffusion is assumed to be the dominant transport process through the aquiclude. In many cases the hydraulic conductivity of the clay formation is below the detection limit of conventional hydraulic measurement methods. Hence, characterisation of such an aquiclude may be limited to qualitative investigations demonstrating its tightness. The assessment of the long-term barrier function of clay formations in the framework of radioactive waste disposal, however, requires more rigorous quantitative site characterisation procedures (chapter 4.3) and a careful analysis of flow and transport processes. The key elements of this analysis are:

- An assessment of groundwater flow mechanisms and coupled processes (chapter 4.4).
- An assessment of relevant scales (chapter 4.5).
- Evidence for a continuous distribution of porewater pressure in the formation (chapter 4.6).
- An evaluation of hydrogeological site understanding (chapter 4.7).

The range of applicability of Darcy's law is a key issue to be addressed in the *assessment of groundwater flow mechanisms* in clay formations. The phenomenological explanation for deviations from Darcy's law may be founded in coupled processes involving chemical, mechanical, thermal or hydraulic components (Horseman et al. 1996). Coupled processes may significantly influence the regional groundwater flow system, for example, by preventing advective groundwater flow. The context of the Mont Terri project demands detailed consideration of the following two processes:

- Chemico-osmotic flow as a result of membrane effects in the clay formation.
- Hydro-mechanical processes stemming from pore pressure – stress coupling and porosity-permeability coupling of the porous rock.

In tight formations site characterisation delivers hydraulic properties of the rock which are, at most, representative for a scale of centimeters up to meters (packer testing, permeameter testing – cf. chapter 4.3). Modelling groundwater flow, however, requires representative values of rock properties typical on the scale of deka- to hectometers. The a*ssessment of relevant scales* and detailed geological information about relevant structural features on all scales is a pre-requisite for any upscaling of the measured hydraulic properties. *Spatial distribution of porewater pressure* at the site is a key for testing model concepts including groundwater flow mechanisms, coupled processes and hydraulic boundary conditions, and for confirming the spatial representativity of the measured hydraulic parameters. Hydrodynamic modelling of the observed in-situ pore pressures provides a valuable tool for model discrimination.

4.3 Hydrogeological data base from Phases 1 to 4

The main hydrogeological investigation techniques applied for the characterisation of the Opalinus Clay at the Mont Terri rock laboratory are:

– Hydraulic packer tests in boreholes,
– Permeameter tests of core samples.

Complementary methods based on microstructural analyses (Kozeny-Carman relationship) and on nitrogen adsorption / desorption techniques were applied to check for internal consistency in the hydrogeological data base.

4.3.1 Packertests

The boreholes which were equipped with packer systems for hydraulic testing and long-term monitoring of pore pressure are indicated in Figure 2.2. A multitude of packer tests was conducted in all lithological facies (sandy, shaly and carbonate-rich sandy) of the Opalinus Clay and the main fault zone. The core mapping logs were compared to the results of the packer tests to check whether the hydraulic properties are significantly influenced by the fracture frequency in the test interval. Hydraulic interference tests were conducted at two locations in the GP and GS experiments. For these, very weak hydraulic pressure responses were monitored in observation boreholes at about 1 m distance from the test boreholes, i.e. at a distance where the prevalence of a mobile fluid phase at testing scale could be inferred. An overview of the range of derived values for hydraulic conductivity and specific storage coefficients is provided in Table 4.1. Only such data sets are presented which passed through the suitability assessment procedure (chapter 3.2). The hydraulic conductivities range from 2×10^{-14} m/s to 2×10^{-12} m/s. The spread of values is a result of (i) the spatial variability of the parameter, (ii) the different methods of interpretation, (iii) uncertainty analyses conducted on a few tests, and (iv) different borehole histories.
Detailed hydrotest analyses including flow model identification, uncertainty analysis and simulations of the entire test sequence were carried out as part of the GP experiment on boreholes BGP-1 and BGP-4 (TN 98-24). The general approach used to analyse the hydraulic tests was that of a parameter estimation procedure using non-linear optimisation and uncertainty analysis:

– Choose initial conceptual flow model
– Provide initial values of fitting and non-fitting parameters
– Specify constraints and objective function and optimise fitting-parameter estimates using non-linear regression to obtain baseline estimates
– Analyse residuals (evaluate conceptual model)
– Check fitting-parameter uncertainty (joint-confidence regions)
– If uncertainties appear unacceptably large, attempt to better constrain the problem to reduce the uncertainties, e.g. by using an alternative well-formation flow model
– Use Jacobian matrix analysis to better understand how fitting parameters are being constrained
– Perturb baseline estimates and re-optimise the fitting parameters to investigate the uniqueness of the solution (check for local minima)
– Sample from assigned uncertainty distributions for the non-fitting parameters and then re-optimise the fitting parameters to quantify how non-fitting parameter uncertainties affect the fitting-parameter estimates

The fitting parameters selected were hydraulic conductivity, specific storage, static formation pressure and wellbore storage. The non-fitting parameters were borehole radius, pressure history and fluid density. Details of the analysis procedure are documented in TN 98-24.
Figure 4.1 to 4.3 illustrate individual steps of the approach as applied for the analysis of a hydraulic testing sequence performed in borehole BGP-1.
The rigorous analysis approach applied to the BGP-1 and BGP-4 packer test data represents an exception for Phases 1 to 4. Further detailed analyses were carried out in support of hydro-mechanical studies of the BGP-6 interference test (cf. chapter 4.4.3) and the BGS-2 gas test analysis (chapter 5.5). Most of the other packer tests were interpreted using simpler approaches based on diagnostic data analysis. Because of the different levels of detail in the interpretations, the compilation of packer test results presented below cannot fully account for parameter and model uncertainties.
Storage coefficients were not determined for all tests. As a matter of fact, the specific storage coefficient can be better constrained with interference tests, while in most cases only single-hole tests were available. This explains the large range of values of the specific storage obtained: from 2×10^{-7} m^{-1} to 1.7×10^{-4} m^{-1}. In many cases values around 1×10^{-6} and 1×10^{-5} m^{-1} are obtained, which is in a range of expected values for this parameter.
In addition to hydraulic conductivities and storage coefficients, Table 4.1 also lists the tested facies and the frequency of discontinuities which were obtained

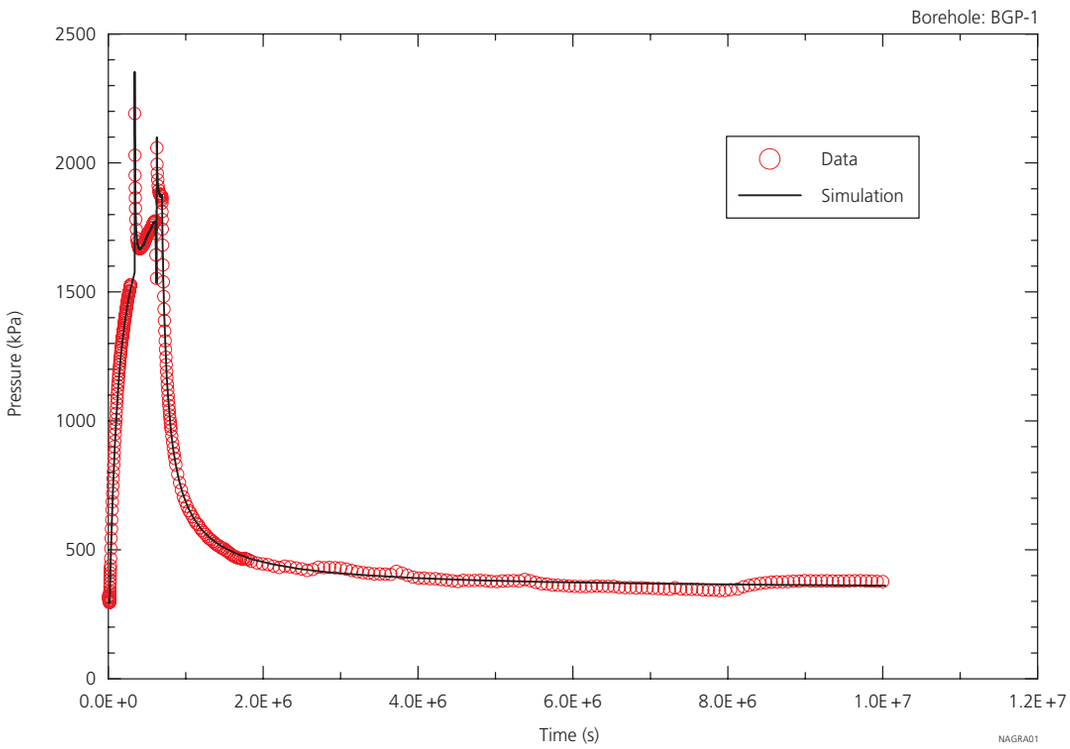

Figure 4.1: Baseline simulation of pressure response in BGP-1 (after TN98-24). The baseline simulation is the result of inverse modelling of the entire test sequence with a given (radial) flow model. Baseline simulations represent the starting point for uncertainty and perturbation analyses.

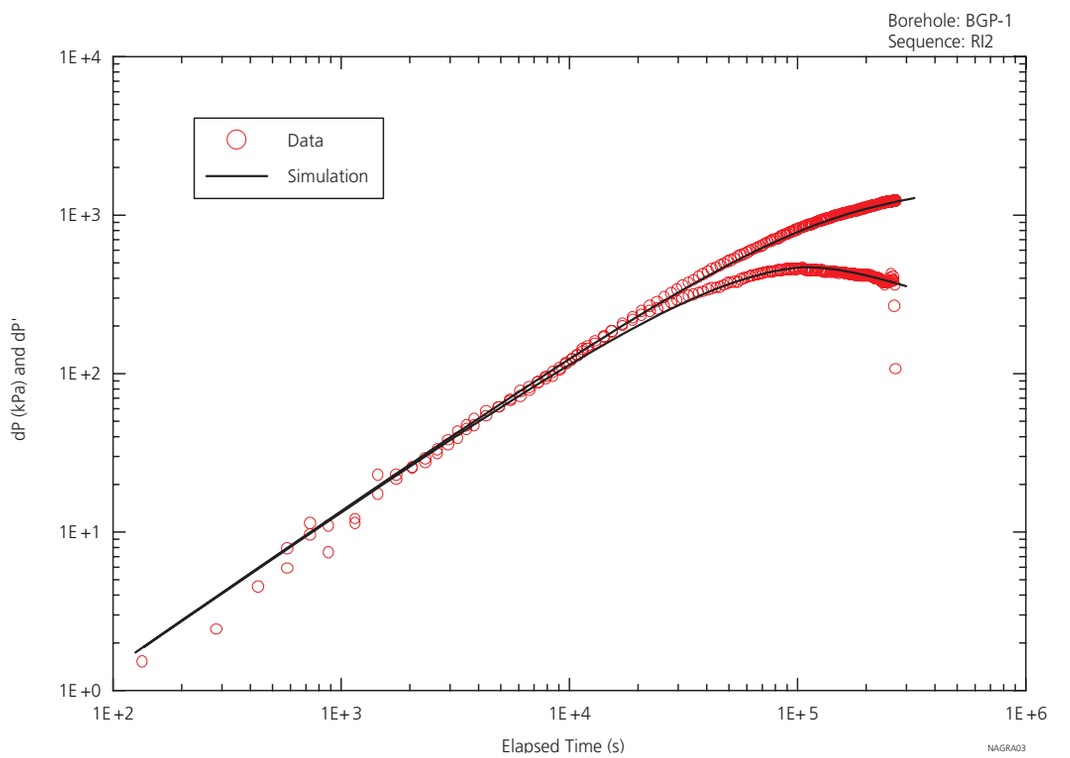

Figure 4.2: Baseline simulation of pressure change (dP) and log-derivative (tdP/dt) during BGP-1 – R12 constant-rate injection test (after TN98-24). The diagnostic log-log derivative plot allows for systematic flow model identification.

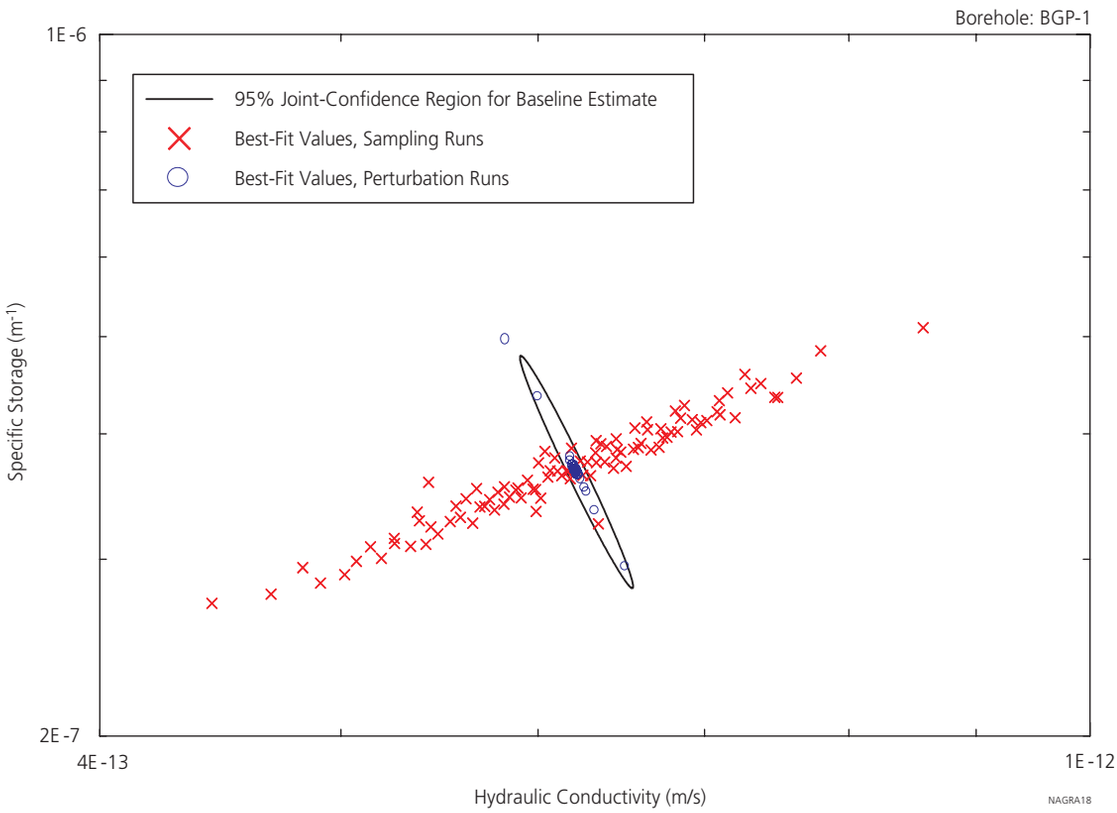

Figure 4.3: Uncertainty analysis of BGP-1 hydraulic conductivity and specific storage estimates (TN98-24): Comparison of the results of the perturbation analyses (perturbation of fitting parameters) and sampling analysis (perturbation of non-fitting parameters) to the 95% confidence regions of the baseline parameters. The best-fit parameter combinations estimated from the perturbation analysis fall within the 95% joint-confidence regions of the baseline parameter set, thus, the inverse problem, as posed, was well constrained.

by locating the test intervals in the core mapping records (see also chapter 4.5.3). Tests were carried out in all facies and the fracture frequency ranged from none to 19 m^{-1}. The data show no significant correlation between the hydraulic conductivity and the lithological facies (cf. chapter 4.5.2). Neither could a definite correlation be detected between the hydraulic conductivity and the fracture frequency in the test section (chapter 4.5.3). The hydraulic tests in the main fault resulted in K values of about 2×10^{-13} to 5×10^{-13} m/s and, therefore, are within the typical range of Mont Terri values.

Borehole / Test interval	Borehole dip (up +) (down -)	Bedding dip (orientation is SE)	Lithological unit	Hydraulic conductivity K [m/s]	Specific storage S_s [m^{-1}]	Frequency of open discontinuities [m^{-1}]
BGP-1 I1.2 8-9 m fbm	inclined (-80°)	44°	carbonate rich sandy facies	4.0×10^{-13} – 9.0×10^{-13}	2.0×10^{-7} – 6.0×10^{-7}	0 (0)
BGP-4 I4.2 9.1-13.6 m fbm	vertical (-90)	44°	main fault: 9.45-12.20 m fbm; in shaly facies	2.0×10^{-13}	3.0×10^{-7} – 3.0×10^{-5}	8.9 (6.2)
BGP-6 I6.2 7.4-8.4 m fbm	inclined (-34°) (⊥ to bedding)	54°	sandy facies	1.5×10^{-14} – 2.7×10^{-13}	not analysed for or fixed at 2×10^{-6}	1 (1)
BGS-1 I1.2 8.0-9.0 m fbm	inclined (-50°)	45°	shaly facies	~2.0×10^{-12}	1.7×10^{-4} [1)]	n.d.
BGS-1 I1.3 5.0-7.0 m fbm	inclined (-50°)	45°	shaly facies	~1.0×10^{-13}	1.6×10^{-4} [1)]	n.d.
BGS-2 I2.2 8.0-9.0 m fbm	inclined (-50°)	45°	shaly facies	~3.0×10^{-13}	1.7×10^{-5} – 8.4×10^{-5} [1)]	n.d.
BGS-2 I2.3 5.0-7.0 m fbm	inclined (-50°)	45°	shaly facies	~1.5×10^{-13}	8.5×10^{-5} [1)]	n.d.
BFM-C1 I1 8.2-11.2 m fbm	vertical (-90°)	50°	main fault: 8.25-9.21 m fbm; in shaly facies	3.0×10^{-13} – 5.0×10^{-13}	1.5×10^{-6} – 1.0×10^{-5}	19 (18)
BDB-1 I1.1 9.9-15.1 m fbm	vertical (-90°)	n.d.	shaly facies	3.8×10^{-13}	3.8×10^{-6}	6.2 (1)
BDB-1 I1.2 3-9.1 m fbm	vertical (-90°)	n.d.	shaly facies	1.2×10^{-13}	8.2×10^{-6}	13.8 (4.4)
BDB-2 I2.1 10.5-20 m fbm	vertical (-90°)	n.d.	shaly facies	3.2×10^{-14}	7.5×10^{-6}	5.3 (1.8)
BDB-2 I2.2 4.5-9.7 m fbm	vertical (-90°)	n.d.	shaly facies	1.3×10^{-13}	9.6×10^{-6}	8.8 (2.9)
BDB-3 I3.1 9.3-16.4 m fbm	vertical (-90°)	n.d.	shaly facies	9.9×10^{-14}	5.6×10^{-6}	—
BDB-3 I3.2 3-8.5 m fbm	vertical (-90°)	n.d.	shaly facies	9.1×10^{-13}	1.8×10^{-5}	8.9 (6.7)

( ) in parentheses: frequency of discontinuities excluding artificial discontinuities
[1)] values determined based on single-pulse sequence and unusually high test zone compressibility, i.e. most likely strongly overestimated
n.d.: not determined

Table 4.1: Overview of the relevant packer test results in the Opalinus Clay formation at the Mont Terri rock laboratory. Values of parameter ranges either stem from different methods of analysis (i.e. analytical vs. numerical) or are the result of uncertainties determined from sensitivity analysis.

4.3.2 Permeameter tests

Five permeameter tests were conducted successfully as parts of the OP and GP experiments. In the OP experiment conducted by the British Geological Survey (BGS), two samples were tested in isostatic cells, whereby flow was imposed perpendicularly to bedding (TN 97-39, Harrington et al. 2001). Figure 4.4 shows a schematical sketch of the BGS controlled flow-rate permeameter. It consists of five main components: (i) a sample assembly, (ii) a 40 MPa rated pressure vessel and associated confining pressure system, (iii) a fluid injection system, (iv) a back pressure system and (v) a micro-computer based data acquisition system. The specimens were sandwiched between two stainless steel end-caps, each with a sintered stainless steel porous disc, and jacketed in heat-shrink teflon to exclude confining fluid. The specimen is subject to an isotropic confining stress – the effective stress varied between 4.2 and 6.4 MPa. The observed K values ranged from 6 to 12×10^{-14} m/s. No significant correlation could be found between the conductivity and the effective stress. The derived storage coefficient was notably high with a value of about 5×10^{-4} m^{-1}.

The permeameter tests as part of the GP experiment were carried out by SCK•CEN (TN 98-15, TN 99-58). The test equipment was similar to the one used by BGS (cf. Figure 5.1). Confining pressure and effective stress were also similar to those for the OP permeameter tests. The flow direction was at about 35°, 50° and normal to bedding. The hydraulic conductivity was derived to be about 1 to 2×10^{-13} m/s.
A summary of results from the permeameter tests is provided in Table 4.2.

Experiment	**Core sample**	**Lithological unit**	**Hydraulic conductivity K [m/s]**	**Specific storage S_S [1/m]**
GP-Experiment	SED-B3 06 (GP)	shaly facies	2.2×10^{-11} (full saturation)	-
	flow parallel to bedding; most probably disturbed sample			
	BFP-16 (GP)	shaly facies	$1.5\times10^{-13} - 1.8\times10^{-13}$	-
	flow ca. 50° to bedding; effective stress ca. 5 MPa			
	BWS-E4 06	sandy facies	$1.9\times10^{-13} - 2.1\times10^{-13}$	-
	flow normal to bedding; effective stress ca. 4.5 – 5 MPa			
	BED-C5/7	shaly facies	1.9×10^{-13}	-
	flow ca. 35° to bedding; effective stress ca. 4.5 – 5 MPa			
OP-Experiment	2 samples from SHGN niche	shaly facies	mean K⊥ 7.5×10^{-14} ($6\times10^{-14} - 12\times10^{-14}$)	4.8×10^{-4}
	for effective stresses, typically in the range of 4 – 5 MPa			

Table 4.2: Summary of results from the permeameter tests and structural investigations.

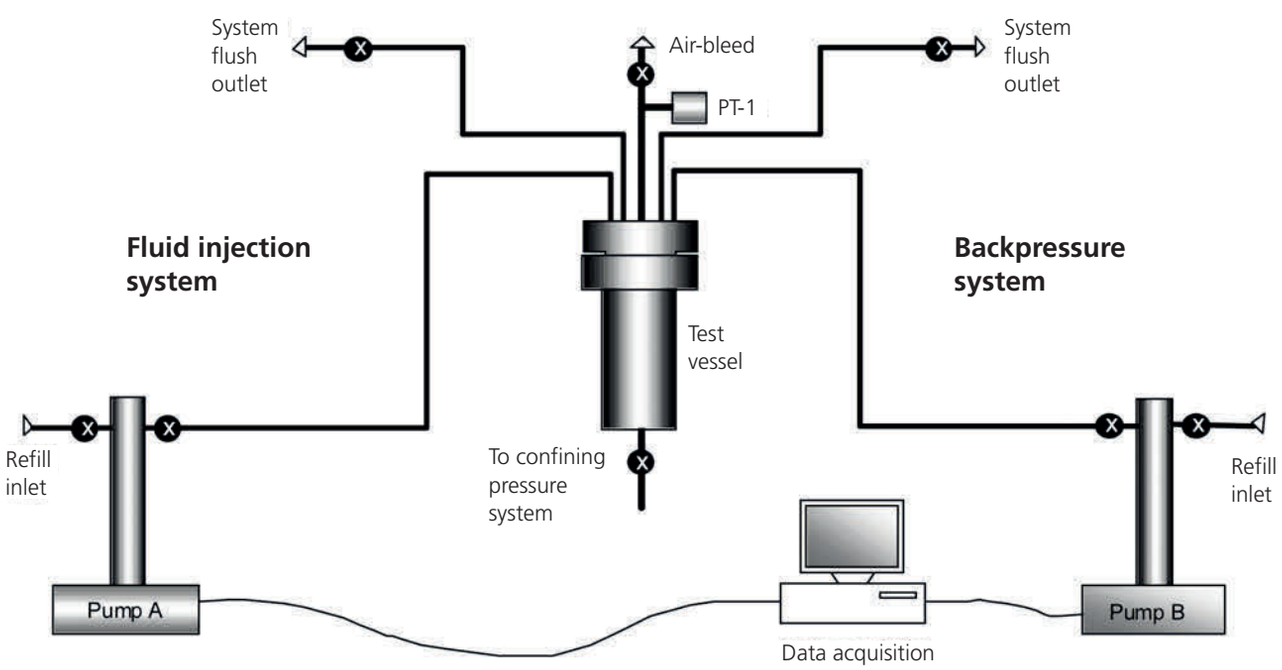

Figure 4.4: Schematic configuration of the BGS permeameter after Harrington et al. (2001).

4.4 Assessment of coupled processes

4.4.1 Threshold gradient

Conceptual framework

Darcy's law represents the general base for quantitative descriptions of groundwater flow. It denotes the linear correlation between the specific discharge v_f through a representative elementary volume and the hydraulic gradient. The proportionality constant for the relationship is provided by the hydraulic conductivity K. Darcy's law is applicable only within certain limitations. For the case of the Opalinus Clay porewater flow at low hydraulic gradient is the range where deviations from the linear flow law may be expected. The small pore radii cause electro-molecular rock-water interactions to gain significance in comparison to the viscous fluid properties, i.e. friction. In response, the formation water no longer behaves like a Newtonian fluid when exposed to a low hydraulic gradient. A comprehensive discussion of possible causes for non-linear porewater flow in clay-rich rock is found in Horseman et al. 1996. In empirical terms, this situation may be accounted for by introducing a hydraulic threshold gradient$_o$ (see, e.g. Bear 1972, de Marsily 1986):

$$v_f[m/s] = \begin{cases} K \cdot \text{grad } h \cdot \left[1 - \dfrac{i_o}{|\text{grad } h|}\right] & \text{for } |\text{grad } h| \geq i_o \\ 0 & \text{for } |\text{grad } h| < i_o \end{cases} \qquad (4.1)$$

In clay-rich rock deviations from Darcy's law are often interpreted as a consequence of competing (coupled) flow processes (Miller & Low 1963, Swartzendruber 1962a&b, Russel & Swartzendruber 1971, Horseman et al. 1996). A chemical disequilibrium in the system rock/porewater, for example, gives rise to an osmotic flow. Hence, the hydraulic threshold gradient can be interpreted as the limiting case, below which the osmotic flow due to the chemical disequilibrium dominates the hydraulically driven flow. Therefore, the hydraulic threshold gradient is not an intrinsic rock property, but depends on the geomechanical and geochemical conditions in the porewater / rock system. Literature offers very little quantitative information for threshold gradients which would be appropriate for very low-permeability formations. Voigt & Bamberg (1995) published a compilation of results obtained in laboratory experiments. These indicate threshold hydraulic gradients in the range of 100–1000 m/m for hydraulic conductivities of about 10^{-13} m/s. In the following sections methods and parameter estimates of the threshold gradient are presented for the Opalinus Clay at Mont Terri.

Experimental data base

Experimental evidence for the range of validity of Darcy's law was gained by the following laboratory and field experiments:
- permeameter tests with core samples
- packer tests: single hole and crosshole
- long-term monitoring of pore pressures in piezometer boreholes

Permeameter tests with core samples

Permeameter experiments on core samples of Opalinus Clay from the Mont Terri site generally have been conducted with gradients > 1000 m/m (TN 97-39, TN 98-15, TN 99-58; cf. chapter 4.3.2). At such hydraulic gradients Darcy's law has been proven. Figure 4.5 shows the flow transients of a permeameter experiment, conducted as a multi-step pressure test (TN 97-39). Clear evidence is given for linearity between the stabilised flow rate and water pressure.

Packer tests in boreholes

As part of the GP experiment, long-term packer tests (single hole and crosshole) with flow periods of weeks and recovery periods of months were conducted. These tests were analysed using diagnostic tools (diagnostic plots, straight line analyses, etc.) and by numerical simulation of the entire test sequence (e.g. TN 98-24 and Figure 4.6). In many cases excellent fits of the pressure and flow transients were seen in the test simulations. Figure 4.6a presents a sketch of the pressure gradient radially outward from the testing borehole and Figure 4.6b shows the best fit results of a hydrotest performed in interval I4.2 of borehole BGP-4. The abbreviations for the testing sequences denote the following: PSR = pressure static recovery, RI = constant rate injection, RIS = recovery rate injection, HIS = recovery after head injection. The deviations between simulations and field data are minimal, suggesting an appropriate choice of flow law (Darcy's), well-formation flow model (radially homogeneous) and hydraulic properties. The determination of hydraulic gradients in the immediate vicinity of the borehole, as derived from numerical test simulations, is represented in Figure 4.6c. In the course of the test sequence, hydraulic gradients exhibit typical values in the range 50–500 m/m. It can be concluded that groundwater flow follows Darcy's law at hydraulic gradients higher than 50 m/m.

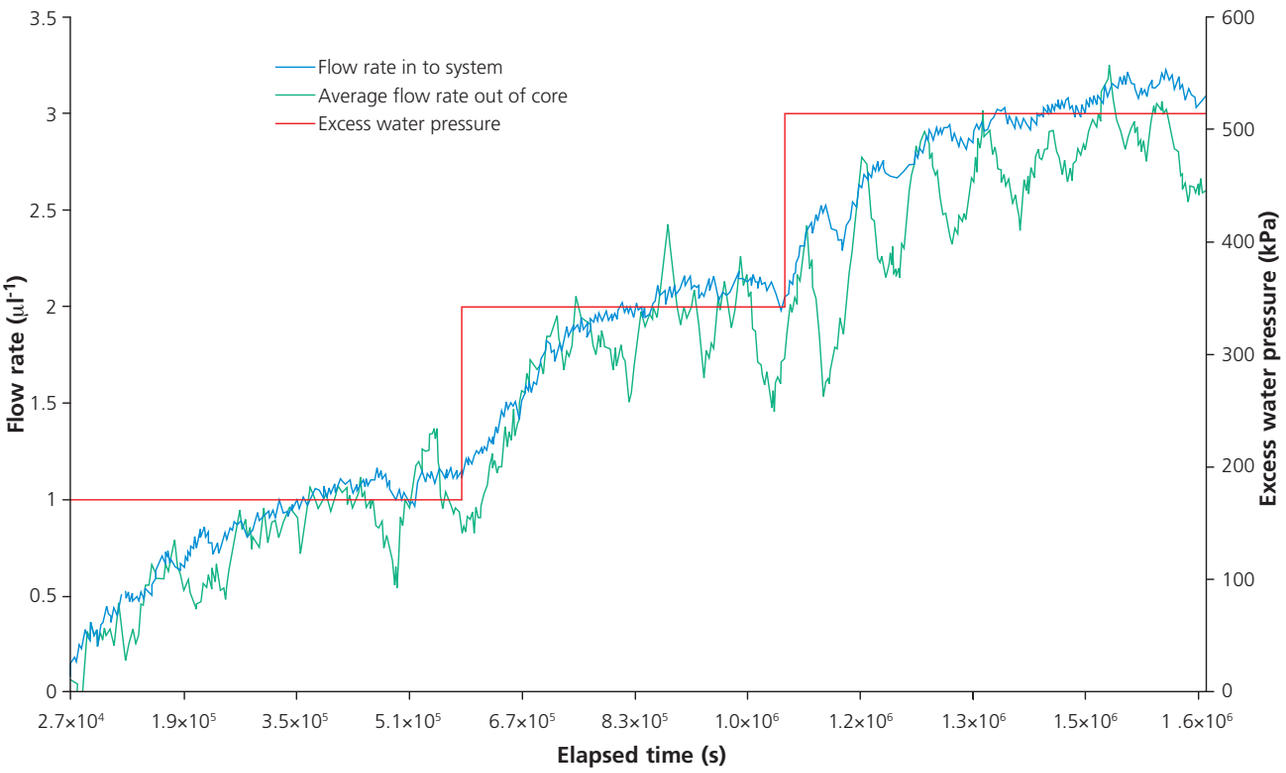

Figure 4.5: Permeameter test conducted in the OP experiment (TN 97-39). Linearity between flow and pressure is proven for hydraulic gradients > 1000 m/m (Figure taken from TN 97-26).

Observations from hydraulic crosshole testing may also be used to explore the range of validity of Darcy's law. The crosshole response in interval I3.1 of borehole BGP-3 on the source signal in BGP-4/I2 was simulated using the numerical borehole simulator MULTISIM, which is based on Darcy's law and the continuity equation (TN 98-24). The distance between source and observation borehole was 1 m. Although a response was observed in BGP-3/I1 (cf. Figure 4.7a), a satisfactory fit of the crosshole response was not achieved, even though a complex flow model was chosen. Neither the early arrival time of the pressure signal nor the flattening out of the pressure after increase was reproduced by the simulation. The misfit was interpreted as evidence for the impact of hydro-mechanical coupling (early arrival time of the pressure signal) or for a possible deviation from Darcy's law (threshold pressure gradient for flow at the observation borehole BGP-3). Figure 4.7b demonstrates based on a radial pressure field that the hydraulic gradients at a distance of 1 m from the source borehole are significantly lower than in the immediate vicinity of the source borehole, typically lower than 0.5 m/m. If threshold gradients do exist (which is not proven by the observations), they should be low, possible smaller than 1 m/m.

Estimate of an upper limit of the hydraulic threshold gradient

Further evidences of a hydraulic threshold gradient are presented in Table 4.3. The threshold gradient necessary to establish Darcy flow in the Opalinus Clay is seemingly in the order of magnitude of 1 m/m. However, for technical reasons no direct measurement of the threshold gradient is possible. The range of uncertainty of the assessed threshold gradients is therefore quite high, i.e. one order of magnitude.

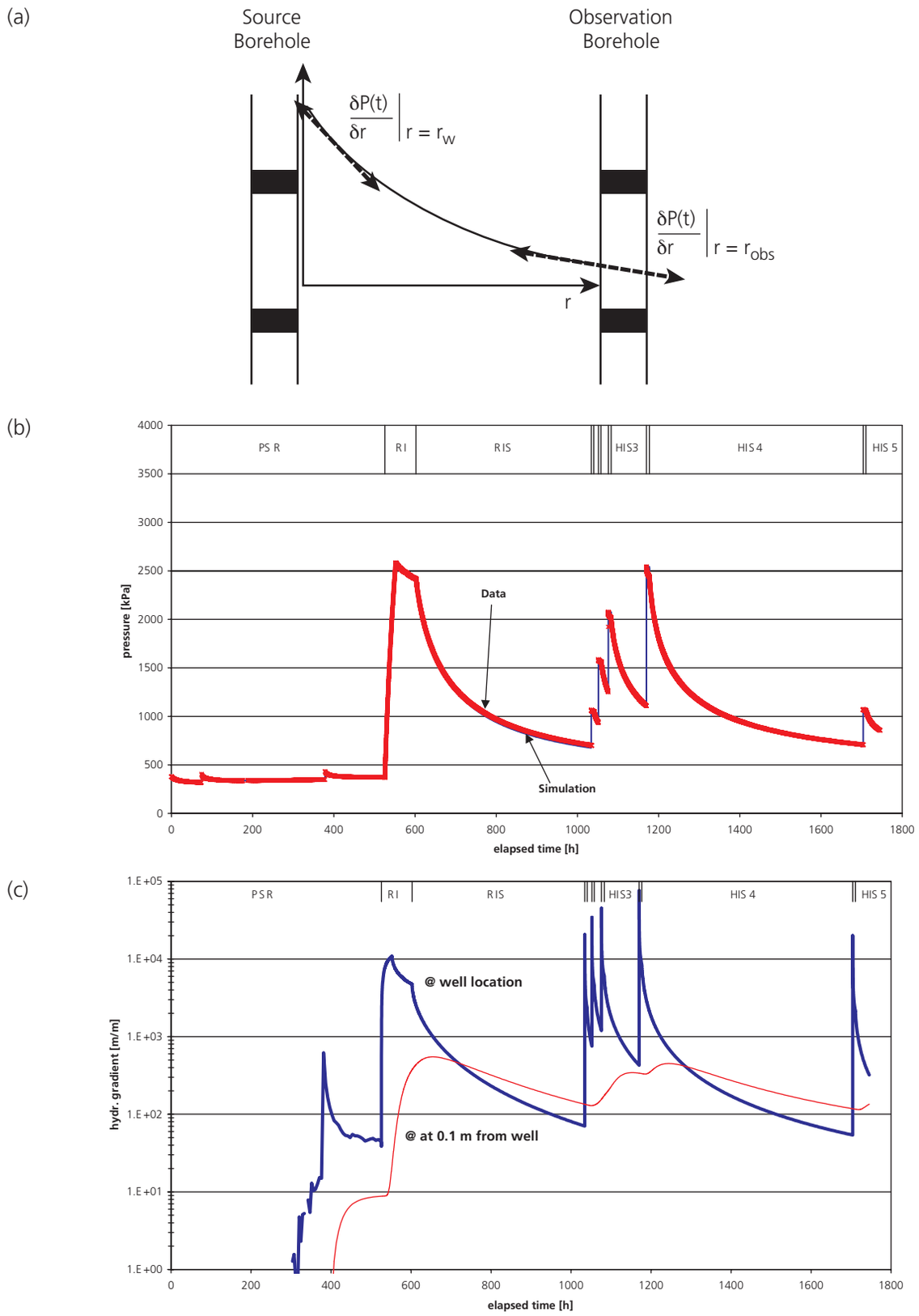

Figure 4.6: Simulation of a sequence of rate injection and head injection tests in BGP-4 as part of the GP experiment (TN 98-24): (a) schematic pressure gradient between boreholes, (b) best-fit simulation by inverse modelling, and (c) hydraulic gradient in the immediate vicinity of the borehole.

(a)

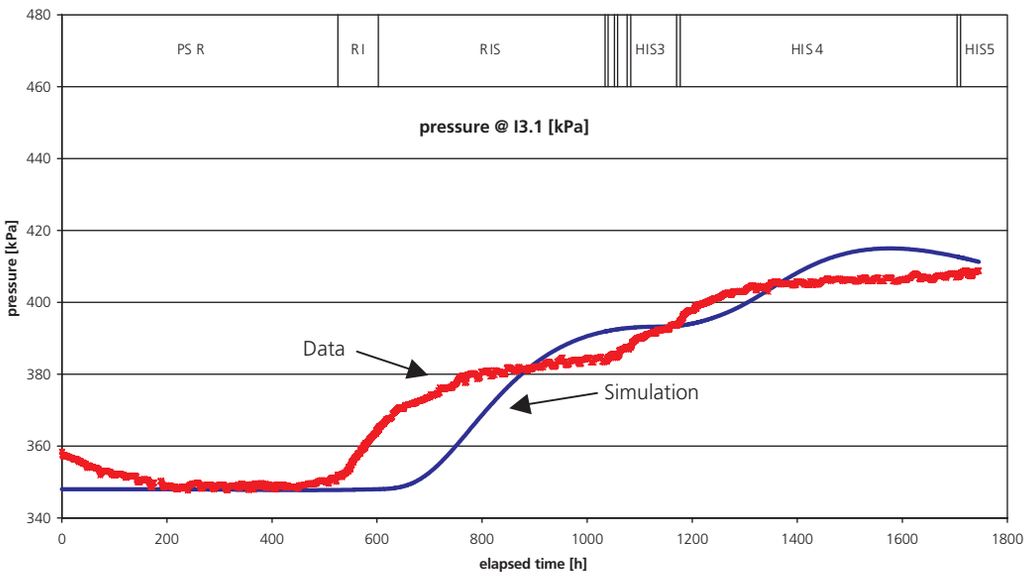

(b)

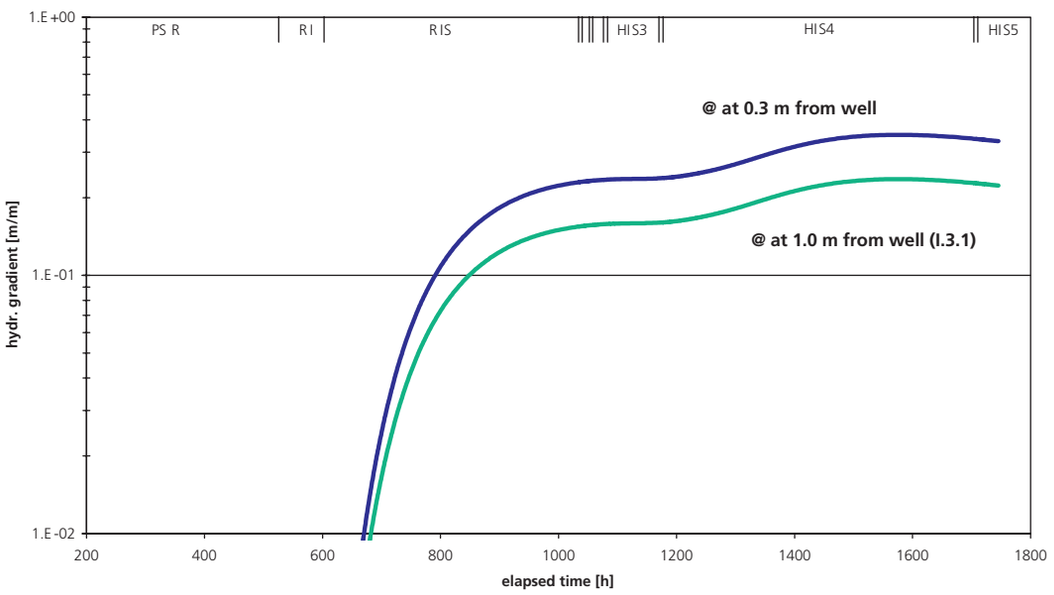

Figure 4.7: Simulation of the crosshole response in BGP-3/I1 to a sequence of rate injection and head injection tests in BGP-4 (TN 98-24): (a) a satisfactory fit of the response in BGP-3 by inverse modelling was not achieved; (b) hydraulic gradient at a distance of 0.3 m and at the location of borehole BGP-3/I1. The gradients are computed based on a radial flow model.

Hydraulic investigation method	Typical hydraulic gradient imposed [m/m]	Validity of Darcy's law
Permeameter tests on cores	1000–10000	The assumption of Darcy flow is proven experimentally.
Single-hole packer tests	50–500 (gradients during the pressure recovery phases)	The assumption of Darcy flow is proven experimentally.
Hydraulic interference tests	much less than one at the observation borehole	Inconsistency between the pressure evolution observed during the flowing and the pressure recovery phases (especially: abnormal "flattening" of the pressure observed in the observation borehole). These might indicate non-Darcy behavior.
Long-term monitoring of the pressure evolution in the vicinity of the tunnel near field	Radial gradient at the distance of less than 10 m is 1–20	Long-term pressure monitoring in the tunnel nearfield, does not show any indication for deviation from Darcy's law (see preliminary interpretation of the pressure measurements in chapter 4.6)

Table 4.3: Range of validity of Darcy's law and threshold gradient estimates. Typical ranges of hydraulic gradients are listed for different hydrogeological investigation techniques. For those techniques for which no deviation from Darcy's law was observed, it can be inferred that the pressure gradient was above the threshold gradient in the investigated domain.

4.4.2 Osmosis

The phenomenon of osmosis bears relevance for the hydrogeological considerations of the Opalinus Clay in terms of both a potential fluid transport mechanism and a potential cause for instability problems in boreholes and engineered subsurface structures. Literature provides numerous evidences that strongly consolidated clay formations like the Opalinus Clay may act as semi-permeable membranes and that high geochemical gradients in the formation water may drive osmotic flux (e.g. Hanshaw 1962, Young & Low 1965, Fritz 1986, Neuzil 2000). It is also known that such effects may be the cause of borehole instabilities partly due to swelling effects (van Oort 1994, Wong & Heidug 1994). Osmotic flow and osmotic differential pressures have been demonstrated repeatedly in clay formations in both laboratory and field experiments.

Chemo-osmotic flow

Osmosis is a process taking place only in materials with extremely small pores. Its underlying principle is that of a semi-permable membrane, i.e. water molecules may pass through the porous medium while molecules dissolved in that water may not. If such a semi-permeable membrane separates two solutions with different concentrations, a flux is induced through the membrane as a result of osmosis and an osmotic pressure difference arises between the two sides of the membrane. In analogy to Darcy's law, the osmotic flux v_Π is proportional to the gradient of the osmotic pressure π (e.g. Horseman et al. 1996):

$$v_\Pi[m/s] = \zeta \cdot K \ \frac{\text{grad}\,\Pi}{\rho \cdot g} \qquad (4.2)$$

K and ζ are the hydraulic conductivity and the osmotic efficiency, respectively. Osmotic efficiency is defined as the ratio of the developped hydraulic pressure and the osmotic pressure at zero flux conditions derived from the chemical activity of thewater on the sides of the semi-permeable clay membrane.

$$\zeta = \left.\frac{\Delta P}{\Delta \Pi}\right|_{v_\Pi=0} \qquad \text{where } \Delta\Pi = \frac{R \cdot T}{V_w} \cdot \ln\frac{a_1}{a_2} \qquad (4.3)$$

a_1 und a_2 are the chemical activities of the water on the sides of the semi-permeable clay membrane and V_w is the volume of one mole of water.

After Fritz (1982) the van't Hoff equation is applicable for NaCl concentrations < 1 mol:

$$\Delta\Pi \approx \nu \cdot R \cdot T \cdot \Delta C \qquad (4.4)$$

where C is the molar concentration of each of the ions and ν=2 represents the number of number of ions of the dissociated solute. Assuming a 0.245 mol NaCl solution (equivalent to 14.3 g/l NaCl) the osmotic pressure at room temperature is in the order of 1 MPa (with reference to deionised water). Ultrafiltration is the inverse process of osmosis, describing the concentration gradient, which is

observed when an aqueous phase is pressed through a semi-permeable membrane. Horseman et al. (1996) mention osmosis and ultrafiltration as possible causes for deviations from the linear flow law (hydraulic threshold gradient, cf. chapter 4.4.1).
In the framework of the OP experiment, laboratory and field experiments were conducted in order to determine the osmotic efficiency / pressure of the Opalinus Clay (TN 97-39). Furthermore, Soler (1999) computed the theoretical osmotic pressures resulting from the salinity of the Opalinus Clay and the aquifers below and above.

Osmotic efficiency

In order to determine the osmotic efficiency of the Opalinus Clay under in-situ conditions, the 8 m long vertical borehole BOP-1 in the Reserve niche was equipped with a PP system (TN 2000-43). The borehole was drilled with air and the testing interval was saturated with a synthetic porewater (Pearson recipe). With the exception of some unforeseen events, the test interval was fully closed off for 2 years, and a thorough equilibration of the testing fluid with the formation was attained (Figure 4.8a). On February the 16th, 2000, the fluid was at once replaced with deionised water (Figure 4.8b). Replacement of the fluid in the monitoring interval took place in a closed circulation system to avoid any hydraulic disturbance (i.e. advective flow towards the borehole due to the drop of interval pressure). A marked pressure decrease of around 80 kPa was observed, which is due to the chemical disequilibrium between the formation porewater and the test fluid. A numerical simulation of the experiment rendered a value for the osmotic efficiency of about 12% (TN 2000-44).

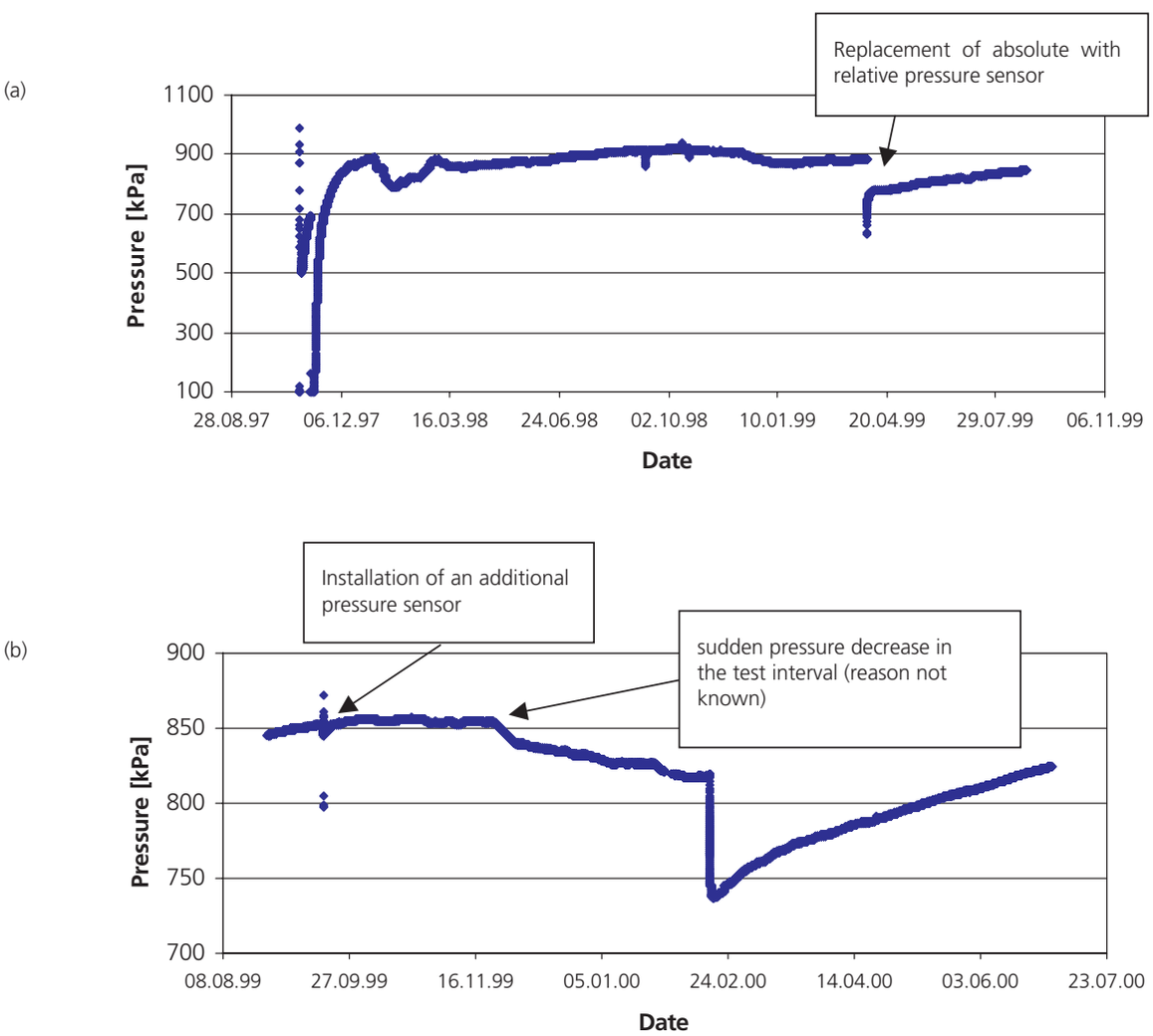

Figure 4.8: Pressures recorded in borehole BOP-1, (a) prior to fluid exchange, and (b) shortly before and after the fluid exchange with deionised water on February 16th, 2000.

The lab and in-situ experiments performed within the framework of the OP experiment present relatively low osmotic efficiencies of the Opalinus Clay. The osmotic efficiency was determined on two cores of the Opalinus Clay (shaly facies) under effective stresses of 4.5 MPa and 6.5 MPa (Harrington et al. 2001; TN 97-39, TN 99-81). The resulting values range from 0.03 to 0.10. In the in-situ experiment (TN 2000-42; TN 2000-43, TN 2000-44), the osmotic efficiency was derived from the measured pressure evolution in the testing borehole filled with deionised water. A maximum value of 0.12 was obtained. The impact of chemo-osmosis on packer tests was shown to be small. Further evidences suggesting small impact of osmosis were found:

– The DB experiment investigated the impact of different test fluids (synthetic porewater, KCl-based mud, silicate-polymer mud, see Enachescu et al. 1999). The analysis of the tests does not show a significant dependency of the hydraulic test results on the testing fluid used (cf. chapter 3.4).
– Soler (1999) used the results of the preliminary analyses of porewater samples collected along the reconnaissance gallery to compute osmotic pressures based on the water activities (Figure 4.9). The neighbouring formations on either side, i.e. the Lower Dogger Blaukalke limestones to the SSE and the Lias Gryphaea limestones to the NNW, showed small values of less than 0.1 MPa, while the osmotic pressure toward the centre of the Opalinus Clay formation was found to be up to 1.3 MPa, with an average osmotic gradient in the order of 1–2 m/m. If it is considered that the clay membrane is not ideal with measured values of the osmotic efficiency of max. ζ=0.12, the corresponding (hydraulic) overpressure will be less than 0.16 MPa and the hydraulic gradient will even be as low as 0.2 m/m. The osmotic fluxes would then have little impact on the hydraulic pressure within the Opalinus Clay at Mont Terri. Note in comparison the hydraulic gradients in the zone of influence of the galleries which are typically larger than 5 m/m in the immediate vicinity of the galleries. Figure 4.9 also indicates that, should chemical osmotic flux occur, it would be directed towards the Opalinus Clay as chemical osmosis promotes the flow of fluid up the salinity gradient.
– Recently, a more comprehensive chloride profile was reported as part of the GM experiment (Pearson et al. 2003; cf. Figure 4.15). The maximum salinity was in the order of 13 g/l (equivalent to 0.35 mol/l). According to the van't Hoff equation the corresponding osmotic pressure is 1.7 MPa (with reference to deionised water) – and, assuming an osmotic efficiency of 12% the hydraulic overpressure is in the order of 0.2 MPa.

4.4.3 Coupled hydro-mechanical processes

Relevance and conceptual framework

The hydromechanical processes are, for several reasons, of marked significance for the hydrogeological studies of the Opalinus Clay. First, they may affect the interpretation of hydraulic tests, leading to biased estimates of hydraulic properties (e.g. overestimation of

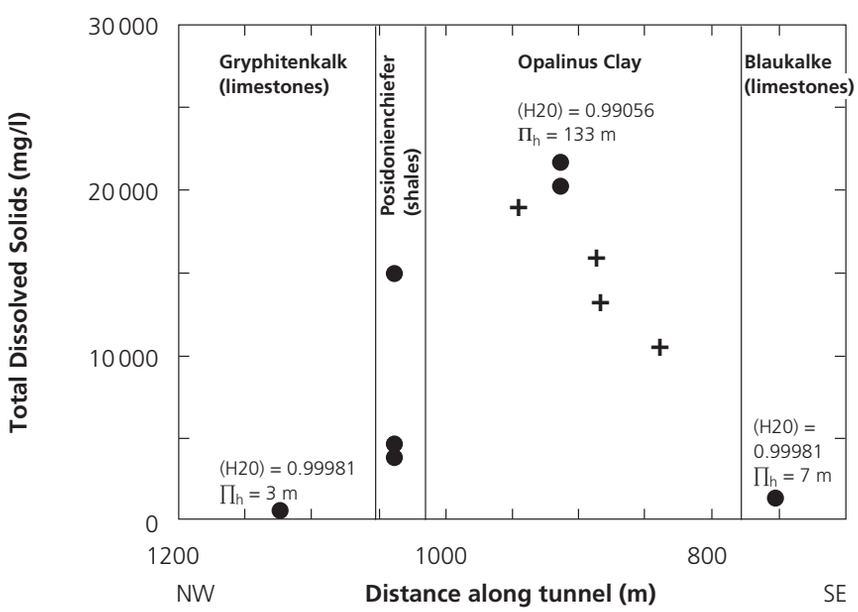

Figure 4.9: Schematic diagram showing Total Dissolved Solids vs. Distance along the Mont Terri reconnaissance gallery. Dots and plus signs are indicating different experimental values. Activity of water (H2O) and osmotic pressure head (Π_h) are also given for the sample with the highest salinity in the Opalinus Clay, and for two low salinity sample above and below the Opalinus Clay (after Soler 1999).

K-values due to borehole closure effects, breakouts). Second, the mechanical behaviour influences the storage capacity of the Opalinus Clay at the large scale and – to lesser extent – on hydraulic conductivity. Finally, the deformation behaviour of the rock is of great importance in the excavation disturbed zone (Harrington et al. 2001): not only the property of self healing, also is the transition between ductile and brittle strongly related to the stresses in the immediate vicinity of the underground structures. In this study, emphasis is given to the first two issues.

The well-established theories of consolidation and poroelasticity (e.g. Horseman et al. 1996) form the foundation for conceptualisation of hydromechanical processes. Coupling of hydraulic and mechanical quantities is expressed by the concept of effective stress. Assuming a fully saturated porous medium at a given porewater pressure p_{pw} is subjected to mechanical stress σ, the mean effective stress p_m' [Pa] is defined as:

$$p'_m = \frac{1}{3} \cdot (\sigma_1 + \sigma_2 + \sigma_3) - p_{pw} \qquad (4.5)$$

where σ_1, σ_2 and σ_3 represent the principle directions of the stress tensor.

The Opalinus Clay at Mont Terri is an indurated, slightly overconsolidated claystone. Assuming the rock is exposed to changing stress conditions in an elastic deformation regime, a logarithmic relationship holds for the inter-dependence between porosity n [-] and mean effective stress (Wood 1990):

$$n \approx n_o - \kappa \cdot \ln \frac{p'm}{p'o} \qquad (4.6)$$

where κ is the negative slope of the rebound-reconsolidation line (RRL). The intercept value n_o is conventially chosen in a way that it represents the porosity at an effective stress p'_o = 1 kPa. Drawing on critical state concepts, the drained bulk modulus of an overconsolidated clay, *B* [Pa], can be estimated from the mean normal effective stress, p'_m, and the negative slope of the rebound-reconsolidation line, κ, using:

$$B = p'_m \left[\frac{1}{(1-n)\,\kappa} \right] \qquad (4.7)$$

The specific storage coefficient S_s, is usually defined as:

$$S_s = \rho_w \cdot g \cdot \left[\frac{1}{B} + \frac{n}{K_w} \right] \qquad (4.8)$$

where B and K_W are the compressibility of rock and water, respectively, and ρ_W is the density of water. In the context of groundwater flow modelling the drained compressibility of the rock is used to determine specific storage, whereas the undrained modulus is more appropriate for hydrotest analysis.

According to the Kozeny-Carman equation (e.g. Horseman et al. 1996) intrinsic permeability k and hydraulic conductivity K [m/s] can be expressed in terms of porosity n and specific surface S:

$$k = \frac{n^3}{(1-n)^2} \left[\frac{1}{\tau^2 \cdot C_s \cdot (\rho_s S)^2} \right]$$

and

$$K \left[m/s \right] \approx 1 \cdot 10^7 \cdot k \left[m^2 \right] \qquad (4.9)$$

where τ is the tortuosity and C_s represents a geometry factor with typical values between 2 and 3. Specific surface and porosity can be determined by microstructural analysis of porespace.

Combining equations (4.6) and (4.9) leads to a relationship between permeability and mean effective stress. In the case of elastic deformation, the changes of permeability with stress are rather small. However, when the stress conditions approach a critical state boundary of plasticity, i.e. irreversible deformation, dilatancy or compaction may occur and the permeability changes are much more pronounced and can not be described by equations (4.6) and (4.9).

In oilfield exploration (e.g. Settari & Walters, 2001), it is a well-known procedure to decompose sequentially the hydro-mechanical coupling process into:

- Pore volume coupling - that is, any changes in effective stress (and the resulting volumetric strain) cause changes in the porosity (translating to pressure changes) of the porous medium.
- Permeability coupling, which relates permeability changes to porosity changes due to volumetric deformation

For the hydro-mechanical modelling excercise described below (coupled hydro-mechanical modelling of the interference test in BGP-6), the pore volume coupling alone was used as the changes in permeability due to porosity changes with effective stress were assumed to be negligible (due to lack of data to support otherwise). The approach was simplified by neglecting the porosity-permeability relationship and, instead, introducing so-called transmissibility multipliers. Thus, the coupling between effective stress and pore volume is modelled explicitly, whereas the effective permeability is the product of the intrinsic permeability and a stress dependent dimensionless coeffi-

cient. The functional relationship between effective stress and transmissibility multiplier is a smooth function which has to be fitted to the data.

Experimental evidence for coupled hydro-mechanical processes

Interference tests were conducted in the FM niche with the GP experiment in Phase 4, and at the GS site in the new gallery with the GS experiment of Phase 5 in search of evidence for hydro-mechanical processes on the scale of the in-situ experiment. The experimental set-up was similar in both experiments. Figure 4.10a shows the borehole configuration applied in the FM niche: triple packer systems were installed in BGP-5 and BGP-6 for hydraulic testing. Fixed installed micrometers (FIM) with five measuring sections were emplaced in BGP-8 and BGP-9 to monitor displacements along the boreholes (the configuration was completed by a TDR system for monitoring possible changes of water content during gas injection tests). A three-step constant-head water-injection test (pressure steps HI1, HI2 and HI3) was carried out in interval I2 of borehole BGP-6 (Figure 4.10b) and hydraulic responses were observed in all monitoring intervals of BGP-5 and BGP-6. In addition, displacements were recorded in BGP-8 and BGP-9. Figure 4.10c presents the crossplots of displacements in BGP-8 versus injection pressure in BGP-6/I2. The correlation of displacements and interval pressure is evident. In section F8.2 of BGP-8, a maximum (compressive) strain of -0.02 mm/m is observed. The other sections tend to show dilatant behaviour. In BGP-9 the same pattern is observed, however, the deformations are less pronounced because the distance to the source borehole is longer.

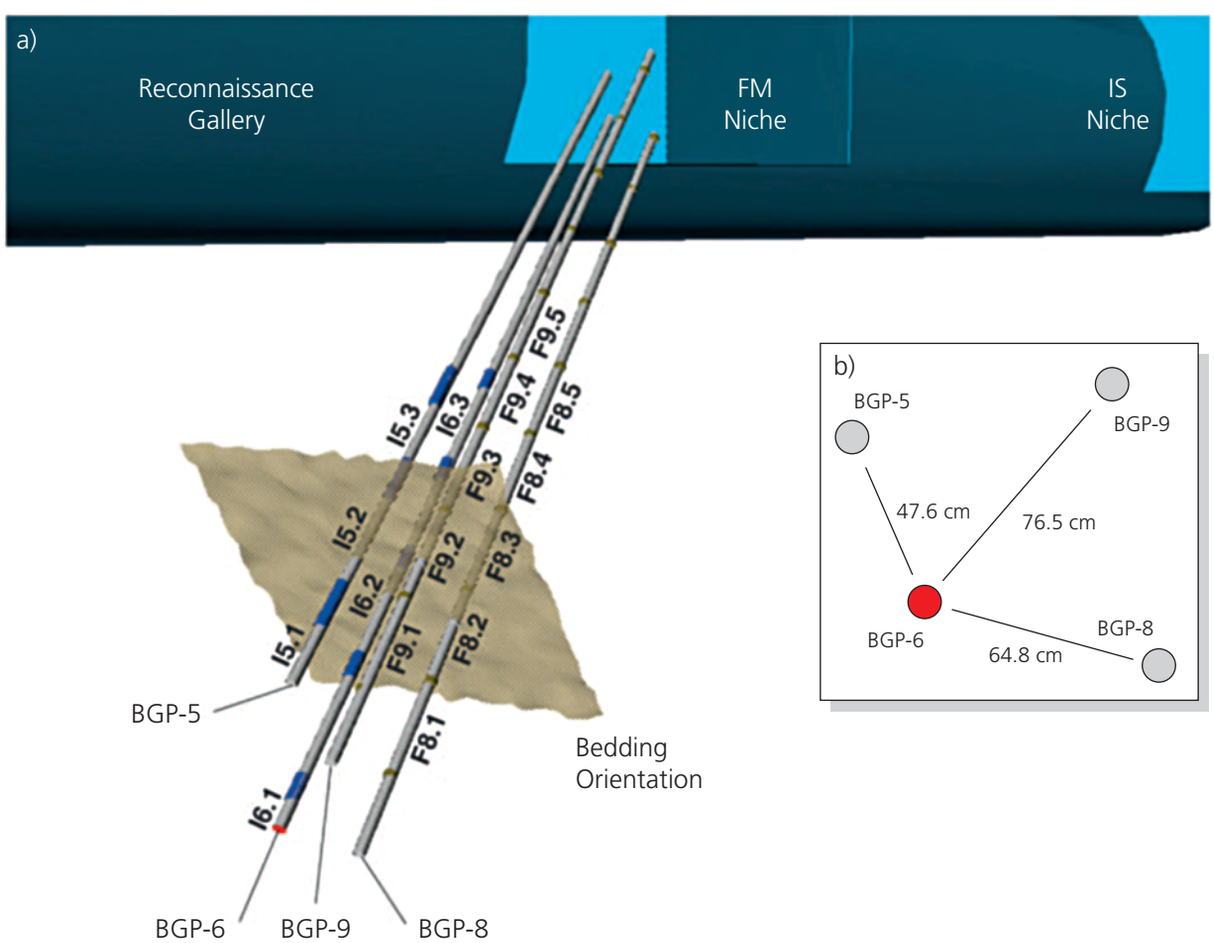

Figure 4.10: Interference test in the FM niche with a water-injection test in BGP-6: test configuration with the four boreholes (a) in 3D with a schematic plane indicating the bedding orientation roughly at right angle to borehole orientation and (b) in plan view perpendicular to BGP-6 at the centre of the test interval. (c) Pressure vs. time plot for the three-step constant-head water-injection test in BGP-6/I2 and (d) corresponding displacement records from FIMs installed in BGP-8 and BGP-9. (c) and (d) on page 46.

c)

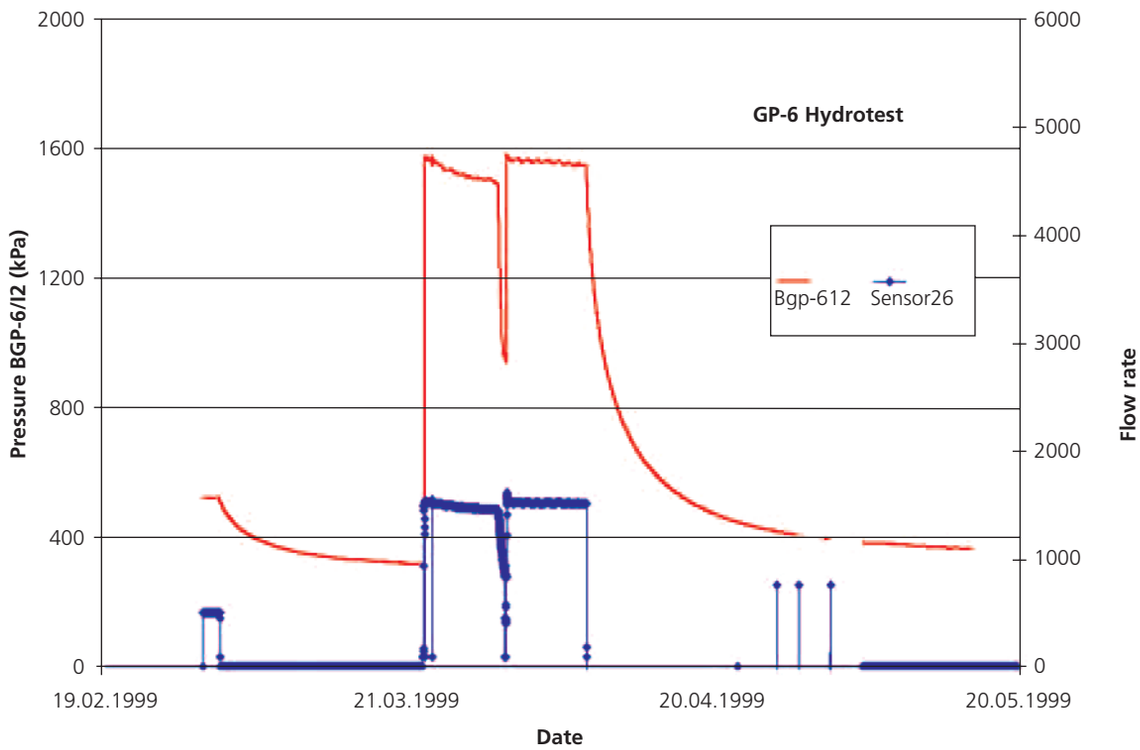

d)

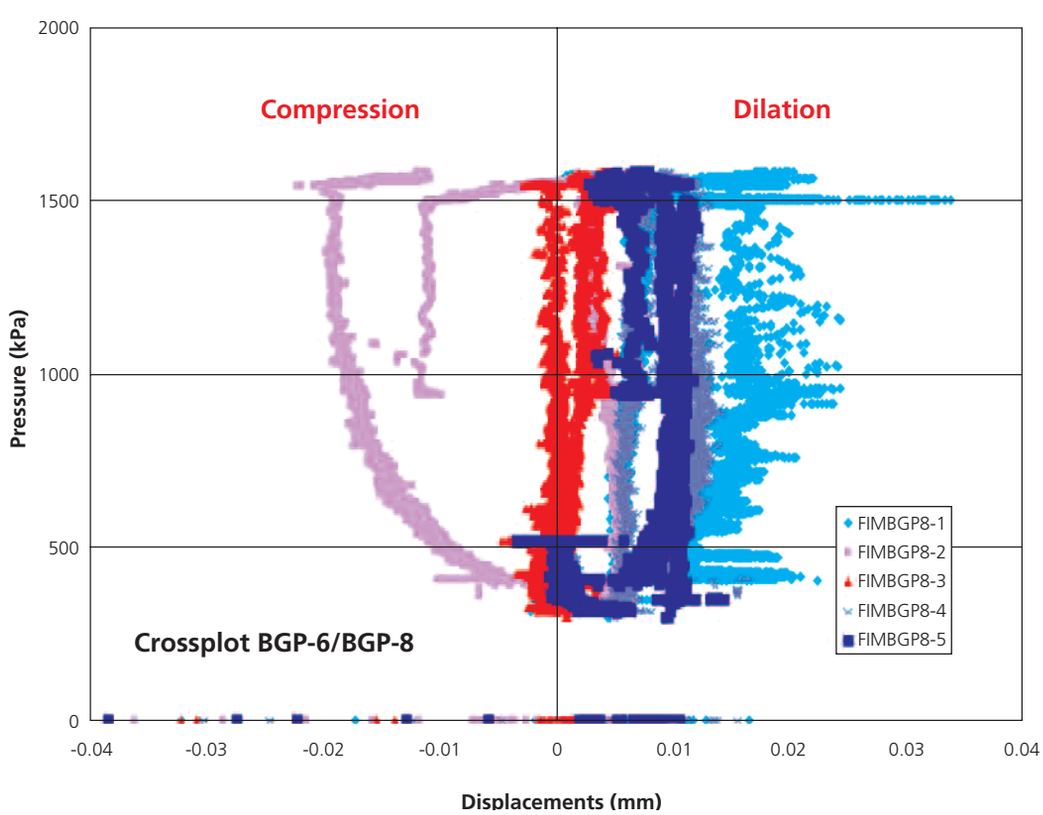

Figure 4.10 continued

Coupled hydro-mechanical modelling of the hydraulic interference test in BGP-6

The hydro-mechanical analysis of the interference test in BGP-6 was conducted in two steps (cf. TN 2000-21):

– In a first step, a detailed (hydraulic) analysis of the hydrotest response in the test interval I6.2 of borehole BGP-6 was performed with the welltest simulator GTFM (Pickens et al. 1987). The analysis focussed on the measured flow rates during the constant head injection sequences and on the pressure response during the subsequent recovery periods.
– In a second step, the coupled hydro-mechanical code GEOSIM (TN 2000-21) was applied, considering both the hydraulic (e.g., porewater pressure response) and the geomechanical response. For this task, the test configuration was implemented with a 3D numerical model covering boreholes BGP-6 and BGP-5 for hydraulic responses, and BGP-8 and BGP-9 for geomechanical responses.

The hydraulic test interpretation was aimed at detecting potential changes in hydraulic properties with injection pressure. The detailed analyses were done through diagnostic plot analysis and inverse modelling of individual test events and of the entire hydrotest sequence. Figure 4.11 illustrates the difficulties in matching the entire test sequence by inverse modelling. Fitting the individual test events HI1 / HIS1 and HI2&3 / HIS2&3 leads to acceptable matches, whereas the fit of the entire test sequence is not satisfactory.

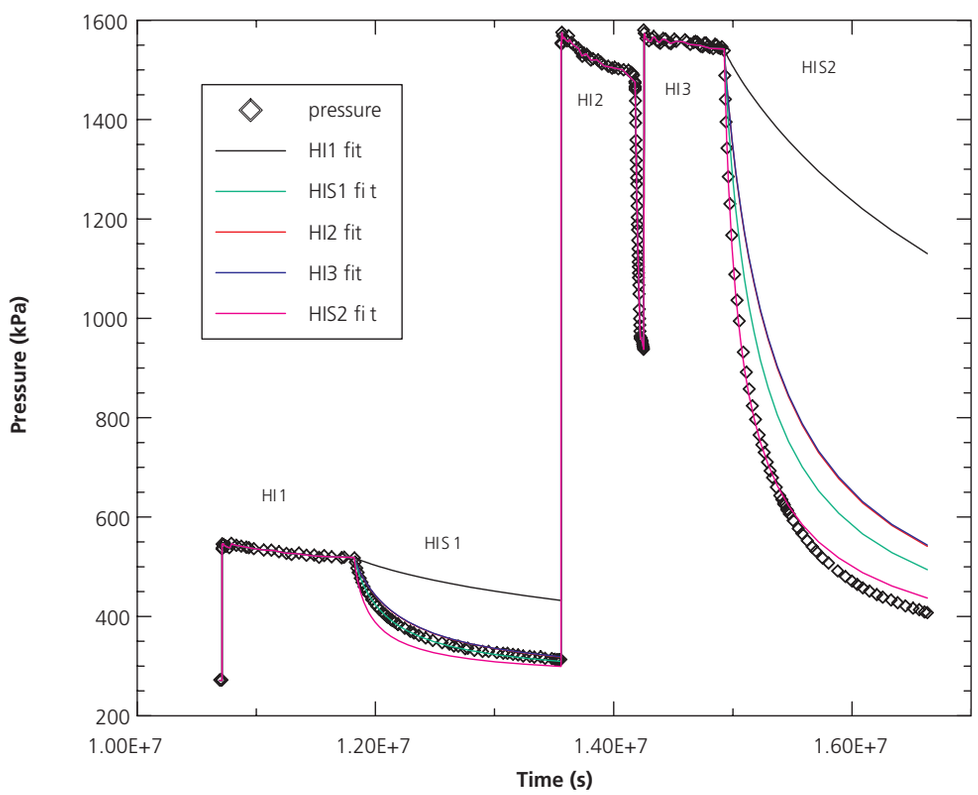

P: Static formation pressure
S_s: Specific storage
K_{inner}: Hydraulic conductivity of the inner zone in a 2 shell radial composite model
K_{outer}: Hydraulic conductivity of the outer zone

	Kouter (m/s)	Kinner (m/s)	Rinner (cm)
HI1	1.18E-14	3.27E-13	12.65
HI2	1.56E-14	2.02E-13	179.95
HI3	3.43E-14	1.99E-13	153.15
HIS1	6.86E-14	3.22E-13	272.05
HIS2	1.53E-13	8.14E-13	582.35

P = 271 kPa
Ss inner = Ss outer = 2E-06 1/m

Figure 4.11: Inverse modelling of the packer test conducted in BGP-6 using a finite skin model (inner zone / outer zone) exhibits difficulties in simulating jointly the HI1 / HIS1 sequence and the HI2&3 / HIS2&3 sequence. The analysis of HI1 / HIS1 gives a hydraulic conductivity in the order of 1 to 3 E-14 m/s. The two latter test sequences suggest values in the range 7E-14 and 2E-13 m/s (after TN 2000-21).

Fitting of HI1 / HIS1 leads to K-values in the order of 1 to 3×10^{-14} m/s; putting the weight on H2&3 / HIS2&3, however, gives value between 7×10^{-14} and 2×10^{-14} m/s. This fact suggests dependence between hydraulic conductivity and injection pressure. More generally, a relation between intrinsic permeability and effective stress may be deduced.

Coupled hydro-mechanical modelling was performed with the code GEOSIM (TN 2000-21). In GEOSIM, a sequential coupling procedure was implemented which consists of pore volume coupling followed by permeability coupling. Due to the lack of site specific data, the porosity-permeability coupling was neglected and a simple transmissibility multiplier was introduced. Geomechanical properties of the Opalinus Clay were taken from TN 98-35. Pressure responses in the observation intervals of BGP-5 and BGP-6 were modelled as well as the mechanical responses in BGP-8 and BGP-9. Four different cases were considered:

Case 1: Opalinus Clay exhibits homogeneous and isotropic hydraulic properties. Geomechanical behaviour is characterised by elastic properties, based on TN 98-35. An additional sensitivity run (Case 1a) was carried out using anisotropic hydraulic conductivity (K enhancement by a factor of 2.5 parallel to bedding).

Case 2: Flow takes place in mechanically weakened zone which is parallel to the bedding plane and called "fracture zone" in the following. It has a thickness of 2.5 cm. The transmissivity of this fracture zone is stress dependent. The initial transmissivity of the fracture is 2.5×10^{-14} m²/s. Its elastic properties are the same as in Case 1.

Case 3: Comparable to Case 2, except that softening of the fracture zone during fluid injection is assumed.

Case 4: Comparable to Case 2, except that the geomechanical behavior is no longer linearly elastic. A hyperbolic model is used, as it was proposed in TN 98-56.

The results of hydro-mechanical modelling are discussed in TN 2000-21. A brief summary is given below.

Case 1 (isotropic properties) results in a poor overall fit of the test sequence both in pressure response and in displacement modelling. The sensitivity run with anisotropic rock properties (Case 1a), however, showed an acceptable overall match. In particular, the general pattern of the simulated displacements at the FIM locations (compression/extension) was in agreement with the observations. The magnitudes of the simulated displacements were slightly lower than the measured ones.

In Case 2 the potential of a permeability increase as a result of the increase in injection pressure during the hydrotest was examined. That is, as the fluid pressure increases during the constant-head injection tests, the effective stress decreases causing an increase in the fracture transmissivity. The magnitude of the permeability change is a factor 3. Figure 4.12 shows the simulated interval pressures. Note that only the fall-off events (HIS events) were fitted, whereas the HI events were given by prescribed pressure. The overall fit of the interval pressure and the diagnostic plots of the fall-off events are satisfactory. Furthermore, the calculated displacements matched the observed extensions/compressions reasonably well (not presented here, cf. TN 2000-21).

Case 3 corresponds to Case 2, except that the fracture zone was assumed to have a higher compressibility (e.g., decreasing E modulus from 4 GPa to 1 GPa). This softening of the fracture zone during fluid injection was designed to account for potential dilatancy prior to the failure of the samples as suggested in the triaxial tests (TN 98-35 and TN 98-55). The impact of the softer fracture zone did not noticeably affect the fluid pressure response in BGP-6/I2. The mechanical effect however is noticeable: an increase in the extension in BGP-8/I2 (from about 0.04 to 0.08 mm) is observed, which is significantly greater than the measured displacements.

Case 4 also corresponds to Case 2, except that a hyperbolic geomechanical model is assumed. Similar to Case 3, the impact of the hyperbolic model on the fluid-pressure response is small. The results of the calculated displacements at the corresponding FIM segments in BGP-8 indicate significantly lower extension (0.01 mm) as compared to Case 2. However, variations in the parameters describing the hyperbolic model may result in calculated displacements that show a better fit with the observed data. In conclusion, the introduced complexities of the material law are not required to explain the data.

Concluding remarks

The results of the coupled hydro-mechanical modelling indicate that the observed FIM measurements can be reproduced reasonably well with an overall elastic constitutive model for the clay. However, non-linear behaviour represented by a hyperbolic constitutive model cannot be excluded. More importantly, the coupled modelling indicates that the increased injection

pressure during the HI events caused a significant permeability increase associated with a decrease in effective stress. For the interference test in BGP-6 with a maximum injection pressure of about 1.6 MPa, the permeability enhancement factor was about 3. Hydromechanical modelling of hydraulic interference tests at Mont Terri suffers from the fact that the understanding of stress conditions at the site is quite rudimentary. Neither the principal stress directions, nor stress magnitudes are well known. Moreover, the test boreholes in the FM niche are located close to the tunnel excavations. Thus, complex stress redistribution in the test zone may be expected. Recent geomechanical studies as part of the RA project will place emphasis on an improved understanding of rock stress in the tunnel nearfield. In future phases of the HA project this information will be integrated in the assessment of hydromechanical coupled processes.

4.5 Groundwater flow at different scales

The hydraulic properties of the undisturbed Opalinus Clay formation are governed in part by the hierarchy of pore structures, with the spatial distribution of the various pore structures being scale-dependent. The hydraulic conductivity, too, is a scale-dependent property. In practice – given the low permeability of the Opalinus Clay – hydraulic conductivity may be determined only at small scale. With hydraulic in-situ tests and laboratory experiments it was possible to obtain hydraulic conductivity estimates representative for the centimeter to meter scale. However, attempts to draw conclusions on groundwater flow on the site scale require effective hydraulic conductivity values on the deka- to hectometer scale. In addition to deriving representative hydraulic parameters from testing on the small scale, it is therefore also necessary to establish a (conceptual) modelling approach which allows for the upscaling of these observations to the required region-

a)

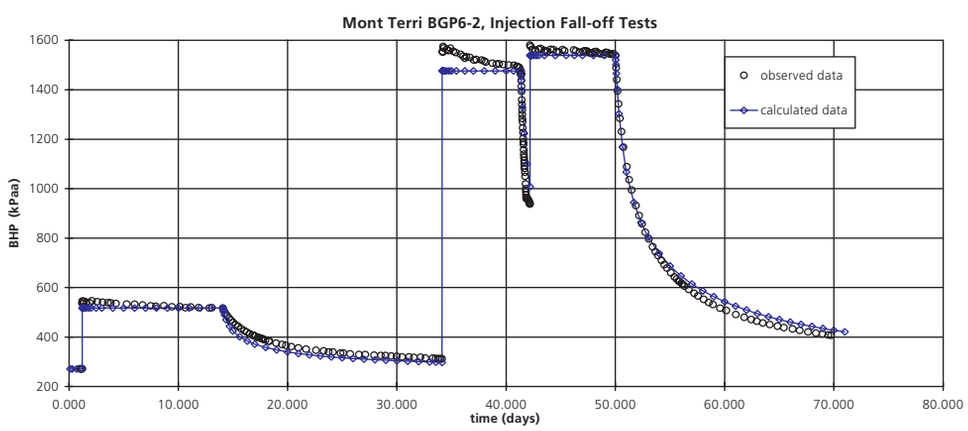

b)

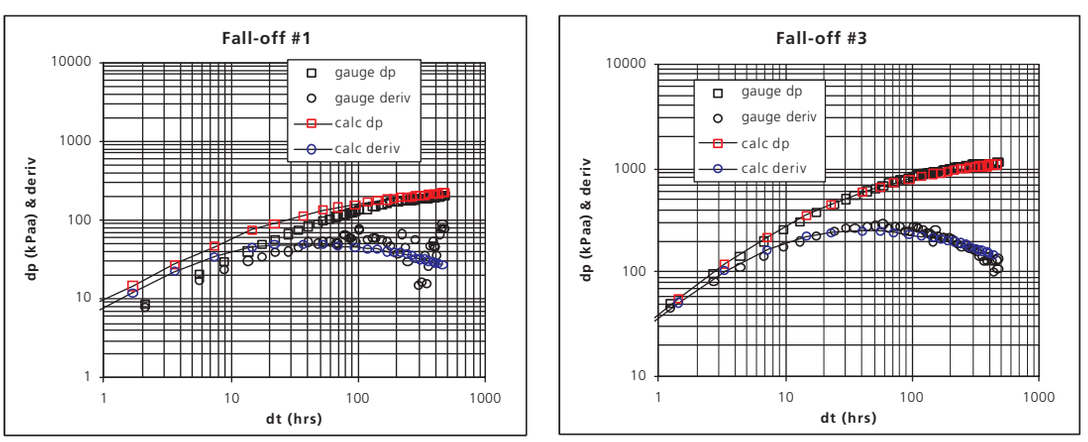

Figure 4.12: Hydro-mechanical modelling of the interference test in BGP-6 – simulated interval pressures. Note that only the fall-off events (HIS events) where fitted, whereas the HI events were given by prescribed pressure: (a) The overall fit of interval pressure and (b) the diagnostic plots of the fall-off events are satisfactory (after TN 2000-21).

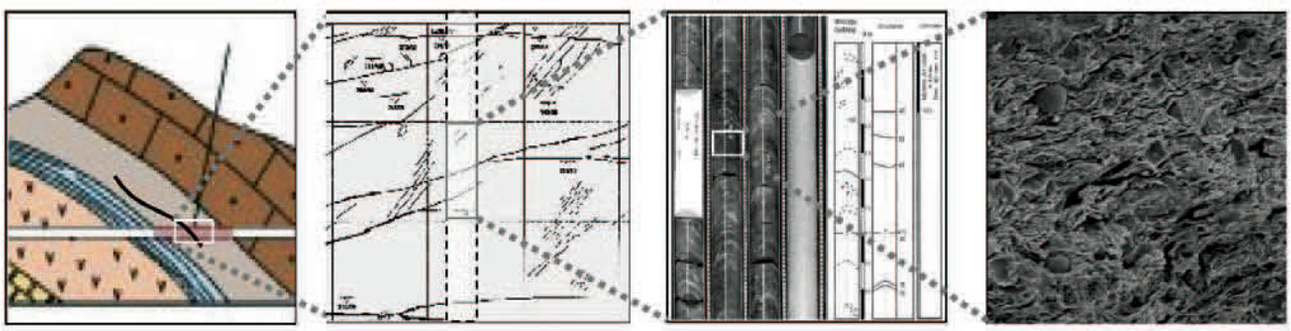

Figure 4.13: Hydraulically relevant structural and stratigraphic elements at various scales of observation: (a) geological formations and regional flexure at the Mont Terri site; (b) facies, fracture zones and single fractures of the decimeter to dekameter scale in the Opalinus Clay formation; (c) lithofacies and bedding as well as various small discontinuities in the order of millimeters to decimeters; and (d) microfractures, and micro/mesopores in the sub-millimeter range (Remark: the figure does not necessarily adhere to the scales introduced above but covers the complete range of scales described).

al scale where no direct measurements are possible. The first step in the analysis of the scale dependency of the hydraulic conductivity is the identification of the hydraulically relevant structural elements at the various scales of observation. In total, four different observation scales have been defined for the Mont Terri site. Their dimensions serve as guidelines rather than exact sizes (Figure 4.13):

- On the site scale (10^1–>10^3 m) the Opalinus Clay formation represents an aquitard sandwiched between the more permeable formations of the Jurensis Marls and the Lower Dogger Limestones. The Opalinus Clay acts as a hydraulic barrier. The only element which may affect this barrier function at the site scale is the main fault. The impact of the main fault on the hydrogeological system may not be assessed effectively by in-situ experiments. However, it is possible to assess the hydraulic efficiency of the Opalinus Clay barrrier qualitatively by means of independent experimental evidences such as the observed pore pressure distribution at the site, porewater chemistry and isotope profiles.
- Tunnel mapping allows for the differentiation of facies and the detection of discrete structural features on the scale of decimeters to dekameters (10^{-1}–10^1 m). Within the individual facies, layers of various sand and clay content but of critical lateral extent exist. Hydraulic characterisation of all these features on the decimeter to dekameter scale is carried out through packer testing in boreholes, both in single and cross-hole arrangements. Hydraulic conductivities determined from the results of packer tests with test intervals of several decimeters up to about 10 m in length, are representative for radial extensions of several decimeters to several meters, i.e. corresponding to the radius of influence of the hydraulic test.
- At the core scale (10^{-3}–10^{-1} m) and also at the tunnel mapping scale, well structured parallel interlayering of clayey and sandy layers is observed. Layering can be interpreted as an indication for pronounced anisotropy of the hydraulic conductivity at the centimeter to decimeter scale. Permeameter tests allow for the determination of hydraulic conductivity both parallel and perpendicular to the layering.
- The mineralogical composition and the microstructure of the Opalinus Clay were determined in the laboratory for an investigation domain of < 0.002 mm. The microstructure was analysed with various methods like gravimetric methods, helium pycnometry and mercury injection. The equivalent microscopic pore spaces of the Opalinus Clay are classified in the category of micro/meso- and macropores; microfractures may also contribute to porewater flow, altough they are rarely observed in the Opalinus Clay. Within the mesopores, the mobility of the porewater is limited by capillary forces and electrical intermolecular forces. Indirect indication of hydraulic conductivity on this microscale is derived from empirical porosity-permeability relationships (e.g. Kozeny-Carman).

4.5.1 Site scale (10^1 –> 0^3 m)

On the site scale (dekameters to kilometers), the physical framework for the conceptual hydrogeological model is provided by the local geological setting. The Opalinus Clay is a lithostratigraphic unit of the Mont Terri anticline, a structure belonging to the Folded Jura. Figure 4.14 shows a geological map of the Mont Terri anticline and a cross-section along the Mont Terri road tunnel between St-Ursanne and Courgenay. Today's lithostratigraphic and structural elements are the rudimentary elements responsible for the general

hydrostratigraphy, i.e. the definition of hydrogeological units and determination of water-conducting features. However, one also needs to consider the historical evolution, particularly of tectonic and sedimentological/erosional nature for an enhanced understanding of the presently observed groundwater flow systems. The primary references published within the Mont Terri investigation program are Wermeille & Bossart (1999a), TN 99-22 as well as contributions to Thury & Bossart eds. (1999). Eventually, an excellent overview of the regional geology and the paleogeology of the site is given in Pearson et al. (2003).

(a)

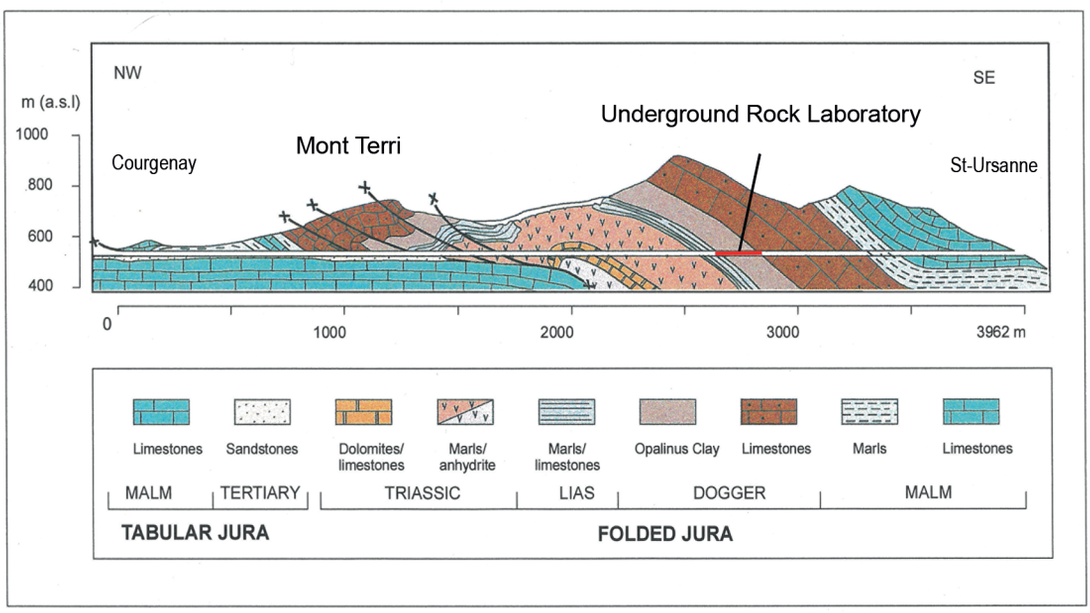

(b)

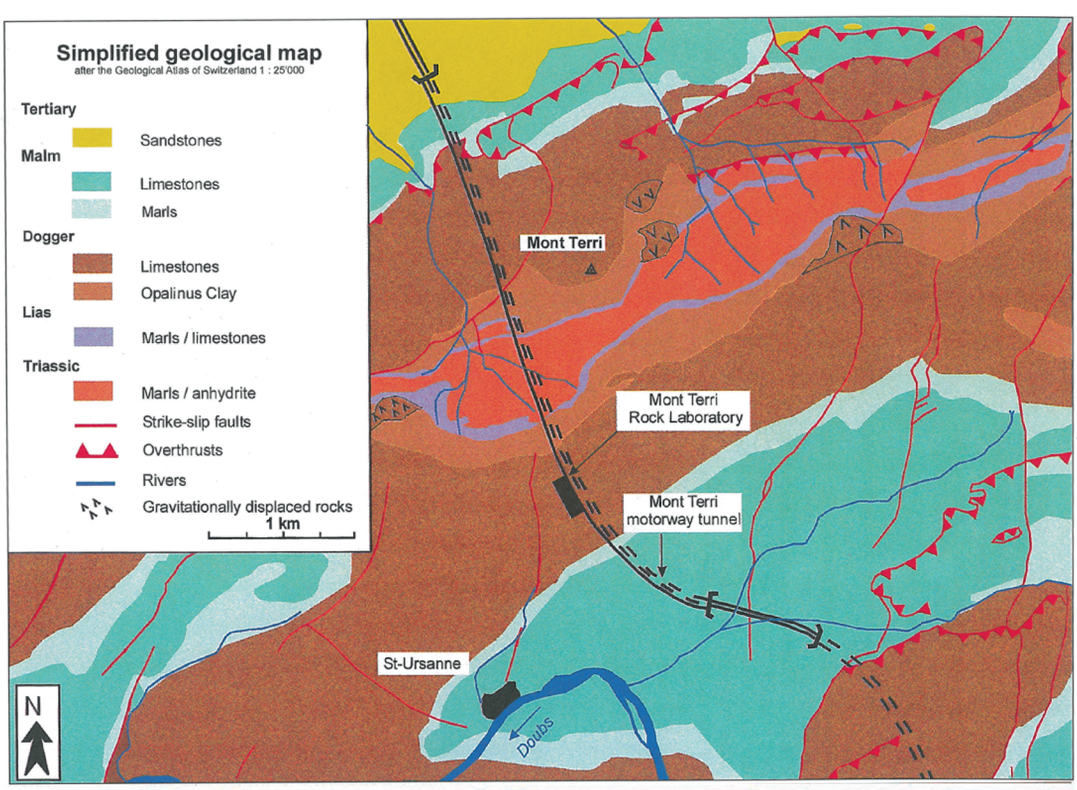

Figure 4.14: (a) Simplified geological cross-section through the Mont Terri anticline along the motorway tunnel, showing the location of the Mont Terri rock laboratory (Thury & Bossart 1999) and (b) simplified map of the Mont Terri anticline.

Definition of hydrogeological units

The purpose of defining the regional hydrostratigraphy is to divide the regional groundwater flow domain into hydrogeological units. These units merge adjacent stratigraphic units of similar hydrogeological properties and are generally classified into aquifers and aquitards. Obviously, the final definition of the hydrogeological units is based on the available hydrogeological data. The hydrogeological investigations for the Mont Terri project focussed almost exclusively on the characterisation of the Opalinus Clay. Little knowledge has been acquired about the adjacent formations. Important sources of information for these formations, therefore, are the records of hydrogeological investigations conducted in the course of construction of the motorway tunnel (TN 99-22). Additional information on the regional hydrogeology has been summarised by Wermeille & Bossart (1999a). Table 4.4 presents the current knowledge base of the hydrogeological setting at site scale.

Clearly identifiable as aquifers are the limestones of the Upper Malm and the limestones of the Lower Dogger. The limestones of the Upper Malm represent a regional aquifer of relevance for the regional water supply. The Lower Dogger limestones form a local aquifer which, nevertheless, produced substantial discharge rates during the construction of the motorway tunnel. The significance of the Jurensis Marls is less clearly defined. Water influx was observed from this formation during construction, but appeared to have originated in localised water conducting features. The measured chloride concentrations in the porewater and along the tunnel present an indirect evidence for this hydrogeological situation (Figure 4.15). The chloride profile shows a gradual decrease in concentrations towards the Lower Dogger which is an indication for more intense groundwater flow in the Lower Dogger. In the Jurensis Marls and the Posidonia Shales some considerable concentrations have been observed in samples obtained from porewater squeezing or leaching, while water samples collected in boreholes tend to imply short-term residence times.

Typical aquitards besides the Opalinus Clay are the Malm Marls, and the marl and anhydrite formations of Trias. The hydraulic barrier function of the Opalinus Clay was investigated rigorously in the Mont Terri investigation program. Not much is known, however, about the other aquitards.

Regional faults

Several thrust faults and strike slip faults intersect the motorway tunnel in the northern section (cf. Figure 4.14). The fault zones were mapped during the exploration phase in 1992 and inflow zones with flow rates of 1–2 l/s observed. The main fault in the Opalinus Clay did not show any water inflow. In addition, the chloride profiles in Figure 4.15 do not suggest enhanced groundwater flow along the main fault, as would be indicated by a drop in salinity.

Tectonic and stratigraphic evolution of the site

Wermeille & Bossart (1999a; Chapter 1.2 in TN 99-73) conducted a comprehensive literature review of the tectonic and stratigraphic evolution of the Folded Jura including the erosional history. The results may be summarised as follows: 40 My ago the area was covered by a sea which led to the deposition of the UMM, the Lower Marine Molasse. The period from 40 My ago to 21.5 My ago saw the subsidence of the

Lithostratigraphy	Hydrogeological classification
Limestones of the Upper Malm	Regional aquifer (karstified):
(Oxfordian/Kimmeridgian/Thionian)	fissured and karstic limestones; inflow rates > 1 l/s
Malm Marls (Lower Oxfordian/Callovian)	Aquitard: (shaly) marls, limestones, marly clay; impermeable
"Lower Dogger" (Lower Aalean/Lower Bajocian)	Local aquifer (karstified): sandy limestones, fissured and karstic; inflow rates 12–200 l/s
Opalinus Clay (Lower Aalenian)	Aquitard: silty and sandy shales; impermeable
Jurensis Marls and Posidonia Shales (Upper Toarcian)	Hydrogeological unit with localised water circulation (weakly karstified): Marls and limestones; spontaneous water inflows into the tunnel of 1–5 l/s
Triassic marls/anhydrite/dolomites/limestones Aquitard:	Marls, anhydrite, dolomites, limestones; partly fissured and karstic; tight rock with localised inflow rates << 1 l/min

Table 4.4: Hydrogeological classification of the lithostratigraphic units in the Mont Terri region (after Thury & Bossart 1999). Hydrogeological conditions during construction of the motorway tunnel between 1989 and 1999 (after Haapainter & Schaeren TN 99-22).

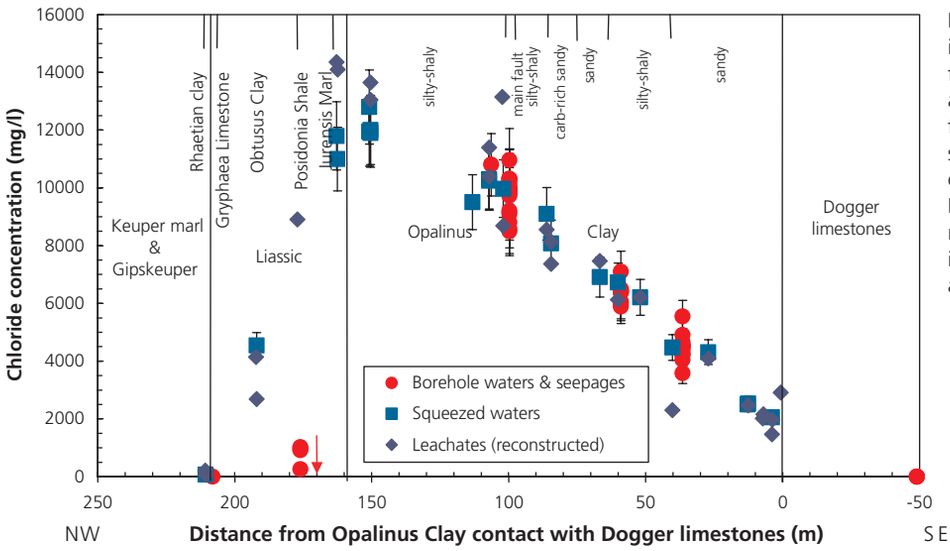

Figure 4.15: Chloride profiles as an indirect evidence for groundwater flow conditions in the Opalinus Clay and in the adjacent stratigraphic formations. The chloride profile shows a gradual decrease in concentrations towards the Lower Dogger, which is an indication for more intense groundwater flow in this formation (after Pearson et al. 2003).

Delémont Basin with the formation of N-S trending faults east of St-Ursanne and the Mont Terri flexure. Sedimentation of the UMM continued initially but was taken over increasingly by the sedimentation of USM, i.e. Lower Fresh Water Molasse, due to freshwater lakes and braided rivers. As the subsidence of the Delémont Basin continued until about 10.5 My ago, the area of St-Ursanne emerged and became hydraulically separated from the Delémont Basin. The erosive period for the Doubs valley also started during this time and a primitive Doubs river formed. The evolutionary history from 10.5 My ago to the present includes the formation of the Folded Jura which was thrust over the flat-lying Tabular Jura into its current position by about 3 My ago. The tectonic process led to the formation of anticlines which also prevented the Doubs river from flowing northwards, eastwards and southwards, i.e. forced it to double back approximately in a westerly direction. In their own interpretive work, Wermeille & Bossart (1999a) derived erosional rates which indicate that the Doubs River at St-Ursanne reached the level of the future Mont Terri underground laboratory between 3 My and 1 My before present. The current overburden at the rock laboratory is about 250–320 m (Thury & Bossart 1999). The estimated overburden in the past was at least 1000 m.

This tectonic and sedimentary evolution has strongly influenced the hydrogeological evolution in the area. It is important to recognize that paleohydrogeological effects may still be evident in the present hydrogeologic regime. According to Wermeille & Bossart (1999a) the two main geological developments with major impact on the paleohydrogeology at the Mont Terri site are (i) the progressive downward erosion of the Doubs valley, responsible for the change in groundwater flow direction in the Opalinus Clay with a reversal from infiltration to exfiltration along the Doubs river, and (ii) the progressive erosion of the Mont Terri anticline which affected the flow direction and mainly the groundwater chemistry.

The focus of the hydrogeological analyses at the Mont Terri rock laboratory lies on the Opalinus Clay, an aquitard and a sedimentary product of the Jurassic Sea of approximately 180 My ago. Within the bounds of the rock laboratory, the formation is traversed by a major inverse fault zone (Haarpaintner & Schaeren, TN 99-22). The neighbouring formations to the Northwest and Southeast of the Opalinus Clay are the aquifers of the Jurensis Marls and Lower Dogger Limestones, respectively. Being situated in the southern limb of the Mont Terri anticline, the strata exposed in the rock laboratory dip with an angle of approximately 45° to the southeast (Thury & Bossart 1999).

4.5.2 The scale of tunnel investigations (10^{-1} – 10^{1} m)

At Mont Terri extensive sedimentological mapping of freshly excavated niches, of outcrops in the reconnaissance gallery and of the tunnel walls has resulted in a more detailed lithological partitioning of the Opalinus Clay (Figure 4.16). Geological and hydrogeological characterisation of the tunnel surface mapping covered lithological and structural features on the decimeter to dekameter scale (Figure 4.17). Packer testing in boreholes was used to determine hydraulic properties of the Opalinus Clay on this scale.

Lithology / facies

The Opalinus Clay formation has been divided into three major facies which are generally referred to as the shaly facies, the carbonate-rich sandy facies and the sandy facies (see Figure 4.16). According to Bossart & Wermeille (Chapter 2.1 in Thury & Bossart 1999), the three facies are the result of different sedimentary environments in the shallow basin during the time of deposition. The shaly facies is predominant, making up about 135 m of the new gallery. It, therefore, has been subdivided further into three lithofacies which alternate in the range of decimeters to meters: shale, silty shale and argillaceous marl (TN 99-73, S1.2).

Structural Elements

Particular attention has been paid to the fault zone, representing the "Main Fault" in the central section of the Opalinus Clay formation. In the three galleries excavated parallel to each other, this feature has been observed to be one to several meters thick (see Figure 4.16). It is referred to as the main fault and represents a thrust fault (3rd order fault) with a displacement in the order of 5 m and an extent of at least 60 m (TN 99-73, S1.2). Its orientation is slightly steeper than that of the bedding and runs subparallel to bedding. The main fault is further characterised by a large number of fault planes, i.e. > 20 1/m. Most of the fault planes within the main fault show slickensides and shear fibres on a polished surface. These small-scale structures consistently indicate overthrusting. Additionally, there are highly deformed intervals similar to fault breccia which show loss of cohesion and completely disturbed bedding (drag folds).
One of the highly tectonised samples from the main fault was impregnated with epoxy resin (chapter 2.3 by Bossart & Adler in Thury & Bossart 1999). Thin section analysis of this section of the main fault revealed that the open fractures likely formed as a result of the tunnel excavation and are not likely candidates for advective water flow. Only the interface between the fracture wall and the fracture infill might have been reactivated in a brittle manner. But the corresponding apertures are small and estimated to be in the micrometer range. Mazurek (2001) concludes as well that the hydraulic character of the main fault is no different than that of the surrounding, undisturbed matrix of the shaly facies.
Strong fabric anisotropy, i.e. layering/bedding planes, is observed in the undisturbed matrix.

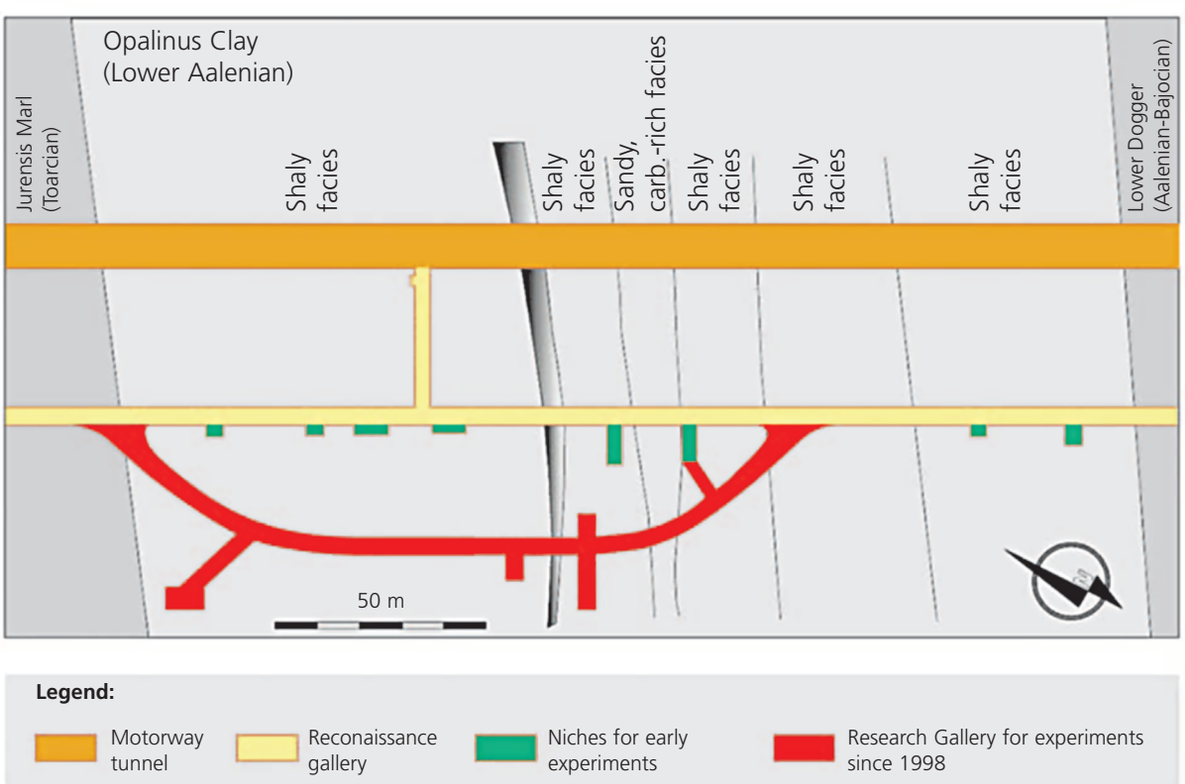

Figure 4.16: The scale of tunnel investigations (10^{-1}–10^{1} m).

Hydraulic relevance of facies and structural elements

Packer tests and permeameter tests were carried out in all facies (cf. Table 4.1 and Table 4.2). Hydraulic conductivities cover a range between 2×10^{-14} and 1×10^{-12} m/s. The K values do not indicate a significant correlation between hydraulic conductivity and the different facies. The measured variabilities in hydraulic conductivity are related to uncertainties in hydraulic testing and test analysis rather than in a systematic change of hydraulic conductivity with changing facies. Extensive hydraulic testing of the main fault was conducted (e.g. packer tests in BFM-C1 and BGP-4, cf. Table 4.1). Fracture frequency along the test intervals was up to 19 1/m. The reported K values are in the range 2×10^{-13} – 5×10^{-13} m/s. No significant differences in hydraulic conductivity were detected as compared with undisturbed matrix of the Opalinus Clay.

Lithological unit	Hydraulic conductivity K[m/s]	Specific storage S_S [1/m]
Carbonate-rich sandy facies	4×10^{-13} – 9×10^{-13}	2×10^{-7} – 6×10^{-7}
Sandy facies	2×10^{-14} – 2×10^{-13}	–
Shaly facies	2×10^{-14} – 2×10^{-12}	3×10^{-7} – 3×10^{-5}

Table 4.5: Ranges of hydraulic properties in the 3 facies of the Opalinus Clay (based on packer test results; cf. Table 4.1).

4.5.3 The scale of core mapping (10^{-3}–10^{-1} m)

Structural mapping was done concurrently with the lithological mapping for all recovered drillcores. A systematic mapping key was defined in TN 96-02 to classify the features, including bedding, fault planes, joints, veins and artificial discontinuities. The mapping key is essentially the same as used for tunnel mapping. Figure 4.18 shows photo documentation of drillcore mapping and lithological / structural classification schemes. Hydraulically the scale of drillcore mapping can be treated in the same way as the scale of tunnel mapping. Permeameter tests (Table 4.2) did not show significant variability in hydraulic properties on the scale of core mapping.

4.5.4 The sub-millimeter scale

Extensive investigations were carried out to describe mineralogy and microstructure of the Opalinus Clay (Nagra 2002). The investigation methods included:

– mineralogical analyses of drillcores
– various techniques of porosimetry
– various techniques for determination of specific surface (BET, EGME)
– scanning electron microscopy (SEM)
– adsorption / desorption methods

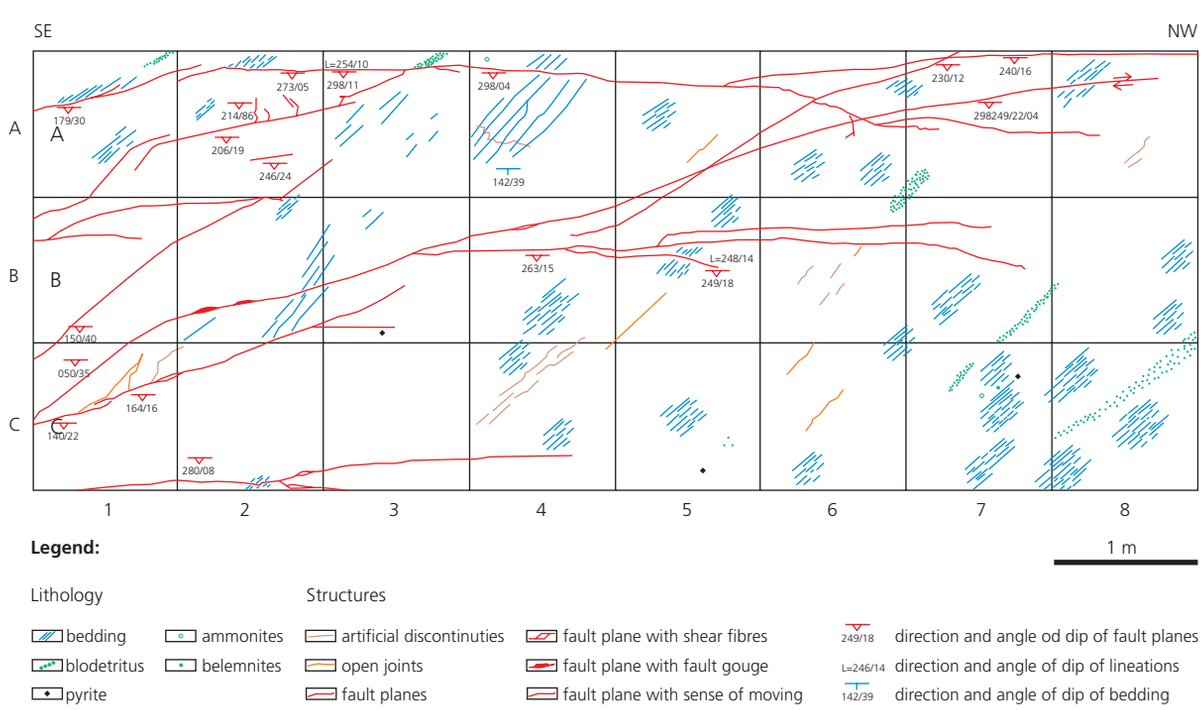

Figure 4.17: Small scale mapping of structural features in the BF niche of the reconnaissance gallery, i.e. in the shaly facies of the Opalinus Clay (Figure 4.13, TN 96-02).

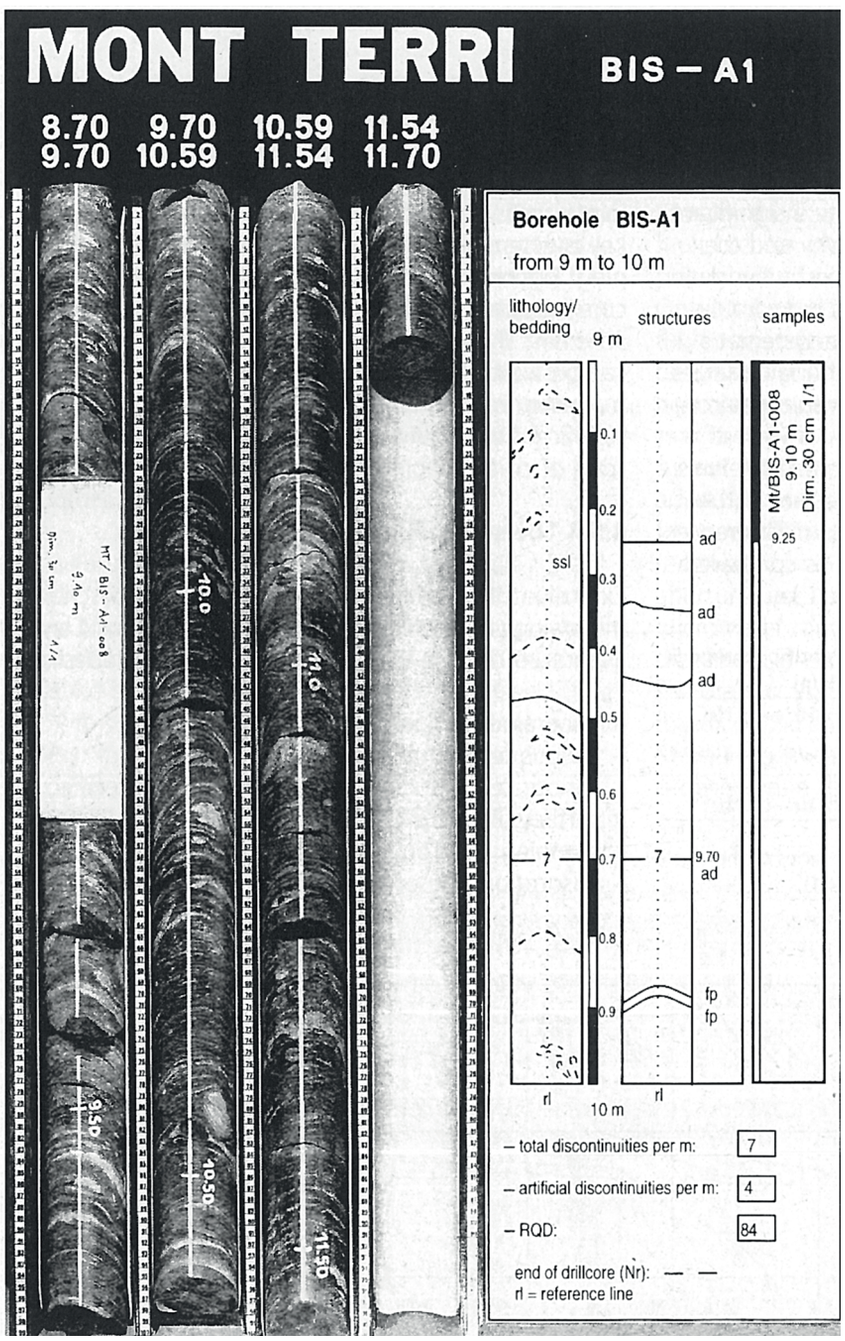

Figure 4.18: Photographic documentation of drillcores and classification of lithological/structural features.

	Calcite	Siderite	Quartz	K-Feld-spar	Total layered silicates	Illite	Illite / smectite	Chlorite	Kaolinite
Mean value weight (%)	13	3	14	1	66	23	11	10	22
Standard deviation	±8	±1.8	±4	±1.6	±11	±2	±2	±2	±2
No. of 8 analyses		8	8	8	8	8	8	8	8

Table 4.6: Mineralogy of the clay-rich shaly facies of the Opalinus Clay at Mont Terri after Mazurek (2001). Data from the sandy facies are not included.

From the hydrogeological point of view, mineralogy of the Opalinus Clay is of relevance in the context of coupled hydro-chemical processes such as swelling or chemico-osmotic flow. Table 4.6 gives an overview of the main mineralogical components of the shaly facies at Mont Terri (Nagra 2002). It is evident, that the fraction of the main swelling clay mineral, illite-smectite mixed layers, is quite low.

Some hydrogeologic properties of the Opalinus Clay can be inferred indirectly from the analysis of its microstructure. Figure 4.19 visualises the microscopic arrangement of the clay aggregates using SEM techniques. Feldspar and quartz grains are wrapped in a complex structure. The magnification achieved by conventional SEM techniques is not sufficient to visualise the microscopic system of mesopores (1–30 nm), which represent the main features for fluid transport in the Opalinus Clay. Adsorption/desorption methods and Hg porosimetry are tools for the determination of equivalent pore radii of the microscopic clay structures. As shown in Figure 4.20 and in Table 4.7, equivalent pore radii are in the range of 1–50 nm (mean: 4 –11 nm).

Mean equivalent pore radius [nm]	4 – 11
Porosity [-]	0.156
Rock density [g/cm^3]	2.32 – 2.42
Specific surface (BET N2) [m^2/g]	24 – 37
Specific surface (adsorption) [m^2/g]	112 – 147

Table 4.7: Microstructural properties of the Opalinus Clay at Mont Terri after Nagra 2002.

Hydraulic conductivity can be inferred using the Kozeny-Carman relationship (equation 4.9) when porosity and specific surface are known. Specific surface was determined by BET methods as 24–37 m^2/g (outer surface) and by adsorption methods as 112–147 m^2/g (total surface). The geometry factor C_s is taken to be 2.5 and the tortuosity τ is 1.41. Thus the Kozeny-Carman relationship leads to a range of K values in the order of 1×10^{-13} – 1×10^{-12} m/s, which is slightly higher than the permeameter measurements suggest.

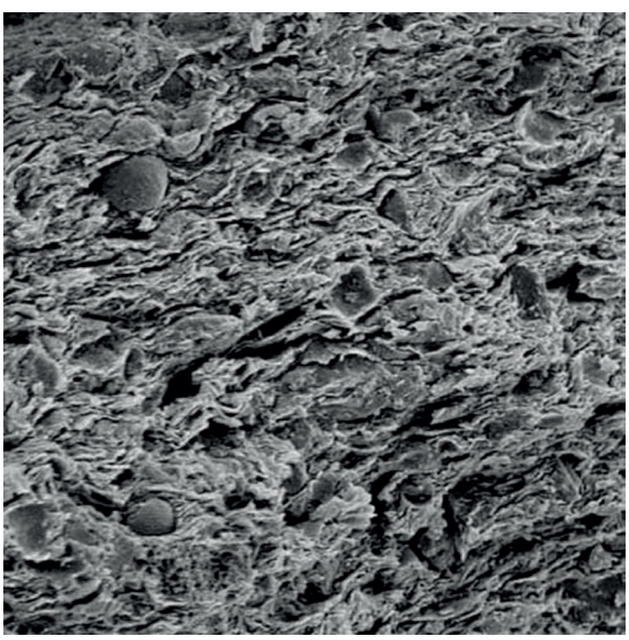

Figure 4.19: Visualisation of the microstructure of Opalinus Clay by SEM (Möri 2000, personal communication).

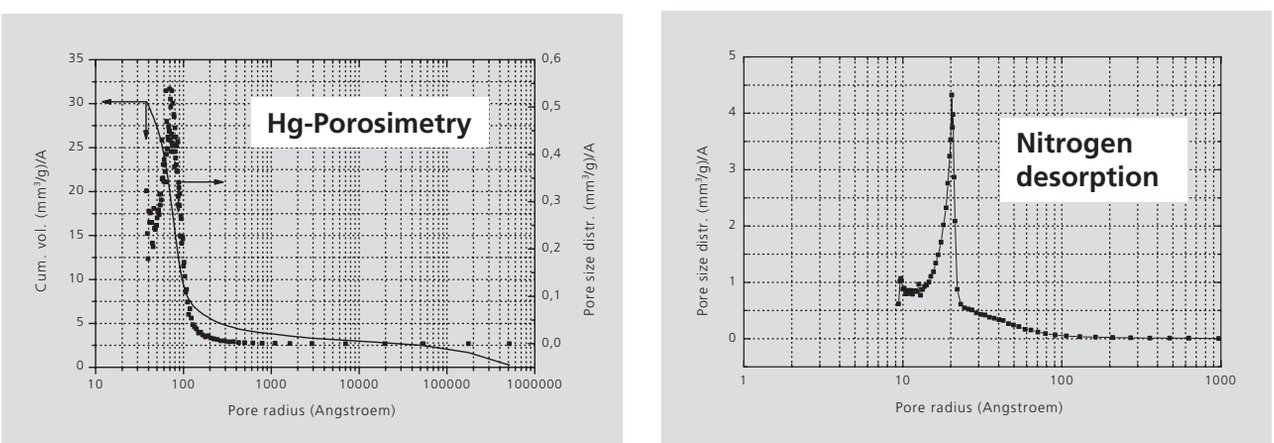

Figure 4.20: Determination of equivalent pore radii by Hg porosimetry and nitrogen desorption (from Bardot et al. 2001).

4.6 Pore pressure distribution at the Mont Terri site

4.6.1 Data base

With the exception of the Opalinus Clay formation, the pore pressures in the Mont Terri site are not very well known. Less than 10 piezometers were installed over the full length of the motorway tunnel previous to its construction in 1992 (i.e. after reconnaissance tunnel excavation in 1989; cf. TN 99-22). Even fewer observations are available for the time since excavation. Figure 4.21 illustrates the approximate depth of the groundwater level, measured before and after construction in the rock formations adjacent to the Opalinus Clay. In the Triassic and Liassic formations to the Northwest of the Opalinus Clay, pore pressures of 2.0–2.3 MPa (reference level: altitude of the motor way) are reported. In the Lower Dogger aquifer to the Southeast, a pressure of about 0.8 MPa was measured in a borehole in lead of the tunnel excavation.

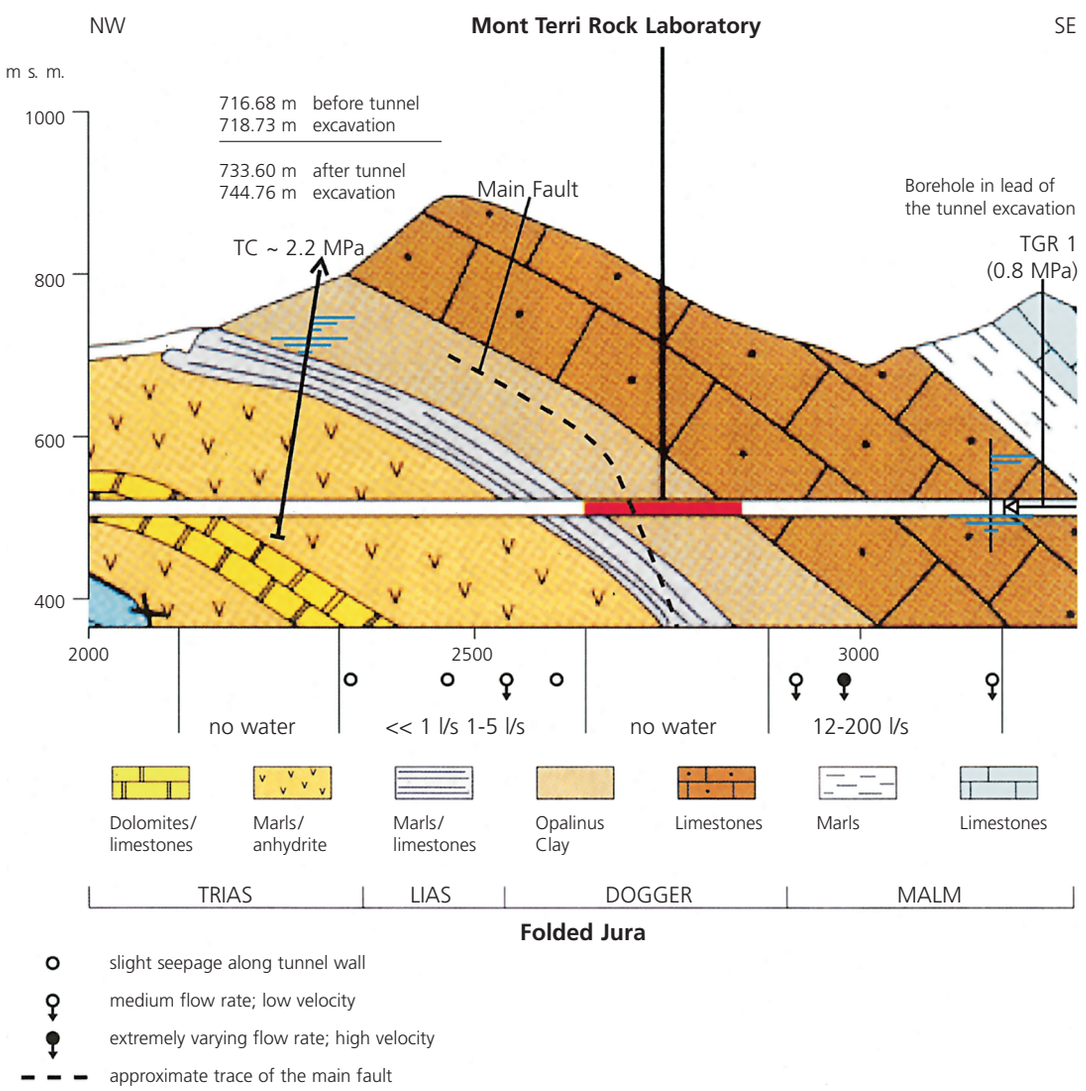

Figure 4.21: Cross-section through the Mont Terri site with piezometric levels (TN 99-22).

Bossart & Wermeille (TN 99-73, Section 1) reason that the drawdown in the vicinity of the Mont Terri rock laboratory due to the excavation of the motorway tunnel is about 30 m as indicated by the water level records. They state further that the expected groundwater level above the rock laboratory corresponds to about 740 m.a.s.l. (around 2.3 MPa) and is not in contradiction with pore pressures observed in the Opalinus Clay. Pore pressures below and above the Opalinus Clay are not know to date.

Since the beginning of the Mont Terri project in 1996, numerous boreholes have been drilled and equipped with long-term monitoring systems to determine pore pressure evolution in the Opalinus Clay formation. In particular, pressure was recorded continually since mid 1997 in the horizontal boreholes BPP-1, BED-B0, BED-B1, BED-B2, BED-B3 and BED-B4 (see Figure 2.2 for locations). Furthermore, the pressure in the vertical BDI borehole was also recorded. Figures 4.22a to e present the pressure records from mid 1997 to early 1999.

(a)

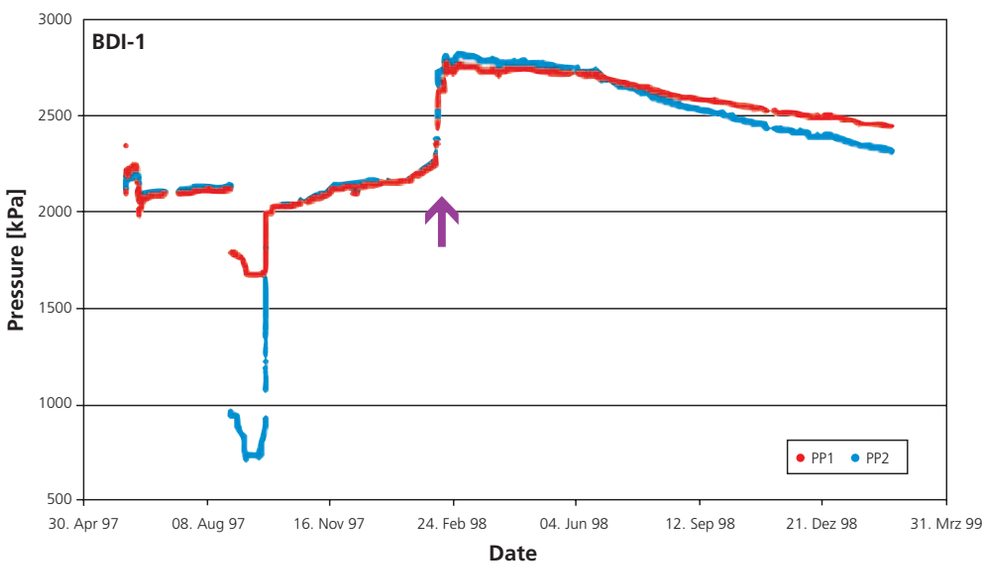

(b)

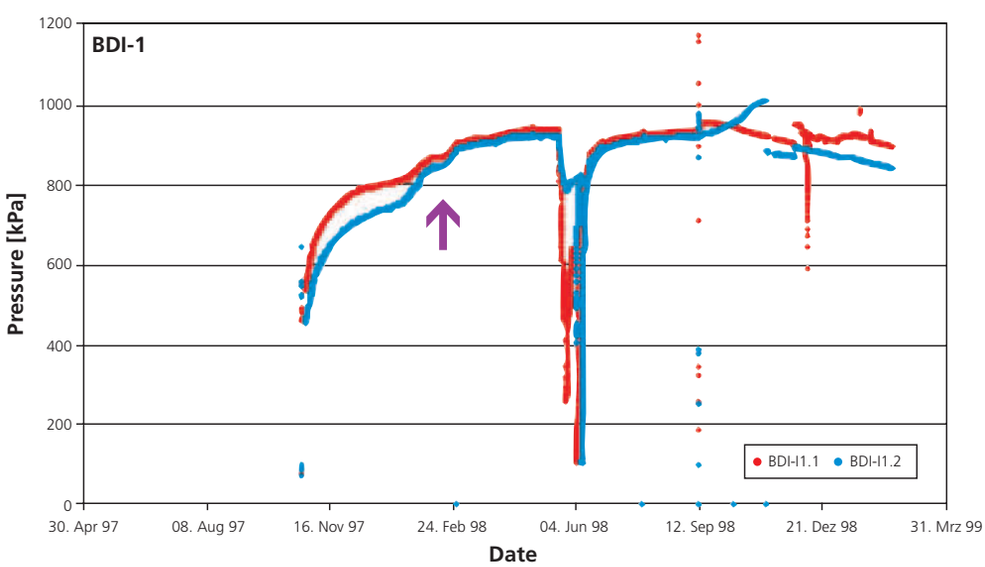

Figure 4.22: Pressure monitoring from mid 1997 to early 1999 in boreholes (a) BPP-1, (b) BED-B1, (c) BED-B2, (d) BED-B3, and (e) BDI-1. The purple arrows indicate the impact signatures caused by the excavation of the new gallery by blasting and a road header. (c), (d) and (e) on page 60.

(c)

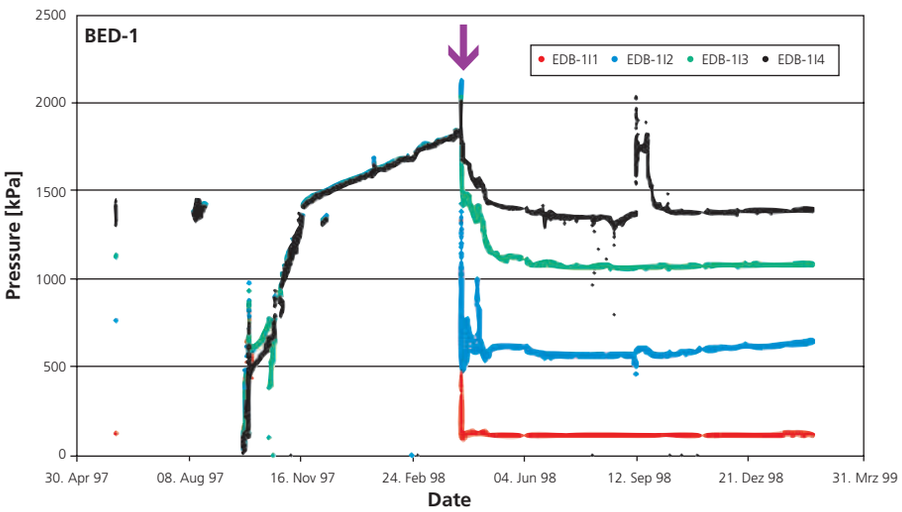

(d)

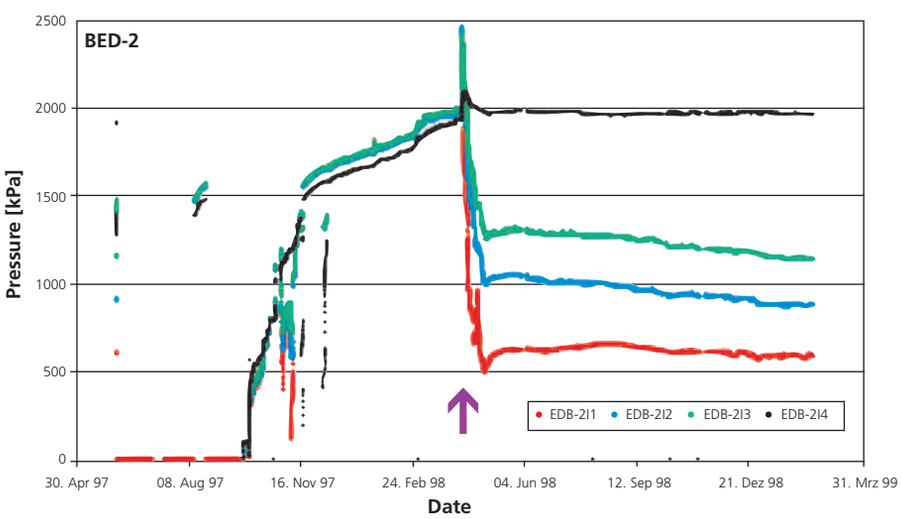

(e)

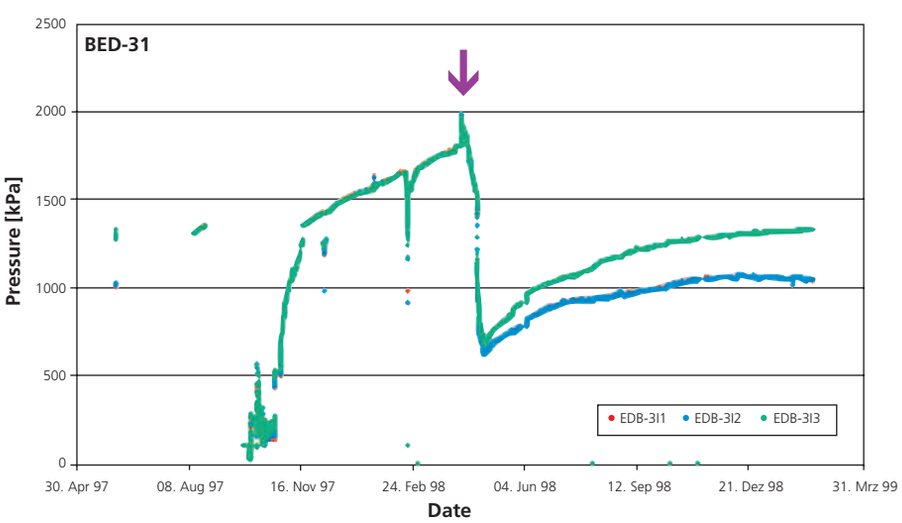

Figure 4.22 continued

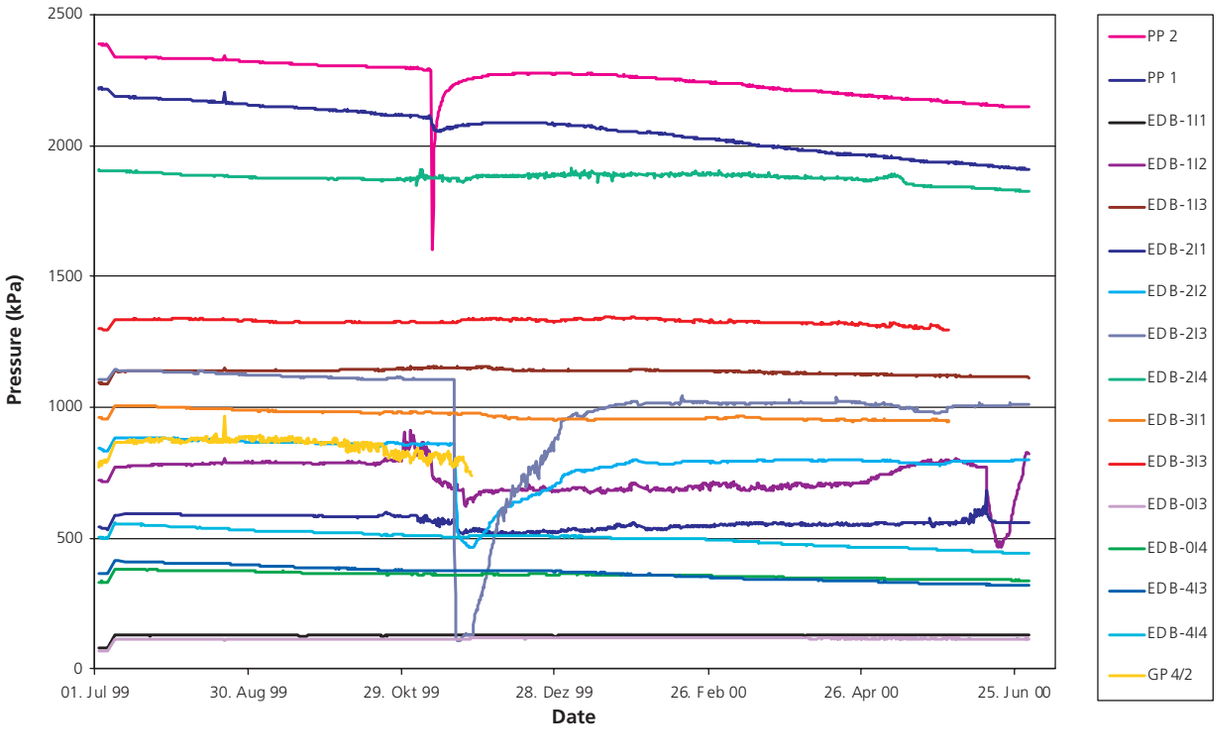

Figure 4.23: The pressure transients in the period from July 1999 to June 2000.

Whereas the changes in pressure prior to spring 1998 denote a gradual re-equilibration with the formation pressure, the sudden increase or decrease observed during spring 1998 is due to the excavation of the new gallery by blasting. Also in the test intervals of the boreholes located the farthest away from the new gallery (e.g. 10 m), the amplitude of the disturbance is quite large on the horizontal boreholes (sometimes larger than 0.5 MPa). In the vertical BDI-1 the impact of the blasting on the pressure is more limited (a few bar pressure increase).
Furthermore, the hydraulic influence of the new gallery is visible in several intervals either clearly situated within the EDZ or in the "hydraulic influence radius" of the new gallery (lower pressure as prior to the excavation).
After installation of the central data acquisition system in Phase 5, the pore pressures in many of the long-term monitoring systems were recorded continuously. Figure 2.2 gives an overview of locations and orientations of the long-term monitoring boreholes. The pressure transients in the time period between June 1999 and June 2000 are given in Figure 4.23. A general trend of decreasing pore pressures is observed in many of the observation intervals, indicating the impact of the tunnel drainage.

4.6.2 Interpretation of the pore pressure distribution in the Opalinus Clay formation

Data observations

From the hydraulic point of view, the pore pressure distribution in the Opalinus Clay might be controlled by any one or several of the following mechanisms:

- differences with respect to the piezometric heads of the adjacent hydrogeological units in the NW and SE directions: Triassic Marls with high freshwater heads corresponding to a pressure of 2.2 MPa at tunnel niveau, and the Dogger aquifer for which merely one measurement of very low value (0.8 MPa) at tunnel niveau is known,
- a hydraulic gradient between the reconnaissance gallery and new gallery causing (slow) drainage of the Opalinus Clay,
- the main fault acting as a "sealing fault" between the NW and SE parts of the Opalinus Clay , i.e. a hypothesis supported by very low permeability values attained in tests conducted in the main fault,
- it cannot be precluded, that geomechanical effects due to stress redistribution after the excavation of the galleries and also to changes within the borehole (e.g. partial collapse of borehole) might have

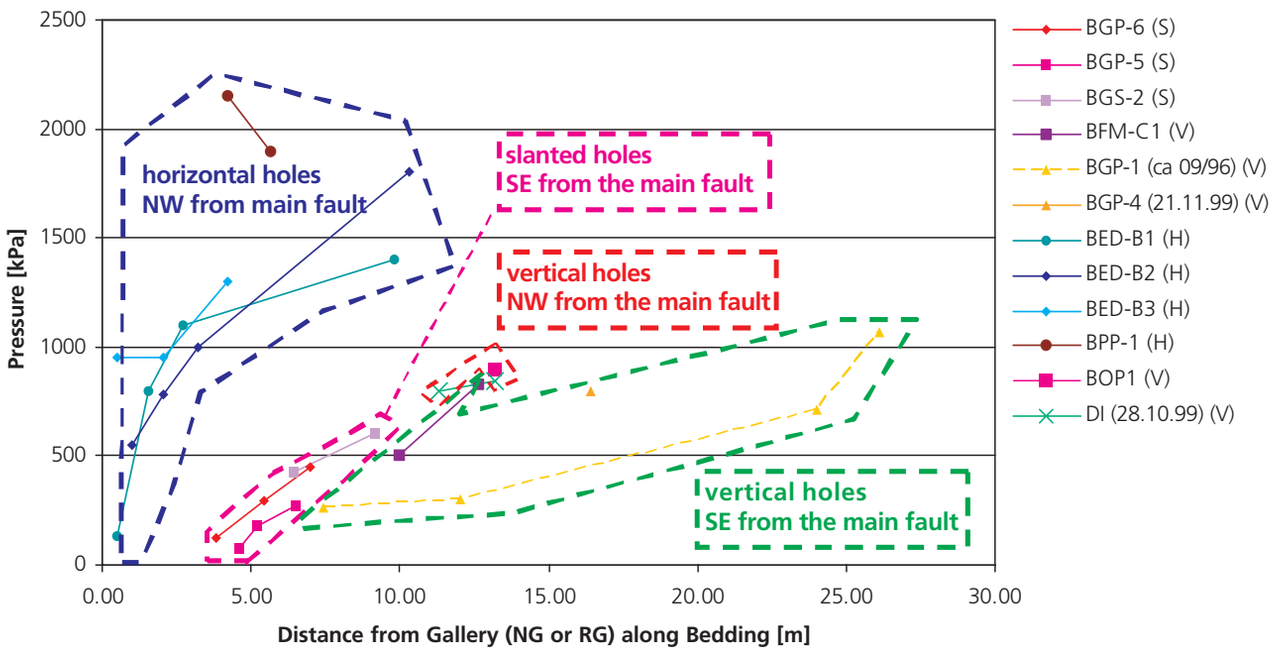

Figure 4.24: Compilation of pressure observations in boreholes of the Mont Terri rock laboratory on 30.06.2000 (unless indicated otherwise in the figure legend), illustrated with respect to the distance along bedding to the nearest gallery.

had an impact on the measured pressure (see Martin & Lanyon 2004),
- it cannot be precluded, that chemico-osmotic flow due to the concentration profile in the site (Figure 4.15) gives rise to an additional anomaleous component of the measured pore pressure. The impact of osmotic pressures, however, is small due to the low osmotic efficiency of the rock formation.

Most likely, it is a combination of these effects which is responsible for the pattern of pressure distribution observed in the Opalinus Clay at the Mont Terri site.
The pore pressure measurements gathered by the end of June 2000 are presented in Figure 4.24 and Figure 4.25. Where no values were available by June 2000, younger measurements have been added in the diagrams instead and are indicated as such in the figure legends. The particular point in time was selected as the „longest" re-equilibration time available.
In Figure 4.24 all measurements are presented as distances along bedding either to the reconnaissance gallery or to the new gallery, whichever is closer to the observation interval. Indications of the borehole orientation are also provided in terms of vertical, slanted or horizontal. In Figure 4.25, all measurements are illustrated along an imaginary axis projected between the reconnaissance and the new gallery.

The following observations may be expressed:

- The gradients near the new gallery (boreholes BED: up to 20 m/m) are much higher than those near the reconnaissance gallery (1 m/m). This is consistent with the fact that the reconnaissance gallery was excavated 10 years prior (1989) to the new gallery (1998).
- In horizontal boreholes NW from the main fault and inside the shaly facies, the pressures away from both NG and RG are high up to 2.0 MPa.
- In vertical boreholes SE from the main fault (mainly in the sandy facies), the pressure located more than 7 m away from the RG or NG are low, between 0.3 and 0.8 MPa.
- All the vertical and slanted boreholes deliver pressure observations smaller in magnitude than the horizontal boreholes.

4.6.3 Simple assessment of the galleries' drainage effects with numerical simulations

A 2D transient groundwater flow simulation was performed with the Colenco Code MHYTIC in order to assess the potential drainage effects caused by the reconnaissance and new galleries. It simulated the period from the time of excavation of the reconnaissance gallery in 1989 to mid 2000.

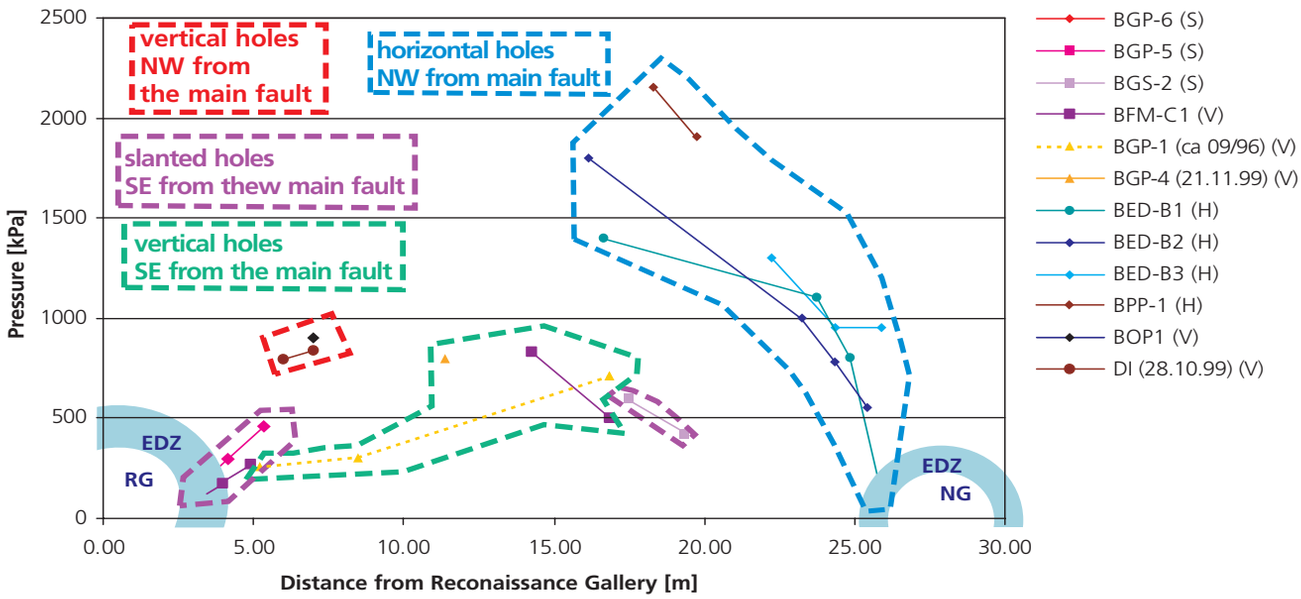

Presssures in Formation adjacent to the Opalinus Clay:
Lias Gryphaea Limestones to the NNW: 2000–2300 kPa
Lower Dogger Blaukalke Limestones to the SSE: 800–1000 kPa (?)
Simulation parameters:
Hydraulic Conductivity K = 1×10^{-13} m/s Specific Storage Ss = 1×10^{-6} 1/m
Borehole orientation:
S: slanted V: vertical H: horizontal
Structural elements:
RG: reconnaissance gallery NG: new gallery EDZ: excavation disturbed zone

Figure 4.25: Compilation of pressure observations gathered in boreholes at the Mont Terri rock laboratory on 30.06.2000 (unless indicated otherwise in the figure legend), illustrated along an axis projected between the reconnaissance gallery and the new gallery.

The 2D finite element domain is presented in Figure 4.26 and is representative of a vertical slice situated in the area of the BED boreholes (see Figure 2.2). The initial pressure head is assumed to be constant and equivalent to 2.2 MPa at the gallery level. The boundary conditions are no flow along the sides and along the bottom, and a constant head of 2.2 MPa along the top boundary. The new gallery is assumed to have been excavated "instantaneously" in mid 1998.
The resulting simulated head distributions just before the excavation of the new gallery and by July 2000 are shown in Figure 4.27a and b, respectively.
Figure 4.28 presents the projection of the measured pressures and the numerically generated pressure curve on an axis joining the reconnaissance gallery and the new gallery. The following conclusions may be drawn:

- The simulated asymmetric pressure profile is consistent with field observations.
- The simulation matches to a certain extent the pressures observed in the horizontal boreholes and in the vertical boreholes in the first 7 m from the midpoint of the reconnaissance gallery.
- The measurement points assembled in a cloud not matched by the simulations were issued from the downwards vertical and slanted holes with distances to the galleries larger than about 7 m.

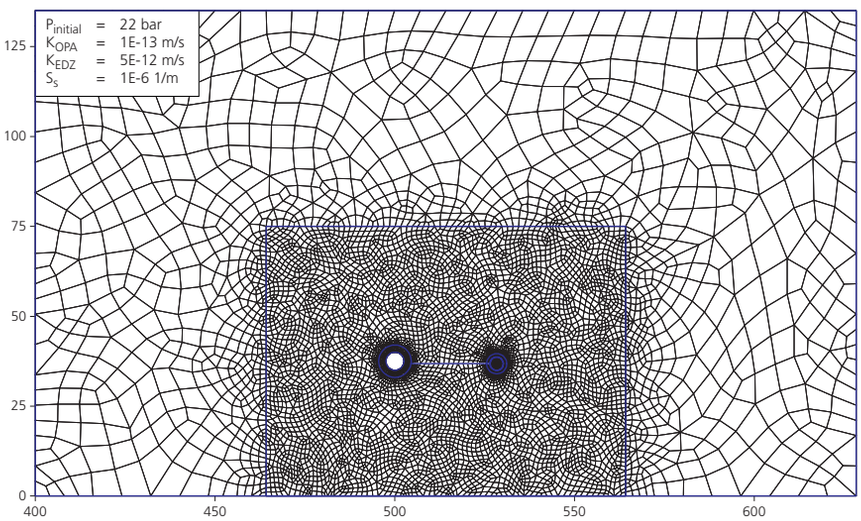

Figure 4.26: Vertical configuration and 2D finite element mesh used to simulate the pressure head on a plane projected perpendicularly through the reconnaissance gallery (left) and the new gallery (right) approximately at tunnel meter RG 970.

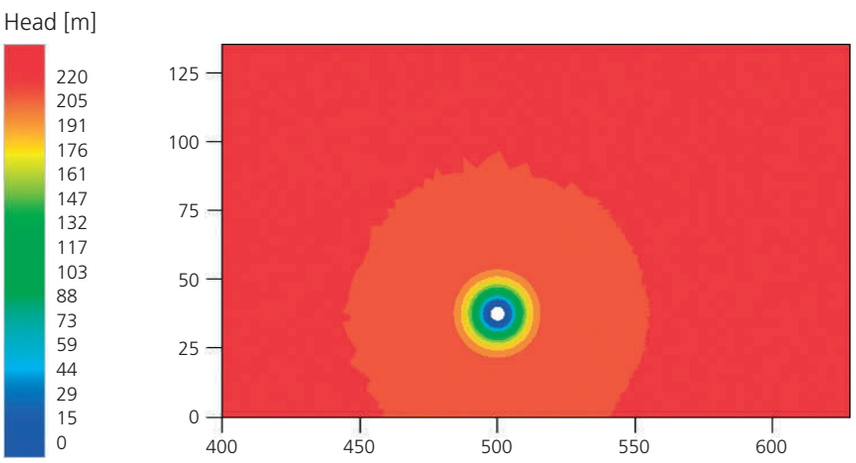

Figure 4.27: Simulation of the distribution of pressure head on a plane projected perpendicularly through the reconnaissance gallery and the new gallery at approximately tunnel meter RG 970. Hypothetical points in time: (a) end of April 1998, (b) end of July 2000.

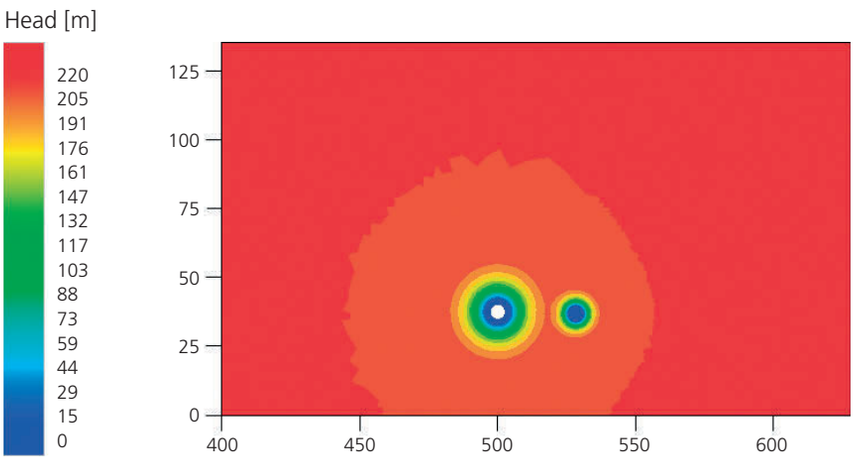

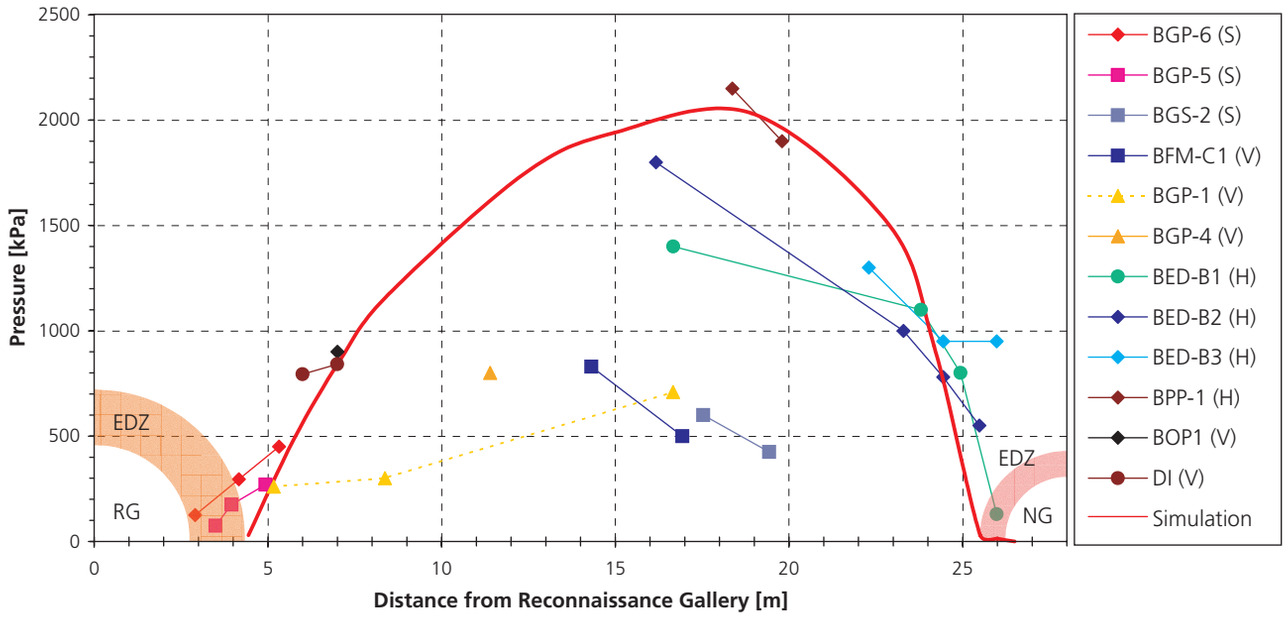

Pressures in formations adjacent to the Opalinus Clay:
Lias Gryphaea Limestones to the NNW: 2000-2300 kPa
Lower Dogger Blaukalke Limestones to the SSE: 800-1000 kPa

Simulation parameters:
Hydraulic Conductivity K = 1E-13 m/s
Specific Storage Ss = 1E-6 1/m

Borehole orientation:
S: slanted / V: vertical / H:horizontal

Structural elements:
RG: Reconnaissance Gallery
NG: New GalleryEDZ: Excavation Disturbed Zone

Figure 4.28: Comparison of pressure observations (mostly on 30.06.2000) and the results of the numerical simulation with K = 1×10^{-13} m/s and S_s = 1×10^{-6} 1/m, along an axis projected perpendicularly through the reconnaissance gallery and the new gallery at approximately tunnel meter RG 970.

The measurements located within a few meters of the EDZ of both galleries fit well with the simulation results. Simulations for the region to the NW of the main fault, inside the shaly facies, do fit the high pressures measured (larger than 1.4 MPa) reasonably well. A clear mismatch of the measurement is observed in the vertical boreholes SE of the main fault, mainly situated in the sandy facies.
As no difference in hydraulic conductivity was observed between shaly and sandy facies, two hypotheses can be drawn up with respect to the mismatch observed:

– Either: The part of the Opalinus Clay situated SE of the main fault is largely affected by the low hydraulic head in the adjacent formation of the Dogger limestones and a certain hydraulic separation is created by the main fault which would act as a sealing fault.
– Or: The horizontal borehole intervals are highly affected by the stress field (including borehole collapse) and the pressures measured result from coupling of hydraulic and geomechanic effects.

Effects of chemical osmosis on the pressure measurements do not appear likely because no "abnormal" pressure, i.e. larger than 2.2 MPa, were measured and the osmotic efficiency of the clay membrane is low.
A more complex hydraulic model is needed to fully explain the observations. One of these models could be a model consisting of two domains, separated by the main fault as an impervious boundary. The hydraulic head would be 2.2 MPa, i.e. matching the Triassic Marls, to the NNW of the mail fault, and 1.0 MPa to the SSE, i.e. conforming with the Lower Dogger. Such a model would be supported by the chloride measurements (c.f. Figure 4.15).
Additional work both in terms of field investigations (e.g., additional pressure observation boreholes at selected locations, for example within the sandy facies and the adjacent formations of the Lower Dogger and Lias aquifers) and in terms of numerical modelling (e.g., 3D hydrogeological modelling, NW/SE gradient) is required to better constrain the hydrogeological situation.

4.7 Evaluation of current hydrogeological site understanding

The geoscientific characterisation of the Opalinus Clay and the adjacent stratigraphic formations at the Mont Terri site was to demonstrate primarily the barrier function of the clay formation. This, in fact, requires an integrated assessment of the available hydrogeological site characterisation data and the cross-comparison with independent evidence to consolidate confidence in the overall performance of the clay formation as a flow barrier. The hydrogeological assessment consists of the following elements:

- identification of relevant hydrogeological features on the site scale
- description of relevant flow mechanisms
- determination of representative hydraulic properties on the site scale
- characterisation of in-situ pore pressure conditions

On the site scale, six *hydrogeological units* were defined (cf. Table 4.3). Focusing on the immediate vicinity of the rock laboratory, the "Lower Dogger" was identified as a local karstified aquifer which exfiltrates substantially into the tunnel systems. The significance of the Jurensis Marls to the North of the Opalinus Clay formation is less clearly defined. Water influx was observed from this formation during construction of the motorway tunnel, but appeared to have originated in localised water conducting features. The measured chloride profiles along the tunnel (cf. Figure 4.15) suggest no significant groundwater flow in this unit.

The Opalinus Clay is a pronounced aquitard. No groundwater influx into the galleries was detected. The chloride profile indicates that diffusion is the dominant transport process. Hydraulic packer testing and permeameter testing exhibit consistently low values of hydraulic conductivity. No significant variations of hydraulic conductivity are seen among the different *facies* of the Opalinus Clay. Even more so, no marked enhancement of hydraulic conductivity is apparent in the vicinity of *tectonic features*: extensive packer testing in the main fault did not reveal any correlation between hydraulic conductivity and fracture frequency along the boreholes.

At elevated hydraulic gradients *groundwater flow is governed by Darcy's law*. Linearity between hydraulic gradient and specific flow was demonstrated in the context of permeameter tests at hydraulic gradients > 1000. No deviations from Darcy's law were seen in the course of single-hole packer testing at gradients around 50. Hydraulic interference tests, however, exhibited anomalous crosshole responses, suggesting non-linear flow behavior at hydraulic gradients < 1. Hence, an estimate for a hydraulic threshold gradient (if in fact existing) might be less than 1. The validity of Darcy's law is supported by the observed cone of pore-pressure decline towards the galleries, suggesting a gravitationally driven groundwater flow at typical hydraulic gradients between 1 and 10, clearly consistent with the hydraulic parameters.

Coupled hydro-chemical and hydro-mechanical processes may affect groundwater flow and transport processes in the Opalinus Clay. Due to its low membrane efficiency, which was determined experimentally (whenever subject to discussion), it is not likely that the pore pressure within the Opalinus Clay of Mont Terri is significantly affected by substantial osmotic flow processes. Hydro-mechanical coupled processes, however, may become relevant when the effective stress in the formation is lowered (e.g. hydraulic testing at elevated injection pressures). In the context of packer testing, evidence was seen for permeability enhancement at elevated injection pressures.

Hydraulic conductivity in the Opalinus Clay exhibits low spatial variability. Independent of the facies and of the degree of tectonic disturbance, K-values of the intact Opalinus Clay (without the EDZ) were measured in the range of 2×10^{-14} – 2×10^{-12} m/s (Table 4.5*). Storage coefficients* derived from packer testing were in the range 3×10^{-7} – 3×10^{-5} 1/m.

The *pore pressure distribution* at the Mont Terri site is being monitored continuously since Phase 3. Since that time, a continuous decrease of pore pressure has been observed in all observation intervals of the long-term monitoring system. Pore pressure monitoring indicates a clear cone of depression of hydraulic head towards the laboratory galleries. Beyond this, additional trends are observed: the subvertical boreholes generally exhibit lower pressures than the horizontal and the upwards directed boreholes. Also, pore pressure decreases towards the South. Although the spatial distribution of pore pressures at the Mont Terri site is not yet fully understood, it is believed that porewater flow in the Opalinus Clay is governed by the superposed effects of drainage towards the galleries and the pressure boundaries imposed by the adjacent rock formations. Stress redistribution effects due to the excavation of the tunnel might have an influence on the pore pressure currently monitored.

5 Gas Migration Mechanisms in the Opalinus Clay

5.1 Introduction

Radioactive wastes considered for disposal in repositories in deep, low permeability formations are expected to produce a significant amount of gas due to corrosion and microbial degradation processes. Gas generation may continue for long periods after repository closure. The accumulation of the gas may lead to unacceptable build-ups of the gas pressure in the disposal tunnels, if the gas cannot escape through the low permeability host rock.
The investigation of gas migration processes through argillaceous formations is, therefore, a key issue in the assessment of repository performance. The investigations on gas migration carried out at the Mont Terri rock laboratory during Phases 1 through 5 were aimed at collecting a comprehensive data base as a prerequisite for the development of enhanced process understanding. Although a full compatibility of the in-situ conditions at Mont Terri to the conditions at an actual repository site may not be achievable, the basic gas migration mechanisms are expected to be comparable. The Mont Terri site offers the opportunity to do both small scale experiments with drillcores in a laboratory and in-situ experiments in the underground facility.
This part of the hydrogeological synthesis is aimed at reviewing the achievements in the experimental work and in the interpretation of gas migration studies conducted in Phases 1 to 5 of the Mont Terri project. The outline of the chapter is as follows:

- Review of conceptual approaches for gas migration in clay-rich formations.
- Critical assessment of gas related experiments carried out in Phases 1 to 5 through quality assurance with respect to execution, analysis and documentation.
- Survey of the experimental data base for two-phase flow properties of the Opalinus Clay.
- Assessment of the modelling approaches applied in Phases 1 to 5 for the interpretation of gas related experiments.

5.2 Conceptual approaches of gas migration in clay formations

The gas migration in the Opalinus Clay is controlled not only by the hydro-mechanical properties of the rock mass but also by the gas pressure p_g at the generation locus and the hydro-mechanical state of the rock (i.e. saturation with water, porewater pressure, stress state). The in-situ stress of the rock mass is an essential parameter and is described by its three principal components σ_1, σ_2 und σ_3. Any gas release through the Opalinus Clay may be accommodated by the following mechanisms:
- advective-dispersive transport of gas dissolved in the porewater
- generalized Darcy flow, i.e. two-phase flow
- microscopic fracturing driven by the gas production rate, i.e. stationary processes
- macroscopic gas- and hydro-fracturing, i.e. instationary processes

Table 5.1 presents an overview of the migration mechanisms, pressure regimes and the efficiency of the different mechanisms in the Opalinus Clay. The remainder of this section is dedicated to a discussion of the individual migration mechanisms on a phenomenological base and, where appropriate, in terms of a conceptual modelling approach. Furthermore, the link between gas migration and the deformation of the Opalinus Clay is illustrated.

Gas migration mechanism	Gas pressure regime[1]	Remarks
Advective and dispersive transport of dissolved gas	For any gas pressure p_g	Gas transport by advection is not very efficient in the Opalinus Clay because of the low advective fluxes
Two-phase flow	$p_{ae} < p_g < \sigma_3$	Gas transport efficiency is limited by the high gas entry pressure of clay
Microscopic fracturing	$p_g \approx \sigma_3$	The microfracturing process is controlled by the gas production rate High gas transport capacity due to the pressure- dependent gas permeability
Macroscopic gas frac/ hydro frac	$p_g > \sigma_3$ + tensile strength	Creation and propagation of macroscopic fracs is initiated and controlled by gas pressure Extremely high transport capacity due to high frac transmissivity

[1] - the values represent rough estimates for the expected pressure ranges

Table 5.1: Overview of potential gas migration mechanisms. The transport capacity of the various mechanisms is influenced by the gas pressure p_g, the minimum main stress σ_3 and the various hydro-mechanical properties of the formation (p_{ae} – gas entry pressure, T_{opa} – tensile strength).

Transport of dissolved gas

Advective and dispersive transport of gas in porewater is a straightforward migration mechanism which is characterised by three fundamental laws: (i) the advective groundwater flow is governed by Darcy's law, (ii) Fick's law represents the diffusion of dissolved gas due to concentration gradients, and (iii) Henry's law describes the solubility of gas in porewater.
The transport of dissolved gas occurs even at low gas pressures; the pressure-dependent solubility of gas in porewater and the increased groundwater flux cause the specific flux of the dissolved gas to increase with an increase in the gas pressure. However, the low hydraulic conductivity of the Opalinus Clay significantly restricts the efficiency of this transport mechanism. The main parameters affecting the transport behavior of dissolved gas are the (gas) diffusion constant, the solubility coefficient, the flow porosity and the hydraulic conductivity.

Two-phase flow

In its conventional form two-phase flow is described as the process whereby the pore volume of a rock formation fills with gas by replacing porewater under the influence of visco-capillary forces (e.g. Baer 1972). This process causes the pore space to deform reversibly, i.e. elastically. Because the pore space of the Opalinus Clay at Mont Terri consists mostly of mesopores (equivalent pore radii: 2 – 50 nm), very high gas pressures are necessary to displace the porewater. The controlling factor for the two-phase flow characteristics of a porous medium is the gas entry pressure p_{ae} with a typical range for the Opalinus Clay of 1–10 MPa. Once the gas entry pressure has been exceeded, the gas mobility is controlled mostly by the intrinsic permeability k of the formation, the permeability-saturation relationship or relative permeability, and the relationship between the capillary pressure and the water saturation. The functional dependency between the pore-space saturation and the relative permeability or the capillary pressure are commonly described with parametric models (e.g. Brooks-Corey model, van Genuchten model, see also TN 98-25). One has to note, though, that only the free or mobile water may be displaced from the pore space whereby the residual water saturation in the Opalinus Clay tends to be at least 50%. The residual gas saturation in the Opalinus Clay, however, is negligible (very low gas content was measured in the Opalinus Clay).

Microfracturing

The tensile strength of the Opalinus Clay is relatively low. Therefore, it is most likely that the rock will not withstand long-term gas pressures with a level higher than the minimum principal stress σ_3. Based on the expected micro-scale variability of the rock strength it even seems plausible that microfractures will form in the Opalinus Clay before the macroscopic tensile strength of the formation is exceeded. This microscopic fracturing causes an irreversible deformation of the pore space, i.e. dilation, and a detectable increase in intrinsic permeability. While the regime of the conventional two-phase flow sees the intrinsic permeability quasi independent of the absolute gas pressure, for microscopic fracturing the permeability is observed to increase with an increase in gas pressure. This phenomenon of microfracturing occurs when the gas pressure is allowed to grow slowly: the additional pore volume – which is the result of dilation – has to hold a steady balance with the volumetric gas production rate so that a quasi-stationary gas flow may evolve along the newly opened gas flow path.

Macroscopic fracturing

A macroscopic tensile fracture develops when the gas pressure is larger than the sum of the minimum principal stress σ_3 and the tensile strength T_{opa} of the Opalinus Clay, as determined in geomechanical short-term tests. This critical gas pressure is known as the frac-pressure. A macroscopic frac develops only when the gas pressure build-up is fast, i.e. when the formation of microscopic fractures (dilatency) no longer counterbalances the gas production rate. The macroscopic frac is initiated quasi instantaneously and propagates at about the velocity of a shear wave. The propagation comes to a halt when the gas pressure in the macroscopic fracture becomes less than the value of the minimum principal stress (shut-in pressure). When the gas pressure is increased once more, the re-frac pressure is reached when the previously created fracture is re-opened. The value of the re-frac pressure is intermediate between shut-in pressure and frac pressure. The conceptual, theoretical and experimental framework for fracture propagation is well documented in standard hydrocarbon exploration literature (Valko & Economides 1997).

Propagation of gas induced fracture patterns

Independent of the fracture mechanism, fracture orientation and propagation are controlled primarily by the in-situ stress conditions and the geomechanical/

structural properties of the formation. The following factors of influence are particularly noteworthy:

– In an anisotropic stress field, fracture propagation occurs perpendicular to the direction of minimum principal stress or – in general terms – along the steepest stress gradient.
– Under anisotropic mechanical formation conditions, fracture propagation occurs perpendicular to the direction of minimum tensile strength. One may assume, therefore, that fractures develop preferentially along bedding.
– Geological deformation structures may have geomechanical properties which potentially allow them to function as discontinuities. Gas induced fractures may form along these discontinuities. Likewise, the geological structures may be re-activated if their mechanical properties, e.g. tensile strength, cohesion, friction angle, are lowered with respect to the intact Opalinus Clay.

5.3 Quality assurance of gas related experiments

Similar to the suitability assessement of the hydraulic experiments (cf. chapter 3.2) a quality assurance procedure was applied on all gas related experiments that were carried out in Phases 1 to 5. The QA process for the gas related experiments, however, was different in some details because gas migration mechanisms in claystone are much less understood when compared with (single phase) hydrogeological processes. Therefore, the gas related experiments at Mont Terri were mainly aimed at process understanding rather than on the determination of material properties. These differences in emphasis gave reason for developing a slightly different QA approach (TN 00-58). The aspects that were addressed in the QA procedure were (i) field and laboratory methods, as well as (ii) data analysis.
Similar to the suitability assessment in chapter 3.2 an attempt has been made to adopt a systematic approach to address the two key points given above for each of the experiments reviewed. Performing the review in a structured way is intended to allow a systematic inter-comparison of the experiments and analyses, thereby bringing out where comparisons can be drawn and ensuring that consistencies or inconsistencies are properly identified. The overall driver for the task was to identify the key gas migration mechanisms and to define the basic dataset for effective gas and two-phase flow parameters for relevant experiments performed as part of Phases 1 to 5 of the Mont Terri project.

Three groups of field experiments were included in the review; these took place in different areas of the Mont Terri rock laboratory. The first group of tests, performed as part of Phases 1 and 2 of the project, concentrated on hydraulic tests and gas threshold pressure tests in boreholes BGP-1, BGP-2, BGP-3 and BGP-4 in the SHGN niche (cf. Figure 2.2; TN 97-28, TN 98-24 and TN 98-25). The next group focused on gas threshold pressure tests and long-term gas injection tests in boreholes BGP5, BGP-6, BGP-8 and BGP-9 in the FM niche (TN 99-07, TN 99-08). The final group of experiments emphasised long-term experiments in boreholes BGS-1, BGS-2, BGS-3 and BGS-4. A series of hydraulic tests were performed in BGS-1 and BGS-2, followed by a long-term gas injection test in BGS-2 (TN 2000-07). Technical Note 2000-10 describes hydraulic fracturing in borehole BGS-2.
In addition to the field experiments, permeameter experiments in the laboratory were carried out with core samples. The main objective of these tests was the determination of the hydraulic and gas related properties of the Opalinus Clay (TN 98-15, TN 99-58).

For the first aspect of the quality review, the *field and laboratory methods (FLM)*, a number of key issues were identified that would enable conclusions to be drawn from the work in a systematic manner:

FLM 1: Has standard equipment been used? Is the application of the equipment
- ✓ well within its limits of design?
- × beyond its limits of design?
- ? at the limit of design for the range of parameters expected, or is this not really adequately known or properly understood?

FLM 2: Has a sound experimental methodology been used? This covers such issues as:
- FLM 2.1: Has there been adequate time allowed for testing? (✓ yes, × no, ? not known)
- FLM 2.2: Is the test free of issues concerning the stabilisation of pressure or the prehistory? (✓ yes, × no, ? not known)
- FLM 2.3: Has the test been designed appropriately with respect to the general test objectives? (✓ yes, × no, ? not known)

FLM 3: Do the results look compatible or incompatible with what is expected from the action of various standard processes, as indicated by visual inspection of diagnostic plots? Are there obvious problems (and if so have these been properly identified) such as:
- FLM 3.1: Equipment appeared to function satisfactorily?

(✓ yes, ✕ no, ? not known)

FLM 3.2: Evidence for coupled processes?
(✓ yes, ✕ no, ? not known)

FLM 3.3: Wellbore storage has been quantified?
(✓ yes, ✕ no, ? not known)

FLM 3.4: Is test free of domination by wellbore storage?
(✓ yes, ✕ no, ? not known)

FLM 4: Is there evidence for adequate motivation for carrying out the experiment in the way it has been carried out?

FLM 4.1: Were the specific objectives clear from the start?
(✓ yes, ✕ no, ? not known)

FLM 4.2: Were the objectives achievable given the equipment?
(✓ yes, ✕ no, ? not known)

FLM 4.3: Were the objectives achieved?
(✓ yes, ✕ no, ? not known)

FLM 5: Has the methodology tested appropriate flow and gas transport pathways? For each of the experiments:

FLM 5.1: Has an appropriate conceptual model (or range of conceptual models) been developed for the test?
(✓ yes, ✕ no, ? not known)

FLM 5.2: Has the 'support scale' of the experiment been identified, i.e. the scale on which the hydrogeological, gas parameters vary?
(✓ yes, ✕ no, ? not known)

For each of the issues FLM 1 to FLM 5, a suite of detailed assessment criteria were defined. In the context of field testing, for example, some of the important FML 1 assessment criteria were: (i) design of downhole equipment (length of packer seals, guard packers, control of packer pressures, minimisation of system compressibility, minimisation of test interval volume, independent flow and pressure lines to the test interval) and (ii) design of surface equipment (flow control system, pressure monitoring and data acquisition system). A detailed description of the assessment criteria is given in TN 99-58.

The conclusions from the standard questions given above are recorded in Table 5.2. The checkbox approach to providing an overall review of the complete suite of field experiments necessarily provides only a simplified commentary on the experiments, with an element of subjectivity in the analyses. Further comments to each of the experiments are given in TN 99-58.

The *data analysis (DA) review* was conducted in a way similar to the approach for the review of the *field and laboratory methods*. The intention was to flush out various issues:

DA 1: How was the analysis performed?

DA 2: Was there adequate logic behind using one analysis tool rather than another and was this an issue?
(✓ yes, ✕ no, ? not known)

DA 3: Were appropriate conclusions drawn? For example, were stronger conclusions drawn than were supported by the non-unique nature of the analysis?
(✓ yes, ✕ no, ? not known)

DA 4: Has the scale of the experiment been determined, as for example embodied in the simplifying assumptions made in the conceptual model used to interpret the experiment, i.e. is this on a sub-cm, sub-m or more generally on what support scale (or radius of interest)?
(✓ yes, ✕ no, ? not known)
Note that reference here is to the scale over

Filed and Laboratory Methods hydro and gas testing	FLM1	FLM2.1	FLM2.2	FLM2.3	FLM3.1	FLM3.2	FLM3.3	FLM3.4	FLM4.1	FLM4.2	FLM4.3	FLM5.1	FLM5.2
BGP-4 Gas	✓	?	?	✓	✓	?	✓	-	✓	✓	✕	✓	✕
BGP-6 Gas (TN99-07)	✓	✓	✓	✓	✓	✓	✓	✓	✓	✓	✓	?	✓
BGS-2 Gas (TN00-07)	✓	✓	✓	✓	?	?	✓	✓	✓	✓	✓	?	?
GP core test (TN98-15)	✓	✕	✓	✓	✕	✓	?	?	?	?	?	✓	✓

Table 5.2: Summary of the quality review of the field and laboratory methods. The symbol ✓ indicates an affirmative or clear response to the question. The symbol ✕ indicates a negative response to the question or incorrect conclusion drawn. The symbol ? indicates an inconclusive or not known response to the posed question.

Data analysis	DA 1	DA 2	DA 3	DA 4	DA 5	DA 6.1	DA 6.2	DA 6.3	DA 6.4	DA 6.5	DA 7
BGP-4 Gas (TN98-25)	IT2, T2	✓	?	?	✓	✓	✓	✓	✓	?	✓
BGS-6 Gas (TN99-07)	SLA, SSA	?	✓	?	×	×	✓	✓	✓	?	✓
BSG2 Gas (TN00-07)	I2	?	?	?	✓	×	✓	✓	?	?	✓

Table 5.3: Summary of the quality review of the data analysis of gas tests performed in Phases 1 to 5. Methods of analysis: TOUGH2 (T2), ITOUGH2 (IT2), INTERPRET2 (I2), Sabet and Horne (SLA), Sabet (SSA), sensitivity analysis (+S). Symbol legend: ✓ yes, × no, ? not known.

which the hydrogeological model assumed has been demonstrated. A scale over which some experimental response has been seen in observation boreholes may well have been identified.

DA 5: Is the conceptual model sufficient to explain the results?
(✓ yes, × no, ? not known)

DA 6: Was adequate attention given to:
DA 6.1: sensitivity of the results to data fit?
(✓ yes, × no, ? not known)
DA 6.2: apparent inconsistencies?
(✓ yes, × no, ? not known)
DA 6.3: consistencies in argument, i.e. have some of the conclusions been supplemented by other information?
(✓ yes, × no, ? not known)
DA 6.4: problems with the test?
(✓ yes, × no, ? not known)
DA 6.5: possibilities of different flow/gas pathways?
(✓ yes, × no, ? not known)

DA 7: Are there any issues to be considered about the quality assurance of the wide range of models referenced (e.g. in TN 98-25)?
(✓ yes, × no, ? not known)

The results of this analysis are given in Table 5.3. As with the analysis shown in Table 5.2, the overview provided in this table is necessarily simplified; further explanation is provided in TN 99-58.

5.4 Experimental data base

Gas related laboratory and field tests have been conducted in the framework of experiments GP, GP-A and GS. Those documents issued by the middle of Phase 5 were included in the quality assurance process described in chapter 5.3. Since that time, two additional documents discussing experimental studies have been released: (i) a report on the second laboratory experiment with a core sample (TN 99-58) and (ii) a summary report of all field activities in the GP-A/GS experiment (Enachescu et al. 2002). In the next sections, results of the gas related experimental investigations in Phases 1 to 5 will be summarised according to the following outline:

– Gas permeability tests on core samples,
– Gas threshold pressure tests in boreholes,
– Long-term gas-injection tests in boreholes,
– Hydrofracturing and gas fracturing experiments in boreholes.

5.4.1 Gas permeability tests on core samples

Gas permeability tests were conducted as part of the GP experiment (TN 98-15, TN 99-58). The experiments were aimed at

– The evaluation of enhanced gas permeability at high injection pressures, and
– The self-healing capacity of the Opalinus Clay after a gas breakthrough.

A total of four core samples were tested. Their sample ID's are BED-B3 06, BFP-16, BED-C5/7 and BWS-E4 06. The samples were taken from the sandy and shaly facies. The tests were designed to match the expected in-situ stress conditions. The confining pressure was 6 MPa and the downstream porewater pressure was 2 MPa. One core sample each was subjected to flow parallel and perpendicular to bedding. The flow direction for the other two samples was oblique to bedding. It was also ascertained that the core samples were saturated completely before the water/gas injection phase was started. Each test started with a hydrotest phase to determine the intrinsic permeability. Subsequently the gas injection phase was initated as a constant rate resp. constant head event. Figure 5.1

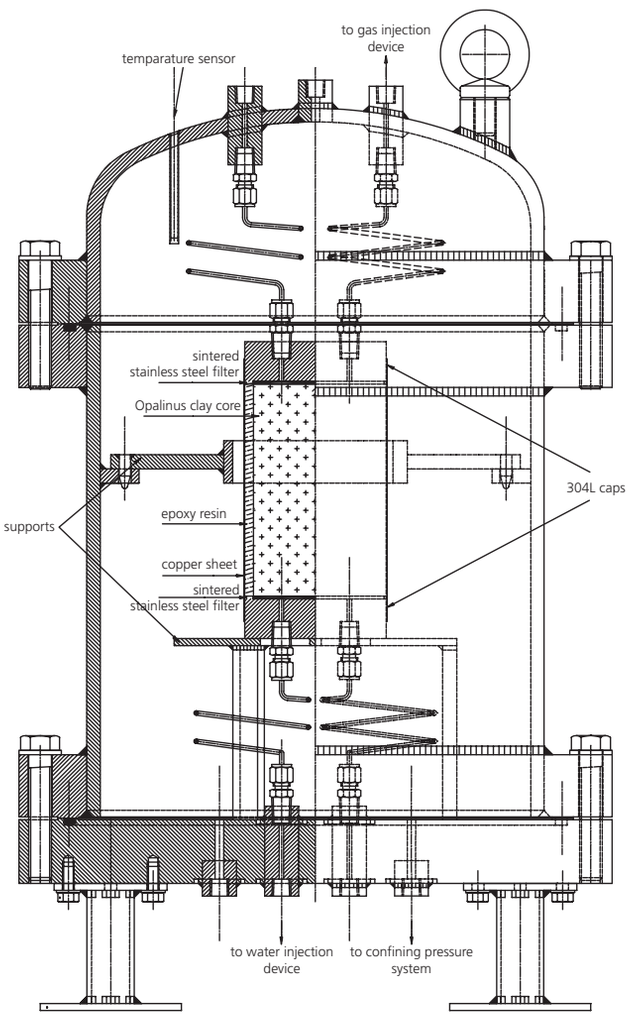

Figure 5.1: Schematic view of SCK·CEN's isostatic cell and sample assembly for the Opalinus Clay samples as part of the GP experiment (after TN 99-58).

shows a schematical sketch of the isostatic cells used for hydraulic testing and gas testing of core samples. The tests were carried out at SCK·CEN's Laboratory. The gas injection periods ranged from 3 to 8 months. The intrinsic permeabilities were consistently in the range of $1\times10^{-20}-2\times10^{-20}$ m^2, with the exception of sample BED-B3 06. This specimen was damaged during the sample preparation process and exhibited a visible fracture in flow direction. The recorded gas entry pressures are all ≤ 0.5 MPa (cf. Table 4.4). The gas saturation of the core samples after the gas injection phase was generelly low (typically below 10%; in case of sample BED-B3 06 the upper limit of gas saturation was determined to be < 0.22).

The disturbed sample BED-B3 06 was tested hydraulically again after the gas injection phase to investigate for potential changes in the hydraulic conductivity. This indicates that the presence of the former gas pathway, represented by the initial planar fracture, did not give rise to an enhanced permeability. Several hypotheses could explain this observation: a self-healing of the sample took place, the lower permeability is due to the de-saturation of the clay, or gas microbubbles might block a portion of the connected porosity. None of these hypotheses can be excluded with the given level of experimental evidence.

Another before-and-after measurement set of hydraulic conductivity was conducted with sample BWS-E4 06. Within the uncertainty limits of the measuring technique, the hydraulic test after gas injection exhibits the same conductivity as the one done before gas testing (2.1×10^{-20} m^2).

Gas testing of sample BED-C5/7 lasted approximately 6 month. A clear gas breakthrough was achieved. After termination of the gas injection test the sample was dismantled. Visual inspection of the core indicated a sharp separation front between a lighter (unsaturated) and a darker (saturated) zone located at about 4.5 cm from the gas injection side (Figure 5.2). Subsequently, the core was cut into slices and the water

Core sample	**Injection period [d]**	**Direction of flow relative to bedding**	**Intrinsic permeability[1] k [m²]**	**Gas entry pressure p_{ae} [MPa]**
BED-B3 06 2)	60	0°	2.0×10^{-18}	<0.03
BFP 16	110	50°	1.5×10^{-20}	0.5
BWS-E4 06	180	90°	2.0×10^{-20}	0.2
BED-C5/7	174	35°	2.0×10^{-20}	0.2

[1] Intrinsic permeability k (m²) as derived from hydraulic conductivity K (m/s): k = 1E-7 · K
[2] Core sample is not representative of undisturbed Opalinus Clay (visible fracture in flow direction)

Table 5.4: Two-phase flow parameters as derived from laboratory experiments on core samples of the Opalinus Clay from the Mont Terri rock laboratory. The intrinsic permeability was derived from hydraulic permeameter tests.

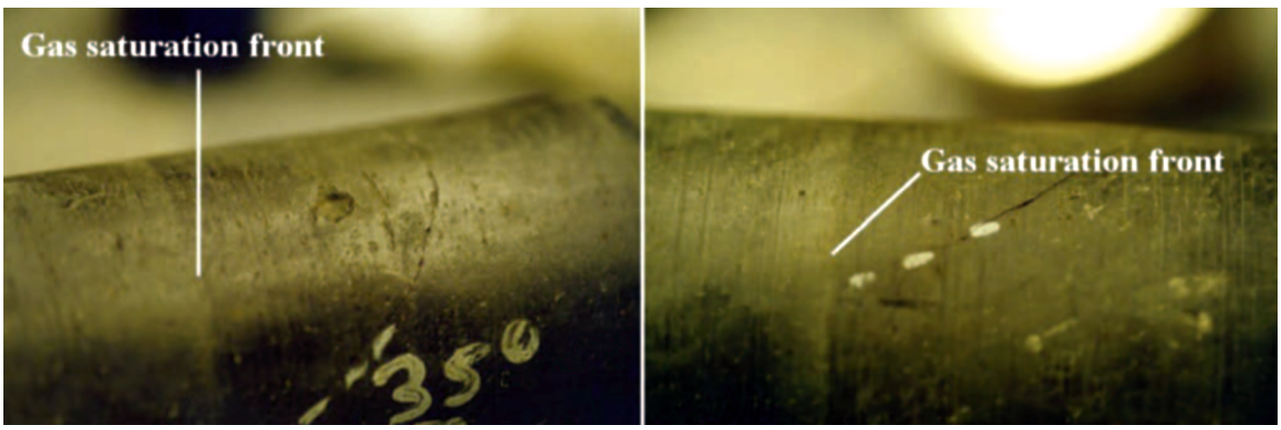

Figure 5.2: Photographs of the BED-C5/7 sample taken right after the gas injection test (after gas breakthrough) and showing a sharp gas saturation front (after TN 99-58).

content of each piece was determined. The water saturation of the different slices varied between 92.8 and 99.8%. This observation is interpreted as follows:

– During the early stages of the gas injection sequence, the gas phase propagates along the system of macropores until it breaks through at the downstream end of the sample. The gas migration mechanism is either water displacement or microscopic pathway dilation. The total volume of gas stored in the sample is negligible.
– A delayed migration into the pore spaces with smaller pore radii starts in the late time stages of the experiment. This delayed migration is extremely slow, nevertheless exhibits an important feature: an increasing amount of gas is stored in the rock sample.

5.4.2 Gas threshold pressure tests

Two gas threshold pressure tests were conducted in boreholes BGP-4 and BGP-6. The purpose of these tests was:

– To determine the gas entry pressure of the Opalinus Clay.
– To provide a data base for a more sophisticated analysis of gas migration in the framework of two-phase modelling and hydro-mechanical modelling (cf. chapter 5.5).

The length of the test interval was 1 m and 4.5 m for boreholes BGP-6 and BGP-4, respectively. The testing sequence consisted in both cases of a hydraulic test, fluid exchange (i.e. replacement of fluid in test interval with gas) and gas injection with a constant flow rate (i.e. "constant rate test"). In BGP-4 the gas injection phase was followed by a long-term pressure recovery phase. In BGP-6 the constant rate event was turned into a long-term constant pressure event before and then ended with a long recovery period. The determination of the gas entry pressures was done diagnostically (Senger et al. 2002) from the analysis of the gas injection phase (particularly of the deviation from the linear pressure increase during the gas injection phase) and of the recovery phase (Horner plot). In addition, the test in BGP-4 was analysed through numerical modelling (TN 98-25). The specifics are summarised in Table 5.5.

The gas injection test in borehole BGP-4 with its test interval length of 4.5 m was carried out in the "main fault" (cf. Figure 5.3) using a rather high gas injection rate of 0.04 l/min (STP). During the pressure recovery a maximum specific gas flux into the rock of 4×10^{-7} $m^3/m^2/min$ (STP) was determined. Diagnostic analysis of the gas injection phase suggests an air entry pressure of about 0.4 MPa. The Horner plot leads to an estimate for the upper limit of about 1.2 MPa. Finally, inverse modelling of the entire test phase was carried out using the multi-phase flow simulator ITOUGH2 (cf. chapter 5.5): the recommended air entry pressure was in the range 0.4 to 0.8 MPa.

The test in borehole BGP-6 with an interval length of 1 m was conducted in the sandy facies. The gas injection rate was lower than in BGP-4 by the factor of 40. During the constant pressure gas injection event subsequent to the injection phase (cf. chapter 5.4.3), a specific gas flux of into the rock of 1×10^{-5} $m^3/m^2/min$ (STP). A gas entry pressure of 1 MPa was determined from log-log diagnostic analysis of the gas injection phase. It is rather apparent that the attained gas entry pressures are comparable despite the significant differences in the injection rates and the durations of the two tests.

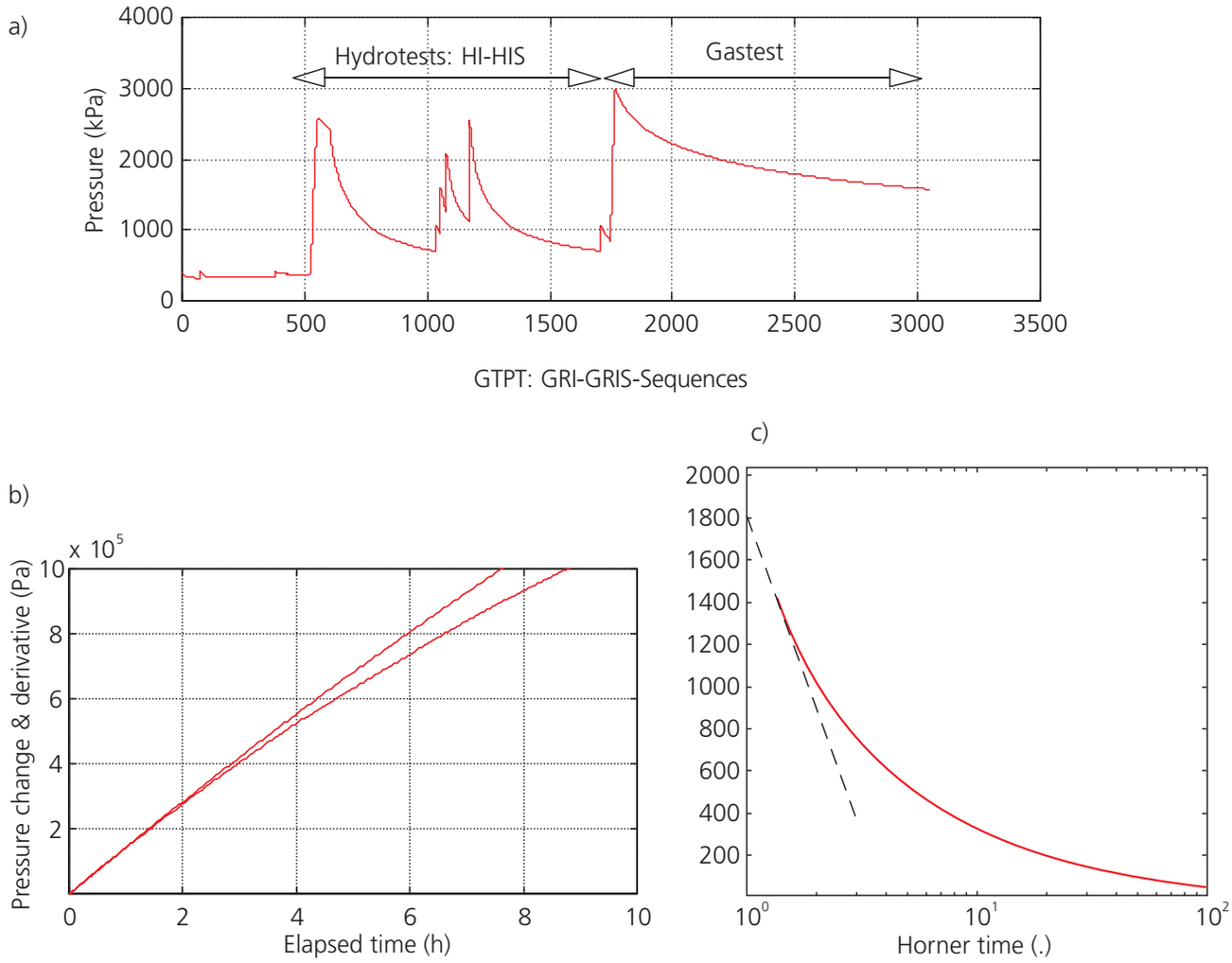

Figure 5.3: Diagnostic analysis of gas threshold pressure test in interval I4.2 of borehole BGP-4: (a) linear plot of the entire test sequence; (b) Cartesian plot of the gas injection phase (deviation from the linear pressure increase during the gas injection phase); (c) Horner plot of the recovery phase (after TN 98-25).

Borehole	**Period [h]**	**Injection rate [l/min STP]**	**Specific gas flux [m³/m²/min STP]**	**Intrinsic permeability [m²]**	**Gas entry pressure p_{ae} [MPa]**
BGP-4	18	0.04	4×10^{-7} [1)]	2E-20 – 6E-20	0.4–0.8
BGP-6	150	0.001	1×10^{-6} [2)]	1.5E-20 (hydro)	~ 1.0

[1)] Gas flow rate per surface of the test interval during the recovery phase
[2)] Gas flow rate per surface area during the subsequent constant head gas injection phase

Table 5.5: Two-phase flow parameters as derived from gas threshold pressure tests at the Mont Terri rock laboratory.

The gas entry pressure are surprisingly low, as for pore diameters of 1–50 nm, the Young-Laplace equation would lead tomuch higher values (factor 10 or more). It seems therefore, that enough macropores (>30 nm) are available inside the Opalinus Clay, which allow for a lesser capillary resistance to flow. The presence of microcracks around the borehole would also explain those low air entry pressures.

5.4.3 Long-term gas injection tests

Two long-term gas injection tests were conducted as part of the GP and the GP-A experiments in the FM niche and at the GS location, respectively. The experimental design was similar: the injection boreholes were equipped with multi-packer systems while the observation boreholes at a distance of decimeters to a meter were equipped either as piezometers for long-term observations or with multiple extensometers for observations of the axial deformation. The aim of these experiments was two-fold:

– To provide a data base for two-phase modelling of gas migration in the Opalinus Clay (cf. chapter 5.5).
– To provide a data base for modelling hydro-mechanical processes (cf. chapter 5.5).

The gas test of the GP experiment lasted for 24 days (TN 99-08). For a constant pressure of 2.1 MPa, the contant flow rate obtained under stationary conditions was about 0.14 mIN/min. The observations in the other boreholes indicated significant mechanical deformation with up to about 30 μm/m. After completion of the gas injection phase, a hydraulic test was performed in order to assess potential changes in the hydraulic conductivity as a result of gas injection. Within the bounds of measurement precision, the hydraulic conductivities derived before and after gas injection were identical with about 1×10^{-13} m/s.

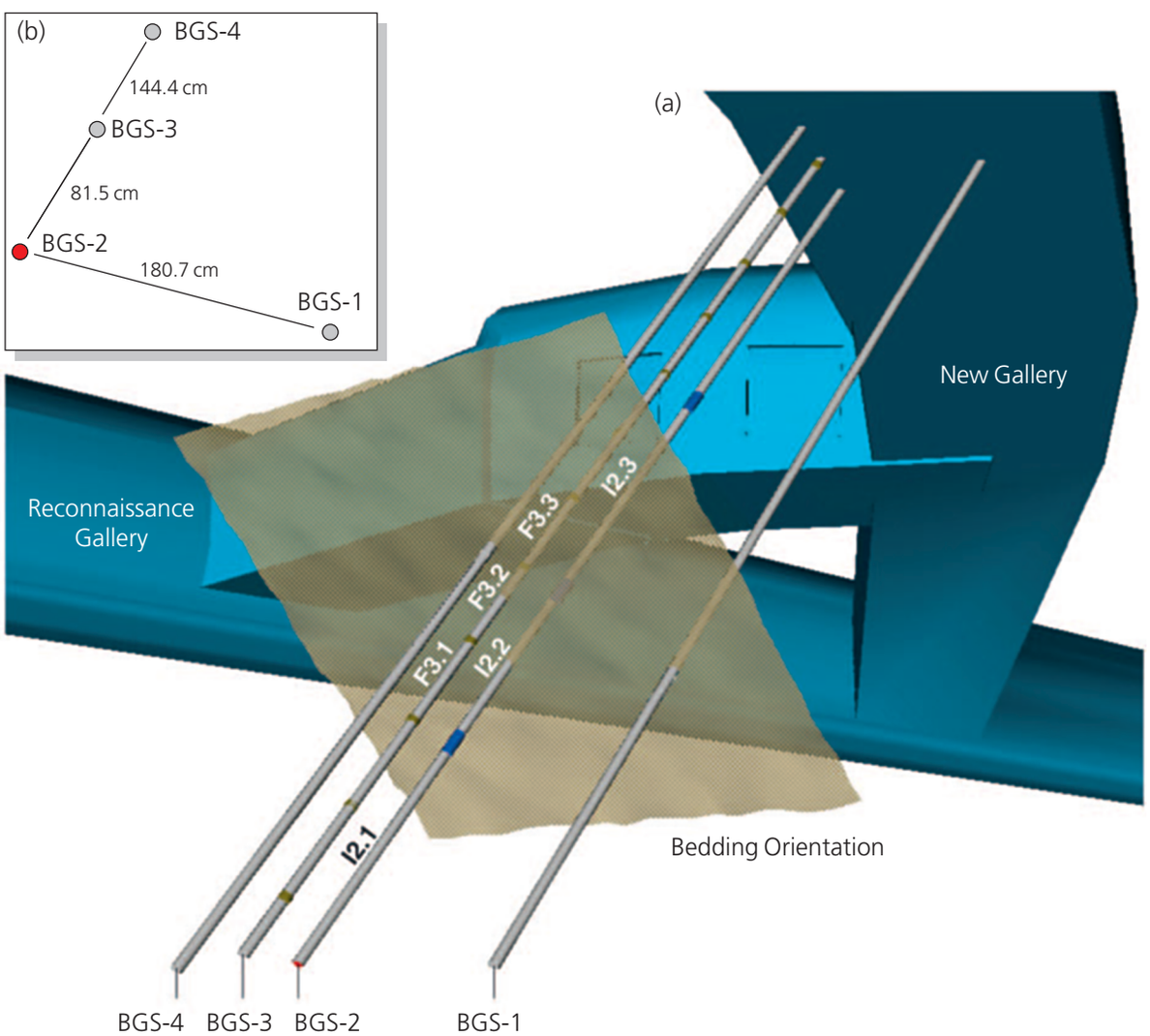

Figure 5.4: Long-term gas injection experiment in the GP-A/GS site. (a) The test configuration consisted of two boreholes: BGS-2 was equipped with a triple packer system, BGP-3 with fixed installed micrometers. (b) Shows a plan view drawn perpendicular to BGS-2 through the centre of test interval I2.2. (c) At gas injection pressures of more than 2 MPa, a significant mechanical response is observed in BGP-3 (after Enachescu et al. 2002). (c) on page 77.

(c)

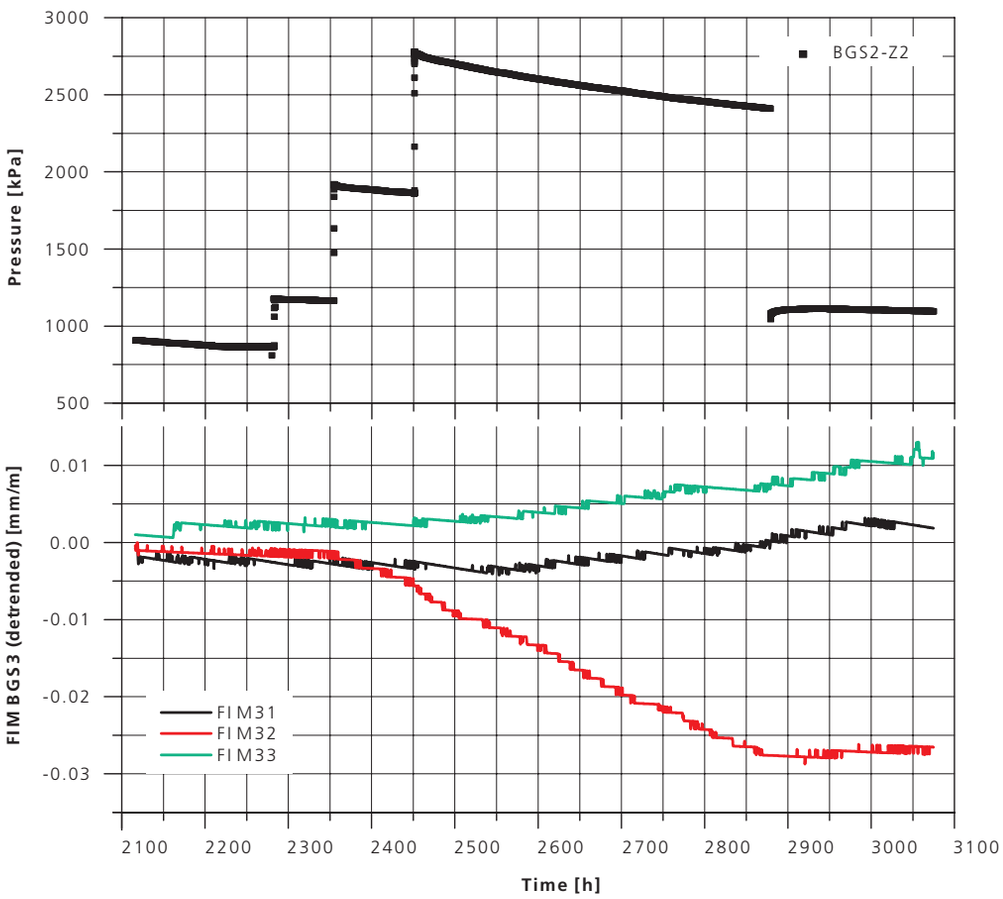

Figure 5.4 continued

The other long-term gas injection test lasted for a total of 30 days and encompassed a testing sequence with three levels (Enachescu et al. 2002). Before testing commenced in the GP-A borehole, the borehole fluid in the test interval of ca. 2.1 l volume was replaced with nitrogen gas. The gas pressure in the test interval was then fixed at differential pressures of about 0.5 MPa, 1.0 MPa and 2.0 MPa, respectively, and the interval closed off. Figure 5.4 shows the development of the interval pressure and of the gas flow rate in the gas injection borehole BGS-2, as well as the deformation in the observation borehole BGS-3 at a distance of 1 m. For a differential pressure of 0.5 MPa the formation appears practically impermeable to gas as the gas entry pressure has not yet been reached. Low flow rates result for a differential pressure of 1 MPa without any significant deformation in the adjacent extensometer boreholes. The highest pressure level is accompanied by marked increases in the gas flow rate and significant deformation of about 20 μm/m which are not reversible after completion of the gas injection test. This gas test was analysed with a coupled hydrodynamic model (Senger et al. 2002).

The pressure recovery observed in the injection borehole and the deformation recorded in the observation borehole could be simulated remarkably well in terms of time and magnitude (cf. chapter 5.5). The quantitative results prove that the intrinsic permeability increases on the highest pressure level by a factor of 5 as a result of the observed dilation.

5.4.4 Hydrofrac and gasfrac experiments

As a follow-up to the long-term gas injection test (Figure 5.4), a complex sequence of hydrofrac and re-frac tests was performed at the GS site, completed by hydrotests and further gas tests. The objectives of this suite of tests were:

- To investigate the pressure regime of hydro-/gas fracturing in the Opalinus Clay (cf. chapter 5.3).
- To determine frac pressure and re-frac pressure at the GS location.
- To determine pressure dependent transmissivity of a hydrofrac.
- To assess the self-healing capacity of the Opalinus Clay.

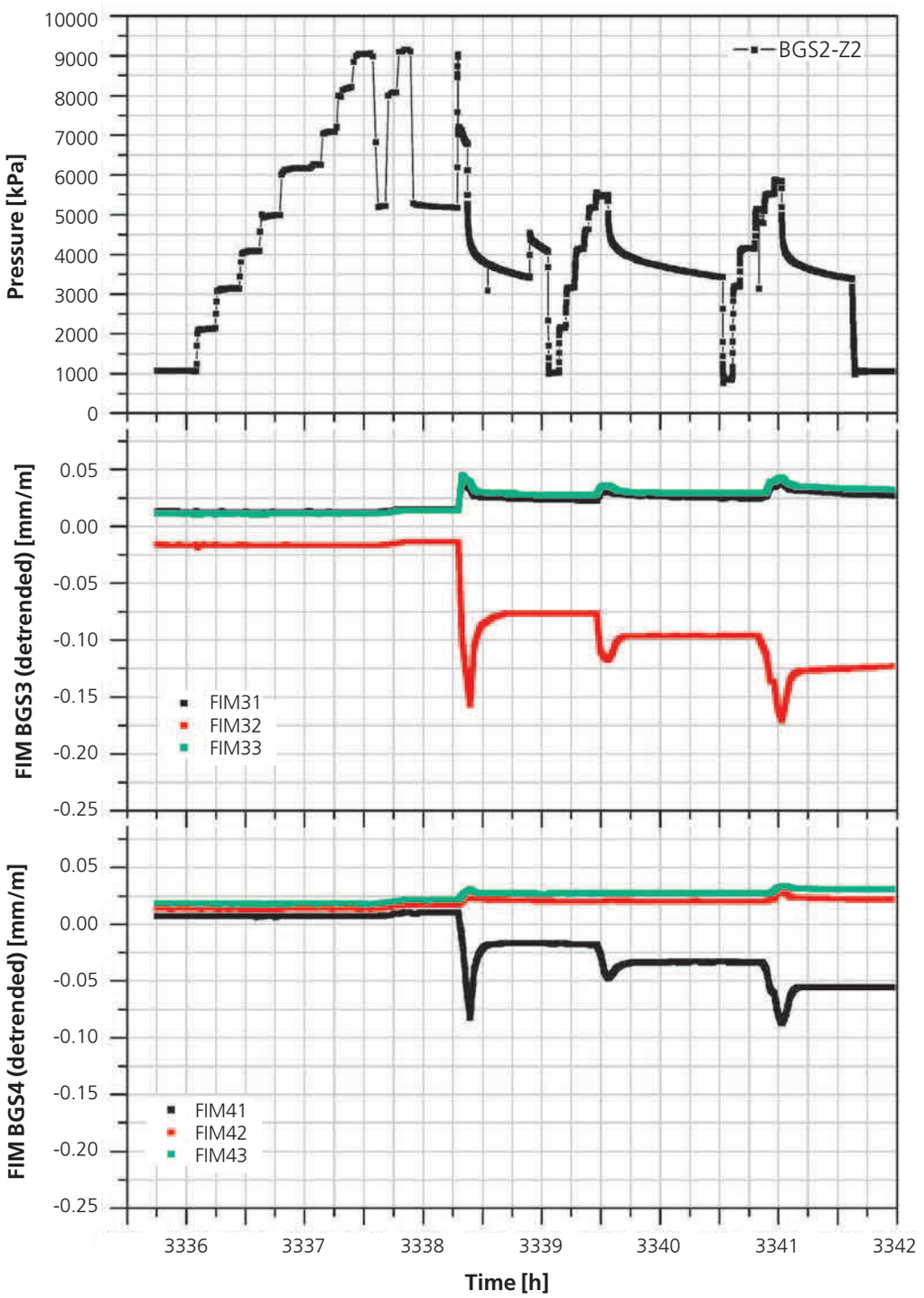

Figure 5.5: Sequence of hydrofrac and re-frac events in test interval I2.2 of borehole BGS-2. Pressure transients in interval I2.2 of borehole BGS-2 and displacements measured in BGS-3 and BGS-4 (after Enachescu et al. 2002).

The hydrofrac/gasfrac sequence was carried out in test interval I2.2 of borehole BGS-2. Pore pressures were monitored in the adjacent observation intervals I2.1 and I2.3 and in borehole BGS-1. Boreholes BGS-3 and BGS-4 were instrumented with extensometers (Fixed Installed Micrometers/FIM). The orientation of all boreholes was approximately perpendicular to bedding. The expected orientation of the hydrofrac was parallel to bedding. The entire test sequence is listed in Table 5.6.

Stage	Remarks
Stage 1: Hydrofrac	- progressive constant gas pressure steps: (first attempt) 0.8–9 MPa (1.5 h); no fracture event
Stage 2: Hydrofrac (second attempt)	- constant gas pressure steps: 5, 8 and 9 MPa - fracture event at a pressure of 9027 kPa - gas injection continued for 0.08 h at an approximate pressure of 7145–6112 kPa. The total volume injected is 4.7 l - shut in, followed by a pressure reduction to the static formation pressure at approximately 0.8 MPa
Stage 3: Refrac test steps each	- two re-frac cycles with several pressure - shut-in after successful fracture re-opening - pressure drop to static formation pressure (approx. 0.8 MPa) - test interval opened to accommodate back-flow (no backflow measured)
Stage 4: Hydraulic test	- multi-step pulse injection test
Stage 5: Gas pulse test	- gas pulse test (gas pressure below frac pressure)
Stage 6: Gas injection test	- constant rate gas injection - long-term pressure recovery

Table 5.6: Hydraulic fracturing experiment in interval I2.2 of borehole BGS-2: stages of the complex test sequence.

Figure 5.5 shows the pressure transients in test interval I2.2 of borehole BGS-2 during stages 1 through 3. In addition, the mechanical response of the FIM equipment in boreholes BGS-3 and BGS-4 is given. Two cycles of pressurisation are needed to create the hydrofrac. Frac pressure is reached during the second hydrofrac cycle at more than 9 MPa. The frac test was followed by two re-frac cycles. Each cycle consisted of several constant pressure injection events until the fracture re-opened. Subsequently, the test interval was shut-in and, finally, pressure was dropped to the static formation pressure. After the second cycle, the valve to the interval was left open to accommodate back-flow. During the entire equilibration time no back-flow was measured. The re-frac pressure was calculated to 4200 kPa.
All Fixed Installed Micrometers (FIM) reacted to the hydrofrac. Zones FIM3.2 and FIM4.1 show a distinct dilation, while zones FIM3.1 and FIM3.3 exhibit contraction. Responses in zones FIM4.2 (slight contraction) and FIM4.3 (slight dilation) are much smaller in magnitude. The mechanical response in FIM3.2 is as high as 15 μm. FIM4.1 exhibits a lower magnitude, because the distance to the gas injection borehole is greater.

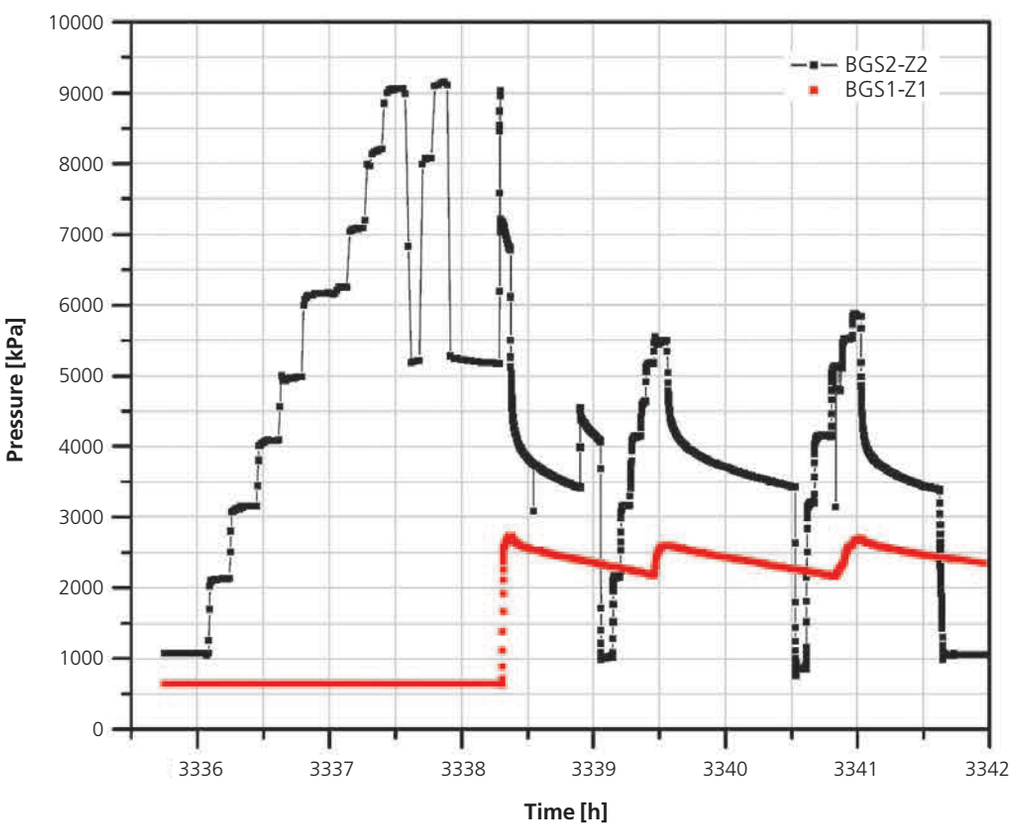

Figure 5.6: Hydraulic response in interval I1.2 of borehole BGS-1 to the hydrofrac and re-frac events in test interval I2.2 of borehole BGS-2 (after Enachescu et al. 2002).

The frac events created an increase in interval transmissivity and a hydraulic communication between intervals I2.1 and I2.2 of borehole BGS-2.

5.5 Modelling of gas related experiments

It was one of the objectives of the gas related field experiments to provide an appropriate data base required for validation of the different conceptual approaches of gas migration (cf. chapter 5.2). Emphasis was given to two-phase flow processes and microscopic pathway dilation because these mechanisms play a key role in the assessment of gas release from the disposal caverns of a repository for radioactive waste.
Two gas experiments were selected for detailed interpretation by numerical modelling, namely the extended gas threshold pressure test in interval I4.2 of borehole BGP-4 (cf. Figure 5.3) and the long-term gas injection test in interval I2.2 of borehole BGS-2 (cf. Figure 5.4). In the following sections, a brief summary of the modelling activities will be given and the achievements will be highlighted. Finally, chapter 5.5.3 is aimed at an assessment of the current level of understanding on gas migration mechanisms in claystones.

5.5.1 Two-phase flow modelling of the gas threshold pressure test in BGP-4 Objectives

A summary and chronology of the BGP-4 testing activities including the hydrotests performed prior to the gas threshold pressure test is reported in TN 97-28. A detailed analysis of the hydrotest events with flow model identification, parameter estimation and extended assessment of parameter uncertainties was documented in TN 98-24. The gas threshold pressure test sequence was also subjected to a detailed two-phase flow analysis (TN 98-25). The objectives of the detailed analysis of the BGP-4 gas threshold pressure test were:

- to interprete the test in terms of constitutive relationships (relative permeability and capillary pressure) based on the conceptual framework of two-phase flow in an Equivalent Poro-elastic Medium (EPM) and taking into account the results of the hydrotests interpretation (TN 98-24)
- to identify signatures in the system response which could be attributed to phenomena not described by an EPM-based two-phase flow modelling approach (e.g. coupled hydro-mechanical behavior)

Interpretation procedure

The interpretation of the gas test was performed according to a standard procedure which has proven successful in the past by Nagra for fractured rocks (Marschall et al. 1998). The procedure includes numerical simulations of pressure transient and water / gas flow transients using the multi-phase flow simulator TOUGH2 and the corresponding tool for inverse modelling ITOUGH2. The key elements of the interpretation procedure are:

- Diagnostic graphical representation of the data for the gas injection and recovery phases.
- Set-up of initial fitting and non-fitting parameters as input parameters for the two-phase flow simulation using TOUGH2.
- Computation of the sensitivity of the two-phase flow model parameters (ITOUGH2).
- Specification of constraints and objective function, and optimisation of fitting-parameter estimates using non-linear regression (ITOUGH2) to obtain best estimates.
- Evaluation of the results of the non-linear regression, and uncertainty analysis.
- Consistency check with the analysis of the hydrotest results from BGP-4.

Two-phase flow parametric models

Capillary pressure/water saturation relationship (CPS):
The two most commonly used CPS models in the two-phase flow literature are given by the Brooks-Corey and the van Genuchten relationships.
The model of Brooks & Corey (1964) – here referred to as BC model – is given by:

$$P_c = P_e \cdot S_{ec}^{-1/\lambda} \quad \text{with} \quad S_{ec} = \frac{S_w - S_{wr}}{1 \cdot S_{wr}} \qquad (5.1)$$

where:

λ	a pore-size distribution index [-]
P_e	the air entry pressure [Pa]
$P_c = P_g - P_w$	the capillary pressure [Pa]
P_g	the pressure of the gas phase [Pa]
P_w	the pressure of the water phase [Pa]
S_w	the actual water saturation
S_{wr}	the residual water saturation
S_{ec}	the effective saturation as defined above

For a uniform pore-size distribution λ tends to large values, whereas for a wide spread distribution it tends to small values. Typical values for sands range from 2 to 5.
The model of van Genuchten (1980) – here referred to as VG model – is given by:

$$P_c = \frac{1}{\alpha} \cdot (S_{ec}^{\frac{n}{1-n}} - 1)^{\frac{1}{n}} \qquad (5.2)$$

where α [1/Pa] and *n* are shape parameters of the CPS model.
The main difference between the BC model and the VG model is that, when the water saturation S_{ec} tends to 1, the capillary pressure approaches a non-zero value (i.e. the entry pressure: P_e) in the BC model whereas a continuous decrease of the capillary pressure to zero is observed in the VG model. Both parameterizations are fitting curves of the experimental data. For further details about the CPS models described above, the reader is referred to a book by Corey (1994).
Relative permeability/water saturation relationship (RPS): Through theoretical consideration of viscous flow at the pore scale, parametric models have been derived. Their mathematical formulations are recalled briefly. For more detail on this the reader is referred to the two-phase flow literature. The theoretical RPS model of Burdine (1953) has been used in conjunction with the BC model, leading to the following expressions for the relative permeability to water (k_{rw}) and to gas (k_{rg}):

$$k_{rw} = S_e^{(2+3\lambda)/\lambda)} \qquad (5.3a)$$

$$k_{rg} = (1-S_e)^2(1-S^{(1+2/\lambda)}) \qquad (5.3b)$$

where S_e is the apparent saturation, given by:

$$S_e = \frac{S_w - S_{wr}}{1 - S_{gr} - S_{wr}} \qquad (5.3c)$$

and S_{gr} is the residual gas saturation which corresponds to the gas saturation which does not contribute to the gas flow.
Similarly, the theoretical RPS model of Mualem (1976) has been used in conjunction with the VG model and leads to the following expressions:

$$k_{rw} = S_e^{1/2}\left[1 - (1 - S_e^{\frac{n}{n-1}})^{\frac{n-1}{n}}\right]^2 \qquad (5.4a)$$

$$k_{rg} = (1 - Se)^{1/2}(1 - S_e^{\frac{n}{n-1}})^{2(1-1/n)} \qquad (5.4b)$$

TOUGH2 is a general purpose simulator for multi-dimensional coupled fluid and heat flows of multi-phase multi-component fluid mixtures in porous and fractured media (Pruess 1991; Pruess 1987). The coupled multi-phase multi-component equations are solved by means of integral finite differences. The solution of the flow of fluids accounts for pressure, viscous, gravity and capillary forces. The equation of motion for each fluid phase is the generalized Darcy equation which represents the phase interference on the basis of relative permeability. Functional relationships are used which describe the relative permeabilities and the capillary pressure as a function of the saturation. Thermodynamic properties of the fluids are represented by steam-table equations while the gaseous phase is treated as an ideal gas and described by local thermodynamic equilibrium. Dissolution of gas into water is described by Henry's law.
In this study, isothermal conditions were assumed and the equation of state module EOS3 (phases: water/air) was used for the simulations of the nitrogen gas injection sequence (GRI) and recovery (GRIS). Because TOUGH2 deals with air mass flow rates, the nitrogen mass flow rates were converted into equivalent air mass flow rates for standard pressure (P = 100 kPa) and temperature (T = 20°C) conditions.
The numerical code ITOUGH2 (Finsterle 1997) solves the two-phase flow parameter estimation problem by means of an inverse modelling technique. For the interpretation of the gas threshold pressure test, the pressure data recorded at the test interval during the test are automatically fitted using a minimization algorithm of the differences between simulated and measured data. Both one-phase and two-phase flow parameters can be estimated together with the standard deviations and the correlation coefficients as measures of the parameters uncertainty and interdependence, respectively.

Modelling results

According to the general interpretation procedure (see above), diagnostic test analysis and set-up of input parameters for baseline simulations (forward modelling) formed the early modelling stages. A sensitivity study of the gas injection phase (GRI) and of the subsequent shut-in phase (GRIS) followed, using the inherent capabilities of ITOUGH2: the sensitivity of the pressure transient to the test interval compressibility, the permeability, the formation compressibility and the air entry pressure is high, whereas the one of residual water saturation and the porosity is lower. Noteworthy, the sensitivity coefficients do vary with time resp. with the test events (GRI, GRIS). This fact exhibits a benefi-

cial effect by reducing the degree the non-uniqueness of the solution of the inverse modelling.
In order to avoid over-parameterization, inverse modelling was limited to 5 unknown parameters (formation compressibility, test interval compressibility, porosity, permeability, air entry pressure), whereas the parametric two-phase flow model, the pore size factor and the residual water saturation were fixed (VG model: n = 2, S_{rw} = 0.1, S_{gr} = 0 and S_{gr} = 0.1, respectively). Further refinement included joint inversion of both, hydraulic and gas test sequence. Finally, the results of inverse modelling can be summarised as follows:

- Strong parameter correlation is seen between gas entry pressure, permeability and porosity. This parameter correlation makes results somewhat ambiguous, although excellent matches of the data are achieved.
- Porosity estimates were between 0.1 and 0.23. It is worth mentioning, that the upper value of 0.23 is not consistent with the porosity estimates gained by laboratory tests.
- Better matches of the data are achieved, when a finite residual gas saturation is assumed.
- The estimated gas entry pressure of approximately 0.8 MPa matches the results of diagnostic analysis (chapter 5.4) quite well.
- The permeability estimates derived from the interpretation of the gas test sequences are by a factor of 2 to 3 higher than those from the analysis of the hydraulic test prior to gas testing.
- During the GIS test event the gas penetrates not more than a few centimeters into the rock formation. Assuming a uniform radial gas flow through the entire length of the test interval (length: 4.5 m) the gas front is expected to propagate less than 5 cm.

Figure 5.7 shows two simulations of the entire hydrotest and gas threshold pressure test sequence on the basis of the parameter estimates from the gas threshold pressure test analysis. The impact of test interval compressibility from the hydrotest analysis is highlighted, the other parameters being those obtained with the GTP analysis.

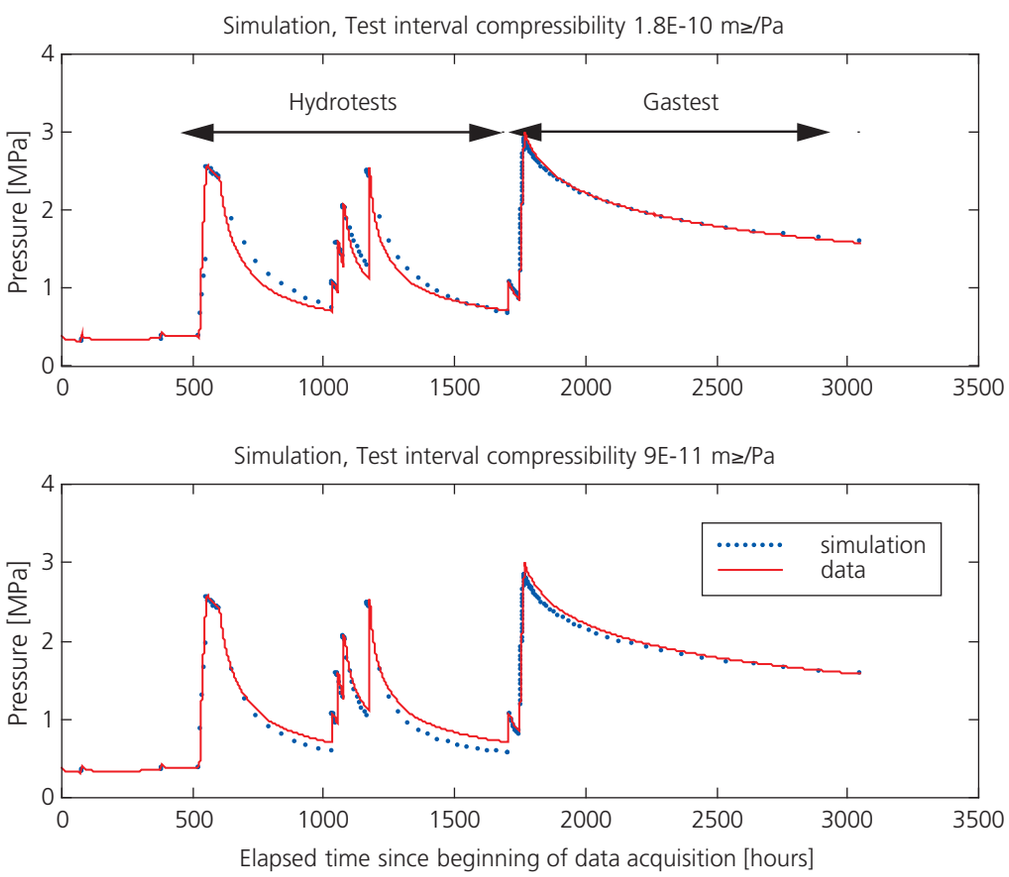

Figure 5.7: Modelling of the extended gas threshold pressure test in interval I4.2 of borehole BGP-4 with a two-phase flow simulator. Note that the entire test sequence is modelled, consisting of a hydrotest, a constant rate gas injection phase and a recovery phase (after TN 98-25).

Concluding remarks

Simulations conducted in the framework of two-phase modelling of the gas threshold pressure test, reproduce the pressure and flow transients observed in test interval BGP-4/I2 satisfactorily. Permeability estimates also compare fairly well with the results of hydraulic testing. Nevertheless, inverse modelling of two-phase flow processes represents an ill-posed problem with non-unique solutions. Consequently, the reliability of parameter estimates and model predictions may be very limited, even if the model calibrations match the data in an acceptable manner.
A way out of this ambiguity is to constrain the problem by introducing independent evidences such as laboratory measurements of porosity, equivalent pore radii (e.g. nitrogen adsorption/desorption), permeability and capillary pressure. Furthermore, a careful analysis of (missing) crosshole responses may help to discard some of the possible solutions. Since the two-phase flow modelling exercise was completed by the end of Phase 3, the geoscientific data base has been broadened significantly and the new evidences might be beneficial in constraining the conceptual uncertainties in two-phase flow modelling. Even so, based on the achievements of this study, the two-phase flow approach seems to be a promising tool for quantitatively characterising gas migration processes in the Opalinus Clay.

5.5.2 Hydro-mechanical modelling of the BGS-2 gas injection experiment Objectives

A summary and chronology of the BGS-2 testing activities, including the hydrotests performed prior to the long-term gas injection test, are reported in TN 00-06, TN 00-07 and in Enachescu et al. (2002). The long-term gas injection test sequence was also subjected to a detailed two-phase flow analysis, combined with simulations of hydro-mechanical coupled processes (Senger et al. 2002). The objectives of the BGP-2 long-term gas test interpretation were:

– to interpret the test in terms of constitutive relationships, i.e. relative permeability and capillary pressure, based on the conceptual framework of two-phase flow in an Equivalent Poro-elastic Medium (EPM) and taking into account the results of the hydrotest interpretations (Enachescu et al. 2002).
– to assess the potential of coupled hydro-mechanical approaches for improving the conceptual understanding of gas migration processes in the Opalinus Clay.

Interpretation procedure and results

The interpretation of the gas test consisted of three major elements (Senger et al. 2002):

1) Analysis of the hydrotest sequence using both diagnostic graphical representations and numerical welltest simulators. A standard hydrotest analysis was conducted of the Hydro-1 test phase using nSight (Avis 2000; updated Windows Version of GTFM) to perform an inverse simulation of the pressure response to the entire test sequence in BGS-2/I2.
2) Two-phase flow simulations of the gas test with ITOUGH2. For consistency, both the hydrotest and gas test sequence were analysed by inverse modelling. The initial estimates for hydraulic properties were based on the results from the hydrotest and appropriate estimates of two-phase flow parameters.
3) Modelling of pressure transients in BGS-1 and BGS-2 and simulation of mechanical responses in the adjacent boreholes BGS-3 and BGS-4 with a fully coupled hydro-mechanical model (GEOSIM, Settari et al. 1999). The results of the Hydro 1 and Gas 1 analyses served as a baseline. The aim of the coupled hydro-mechanical two-phase flow simulation is to identify potential changes in the hydraulic and two-phase flow properties during the gas test that can be related to the displacements observed in BGS-3 and BGS-4.

The analysis of the hydrotest sequence was carried out using the borehole simulators nSight and ITOUGH2. Both codes can be operated in an inverse modelling mode. The best-fit parameters were obtained by inverse simulation of the Cartesian pressure response in BGS-2/I2. Best-fit intrinsic permeability estimates of 1.2×10^{-20} m^2 (nSight) and 2.2×10^{-20} m^2 (ITOUGH2) were determined. The small deviations between the best-fit estimates arise from a slightly different formulation of the storage coefficent in the two codes. Similar to the hydrotest analysis, the gas test was analysed through inverse modelling in a radially-symmetric numerical model using the two-phase flow code ITOUGH2. For the inverse simulation of the gas test sequence, three parameters were estimated, including the permeability and pore compressibility of the formation and the air-entry pressure (P_{ae}) as defined in the van Genuchten two-phase flow parameter model. Other two-phase flow parameters were considered too insensitive to yield well constrained parameters. The results of the inverse simulation indicate a noticeable increase in permeability between the

hydrotest sequence ($k = 2.2 \times 10^{-20}$ m^2) and the gas test sequence ($k = 5.4 \times 10^{-20}$ m^2). The estimated air-entry pressure value (P_{ae} = 148 kPa) was surprisingly low and may not be representative for the undisturbed rock properties: Due to technical problems prior to the first pressure step of the gas test (cf. Figure 5.4), pre-test desaturation of the rock in the vicinity of the borehole cannot be fully ruled out. The first gas test event with its constant pressure plateau may suggest a representative gas entry pressure of about 0.5 MPa. The other two-phase parameters of the van Genuchten model were assumed (i.e., residual water saturation S_{rw} = 0.2, residual gas saturation S_{rg} = 0.001, van Genuchten parameter n = 3). Figure 5.8 shows the results of three simulations of the gas test sequence with different intrinsic permeabilities.

To assess the potential effects of geomechanical processes, the hydrotest and gas test sequences in BGS-2 were simulated with the coupled hydro-mechanical code GEOSIM. Both the hydraulic and two-phase pressure responses in BGS-2 were considered, as well as the geomechanical responses observed in BGS-3 and BGS-4. The focus of the coupled hydro-mechanical analysis under single-phase liquid and two-phase conditions was on improving the process understanding rather than on obtaining a perfect fit of the observed test data. Of special interest were evidences for stress-permeability relationships. For the coupled hydro-mechanical model, the test configuration was implemented in a 3D mesh geometry with the main coordinate axes parallel to the bedding plane and to the borehole orientation, respectively. The boreholes were explicitly gridded such that the stresses and displacements could be accurately calculated in the near-wellbore region. Due to the lack of a solidified data base of rock stress, isotropic stress conditions were assumed.

There are a number of constitutive relations for different rock materials describing the geomechanical behavior in response to stress changes. However, only a limited number of constitutive models exist which relate changes in stress/strain to changes in hydraulic properties. Those models are typically applied to fractured rock whereby the displacements are related to changes in fracture aperture and a corresponding change in fracture permeability (see Stephanson et al. 1996). For this study, an empirical relationship was used based on the inferred increase in permeability during the gas test sequence. The test data suggest that the permeability increase associated with the rock

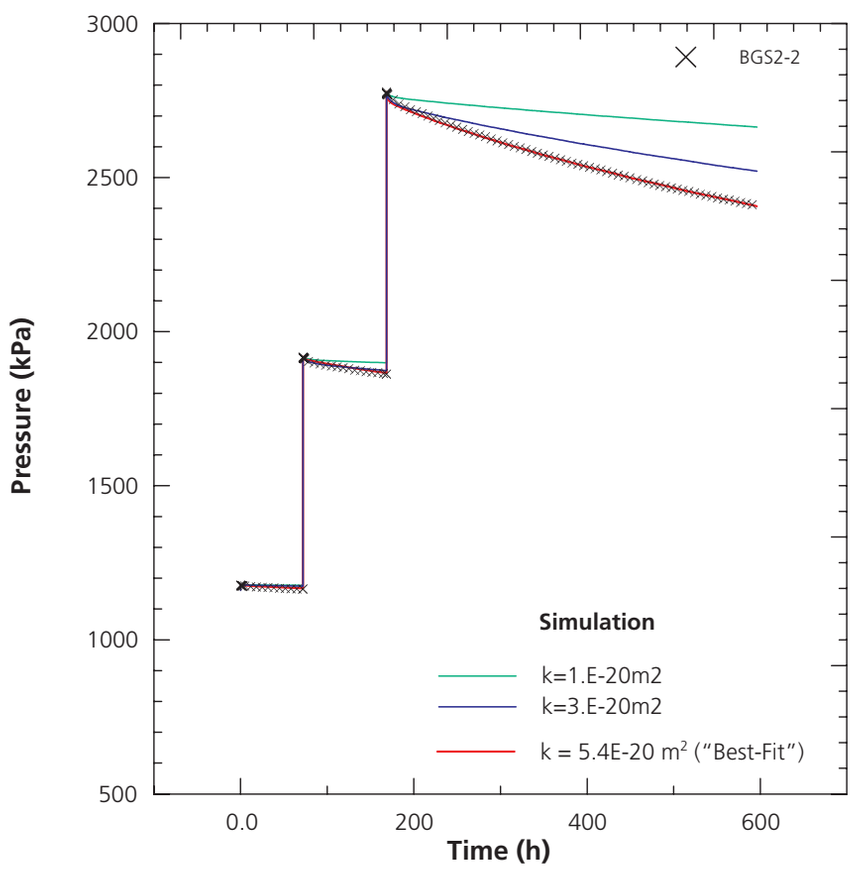

Figure 5.8: Modelling of the gas test sequence in BGS-2/I2 with TOUGH2. The sensitivity of the pressure response to the variation of intrinsic permeability is shown. The third pressure step is most sensitive to permeability. The best-fit intrinsic permeability is 2 to 3 times higher than the best-fit permeability, determined from hydrotest analysis (after Senger et al. 2002).

dilation occurs above a pressure of about 2000 kPa. After the pulse withdrawal test following the last gas pressure event (cf. Figure 5.4), the FIM F3.2 data level off without noticeable rebound suggesting that dilation and the higher permeability are maintained. The resulting change in gas and fluid pressure and the spatial extent of the pressure perturbation away from the injection interval affect the stress distribution which, in turn, causes a geomechanical response as observed in the FIM records.

A number of triaxial tests on the geomechanical behavior of Opalinus Clay cores indicated predominantly elastic properties (TN 98-35, TN 98-55). On the other hand, geomechanical analyses of laboratory tests (TN 98-56) also indicated non-linear elastic behavior as represented by a hyperbolic constitutive model with a stress-dependent elasticity modulus E. For the expected range in differential pressure during the gas test sequence, the hyperbolic constitutive model given in TN 98-56, which was used in the hydro-mechanical analyses (cf. chapter 4.4.3), indicates an overall linear behavior. For this reason, the base case for the subsequent hydro-mechanical models assumed a linearly elastic geomechanical behavior based on an E modulus of 6 GPa (TN 98-49) which is in the range of the corresponding pore compressibilities estimated from the hydraulic tests and gas tests. For the hydraulic and two-phase flow parameters, the best-fit permeability of 2.2×10^{-20} m^2 from the hydrotest was used as initial value and a pressure-dependent permeability increase was assumed such that the permeability increased from 2.2×10^{-20} m^2 below 2000 kPa to 5.4×10^{-20} m^2 at 2800 kPa that corresponds to the best-fit permeability value from the gas test. The permeability increase was assumed to occur uniformly over the entire test-zone interval connecting BGS-2/I2, BGS-1/I2, BGS-3/F3.2 and BGS-4/F4.2. Vertical permeability in the 3D model was assumed to be one order of magnitude lower than the horizontal permeability. The pressure responses in BGS-2/I2, BGS-1/I2 and BGS-3/F3.2 as well as the calculated displacements parallel to the borehole axis for the corresponding FIM zones in BGS-3 and BGS-4 are shown in Figure 5.9 for the gas test in comparison to the measured data. The

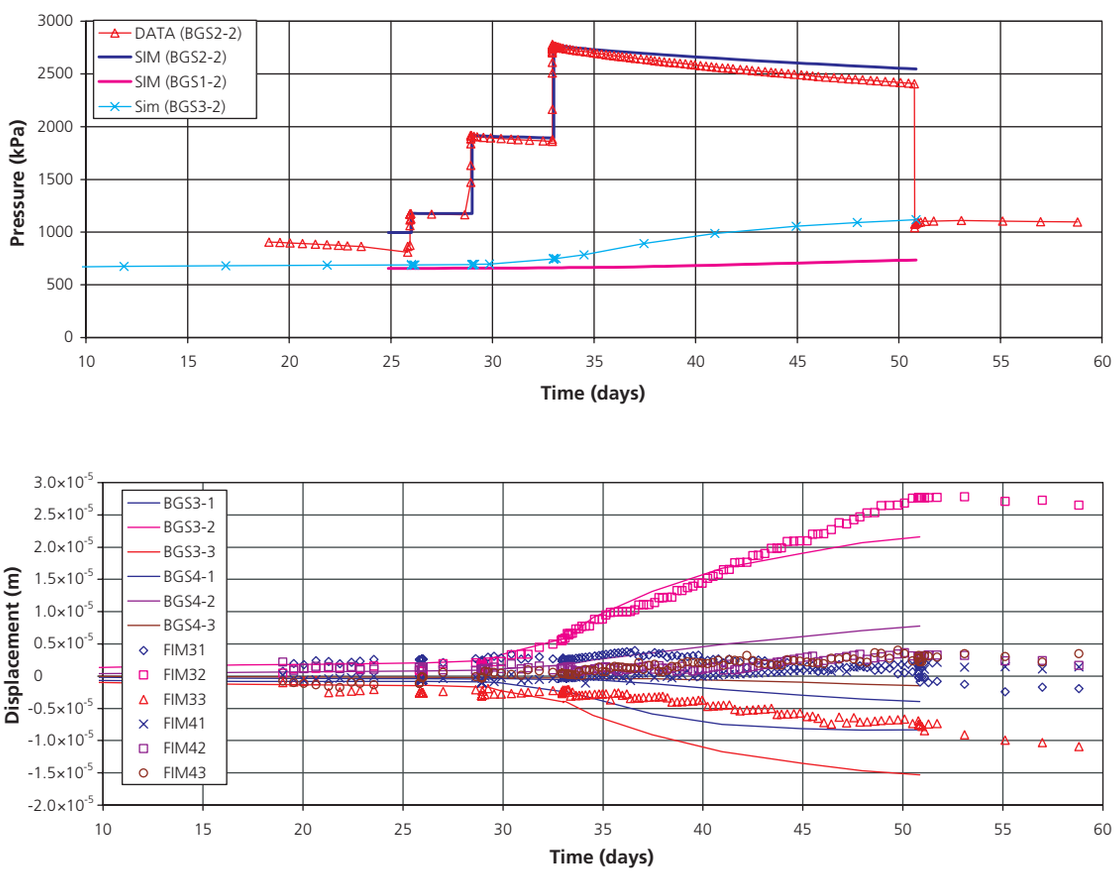

Figure 5.9: Coupled 3D hydro-mechanical simulation: Pressure history in BGS-2/I2, BGS-1/I2 and BGS-2/I3, and FIM data in boreholes BGS-3 and BGS-4. Assumptions: Pressure-dependent permeability over the entire test interval, linear-elastic geomechanical model with an E modulus of 6 GPa (after Senger et al. 2002).

simulated pressures show a reasonably good fit but show less pressure decline during the last pressure step. The corresponding simulated displacements indicate dilation for FIM F3.2 and FIM F4.2, and general compression for the adjacent FIM zones. This compares well with the data, though the magnitude of compression is noticeably greater than the corresponding FIM data. The largest displacements are calculated for the FIM F3.2 zone showing a relatively good fit during the first and the second pressure steps and the early part of the third step. The simulated displacement curve for FIM F3.2 shows a concave shape, with decreasing amounts of dilation, whereas the corresponding FIM F3.2 records indicate a nearly linear increase during the last pressure step.
Several other modelling cases were assessed including a scenario with a limited flow domain ("fracture" model) and a hyperbolic elastic behavior. None of these models showed a significant improvement in the overall performance.

5.6 Evaluation of achievements

In the course of Phases 1 to 5 of the Mont Terri project, a considerable number of laboratory and field experiments were conducted in the general goal of improving the understanding of gas migration processes in the Opalinus Clay. The studies emphasised on

- Improving the conceptual understanding of gas flow mechanisms in the Opalinus Clay.
- Deriving effective parameters to characterise these gas flow mechanisms.
- Assessing possible alterations of rock properties as a consequence of a passed gas phase.

Gas flow mechanisms and effective parameters

Without exception the gas related experiments at Mont Terri have shown that gas transport in the Opalinus Clay starts at low gas pressures, typically in the range 0.2–1 MPa. These pressures are significantly lower than the frac pressure required for macroscopic rock failure to occur. The hydro-frac experiments carried out in borehole BGS-2 (cf. chapter 5.4.4) demonstrate that frac pressures in the order of 9 MPa may be expected. The presumed stress magnitude perpendicular to bedding is in the range of 4–5 MPa.
At low gas pressures, the most probable mechanisms for gas transport are visco-capillary displacement of the porewater (two-phase flow) and microscopic pathway dilation. Two-phase flow is a non-dilatant process whereby the rock matrix is subjected to small elastic deformations rather than irreversible dilation as the gas migrates through. Evidences for two-phase flow processes at low pressures were found in several in-situ experiments such as the gas testing in boreholes BGP-4, BGP-6, BGS-2). The intrinsic rock permeability was determined by laboratory and in-situ tests. The typical range is between 1×10^{-19} and 5×10^{-21} m^2. The measured gas entry pressure ranges between 0.2 and 1.3 MPa. Other two-phase flow parameters like the residual water saturation and gas saturation or the pore size factor are quite uncertain. Laboratory experiments indicate, for example, that residual water saturation may be quite high with a value > 0.8.Microscopic pathway dilation is linked to measurable irreversible deformation. Clear evidence was observed during the in-situ gas tests in boreholes BGS-2 and BGP-6. At gas injection pressures above 2 MPa, significant deformation was measured in the adjacent boreholes. Furthermore, a pressure-dependent rock-permeability was measured. The enhancement factor with respect to the intrinsic permeability (two-phase flow) was up to 2.5 (for a gas pressure of 2.5 MPa).

Alterations of the host rock properties

It is not expected that the two-phase flow processes will significantly affect the hydraulic properties of the Opalinus Clay. Two-phase flow is a non-dilatant process. Therefore, porosity does not change significantly during the passage of a gas phase. In laboratory experiments (cf. chapter 5.4.1), no changes of hydraulic conductivity were detected with respect to before and after gas injection.
In contrast, microscopic pathway dilation is a dilatant process and, therefore, might cause an enhancement of intrinsic permeability. In the GP and GS experiments, hydraulic tests were performed in boreholes BGP-6 and BGS-2 before and after the gas injection tests were conducted. A change in the hydraulic conductivity was not identifiable.

6 Summary and Conclusions

At the onset of the Mont Terri project in 1996, experience with hydrogeological testing procedures in clay-rich formations and the data base for the Opalinus Clay was scant. Over the course of Phases 1 to 4 of the Mont Terri research program, a broad geoscientific data base was compiled and a series of site investigation methods was applied. The latter were, to a large extent, adaptations from hard rock exploration both in terms of the equipment, such as hydraulic long-term monitoring systems, and of the hydrotest analysis and interpretation approaches, e.g. petroleum welltest simulators. Phase 5 introduced a new aspect to the research program: an overall review of the data acquired up until then and their interdisciplinary interpretation. The subjects of this publication are the hydrogeologically relevant investigation methods and data. The report's structure follows the particular points of concern:

- Assessment of the achievements of the hydrogeological investigations both in terms of *development of investigation techniques* and in terms of geoscientific *data analysis*
- Development of a *conceptual model of groundwater flow* at the Mont Terri site
- Development of a *conceptual model of gas migration mechanisms* in the Opalinus Clay

As part of the Hydrogeological Analyses (HA) project, the final objective is to provide a first comprehensive synthesis of the hydrogeological setting of the Mont Terri site based on the workings of Phases 1 through 5.

6.1 Summary of achievements

Phases 1 through 5 of the Mont Terri project saw the execution of many experiments for a variety of different purposes. Key aspects of the *hydrogeological investigations* were (i) the development and testing of site characterisation techniques for clay-rich media, (ii) the demonstration of the barrier function of the Opalinus Clay on the site scale and (iii) the advancement of the understanding of gas transport mechanisms in the Opalinus Clay. Some of the key achievements are high-lighted here:

- A quality assurance procedure ("suitability assessment", cf. chapter 3.2) was implemented, aimed at identifying and assessing those Mont Terri Technical Notes which convey hydraulically relevant information. The QA procedure was designed as a predefined and traceable procedure, equally applicable to all experiments conducted at the Mont Terri rock laboratory. It is recommended that this procedure be adopted for the QA of all hydrogeological data acquired in future phases.
- Different types of hydraulic long-term monitoring systems were tested in boreholes at the Mont Terri rock laboratory, e.g. classical inflatable multipacker systems, the PP system and minipacker piezometers. Even though each system had been designed for specific modes of application, certain clay-specific design criteria are advised to be considered by all (cf. chapter 3.3). Particularly relevant specifications are (i) the minimisation of the effective volume of the observation interval, (ii) the introduction of mechanical support along the entire observation interval to prevent borehole collapse, (iii) an appropriate selection of the materials for the downhole equipment to prevent corrosion and to allow for representative porewater sampling.
- Extensive experimental efforts were undertaken to assess for possible artefacts in the results of hydraulic packer testing as a consequence of the drilling techniques (e.g. drilling fluids) and testing methodologies (e.g. borehole history, test fluid; cf. chapter 3.4) applied. The experiments demonstrated that chemico-osmotic effects may have a minor impact on the transmissivity of the "inner zone", i.e. the zone immediately surrounding the borehole. However, the estimates of the formation properties are not affected significantly. Test perturbations were apparent in the borehole which had been drilled with air.
- A preliminary conceptual hydrogeological model of the Mont Terri site was developed and the understanding of the groundwater flow regime has been enhanced (cf. chapter 4.6). The hydrogeological units of main concern for the underground laboratory and its vicinity are the karstified "Lower Dogger" aquifer and the Opalinus Clay formation, a highly efficient flow barrier. The hydraulic significance of the Jurensis Marls and Posidonia Shales to the North has not been established very well. The main fault, which intersects the rock laboratory, does not affect the barrier function of the Opalinus Clay. The hydraulic conductivity of the Opalinus Clay generally shows low spatial variability and lies in the range of 2×10^{-14} – 2×10^{-12} m/s. The expected range of specific storage is 4×10^{-7} – 3×10^{-5} 1/m. The primary driving force for porewater flow in the Opalinus Clay at the Mont Terri site is gravity: the long-term observations of hydraulic head depict a clear cone of depression towards the gallery system. Furthermore, the "Lower Dogger" aquifer to the South represents a sort of constant pressure boundary for the hydraulic system.

– The investigations of gas transport mechanisms focussed on both laboratory and in-situ experiments (chapter 5). Experimental evidences are found for non-dilatant (classical two-phase flow) and for dilatant (microscopic and macroscopic fracturing) gas transport. The observed gas entry pressure for the Opalinus Clay was generally low (< 1 MPa). Microscopic pathway dilation with an enhancement of gas permeability was observed at pressures (2 to 3 MPa) considerably lower than the refrac pressure. Hydrofrac experiments exhibited frac pressures of 9 MPa and refrac pressures in the order of 4 to 5 MPa.

6.2 Unresolved issues and outlook

The appreciation of hydraulic formation properties and hydrogeological processes active in the Opalinus Clay has grown substantially throughout Phases 1 to 5 of the Mont Terri research program. Site characterisation techniques and interpretation methods have been consolidated, groundwater flow mechanisms have been assessed successfully and hydraulic formation properties have been determined. Finally, the barrier function of the Opalinus Clay was verified in principle on the site scale.
Nevertheless, some issues of hydrogeological relevance remain unresolved and require further studies:

– The pore pressure distribution in the aquifer systems above and below the Opalinus Clay formation is not well known. In particular, the role of the Jurensis Marls as a potential aquifer system has not been well defined.
– Although the main features of porewater flow and pore-pressure distribution in the Opalinus Clay are understood reasonably well, there are some unresolved questions. The large scale anisotropy in hydraulic conductivity is still uncertain. Furthermore, storage coefficients have been determined only on the scale of laboratory experiments and by packer testing. It is expected that site-scale hydrodynamic models which account for the 3D nature of the groundwater system will undoubtedly enhance the integrated understanding of flow processes active at the Mont Terri site.
– Impact of in-situ stress conditions on pore-pressure distribution and groundwater flow at the site: It is expected that stress re-distribution around the galleries may cause extended zones with enhanced hydraulic conductivity, i.e. so-called "stress-dependent permeability". Furthermore, tight fractures may be activated when the effective stress in the site is lowered (e.g. due to pore pressures or due to stress unloading in the vicinity of the tunnel). In the context of a performance assessment, such permeability or transmissivity enhancement at low effective stress is an issue of high importance because these processes may reduce considerably the barrier function of the Opalinus Clay. Due to the poor understanding of in-situ stress conditions at the site, an assessment of coupled hydro-mechanical processes in the excavation disturbed zone is still premature. The results from the Rock Mechanical Analyses project will likely feed into the future task of conceptualising the hydro-mechanical processes active in the Opalinus Clay.
– Consolidation behavior, permeability-porosity relationships and poro-elastic properties of the Opalinus Clay: Stress-strain relationships under undrained conditions were investigated in various rock mechanical experiments. However, merely a few consolidation tests were carried out under drained conditions. Such experiments are required to better understand the burial history of the site. Laboratory testing, e.g. oedometer tests, isostatic and triaxial cell tests, and in-situ testing are recommended to consolidate the available data base.

7 References

Avis, J. (2001): nSIGHTS well test simulator: Users Manual. Duke Engineering & Services.

Bardot, F., Saada, A., Gaboriau, H. & Villiéras, F. (2001): Sondierbohrung Benken: Textural characterization of Opalinus Clay – Use of nitrogen and water adsorption and desorption isotherms. Unpubl. Nagra Int. Rep., Wettingen, Switzerland.

Bear, J. (1972): Dynamics of fluids in porous media. American Elsevier, New York.

Beauheim, R.L., Roberts, R.M, Dale, T.F.,. Fort, M.D &. Stensrud, W.A. (1993): Hydraulic Testing of Salado Formation Evaporites at the Waste Isolation Pilot Plant Site: Second Interpretive Report. SAND92-0533. Albuquerque, NM: Sandia National Laboratories.

Bock, H. (2001): RA Experiment: Data report on rock mechanics. Mont Terri Project Technical Report TR 2000-02 St-Ursanne, Switzerland.

Bock, H. (2002): RA Experiment: Rock mechanics analyses and synthesis: Conceptual model of the Opalinus Clay. Mont Terri Project Technical Report TR 2001-03 St-Ursanne, Switzerland.

Bouchet, A. & Rassineux, F. (1996): Mineralogical study of four samples of shales from Mont Terri (Switzerland). Rapp. ERM 96 151 AB 325, Réf. ANDRA B RP 0.ERM 96-009.

Bradley, G., Croisé, J., Enachescu, C., Horseman, S.T., Jefferies, M., Lavanchy, J.M., Noy, D.& Shuttle, D. (1998): Sondierbohrung Benken – Scoping Study of the Hydraulic Testing in the Opalinus Clay. Unpubl. NAGRA Int. Rep., Wettingen, Switzerland.

Brooks, R.H. & Corey, A.T. (1964): Hydraulic properties of porous media, Hydrol. Pap., 3, 1-27, Colo. State Univ., Fort Collins, USA.

Burdine, N.T. (1953): Relative permeability calculations from pore-size distribution data. Trans. Amer. Inst. Min. Metall. Pet. Eng., 198, 71-78.

Corey, A. (1994): Mechanics of immiscible fluids in porous media. Ed. Water Resources publication, Third Edition, Colorado, USA.

Croisé, J., Marschall, P.& Senger R. (1998): Gas-water flow in a shear zone of a granitic formation: interpretation of field experiments. DisTec'98 - Tracer Hydrogeology. Balkema, Rotterdam, Netherlands.

Duke Engineering & Services. (1998): GEOSIM Reservoir / Geomechanical / Fracturing Coupled Modeling System – User Documentation. Duke Engineering & Services (Canada), Inc., Calgary, Canada.

Enachescu, C., Blümling, P., Castelao, A. & Steffen, P. (2002): Mont Terri / GP-A and GS Experiments - Synth. Rep. Unpubl. Nagra Int. Rep., Wettingen, Switzerland.

Fritz, S.J. (1986): Ideality of clay membranes in osmotic processes: A review. Clays & Clay Mins. 34(2), 214-223.

Greenberg, J.A., Mitchell, J.K. & Witherspoon, P.A. (1973): Coupled Salt and Water Flows in a Groundwater Basin. Journal of Geophysical Research 78 (27), 6341-6353.

Hanshaw, B.B. (1962): Membrane properties of compacted clays. Ph. D., Harvard University, USA.

Harrington, J.F., Horseman, S.T. & Noy D.J.. (2001): Swelling and osmotic flow in a potential host rock. Process assessment and scenario studies. 6th Int. Workshop Key Issues on Waste Isolation Research, Paris, 11/2001.

Horseman, S.T., Alexander, J. & Holmes, D.C.. (1991): Implications of Long-Term Transient Flow, Coupled Flow and Borehole Effects on Hydrogeological Testing in the Opalinus Clay: Preliminary Study with Scoping Calculations. NAGRA Technical Report 91-16, Wettingen, Switzerland.

Horseman, S.T., Higgo, J.J.W., Alexander, J. & Harrington, J.F. (1996): Water, Gas, and Solute Movement through Argillaceous Media. NEA Working Group on Measurement and Physical Understanding of Groundwater Flow Through Argillaceous Media. Report CC-96/1.

Marschall, P., Croisé, J., Fischer, U., Senger, R. & Wyss, E. (1998): Gas flow through water-saturated shear zones: field and laboratory experiments and their interpretation. Proceedings of the 21st Int. Symposium on the Scientific Basis for Nuclear Waste Management - MRS '97. Davos, Switzerland.

Martin, D. & Lanyon, B., with contributions of Blümling P. & Bossart, P. (2004): EDZ in Clay Shale: Mont Terri Rock Laboratory. Mont Terri Project Technical Report TR 2001-01, St-Ursanne, Switzerland.

de Marsily, G. (1986): Quantitative hydrogeology. Academic Press, New York.

Mazurek, M. (2001): Sprödstrukturen und potentielle Migrationspfade im Opalinuston und seinen Rahmengesteinen. Unpubl. Nagra Int. Rep., Wettingen, Switzerland.

Miller, R.J. and Low, P.F. (1963): Threshold gradient for water flow in clay systems. Soil Society of America Proc., 27/6.

Mualem, Y. (1976): A new model for predicting the hydraulic conductivity of unsaturated porous media, Water Resour. Res., 12(6), 513-522.

Nagra (2002): Projekt Opalinuston – Synthese der geowissenschaftlichen Untersuchungsergebnisse. Entsorgungsnachweis für abgebrannte Brennelemente, verglaste hochaktive sowie langlebige mittelaktive Abfälle. Nagra Technical Report NTB 02-03, Wettingen, Switzerland.

Neuzil, C.E. (1994): Characterization of flow properties, driving forces and pore-water chemistry in the ultra-low permeability Pierre Shale, North America.

OECD/NEA Workshop on the Determination of Hydraulic and Hydrochemical Characteristics of Argillaceous Rocks, Nottingham, UK. IBSN 92-64-14485-4.

NEUZIL, C.E. (2000): Osmotic generation of 'anomalous' fluid pressures in geological environments. Nature, 403.

PEARSON, F.J., ARCOS, D., BATH, A., BOISSON, J.-Y., FERNÁNDEZ, A.M., GAEBLER, H.E., GAUCHER, E., GAUTSCHI, A., GRIFFAULT, L., HERNAN,P & WABER H.N. (2004). Geochemistry of water in the Opalinus Clay formation at the Mont Terri Rock Laboratory. Berichte des BWG – Serie Geologie, No. 5, Bern, Switzerland.

PICKENS, J.F., GRISAK,, G.E., AVIS, J.D., BELANGER, D.W. &. THURY, M. (1987): Analysis and Interpretation of Borehole Hydraulic Tests in Deep boreholes: Principles, Model Development and Applications. Water Resources Research, 23/7, 1341-1375.

PRUESS, K. (1987, 1991): TOUGH, TOUGH2, User's Manual. Report LBL-20700, Lawrence Berkeley Laboratory, University of California, Berkeley, CA, USA.

SENGER, R., MARSCHALL, P.& LAVANCHY, J.M.. (1998): Gas threshold pressure tests in deep boreholes for determining two-phase flow properties of the host rock at the proposed L/ILW repository, Switzerland. Proceedings of the 21st Int. Symposium on the Scientific Basis for Nuclear Waste Management - MRS '97. Davos, Switzerland.

SENGER, R., DOMSKI, P. & WALTERS, D. (2002): OPA Geosynthesis: Coupled processes associated with gas flow through Opalinus Clay. Unpubl. Nagra Int. Rep., Wettingen, Switzerland.

SETTARI, A. &. WALTERS, D.A. (2001): Advances in coupled geomechanical and reservoir modeling with applications to reservoir compaction. Society of Petroleum Engineers, Paper SPE 51927.

SOLER, J.M. (1999): Coupled transport phenomena in the Opalinus Clay: Implications for radionuclide transport. Nagra Technical Report NTB 99-09, Wettingen, Switzerland.

STEPHANSON, O., JIN, L., & TSANG, C.F. (1996): Coupled Thermo-Hydro-Mechanical Processes of Fractured Media: Mathematical and Experimental Study, in, Developments in Geotechnical Engineering, 79. Elsevier, Amsterdam.

SWARTZENDRUBER, D. (1962a): Non-Darcy flow behaviour in liquid-saturated porous media. J. Geophys. Res. 67/13.

SWARTZENDRUBER, D. (1962b): Modification of Darcy's law for the flow of water in soils. Soil Sciences 93/1.

THURY, M. & BOSSART, P. (1999): The Mont Terri rock laboratory, a new international research project in a Mesozoic shale formation, in Switzerland. Engineering Geol. 52, 347-359.

THURY, M. & BOSSART, P., eds. (1999): Mont Terri rock laboratory. Results of the hydrogeological, geochemical and geotechnical experiments performed in 1996 and 1997. Swiss National Hydrological and Geological Survey, Geological Report No. 23, Bern, Switzerland.

VALKO, P. & ECONOMIDES, M.J. (1997): Hydraulic fracture mechanics. John Wiley, New York.

VAN GENUCHTEN, M.TH. (1980): A closed-form equation for predicting the hydraulic conductivity of unsaturated soils. Soil Sci. Soc. Amer. J., 44, 892-898.

VAN OORT, E. (1994): A novel technique for the introduction of drilling fluid induced borehole instability in shales. In: Eurock '94, Rotterdam, Holland. Balkema, 293-308.

VINARD, P. & MCCORD, J. (1991): Factors Possibly Affecting Formation Static Pressure Estimates at Wellenberg. Unpubl. Nagra Int. Rep., Wettingen, Switzerland.

VOIGT, H.D. & BAMBERG, H.F.. (1995): Hydrodynamische Eigenschaften poröser Medien. In: Geohydrodynamische Erkundung von Erdöl-, Erdgas- und Grundwasser-Lagerstätten (F. Häfner, H.D. Voigt, H.F. Bamberg, M. Lauterbach, eds.), Wissenschaftlich-Technischer Informationsdienst, Zentrales Geologisches Institut Berlin, Jahrgang 26/1995 – Heft 1. Berlin, Deutschland.

WAWERSIK, W.R., CARLSON, L.W., HENFLING, J.A., BORNS, D.J.,. BEAUHEIM, R.L, HOWARD, C.L. & ROBERTS, R.M. (1997): Hydraulic Fracturing Tests in Anhydrite Interbeds in the WIPP, Marker Beds 139 and 140. SAND95-0596. Albuquerque, NM: Sandia National Laboratories.

WERMEILLE, S. & BOSSART, P. (1999) : Paleohydrological study on the surroundings of the Mont Terri Rock Laboratory. Mont Terri Project Technical Report TR 99-01, Institut Géotechnique SA, St-Ursanne.

WONG, S.W. & HEIDUG, W.K. (1994): Borehole stability in shales: A constitutive model for the mechanical and chemical effects of drilling fluid invasion. In: Eurock '94, Rotterdam, Holland. Balkema, 251-257.

WOOD, D.M. (1990): Soil behaviour and critical state soil mechanics. Cambridge University Press.

YOUNG, A. &. LOW, P.F. (1965): Osmosis in argillaceous rocks. Am. Assoc. Pet. Geol. 49(7), 1004-1008.

Mont Terri Technical Notes

TN 96-02: A. Möri & M. Adler: Small scale mapping of niches (Excavation work during phase 1, spring 1996). Geotechnical Institute; Mont Terri internal, unpublished report.

TN 96-03: Straumann et al.: Excavation of phase 1 niches: technical and engineering aspects. E+B; Mont Terri internal, unpublished report.

TN 96-04: H. Dollinger & A. Möri: Phase 1 drilling and field mapping of drillcores. Geotechnical Institute; Mont Terri internal, unpublished report.
TN 96-05: P. Holub "Borehole logging, Phase 1". Geotest; Mont Terri internal, unpublished report.
TN 96-11: P. Bossart & M. Adler: Fluid logging and borehole fluid effects (experiments FM-A and BF). Geotechnical Institute; Mont Terri internal, unpublished report.
TN 96-17: A. Rübel, J. Lippmann, K. Osenbrück & Ch. Sonntag: Stable isotopes and noble gases in pore water and rock samples of the Opalinus Clay at Mt. Terri (WA-B experiment) – Part I: Stable isotopes and noble gases in pore water". Institut für Umweltphysik, Universität Heidelberg. B.E. Lehmann & I.N. Tolstikhin: Part II: Helium and argon isotopes in rock samples. Physics Institute of the University of Berne & Geological Institute of the Kola Science Centre in Apatity, Russia; Mont Terri internal, unpublished report.
TN 96-18: E. Wyss: GP (phase 1): Screening pulse tests in BGP-1. Solexperts; Mont Terri internal, unpublished report.
TN 96-20: H. Dollinger, P. Bossart & Ch. Bühler: DT Drilling technique, Phase 1. Geotechnical Insitute & Solexperts; Mont Terri internal, unpublished report.
TN 96-21: S.T. Horseman: Guidelines for chemico-osmotic experiments in OPA. British Geological Survey; Mont Terri internal, unpublished report.
TN 96-26: E. Wyss: GP (phase 1): Triple packer system and pressure recovery period PSR1. Solexperts; Mont Terri internal, unpublished report.
TN 96-27: E. Wyss: GP (phase 1): Hydraulic test sequences RI1-RIS1, PSR2, PSR3 & RI1-RIS2. Solexperts; Mont Terri internal, unpublished report.
TN 96-30: K. Watanabe & H. Kazama: Preliminary analysis of evaporation measurements in the Mont Terri Laboratory (Nov. 28 – Dec. 4 1996). Saitama University, Faculty of Engineering, Japan; Mont Terri internal, unpublished report.
TN 97-01: G. Volckaert & T. Fierz: PP Experiment: design & functional tests. SCK·CEN & Solexperts; Mont Terri internal, unpublished report.
TN 97-02: G. Volckaert & T. Fierz: PP Experiment: preliminary in situ test. SCK·CEN & Solexperts; Mont Terri internal, unpublished report.
TN 97-03: G. Volckaert & T. Fierz: PP Experiment: in situ installation and first results. SCK·CEN & Solexperts; Mont Terri internal, unpublished report.
TN 97-04: A. Möri, M. Adler & S. Wermeille: Phase 2 drilling and field mapping of drillcores. Geotechnical Institute; Mont Terri internal, unpublished report.
TN 97-06: B. Vögtli & P. Bossart: DT Experiment: swelling experiment on OPA drillcores. Geotechnical Institute; Mont Terri internal, unpublished report.
TN 97-07: M. Adler & P. Bossart: FM-A Experiment: Results of fluid logging in borehole BFM-A2. Geotechnical Institute; Mont Terri internal, unpublished report.
TN 97-08: A. Möri & P. Bossart: FM-B: Visualisation of in-situ matrix and flow porosity in the Opalinus Clay. Geotechnical Insitute; Mont Terri internal, unpublished report.
TN 97-18: U. Mäder: Flow mechanisms FM-C: diffusion type laboratory experiments on OPA from Mt. Terri – interim report. Rock-Water Interaction Group, University of Berne; Mont Terri internal, unpublished report.
TN 97-21: A. Rübel, J. Lippmann, K. Osenbrück & Ch. Sonntag: Stable isotopes and noble gases in pore water of the Opalinus Clay at Mt. Terri (WS-B Experiment, Borehole BWS-A3). Institut für Umweltphysik, Universität Heidelberg; Mont Terri internal, unpublished report.
TN 97-24: L. Schwark: WS-B Experiment: Organic geochemical and petrological characterisation of organic matter from the Opalinus Clay at the Mont Terri site. University of Köln; Mont Terri internal, unpublished report.
TN 97-26: J.F. Harrington & S.T. Horseman: Osmotic Pressure Experiment (OP): Scoping experiments on osmotic transport in Opalinus Clay – Interim report. British Geological Survey; Mont Terri internal, unpublished report.
TN 97-28: E. Wyss: Experiment GP, Phase 2: Hydraulic tests and gas threshold pressure test in a major tectonic fault. Solexperts; Mont Terri internal, unpublished report.
TN 97-29: H. Rohler: Experiment GP, Phase 2: Ion-selective borehole logging – Borehole BGP-4. ETH Zürich; Mont Terri internal, unpublished report.
TN 97-32: J. Adams & R. Gemperle: ED-A: Results of hydraulic tests performed with the Modular Mini-Packer System (MMPS). Solexperts; Mont Terri internal, unpublished report.
TN 97-36: P. Holub: Borehole logging, Phase 2. Geotest; Mont Terri internal, unpublished report.
TN 97-38: A. Pasquiou & J.C. Robinet: Hydrodynamic characterization of the Opalinus Clay. Eurogeomat; Mont Terri internal, unpublished report.
TN 97-39: J.F. Harrington & S.T. Horseman: Laboratory experiments on hydraulic and osmotic flow in Opalinus Clay. British Geological Survey; Mont Terri internal, unpublished report.
TN 98-11: K. Watanabe, H. Imai, H. Saegusa & F. Shidahara: Evaporation logging in-situ measurement. Saitama University, Hazama Corporation & PNC;

Mont Terri internal, unpublished report.
TN 98-15: L. Ortiz Amaya: GP Core laboratory tests. SCK·CEN; internal, unpublished report.
TN 98-24: P.S. Domski, R.M. Roberts, R.K. Senger, J. Croisé & J.M. Lavanchy: Analysis of the BGP-1 RI2 & RIS2 and BGP-4 hydrotests conducted at the Mont Terri Rock Laboratory. Duke Engineering and Services & Colenco Power Engineering; Mont Terri internal; unpublished report.
TN 98-25: J.M. Lavanchy & R.K. Senger: GP Experiment: Analysis of the BGP-4 GRI & GRIS gas threshold pressure", J. Croisé, D. Gilby. Colenco Power Engineering & Duke Engineering and Services; Mont Terri internal, unpublished report.
TN 98-35: F. Rummel, Th. Hettkamp & U. Weber: DM Experiment: Laboratory experiments for the determination of deformation mechanisms and a constitutive law for time dependent deformation behavior of the Opalinus Clay (Phase 3). Mesy GmbH, Bochum; Mont Terri internal; unpublished report.
TN 98-40: P. Holub: Borehole logging, Phase 3. Geotest; Mont Terri internal, unpublished report.
TN 98-41: M. Mazurek: Mineralogical composition of Opalinus Clay at Mont Terri – A laboratory intercomparison. University of Berne; Mont Terri internal, unpublished report.
TN 98-46: D.J. Noy: Parameter estimates from 1D modelling of osmotic experiments. British Geological Survey; Mont Terri internal, unpublished report.
TN 98-48: P. Bossart & M. Thury: WS-A Experiment: estimation of hydraulic conductivity based on inflow measurements. Institut Géotechnique & SNGHS; Mont Terri internal, unpublished report.
TN 98-49: M. Hohner & P. Bossart: Geological, mineralogical, geochemical, geomechanical and hydraulic parameters of OPA derived by in-situ and laboratory experiments (Phases 1, 2 and partly 3). University of Barcelona & Geotechnical Institute; Mont Terri internal, unpublished report.
TN 98-55: F. Rummel, Th. Hettkamp, U. Weber: DM Experiment: Laboratory experiments for the determination of deformation mechanisms and a constitutive law for time dependent deformation behavior of the Opalinus Clay (Phase 3). Mesy GmbH, Bochum; Mont Terri internal, unpublished report.
TN 98-56: Konietzky: DM Experiment: Numerical back analysis of triaxial lab tests for the Opalinus Clay. ITASCA; Mont Terri internal, unpublished report.
TN 98-58: T. Fierz: EDB Experiment: Rawdata report – Pore water pressures and deformation measurements. Solexperts; Mont Terri internal, unpublished report.
TN 98-62: C. Enachescu, A. Schmid & J.V. Wozniewicz: DB Experiment: Deep borehole hydraulic testing. Golder Associates; Mont Terri internal, unpublished report.
TN 98-63: H.P. Weber: Deep borehole experiment, geological description of drillcores. NAGRA; Mont Terri internal, unpublished report.
TN 98-64: A. Mais: DI Experiment: mercury porosimetry and H2O determination. University of Fribourg; Mont Terri internal, unpublished report.
TN 99-05: T. Fierz & A. Portmann: GP Experiment: Instrumentation of borehole BGP-5 (Triple Packer System) and borehole BGP-6 (PP Piezometer). Solexperts; Mont Terri internal, unpublished report.
TN 99-06: T. Fierz & M. Eichler: GP Experiment: Instrumentation of boreholes BGP-8 and BGP-9 with FIMs (fix installed micrometers). Solexperts; Mont Terri internal, unpublished report.
TN 99-07: H.R. Fisch & M. Piedevache: GP Experiment (Phase 4): Results of hydraulic testing. Solexperts; Mont Terri internal, unpublished report.
TN 99-08: H.R. Fisch & M. Piedevache: GP Experiment: Results of gas testing. Solexperts; Mont Terri internal, unpublished report.
TN 99-18: A. Rübel, J. Lippmann & Ch. Sonntag: WS-A Experiment: Profiles of stable isotopes and noble gases in pore water across OPA. Institut für Umweltphysik, Universität Heidelberg; Mont Terri internal, unpublished report.
TN 99-20: S. Wermeille, A. Möri, H. Steiger, M. Adler, M. Alig & B. Rathmayr: Phase 4, drilling campaign 4a and 4b: Drilling and field mapping of drillcores. Geotechnical Institute; Mont Terri internal, unpublished report.
TN 99-22: R.T. Haarpaintner & G. Schaeren: Conditions géologiques et hydrogéologiques générales. Bureau Technique Norbert, Géologues-conseils; Mont Terri internal, unpublished report.
TN 99-33: P. Holub: BF Experiment: Caliper and fluid logging. Geotest; Mont Terri internal, unpublished report.
TN 99-49: H.R. Fisch: FM-C Experiment: Results of hydraulic testing in borehole BFM-C1. Solexperts; Mont Terri internal, unpublished report.
TN 99-58: L. Ortiz: GP Experiment: Phases 4 and 5 (1998-2000) – Results of the laboratory hydraulic and gas testing. SCK·CEN; Mont Terri internal, unpublished report.
TN 99-73: Various contributors: Second Mont Terri Workshop (1-4 June 1999): Compilation of abstracts and transparencies. 5 volumes; Mont Terri internal, unpublished report.
TN 99-81: D.J. Noy & S.T. Horseman: OP Experiment: Design calculation. Determination of the osmotic pressure response of borehole BOP-1 to a change of borehole fluid. British Geological Survey; Mont

Terri internal, unpublished report.
TN 2000-01: J.L. Fuentes: HE Experiment: Status report and compilation of field data. AITEMIN; Mont Terri internal, unpublished report.
TN 2000-06: K. Jäggi & P. Steffen: GS and GP-A Experiments: Mobilisation and borehole instrumentation of BGS-1 and BGS-2. SJ Geotec; Mont Terri internal, unpublished report.
TN 2000-07: C. Enachescu, K. Jäggi, A. Schmid & J. Wozniewicz: GP-A Experiment: Pre-frac hydraulic and gas longterm tests in borehole BGS-2. Golder Associates & SJ Geotec; Mont Terri internal, unpublished report.
TN 2000-10: C. Enachescu, K. Jäggi, R.J. Pine & A. Schmid: GS Experiment: Hydraulic fracturing in borehole BGS-2. Golder Associates and SJ Geotec; Mont Terri internal, unpublished report.
TN 2000-11: T. Lagler & V. Siegel: GS Experiment: Optical imaging of BGS-1 and BGS-2. BLM; Mont Terri internal, unpublished report.
TN 2000-12: T. Fierz & R. Wälchli: GS Experiment: Instrumentation of boreholes BGS-3 and BGS-4 with FIMs (Fix Installed Micrometers). Solexperts; Mont Terri internal, unpublished report.
TN 2000-13: T. Fierz: GS Experiment: Deformation measurements in boreholes BGS-3 and BGS-4 with FIMs (Fix Installed Micrometers). Solexperts; Mont Terri internal, unpublished report.
TN 2000-21: R. Senger, P. Domski, D. Walters & T. Settari: HA Experiment: Development of a coupled process model of fluid flow in the Opalinus Clay. Duke Engineering; Mont Terri internal, unpublished report.
TN 2000-22a: L. Schlickenrieder & J. Croisé: HA Experiment: Conceptual Hydrogeological Model of the Site / Part A – Review of the Hydrogeological Data Base. Colenco; Mont Terri internal, unpublished report.
TN 2000-42: H.R. Fisch & P. Bossart: OP Experiment: Fluid exchange in borehole BOP-1 with deionised water. The field data set. Solexperts & Geotechnical Institute; Mont Terri internal, unpublished report.
TN 2000-43: D.J. Noy: OP Experiment: Simulation of fluid exchange carried out in borehole BOP-1". British Geological Survey; Mont Terri internal, unpublished report.
TN 2000-44: D.J. Noy: OP Experiment: Simulation of fluid exchange carried out in borehole BOP-1. British Geological Survey; Mont Terri internal, unpublished report.
TN 2000-58: D. Holton, A.R. Hoch & W.R. Rodwell: Mont Terri hydrogeological analyses: Coupled models of gas flow. AEA Technology; Mont Terri internal, unpublished report.

An Experimental and Modelling Study of Chemico-osmotic Effects in the Opalinus Clay of Switzerland

D.J. Noy, S.T. Horseman, J.F. Harrington, P. Bossart & H.R. Fisch

Mont Terri Project – Hydrogeological Sysnthesis, Osmotic Flow
Reports of the FOWG, Geology Series, No. 6 – Bern 2004

Recommended quotation:
Noy, D. J. et al. (2004): An Experimental and Modelling Study of Chemico-osmotic Effects in the Opalinus Clay of Switzerland. In: Heitzmann, P. (Ed.): Mont Terri Project – Hydrogeological Synthesis, Osmotic Flow (p. 95–126). – Reports of the Federal Office for Water and Geology (FOWG), Geology Series No. 6.

Abstract

This programme of work on osmotic flow in Opalinus Clay comprised three main activities, a laboratory pilot study on samples, an *in situ* experiment in a borehole at the Mt Terri Rock Laboratory and a theoretical study supported by mathematical modelling.
The pilot study demonstrated that the shale behaves as a leaky semi-permeable membrane and that it was possible to generate a measurable flow of water by exposing a sample to a solute concentration gradient in the absence of a pressure gradient.
The equations for chemico-osmotically coupled flow and solute transport developed by Greenberg et. al. (1973) were used to assess the results of the laboratory experiments. Some aspects of the transient flows and the long term swelling behaviour seen in the data cannot be explained by the original equations and a modification to the definition of compressibility was proposed which improved the representation of these transient effects.
The modified equations were then applied to the interpretation of an *in situ* field experiment, undertaken at the Mont Terri Rock Laboratory, in which the fluid chemistry within a sealed borehole test interval was first equilibrated with the host rock pore-water and then changed suddenly for either fresh water or a hypersaline brine. A substantial pressure transient, with a magnitude of several metres of equivalent freshwater head, was observed, lasting for several months, which was due solely to the change of fluid chemistry. Matching the magnitude and duration of the response with the solution to the theoretical model equations provided estimates for the osmotic coupling coefficients of Opalinus Clay.
In addition to demonstrating the magnitude of the chemico-osmotic effects in Opalinus Clay and obtaining estimates for the osmotic efficiency, the study also provided evidence for two further important features of these processes. Firstly, the osmotic efficiency of the *in situ* material is greater than that of a laboratory samples. This may be a consequence of the greater disruption caused to the latter by the sampling process. Secondly, the osmotic efficiency of the *in situ* material is lower at high solute concentrations than when the pore fluid is dilute, confirming observations made by previous researchers.

Acknowledgements

We would like to thank the Mont Terri Partners, who have financed the osmotic pressure experiment, and who were quite generous when the budgets of the experiment were exceeded once again. These are: ANDRA (B. Vignal), IRSN (J.-Y. Boisson), NAGRA (M. Hugi and K. Kennedy) and SCK•CEN (B. Neerdael).- Furthermore we would like to thank the experiment delegates for their encouraging comments and good discussions. These are mainly A. Gautschi from Nagra, J.-M. Matray from IRSN and P. DeCannière from SCK•CEN. This report was reviewed by P. Soler, J.-M. Matray and P. DeCannière. We would like to thank the reviewers for their constructive reviews.

Contents

Abstract 97
Acknowledgements 98
Contents 99
List of tables 100
List of figures 101

1 Introduction 103

2 Theoretical model 106
2.1 Numerical solution 108

3 Laboratory study 110
3.1 Apparatus 110
3.2 Procedures 111
3.3 Test conditions 111
3.4 Results 112

4 Field experiment 115
4.1 Experimental set-up 115
4.2 Procedures 116
4.3 Results 116

5 Interpretation 118
5.1 Laboratory study 118
5.2 Borehole experiment 118

6 Conclusions 124

7 References 125
Mont Terri Technical Notes 126

List of tables

Table 3.1: Results of the controlled flow rate (CFR) test stages on the two specimens 112
Table 3.2: Results of the osmotic flow (OF) test stages on the two specimens 112
Table 4.1 Chemical analyses of the formation water in borehole BWS-A1 and samples of the test fluids.....117
Table 5.1: Summary of parameters used in numerical modelling. Porosity was taken as 0.13 in all computer simulations and (*) refers to concentrations on either side of the laboratory sample NS01. (†) Phase 3 prediction was carried out using all the parameters from the Phase 2 interpretation except that the borehole solute concentration was set to 1.497 mol.dm^{-3} 118

List of figures

Figure 1.1 Plan of the Mt. Terri Underground Rock Laboratory showing the site of the Osmotic Pressure ("OP") Experiment and the sampling location for the laboratory test material in the SHGN niche 103
Figure 3.1: Schematic of the apparatus for the laboratory pilot study.....110
Figure 3.2: Schematic of the pressure vessel and specimen assembly for the laboratory pilot study.....111
Figure 3.3: Osmotic flow transient from stage 2 of NS01. Osmotic flow started shortly after the saline solution at one side of the disc was replaced with distilled water. The flow transient asymptotically approaches the steady-state flow condition 113
Figure 3.4: Volumetric strain against average effective stress for NS01 when subject to the pressure variations of CFR test stages 7 to 11, inclusive. Strain was calculated from net pump flows and corrected for apparatus compliance and the compressibility of liquid in the upstream system.....113
Figure 4.1: Schematic of the equipment for the field experiment in the Mt. Terri Rock Laboratory in Switzerland. Pressure transducers are labelled P1 to P5. 115
Figure 4.2: The pressure evolution for Phase 2, replacement of the test section fluid with de-ionised water. The data have been plotted starting from 1 February 2000 117
Figure 4.3: The pressure evolution for Phase 3, replacement of the test section fluid with hyper-saline brine. The data have been plotted starting from 1 March 2002.....117
Figure 5.1: Model predictions of flows and volumetric strain as a function of time using equations (15) and (21) compared to the data from laboratory pilot study NS01 Stage 2. Negative volumetric strain indicates swelling of the sample (the data for volumetric strain are off scale in this plot, c.f. Figure 5.2).....119
Figure 5.2: Model predictions of flows and volumetric strain as a function of time using equations (25) and (26) compared to the data from laboratory pilot study NS01 Stage 2. Negative volumetric strain indicates swelling of the sample 120
Figure 5.3: Field data from Phase 2 of the BOP-1 borehole experiment compared to the model prediction using an osmotic efficiency derived from the laboratory study (see Table 5.1 - Phase 2 prediction).....121
Figure 5.4: Data from Phase 2 of the BOP-1 borehole experiment compared to the model prediction based on optimised parameters (see Table 5.1) 121
Figure 5.5: Field data from Phase 3 of the BOP-1 borehole experiment compared to the model prediction using optimised parameters derived from the Phase 2 interpretation (see Table 5.1).....122
Figure 5.6: Field data from Phase 3 of the BOP-1 borehole experiment compared to the model prediction based on optimised parameters (see Table 5.1).....122

1 Introduction

This report describes a study of chemico-osmotic effects in the Opalinus Clay formation aimed at estimating its osmotic efficiency. The study is comprised of three experimental stages (one laboratory based and two conducted *in situ*) with theoretical assessment and interpretation of each stages. In addition, the interpretations of the first two stages were used to make blind predictions of the outcomes of the following experimental stage.

The Opalinus Clay is a Middle Jurassic (Aalenian) marine shale which underlies large areas of north-western Switzerland. The formation is being studied by a multi-national consortium of companies as a typical example of a rock-type which might prove suitable as a repository host-medium for the geological disposal of radioactive waste (Thury and Bossart, 1999). Tunnelling operations for the N16 Transjuran Motorway connecting Belfort in France to the Swiss highway network afforded an excellent opportunity for research teams to investigate the hydrogeological, geochemical and geotechnical characteristics of this argillaceous rock formation under representative *in situ* conditions. The 3.9 km long Mt. Terri Tunnel links the towns of Delémont and Porrentruy and passes through a mountain ridge which, in structural geological terms, represents the northernmost anticline of the Jura Mountains. The Mt. Terri Rock Laboratory is located in a tunnel (known as the Security Gallery) driven parallel to the main motorway tunnel and through a 230 m long section of the Opalinus Clay. A number of side-branches (or niches) were excavated in this section to provide suitable sites for experimental work (Figure 1.1). The shale formation dips at between 20° and 60° to the south-east and has a local thickness of around 160 m. The depth below ground surface varies between 250 and 320 m.

The Opalinus Clay at Mont Terri has been divided into five lithostratigraphical sub-units, largely on the basis of shale, sand and carbonate contents (Thury, 1999). The most shaly of these sub-units lies at the base of the formation and is around 80 m thick. It comprises argillaceous and marly shales with micas and nodular, bioturbated layers of marl. Clays and micas make up around 65% of the rock and the typical mineralogical composition is 10% illite-smectite mixed-layer clay, 17% illite, 30% kaolinite, 8% chlorite, 20% quartz, 7% calcite, 3% feldspars, 2% siderite, 1% dolomite/ankerite, 1% pyrite and 0.4% organic carbon. Porosity determined from weight loss by drying at 40°C is in the range 13 to 19%.

Osmosis can be defined as a bulk movement of solvent from a region where a solution has a low concentration of solutes to a region where the solute concentration is greater. Since the additional of solutes lowers both the chemical potential and the activity of the solvent, osmosis can also be interpreted as a flow down the chemical potential gradient of the solvent. In order to obtain osmotic flow, it is necessary to place a semi-permeable membrane between the two solutions. This membrane allows water molecules to pass,

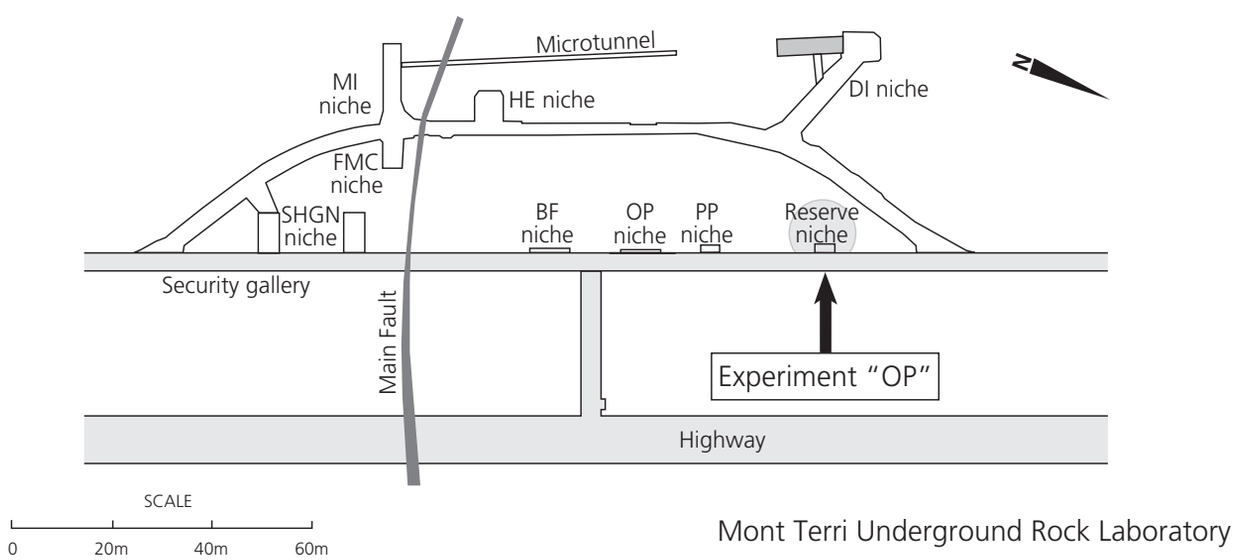

Figure 1.1 Plan of the Mt. Terri Underground Rock Laboratory showing the site of the Osmotic Pressure ("OP") Experiment and the sampling location for the laboratory test material in the SHGN niche.

but restricts the passage of the solute. Chemico-osmosis is a specific example of a variety of so-called "coupled" transport processes in which a flux is driven by a "non-conjugate" thermodynamic force (Fargue et al., 1989; Soler, 1999). Other examples affecting the movement of the liquid phase are thermo-osmosis and electro-osmosis.

The membrane properties of clays are mainly due to electrical restrictions on the movement of the solute ions through the narrow pore spaces between negatively-charged clay mineral surfaces (Fritz, 1986). The charge on the surface of a clay particle together with the charge due to the balancing cations is referred to as the electrical double layer. If the cations are freely diffusing in solution, a very characteristic distribution of charge develops which is termed the diffuse double layer (DDL). Ions within the DDL are subject to two opposing tendencies. Electrostatic forces attract the cations towards the charged surface whereas diffusion tends to make them drift away to regions of lower concentration. Anions behave in the opposite way. Double Layer Theory provides a mathematical framework for the analysis of such problems. The Debye length is a measure of the thickness of the diffuse layer and is found to depend on temperature, the valence of the ions and the concentration of external equilibrium solution (Everett, 1988). When clay particles are in close proximity, the diffuse layers on each surface become overlapped and the negative electrical potential within the pore channels tends to repel any anions that attempt to enter or pass through them. This phenomenon is known as anion or Donnan exclusion (Bolt and de Haan, 1962). During solute transport, the dissociated ions of a salt must move together so as to maintain electroneutrality in the bulk solution. This means that any restriction on the mobility of the anions will also impose a restriction on the movement of the cations. The overall effect is that neutral water molecules can pass through a clay, but the motion of charged species in solution is impeded.

Experimental evidence of membrane behaviour in compact clay systems is now sufficiently conclusive that it cannot be ignored (Hanshaw, 1962; Kemper and Evans, 1963; Young and Low, 1965; Kemper and Rollins, 1966; Letey and Kemper, 1969; Banin and Low, 1971; Greenberg, 1971; Kharaka and Berry, 1973; Fritz and Marine, 1983).

Some of the more recent experimental work on chemico-osmotic effects in shales has been prompted by oil industry concerns about the effect of water-based drilling muds on the stability of exploration and production wells drilled though shale formations (Chenevert, 1970; Sherwood, 1993; Schlemmer et al., 2002). Wong and Heidug (1994) describe a laboratory experiment designed to simulate some of the processes occurring in the borehole. Two porous plates with concave inner surfaces were arranged on opposite curved sides of a 15 mm diameter cylindrical shale sample so as to form two fluid chambers, each in contact with the rock. An axial load was applied to the sample and a constant confining stress was applied to the plates. The two chambers were filled with distilled water at 3.0 MPa pressure. Brine was then introduced into one of the chambers while maintaining the pressure constant. The pressure changes in the other chamber were monitored with time. In the most extreme response reported in this paper, the pressure fell from 3.0 MPa to only 0.2 MPa in around 10 hours. After this initial decline, the pressure gradually increased with time over a period of 200 hours. The authors do not state the salt concentration used in the experiment.

Van Oort (1994) describes a very similar experiment on the Cretaceous Pierre Shale of North America. A cylindrical sample was consolidated in a triaxial cell at a temperature of 65°C and a confining pressure of 5 MPa. Porous discs at each end of the sample enabled a fixed backpressure (i.e. external water pressure) of 0.35 MPa to be applied to the sample during consolidation process. The pressure in the upstream porous disc was then suddenly increased to 3.5 MPa. The pressure in the downstream disc was monitored with time and followed a path which asymptotically approached 3.5 MPa. After a period of about 230 hours it had reached 3.25 MPa. At this time, the fluid in the upstream disc was replaced by a 4.85 $mol.dm^{-3}$ $CaCl_2$ brine, while maintaining the upstream pressure constant. The downstream pressure declined rapidly with time. After about 50 hours it had dropped by 1.95 MPa to around 1.3 MPa. It then slowly increased to 2.05 MPa over the remaining 320 hours or so of the experiment.

These two laboratory experiments confirm that shale samples act as non-ideal osmotic membranes. Water molecules rapidly migrated up the solute concentration gradient causing the low-concentration chamber (or filter) to show a pressure decrease. Because of the non-ideality of the shale membrane, salt was then able to slowly diffuse through the shale in the reverse direction. This gradually eliminated the concentration gradient, so that the osmotic pressure differential between the chambers became smaller with the passage of time.

Neuzil (1994; 2000) reports some field experiments on the effect of osmotic movement of water on head measurements in the Pierre Shale. Four boreholes were drilled, cased and completed with 20 m screens. Waters of differing chemistries were added to these

boreholes. Two contained saline solution (50 g dm^{-3} NaCl), one a solution more or less matched to the pore-water chemistry of the rock (5 g dm^{-3}) and the fourth almost pure water (<0.1 g dm^{-3}). The water levels were monitored for a period of 7 years. The levels in the two boreholes containing the hypersaline solution rose by 3 and 4 metres, respectively. Little change was observed in the borehole containing the pore-water duplicate and there was a small decrease in level (~ 0.2 m) in the hole containing fresh water. Neuzil states "It is clear that osmotic pumping of pore fluids has occurred in this experiment, showing that the Pierre Shale *in situ* has the properties of an osmotic membrane". This is a very important experimental finding and probably represents the first *in situ* experiment to clearly demonstrate the phenomenon of chemico-osmosis in shale. Neuzil also monitored the salinity of each borehole solution with time. The hypersaline solution showed a significant decrease in salinity. The pore-water duplicate showed a fairly minor decrease. In the case of the fresh water, the salinity increased significantly with time. It is clear from the relatively small magnitude of the water level changes with time and the changes in salinity of the borehole fluids that the clay membrane is non-ideal and the osmotic movement of water up the concentration gradient of the pore solution is accompanied by the diffusional transport of ions in the reverse direction.

A number of researchers have suggested that chemico-osmosis might be the source of anomalous heads in some low permeability sedimentary sequences (Berry, 1960; Marine and Fritz, 1981; Neuzil, 2000). Hyperfiltration or reverse-osmosis has also been examined as a possible mechanism affecting brine chemistry in sedimentary basins (Berry, 1960; Coplen and Hanshaw, 1973; Graf, 1982). The implications of osmotic flow to the migration of radionuclides from a repository have also been examined by Soler (1999; 2001).

The theoretical description of the coupled flows have been based upon concepts of irreversible thermodynamics as presented by Kirkwood (1954) for biological membranes. The applicability of these concepts to the coupled flow of solute and water in sedimentary systems was demonstrated by Abd-el-Aziz and Taylor (1964), Letey and Kemper (1969), and Olsen (1969). These ideas have been adapted by Greenberg et. al. (1973) for application to general hydrogeological environments. The equations they developed are used in this report to assess a set of laboratory experimental observations carried out on samples of Opalinus Clay. It is shown that some aspects of the transient flows and the long term swelling behaviour seen in the data cannot be explained by the original equations and a modification to the definition of compressibility is proposed which shows some improvement.

The modified equations are then applied to the interpretation of an *in situ* field experiment, undertaken at the Mont Terri Rock Laboratory, in which the fluid chemistry within a sealed borehole section is first equilibrated with the host rock pore-water and then changed suddenly for first fresh water and then, after a further period of equilibration, for a hypersaline brine. A substantial pressure transient, with a magnitude of several metres of equivalent freshwater head, is observed, lasting for several months, which is due solely to this change of fluid chemistry. Matching the magnitude and duration of the response with the solution to the theoretical model equations provides estimates of the osmotic coupling coefficients for the Opalinus Clay.

In summary, Section 2 of this report describes the theoretical approach used to interpret the chemico-osmotic coupled processes of fluid flow and solute transport. Section 3 outlines the initial laboratory pilot study and its main results, while Section 4 provides details of the three phases of the *in situ* experiment. Section 5 details the steps taken to interpret the various experimental results and Section 6 summarises the main conclusions from the study. During the course of this study a number of Technical Notes were published covering design and manufacture of field and laboratory equipment, development and modification of computer codes, and interim interpretations. A compilation of these notes is provided in the References.

2 Theoretical modell

Following Greenberg et al (1973), we adopt an extension of Darcy's law based on the ideas of irreversible thermodynamics which introduces the effects on groundwater of a solute concentration gradient

$$q = -\frac{k}{\mu}\left(\nabla p + \rho g \hat{z}\right) - k_{hc}\nabla c \tag{1}$$

where q is the volumetric flow rate, k is the intrinsic permeability, μ is the fluid viscosity, ρ is the fluid density, g is the acceleration due to gravity, $\hat{z}$ is a unit vector along the z-axis, k_{hc} is the osmotic coupling coefficient, p is the fluid pressure, and c is the solute concentration. It may be noted that the choice of signs in equation (1) means that k_{hc} will always take a negative value. This emphasizes that osmosis acts in the opposite sense to Darcy flows relative to its respective driving potential (i.e. the solute gradient vs. the head gradient). To obtain the groundwater flow equation, equation (1) is combined with the fluid continuity equation and expressions for the solid and fluid phase compressibilities. The fluid continuity equation is

$$\frac{\partial(\phi\rho)}{\partial t} = -\nabla\cdot(\rho q) \tag{2}$$

where ϕ is the porosity. The left-hand side of equation (2) may be expanded to give

$$\phi\frac{\partial\rho}{\partial t} + \rho\frac{\partial\phi}{\partial t} = -\nabla\cdot(\rho q) \tag{3}$$

The compressibility of the solid phase skeleton may be defined by

$$\alpha = -\frac{1}{V}\frac{\partial V}{\partial\overline{\sigma}_{eff}} \tag{4}$$

where V refers to the total volume of an element of the porous medium and $\overline{\sigma}_{eff}$ is the mean effective stress defined by the Terzaghi relationship

$$\overline{\sigma} = \overline{\sigma}_{eff} + p \tag{5}$$

where $\overline{\sigma}$ is the mean total stress (Bear 1972). Provided that the total stress remains constant, we have $d\overline{\sigma}_{eff} = -dp$, which enables us to write

$$\alpha = \frac{1}{V}\frac{\partial V}{\partial p} \tag{6}$$

Writing the rock element volume $V = V_s + V_p$, where V_s is the solid volume (assumed constant) and V_p is the pore volume, then we can express the porosity as

$$\phi = \frac{V_p}{V_s + V_p} \tag{7}$$

Hence, re-arranging for V_p in terms of V_s and ϕ gives

$$V = V_s + \frac{\phi V_s}{(1-\phi)} = \frac{V_s}{(1-\phi)} \tag{8}$$

Differentiating we have

$$\frac{\partial V}{V} = \frac{\partial\phi}{(1-\phi)} \tag{9}$$

Substituting equation (9) into equation (6) gives

$$\alpha\frac{\partial p}{\partial t} = \frac{1}{(1-\phi)}\frac{\partial\phi}{\partial t} \tag{10}$$

The compressibility of the fluid phase may be defined as

$$\beta\frac{\partial p}{\partial t} = \frac{1}{\rho}\frac{\partial\rho}{\partial t} \tag{11}$$

Combining equation (3) with equations (10) and (11) gives

$$\phi\beta\rho\frac{\partial p}{\partial t} + \alpha(1-\phi)\rho\frac{\partial p}{\partial t} = -\nabla\cdot(\rho q) \tag{12}$$

Introducing the equivalent freshwater head, $h=(p/\rho_0 g)+z$, where ρ_0 is the density of fresh water, and using equation (1) gives

$$\begin{aligned}&\left(\phi\beta + \alpha(1-\phi)\right)\rho\rho_0 g\frac{\partial h}{\partial t} = -\nabla\cdot(\rho q) = \\ &\nabla\cdot\left(\rho\frac{k\rho_0 g}{\mu}\nabla h - \rho_0 g\hat{z} + \rho g\hat{z}\right) + \nabla\cdot(\rho h_{hc}\nabla c)\end{aligned} \tag{13}$$

The specific storage, S_s, and hydraulic conductivity, K, of the

$$S_s = \rho_0 g\left(\phi\beta + \alpha(1-\phi)\right) \qquad K = \frac{k\rho_0 g}{\mu} \tag{14}$$

so that equation (13) becomes

$$\rho S_s\frac{\partial h}{\partial t} = \nabla\cdot\left(\rho K\nabla h + \rho_r\hat{z}\right) + \nabla\cdot(\rho k_{hc}\nabla c) \tag{15}$$

where

$$\rho_r = \left(\frac{\rho}{\rho_0} - 1\right) \tag{16}$$

Greenberg et al (1973) show that the mass flux of solute, J, includes osmotic coupling terms in addition to the usual advective and diffusive transport terms,

$$J = -\left(cK'_{ch}\left(\nabla h + \rho_r \hat{z}\right) + D'\nabla c\right) \tag{17}$$

where

$$K'_{ch} = k_{hc}\left(\frac{\rho_0 g}{RT}\right) + K \tag{18}$$

$$D' = D + ck_{hc} \tag{19}$$

and D is the effective diffusion coefficient, R is the gas constant, and T (K) is the absolute temperature. The continuity equation for solute mass is

$$\frac{\partial(\phi c)}{\partial t} = -\nabla \cdot J \tag{20}$$

Expanding the left-hand side as in equation (2) and using the definition of solid phase compressibility in equation (10) and the mass flux given in equation (17) gives the equation for solute transport as

$$\phi\frac{\partial c}{\partial t} + \left[\alpha(1-\phi)\rho_0 g\right]c\frac{\partial h}{\partial t} = \nabla\cdot\left(cK'_{ch}\left(\nabla h + \rho_r \hat{z}\right)\right) + \nabla\cdot\left(D'\nabla c\right) \tag{21}$$

Equations (15) and (21) together describe a coupled system which exhibits a chemico-osmotic type of behaviour. Initial assessments of the data presented below in Section 3 used these equations. However, it was found that the solutions were unsatisfactory in a number of aspects, particularly in the lack of any long term volume changes due to swelling. A modification to the above development is therefore suggested. It may be noted that equation (1) can be written in the form

$$q = -K\left(\nabla\left(h + \frac{k_{hc}}{K}c\right) + \rho_r g\hat{z}\right) \tag{22}$$

which in turn suggests that the Darcy flow in this modified form of the equation is responding to the gradient of an effective head, h' , given by

$$h' = h + \frac{k_{hc}}{K}c \tag{23}$$

The particular modification to the above development of Greenberg et al (1973) that is suggested is to extend the use of this effective head to the definition of the solid phase compressibility given in equation (10). The new equation for the compressibility is thus

$$\frac{\partial\phi}{\partial t} = \alpha(1-\phi)\rho_0 g\left(\frac{\partial h}{\partial t} + \frac{k_{hc}}{K}\frac{\partial c}{\partial t}\right) \tag{24}$$

Making use of this leads to a modified form of equation (15)

$$\rho S_s\frac{\partial h}{\partial t} + \rho\left(\alpha(1-\phi)\rho_0 g\frac{k_{hc}}{K}\right)\frac{\partial c}{\partial t} = \nabla\cdot\left(\rho K\nabla h + \rho_r\hat{z}\right) + \nabla\cdot\left(\rho k_{hc}\nabla c\right) \tag{25}$$

It can be seen that the second term of this equation contains the solid phase component of the specific storage multiplied by the ratio of the osmotic coupling coefficient to the hydraulic conductivity. Similarly, the solute transport equation (21) becomes

$$\left(\phi + c\left[\alpha(1-\phi)\rho_0 g\right]\frac{k_{hc}}{K}\right)\frac{\partial c}{\partial t} + \left[\alpha(1-\phi)\rho_0 g\right]c\frac{\partial h}{\partial t} = \nabla\cdot\left(cK'_{ch}\left(\nabla h + \rho_r\hat{z}\right)\right) + \nabla\cdot\left(D'\nabla c\right) \tag{26}$$

It is found that the new terms in equations (25) and (26) lead to changes in the transient behaviour of the system that are consistent with that seen in the data and predict a significant degree of swelling as a result of changes in the solute concentration.

It may be noted that the equations presented here consider the osmotic flux to arise from the concentration gradient of a single solute. This relatively simple empirical approach should be adequate provided that the groundwater chemistry is simple (i.e. a single, or strongly dominant, dissolved component) and provided that the parameters are used consistently from cases to case, such as using an interpretation of experimental data in a prediction of borehole behaviour. However, to address more complex fluid chemistries a more rigorous approach will need to be developed, based upon the idea that the groundwater flows in response to a gradient of chemical potential. The chemical potential may then be expressed in terms of the pressure and the concentrations of all solutes to yield equations which could be reduced to those used here with appropriate simplifying assumptions. Such a development is beyond the scope of the current study. Finally, it may be noted that the terms "osmotic permeability" and "osmotic efficiency" are sometimes used when discussing chemico-osmotic effects. The relationship of these parameters to those used in the equations above may be conveniently explored by

considering the osmotic flow across a sample of thickness L in the presence of a solute concentration gradient but no pressure gradient. Equation (1) becomes

$$q = -k_{hc}\frac{\Delta c}{L} \tag{27}$$

where Δ_c is the concentration difference (mol.m^{-3}) across the sample, and k_{hc} is the osmotic coupling coefficient with dimensions (m^{5}mol^{-1}s^{-1}). This osmotic flow can also be written in terms of an "osmotic pressure" difference, $\Delta\Pi_0$ (Pa) by analogy with Darcy's law as

$$q = -\frac{k_\Pi}{\mu}\frac{\Delta\Pi_o}{L} \tag{28}$$

where k_Π is the "osmotic permeability" and μ (Pa·s) is the viscosity. The relationship between solute concentration and osmotic pressure is given by the van't Hoff equation

$$\Delta\Pi_o = n\Delta c \cdot RT \tag{29}$$

where n is the number of dissociated ions formed when the salt goes into solution, R (=8.314 J·mol^{-1}·K^{-1}) is the gas contant, T (K) is the absolute temperature. Equating the flows in equations (27) and (28) and using equation (29) gives

$$k_\Pi = k_{hc}\left(\frac{\mu}{nRT}\right) \tag{30}$$

The "osmotic efficiency" of Kemper and Rollins (1966) is found by equating the flow rate due to an hydraulic pressure difference to the flow rate due to an osmotic pressure difference. The osmotic efficiency is then given by the ratio of the water pressure to the osmotic pressure. Combining Darcy's law for pressure driven water flow with equation (28) for the osmotic flow and rearranging gives

$$\frac{\Delta p}{\Delta\Pi_0} = -\frac{k_\Pi}{k} = -\frac{\left[\frac{k_{hc}\mu}{nRT}\right]}{\left[\frac{K\mu}{\rho g}\right]} = -\frac{k_{hc}}{K}\left[\frac{\rho g}{nRT}\right] \tag{31}$$

Thus, taking a slightly saline ρ = 1030 kg.m^{-3}, g = 9.81 m.s^{-2}, R = 8.314 J.mol^{-1}.K^{-1}, T = 298 K and n = 2 gives the following "rule-of-thumb" relationship:

$$\text{Osmotic efficiency} \approx -2\frac{k_{hc}}{K} \tag{32}$$

It may be noted that the parameter n in the van't Hoff equation (29) may be reduced from the value of 2 assumed here in more concentrated solutions due to ion pairing effects. This would cause the true osmotic efficiency to be somewhat higher than is estimated from equation (32).

2.1 Numerical solution

The pair of equations (15) and (21), or the modified equations (25) and (26), form a system of coupled non-linear partial differential equations. To obtain solutions, the equations were discretized using central finite differences for the spatial derivatives, in Cartesian coordinates for the laboratory experiments and in radial coordinates for the borehole experiments.
The equations were also simplified by assuming a constant fluid density so that only a single spatial dimension needed to be considered, x or r, respectively. For the laboratory experiments it was sufficient to provide specified head and solute concentration values as the boundary conditions.
For the borehole experiments it is necessary to supplement the main equations with equations that represent the response of the sealed borehole section to the flows of fluid and solute. Fluid flows into the sealed borehole section, including for generality an external injection rate, work against the borehole storage to create changes to the head in the section. Thus the new equation required is

$$S_w\frac{\partial h_w}{\partial t} = Q_w - 2\pi r_w L\left(-K\frac{\partial h}{\partial r} - k_{hc}\frac{\partial c}{\partial r}\right)_{r=r_w} \tag{33}$$

where S_w is the borehole storage, defined as the rate of change of fluid volume per unit change of borehole head, Q_w is the rate of external injection of fluid into the sealed section (negative for abstraction), L is the length of the sealed Section, h_w is the head in the borehole and r_W is the borehole radius. It can be seen by comparison with equation (1) that the bracketed term on the right hand side of equation (33) is just the modified Darcy flux at the borehole wall.
In a similar way, an equation for the solute mass balance at the borehole boundary may be written as

$$V_w\frac{\partial c_w}{\partial t} = 2\pi r_w L\left(D'\frac{\partial c}{\partial r} + cK'_{ch}\frac{\partial h}{\partial r}\right)_{r=r_w} \tag{34}$$

where V_w is the volume of fluid in the test section and c_w is the solute concentration there. Thus, equations (33) and (34) provide the rate equations for the borehole boundary nodes and complete the system of coupled non-linear ordinary differential equations which

are integrated in time using Gear's backward difference formulae with either of the subroutine packages LSOIBT (Hindmarsh, 1982) or DASSL (Petzold, 1982). The codes OSMO1 and OSMO1R implement the solutions for Cartesian and radial geometries respectively (Noy, 1998).

3 Laboratory study

The objectives of the laboratory pilot study were to examine both the transient and steady-state osmotic flow of water through disc-shaped specimens of Opalinus Clay subject to a fixed solute concentration gradient. The required outputs were the osmotic efficiency and the resulting osmotic permeability of the shale. This demanded independent measurement of the hydraulic conductivity. Given the known swelling response of de-stressed shale when exposed to water, the apparatus was designed so that an isotropic confining stress could be applied to the shale discs during the flow measurements.

3.1 Apparatus

The apparatus consisted of five main components: (1) a sample assembly, (2) a pressure vessel and associated confining pressure system, (3) a fluid injection system, (4) a back-pressure system, and (5) a microcomputer-based data acquisition system (Figure 3.1).
The pressure vessel, shown in Figure 3.2, comprised an Autoclave Engineers bolted single-closure reactor vessel, made from 316 stainless steel and pressure tested to 40 MPa. The shale disc was sandwiched between two end-caps, each with a sintered stainless steel porous disc, and then jacketed in heat-shrink Teflon tubing to exclude confining fluid and provide a flexible pressure seal. Jubilee hose clamps and thin copper shims were used to compress the Teflon tubing against a Viton "O"-ring in each end-cap so as to provide a leak-tight seal. Each end-cap has a central inflow duct and a circular groove cut into the loading-bearing surface which was linked to an outflow duct. This arrangement allows the permeant to be flushed from the porous disc and connecting tubes when the solution chemistry is changed.
Flow rates were monitored or controlled using a pair of ISCO-500 Series D syringe pumps operating from a single digital control unit. The pump controller has an RS232 serial port that allows volume, pressure and flow rate data to be transmitted to an equivalent port of a personal computer. A program written in QBASIC prompted the pump controller to transmit data to the computer at pre-set time intervals. Data acquisition rates ranged from one scan per 15 minutes to one per 30 minutes. All pressure transducers were calibrated against a Druck PTX610 pressure transmitter using the manufacturer's calibration data.

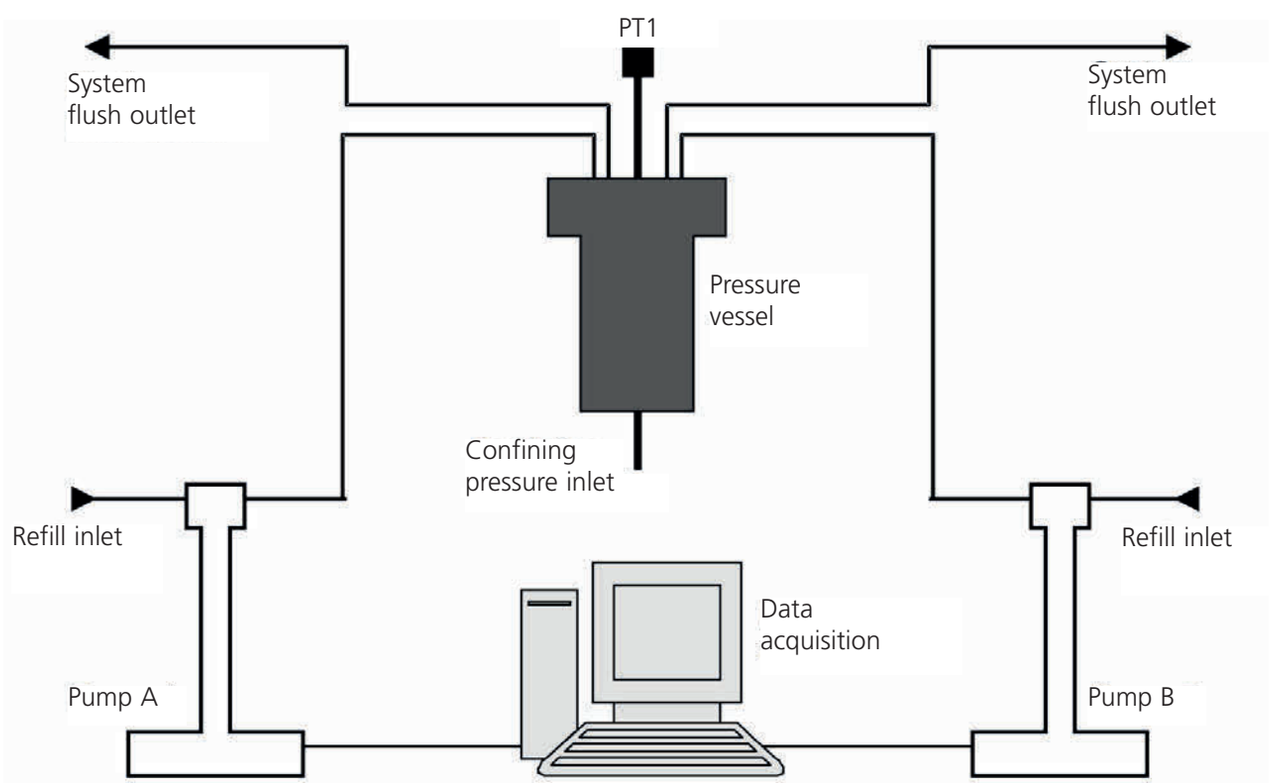

Figure 3.1: Schematic of the apparatus for the laboratory pilot study.

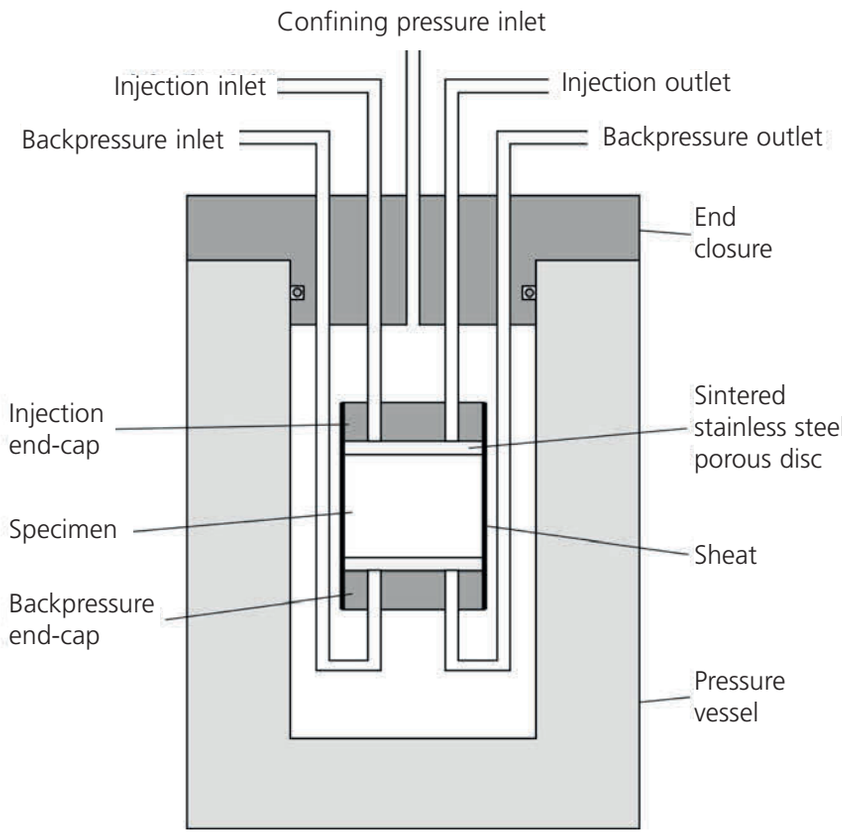

Figure 3.2: Schematic of the pressure vessel and specimen assembly for the laboratory pilot study.

3.2 Procedures

A block sample of Opalinus Clay was taken from SHGN niche of the Mt. Terri Rock Laboratory (Figure 1.1). The block was placed in a heat-sealable aluminized plastic bag. The bag was flushed with nitrogen prior to heat-sealing to prevent oxidation of secondary minerals during shipment. On receipt at BGS, two discs of nominal diameter 5.0 cm and thickness 1.0 cm were prepared from the block using a combination of dry coring, sawing and surface grinding. These discs were orientated so that the direction of flow during the experiments would be normal to the plane of the bedding.

The two porous discs were saturated with saline solution of appropriate chemistry (see below) before being placed in contact with the shale.

The test history for each specimen comprised a sequence of test stages (see Tables 3.1 and 3.2). During an equilibrium (EQ) stage, the specimen was exposed to the saline solution on both faces, with the same pressure at both ends. An osmotic flow (OF) stage was accomplished by replacing the solution at one end of the specimen with distilled water at the same pressure. Since there was no pressure gradient across the disc during an OF stage, the measured water flow was solely due to osmosis. A constant flow rate (CFR) stage was used to evaluate the hydraulic permeability of the specimen and involved pumping the saline solution through the disc at a number of controlled flow rates, with the same solution present as a backpressuring fluid at the downstream end. Anticipating that the osmotic flow rates would be very small, the test programme was carefully designed to minimize systematic errors. Eight separate determinations of osmotic flow were made on the two specimens. The syringe pumps were interchanged and direction of flow varied to reduce uncertainties associated with pump performance and possible leakage of the apparatus. The experiments were performed in an air-conditioned laboratory at a temperature of 20 ± 0.3 °C.

3.3 Test conditions

The vertical total stress acting in the shale at the depth of the tunnel niche was estimated to be 5.5 MPa. This value was selected for the isotropic confining pressure in the experiments, except for stages 13

to 18 of NS01 where confining pressure was increased to 7.5 MPa. A fixed backpressure of 1.0 MPa was specified for all test stages. Guided by the results of previous pore-water squeezing experiments on Opalinus Clay, a 14.3 g dm^{-3} NaCl solution was made up to simulate the natural pore-water of the shale (Cave et al., 1998). The molar concentration of this solution is 0.245 $mol.dm^{-3}$ which, according to equation (29), gives an osmotic pressure of 1.19 MPa.

3.4 Results

Hydraulic permeabilities were calculated from the CFR test data by taking the pressure drop across the specimen at the steady-state asymptote of the pressure transient. The pressure transients were also analyzed using equation (15), neglecting the second term on the right since there was no concentration gradient in these test stages.

Table 3.1 summarizes the results of the controlled flow rate (CFR) test stages on the two specimens. The average effective stress is the difference between the isotropic confining stress and the average pore pressure. Hydraulic conductivity values calculated from flow under a steady-state pressure gradient were close to those obtained by mathematical analysis of the pressure transients. The mean hydraulic conductivity, K, normal to bedding was 7.7×10^{-14} $m\cdot s^{-1}$ and the mean specific storage, S_s, from all reliable determinations was 4.1×10^{-4} m^{-1}.

Table 3.2 summarizes the results of the osmotic tests stages on the two specimens. Osmotic flows were calculated by time-averaging the flow rates of the upstream and downstream pumps in the region of the steady-state asymptote of the flow transient. The osmotic permeability, k_Π, normal to bedding was calculated using equations (28) and (29). The osmotic coupling coefficient, k_{hc}, was then calculated using equation (30). Figure 3.3 illustrates the osmotic flow transient from stage 2 of NS01. The experimental noise seen in the curves is typical of the entire dataset and is indicative of practical difficulties in measuring the exceptionally small osmotic flow rates.

Volumetric strains were calculated assuming the mineral grains to be incompressible, taking the difference between the volume of water pumped in and the volume pumped out of the specimen and dividing the result by the original specimen volume. A correction was applied for apparatus compliance and compression of the liquid in the upstream system. Bulk compressibility, α, was estimated from the stress-strain

Specimen	Test stage	Average effective stress (MPa)	Controlled flow rate ($ml.hr^{-1}$)	Hydraulic conductivity K ($m\cdot s^{-1} \times 10^{14}$)		Specific storage S_s ($m^{-1} \times 10^{4}$)
				From steady-state gradient	From transient analysis	
NSO1	7	4.40	1.0	7.4	5.9	6.2
	8	4.32	2.0	7.8	7.0	4.3
	9	4.23	3.0	7.5	6.3	4.2
	10	4.31	2.0	7.2	-	-
	11	4.40	1.0	6.9	6.6	4.1
	17	6.39	1.0	6.6	6.3	3.4
	18	6.28	2.0	6.4	5.4	3.2
NSO2	5	4.41	1.0	8.4	8.7	3.9
	6	4.34	2.0	9.2	11.2	3.9
	7	4.28	3.0	10.0	11.1	4.1
	8	4.33	2.0	9.0	-	-
	9	4.37	1.0	6.2	-	-

Table 3.1: Results of the controlled flow rate (CFR) test stages on the two specimens.

Specimen	Test stages	Average effective stress (MPa)	Average osmotic flow rate ($\mu L\cdot hr^{-1}$)	Osmotic Permeability, k_Π ($m^2\cdot10^{22}$)	Osmotic coupling oefficient k_{hc} ($m^5\cdot mol^{-1}\cdot s^{-1}x10^{15}$)	Osmotic efficiency
NS01	2-5	4.50	0.4	4.6	-2.3	0.061
	14-15	6.50	0.3	3.5	-1.7	0.045
NS02	2-3	4.50	0.1	1.3	-0.6	0.016

Table 3.2: Results of the osmotic flow (OF) test stages on the two specimens.

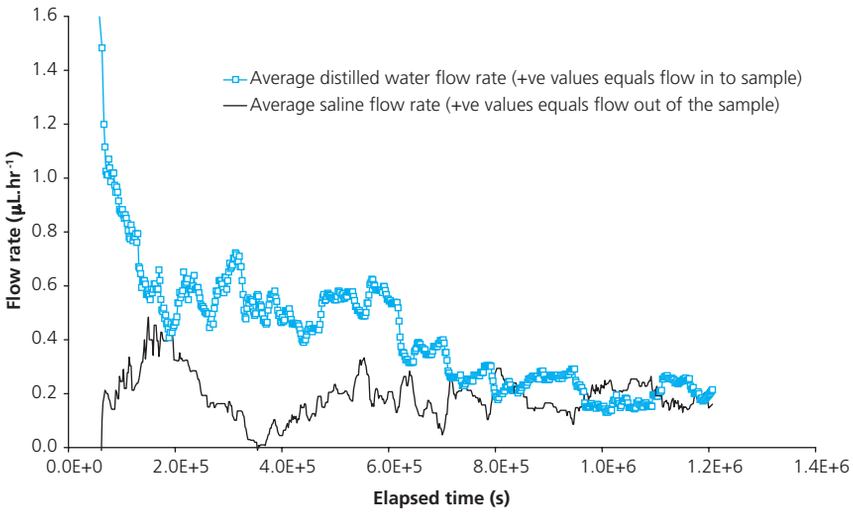

Figure 3.3: Osmotic flow transient from stage 2 of NS01. Osmotic flow started shortly after the saline solution at one side of the disc was replaced with distilled water. The flow transient asymptotically approaches the steady-state flow condition.

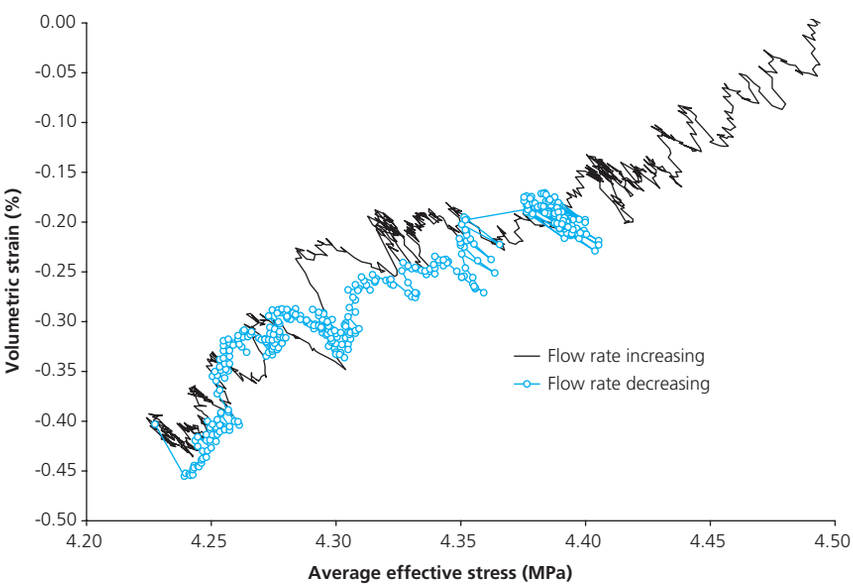

Figure 3.4: Volumetric strain against average effective stress for NS01 when subject to the pressure variations of CFR test stages 7 to 11, inclusive. Strain was calculated from net pump flows and corrected for apparatus compliance and the compressibility of liquid in the upstream system.

plots using least-squares regression analysis and then compared with the values calculated directly from specific storage using Equation (14).

With the application of an isotropic effective confining stress of 4.5 MPa, specimen NS01 exhibited time-dependent swelling for a period of around 5 days. The volumetric strain calculated on the basis of full saturation was around -1.3%, where the negative sign denotes a volume increase. When effective confining stress was increased to 6.5 MPa, a small amount of consolidation was observed. The observed tendency of the shale to swell at the lower stress and consolidate at the higher stress when exposed to a solution matched to the original pore-water suggests that the (pre-excavation) mean normal effective stress at the sampling location in the Mt. Terri Rock Laboratory is bracketed by the values 4.5 and 6.5 MPa.

When one side of the specimen NS01 was exposed to distilled water, the shale swelled by -0.8% over a period of 10 days. Similar behaviour was observed for specimen NS02 which swelled by -0.9% over 26 days. Clearly, a simple change in the salinity of the pore-water can lead to a change in specimen volume. This observation prompted the modifications to the numerical model discussed in Section 5.1.

Figure 3.4 shows a plot of volumetric strain against average effective stress for specimen NS01 during controlled flow rate test stages 7 to 11, inclusive.

Increases in flow rate led to positive pressure transients which were accompanied by swelling. Flow rate decrements led to negative pressure transients accompanied by consolidation.

The strains associated with changes in pore-water pressure were found to be fairly reversible. These data give a compressibility, α, for a history of variable pore-water pressure and constant total stress of 1.3×10^{-8} Pa^{-1}. Stages 17 and 18 at the higher effective stress gave a similar value of 1.7×10^{-8} Pa^{-1}. Compressibility calculated from specific storage using Equation (14) was 5.4×10^{-8} Pa^{-1} for stages 7 to 11, inclusive, and 3.8×10^{-8} Pa^{-1} for stages 17 and 18.

All compressibility values are very high for a shale, suggesting that the volumetric strains must be largely determined by quasi-elastic deformation processes such as swelling and crack dilation. In order to test this hypothesis, a 3-D swelling test was performed on a 40 mm cube of the niche SHGN material (ISRM, 1981). The cube was immersed in distilled water and the resulting swelling strains were measured in three mutually-perpendicular directions using Baty spring-loaded mechanical dial gauges. Within 15 minutes of immersing the cube, fractures began to open and small gas bubbles were expelled from the rock. The cube swelled preferentially in a direction normal to bedding by the combined processes of clay swelling, slaking and bedding plane crack dilation. The total volumetric strain after eight days of monitoring was –2.9%. The volumetric strains of the specimens during hydraulic and osmotic testing were clearly of the same order of magnitude as those during the swelling test.

It is interesting to note that stage 13 of NS01 gave a significantly lower compressibility of 1.7×10^{-9} Pa^{-1} for the condition of variable total stress and constant pore-water pressure. It therefore appears that a change in pore-water pressure at fixed total stress has a significantly larger effect on specimen volume than does a change in total stress at fixed pore-water pressure.

4 Field experiment

The main objective of the *in situ* experiment was to examine the sensitivity of the equilibrium pressure (or head) in a borehole in Opalinus Clay to changes in the salinity of the borehole fluid. Experimental guidelines were that: (a) the pressure measurements should be undertaken within a packered-off test section of a vertical borehole, (b) the packer assembly should be mechanically stiff (i.e. non-compliant), (c) there should be negligible leakage of test fluid, (d) the volume of the test interval should be minimized to reduce the time duration of the pressure transients, (e) the test interval and associated pipework should not contain a compressible gas phase, and (f) temporal changes in the salinity of the test fluids should be monitored (Horseman, 1996).

The field experiment was sited in the OP niche which is adjacent to the Security Gallery of the Mt Terri Rock Laboratory (see Figure 1.1). The Opalinus Clay in this locality corresponds with the lowermost shaly unit identified by Thury (1999). The shale displays strong bedding anisotropy, dips at about 40 degrees towards SSE and is fairly homogenous, with few tectonic fractures. Unloading fractures within the excavation disturbed zones of the tunnel and experimental niche do not extend more than 1 m into the floor.

For the purposes of discussion here, the experiment has been divided into three phases. Phase 1 covers the period starting from 25 September 1997 when the borehole was drilled. Phase 2 starts on 16 February 2000 when de-ionised water was introduced into the test interval and Phase 3 starts on 6 March 2002 when the hypersaline brine solution was introduced.

4.1 Experimental set-up

Borehole BOP-1 was drilled on 25 September 1997 using compressed air as a flushing medium. The 101 mm diameter borehole was drilled vertically downwards to a depth of 8 m. Borehole stability was excellent and no macroscopic borehole breakouts were observed after drilling. The interval 6.2 to 8.0 m was found to comprise unfractured homogeneous gray shale and was selected for the test.

Figure 4.1 is a schematic of the equipment for the experiment. A hydraulic packer and slotted screen were position to give a test interval with a length of 1.5 m, a diameter of 0.096 m and a fluid volume of 0.00425 m^3. The test interval was fitted with a piezometer.

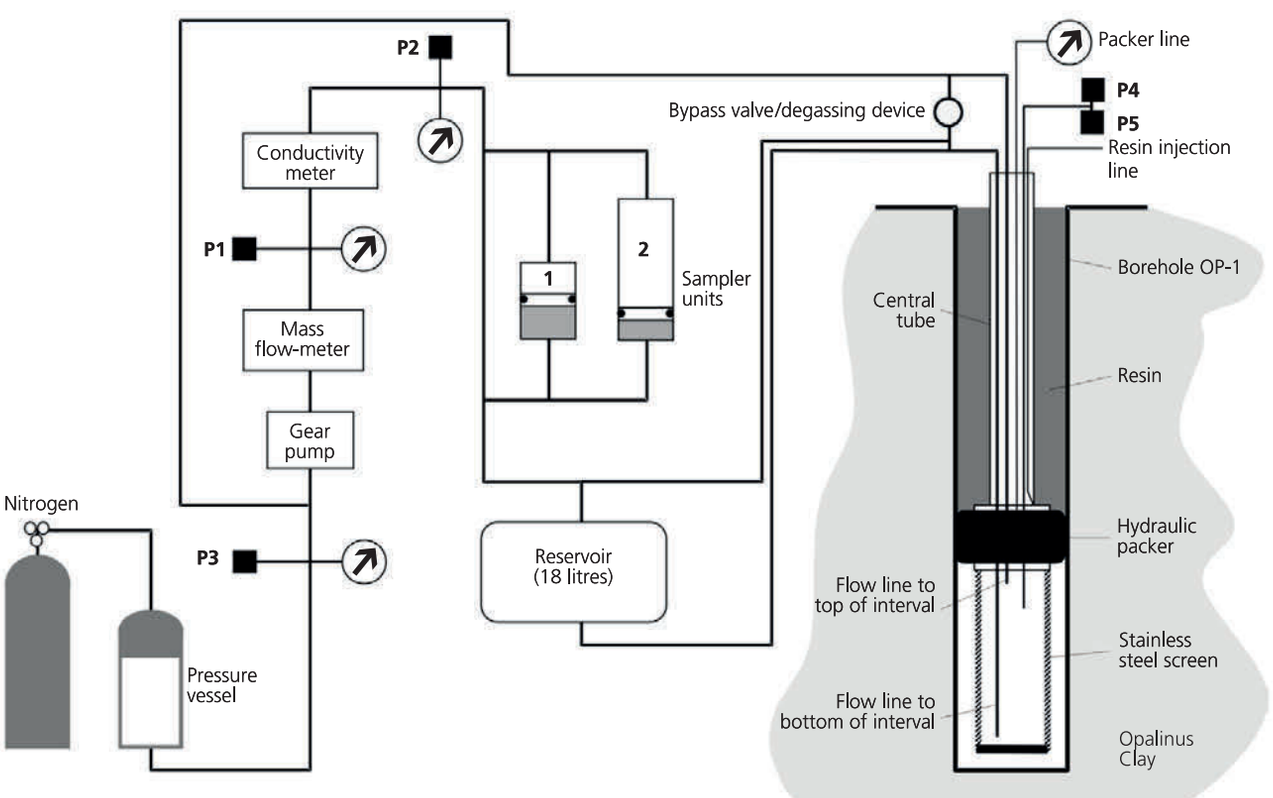

Figure 4.1: Schematic of the equipment for the field experiment in the Mt Terri Rock Laboratory in Switzerland. Pressure transducers are labelled P1 to P5.

The main technical challenge of the experiment was how to exchange the test fluid with a new fluid without changing the downhole pressure. This was considered necessary because the hydromechanical responses associated with any change in interval pressure might lead to unnecessary complications in the interpretation of the data. After some preliminary experimentation, it was found that the test interval could be effectively flushed by passing through the system a volume of fluid at least three times that of the test interval. The reservoir shown in the schematic is made up of inclined stainless steel tubes linked together to give a total capacity of 0.018 m^3. This reservoir also served as a receiver for the displaced fluid. The exchange was accomplished using gear pumps, with a mass flow meter to determine flow rate. The two sampling units allowed some of the fluid in the test interval to be withdrawn for chemical analysis. An electrical conductivity meter was used to indicate the progress of a fluid exchange. The interval pressure was maintained by adjusting the pressure of nitrogen gas in the headspace of a pressure vessel linked into the up-hole pipework. Guided by experience during the first fluid exchange, the surface equipment was slightly modified at the end of Phase 2 to enable trapped air to be more easily removed.
A data acquisition system was installed in the niche to continuously monitor: (a) interval pressure, (b) pressure at selected points in the up-hole circuit, (c) pump flow rate, and (d) electrical conductivity.

4.2 Procedures

The packer was inflated to a pressure of 2 MPa using water. The packer pressure fell by 0.5 MPa over the first day and then remained stable. The tightness of the packer seal was checked by applying an underpressure of 80 mbar using a vacuum pump. Finally, the annulus between packer and borehole mouth was filled with an epoxy resin in order to provide a really tight test interval.
The flow and pressure measuring lines were flushed with CO_2 and then filled with a water. Since the solubility of CO_2 in water is much greater than that of air, this procedure was adopted to remove any free gas from the up-hole system. The water used in this first phase of the experiment was a synthetic pore solution known in the Mt Terri Project as "Pearson Type A1 water". The composition of this solution is close to that of the formation pore-water (Pearson et al., 1999).
After borehole completion, the pressure evolution was monitored for approximately two years. During this first phase of the experiment, the test fluid became fully equilibrated with the surrounding Opalinus Clay pore-water. In the second phase, the original test fluid was sampled and replaced with de-ionised water and the fluid was allowed to equilibrate with formation water for another two years. In the third and last phase, the test fluid was replaced with a 100 g dm^{-3} NaCl solution.

4.3 Results

The fully equilibrated test interval pressure at the end of Phase 1 was 900 ± 20 kPa. The data reveal a small seasonal periodicity, with slightly higher pressures in summer and lower in winter. All pressure values quoted in this section were measured by a transducer reading absolute pressure.
The pressure evolution for Phase 2 after replacement of the original test fluid with de-ionised water is shown in Figure 4.2. At the time of shut-in of the test interval the pressure was 893 kPa. Pressure began to fall and reached a minimum of 812 kPa after 52 hours, a drop of 81 kPa. After reaching the minimum pressure, the interval pressure began to slowly increase, reaching a value of about 850 kPa by the end of March 2000. Pressure continued to slowly increase.
The pressure evolution for Phase 3 after replacing the test fluid with the hypersaline solution is shown in Figure 4.3. At the time of shut-in, the interval pressure was 930 kPa. Pressure then began to rise, reaching a maximum of 1082 kPa after 221 hours, an increase of 152 kPa. After reaching the maximum pressure, the pressure slowly began to decrease, reaching a value of about 1050 kPa by end of April 2002. There were no signs of equilibration and the interval pressure continued to slowly decrease.
Chemical analyses of the test fluid samples at the time of fluid replacement are presented in Table 4.1. Also shown is an analysis of formation water from borehole BWS-A1 which was drilled in the same shaly facies of the Opalinus Clay as the osmosis borehole. Other than easily explained differences in alkalinity and total organic carbon, the fully-equilibrated test fluids at end of Phases 1 and 2 have a compositions which are very close to the formation water from borehole BWS-A1. Since the fluid introduced into the test interval at the start of Phase 2 was distilled water, the analysis shows that the main chemical constituents of the pore-water were able to freely diffuse into the test interval over a period of two years. When measured over this timescale, the shale membrane is clearly very leaky.
The test fluid composition at the start of Phase 3 dif-

Species	Concentration ($mg \cdot dm^{-3}$)			
	Pore-water	**Test fluid**	**Test fluid**	**Test fluid**
	BWS-A1	**End Phase 1**	**End Phase 2**	**Start Phase 3**
Sodium	5610	5750	5330	34900
Potassium	65	55	48	17
Magnesium	344	476	455	17
Calcium	570	715	635	35
Strontium	36	32	39	<10
Chloride	10395	10240	9340	52400
Bromide	36	33	32	<40
Sulphate	1251	1314	1175	25
Alkalinity (HCO_3^-)	36	332	298	63
Total organic carbon	38	5	5	1
Total dissolved solids	18381	18952	17357	87508

Table 4.1 Chemical analyses of the formation water in borehole BWS-A1 and samples of the test fluids.

fers from that of the made-up brine suggesting that some degree of mixing occurred during the fluid exchange.

Taken collectively, the results of the *in situ* experiment demonstrate that hydraulic head measurements in the Opalinus Clay show a measurable but quite small sensitivity to changes in the chemistry of the fluid in the test interval. The transient responses associated with osmotic flow appear to be temporary and of limited duration and eventually diffusive leakage through the leaky shale membrane eliminates the concentration gradient. There are obvious similarities between the field-scale responses from the Mt Terri Rock Laboratory and the laboratory-scale pressure responses in the tests performed by Wong and Heidug (1994) and van Oort (1994), suggesting that this behaviour is not specific to the Opalinus Clay.

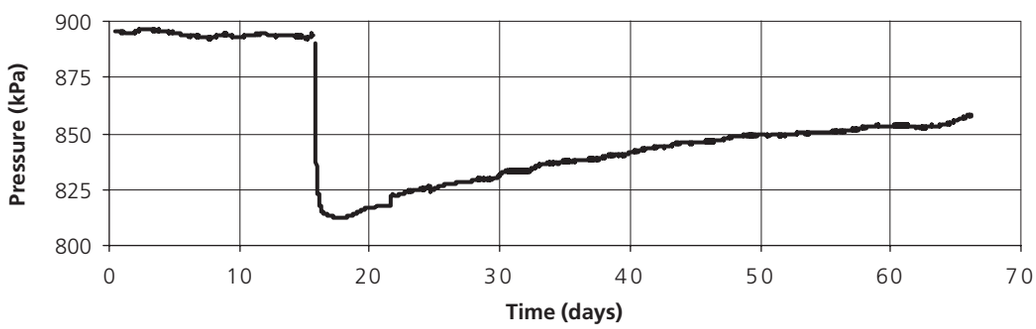

Figure 4.2: The pressure evolution for Phase 2, replacement of the test section fluid with de-ionised water. The data have been plotted starting from 1 February 2000.

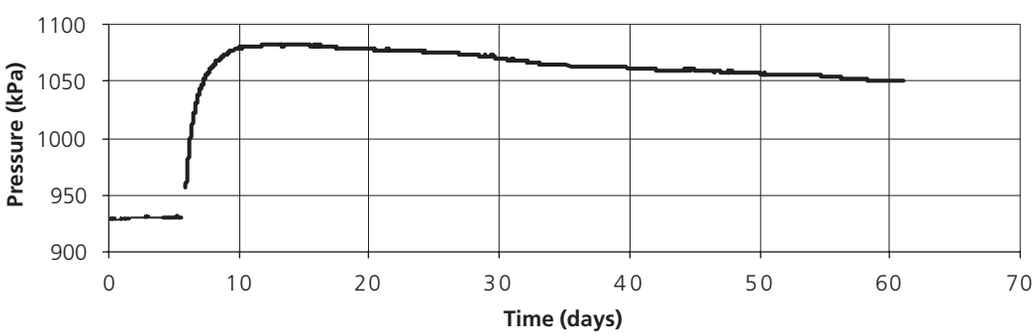

Figure 4.3: The pressure evolution for Phase 3, replacement of the test section fluid with hypersaline brine. The data have been plotted starting from 1 March 2002.

5 Interpretation

5.1 Laboratory study

The pilot study experiments clearly demonstrate the existence of osmotically-driven water flow in Opalinus Clay samples. Long term steady state flow rates that have been measured are readily converted to estimates of the osmotic permeability using the gradient of the solute concentration. However, it was a more detailed examination of the transient behaviour of the system that suggested the modified theoretical treatment indicated by equations (24)-(26).
The response obtained by the solution of equations (15) and (21), the original version of the model, using the parameter values listed in Table 5.1, is shown in Figure 5.1. There are two important features to note about these plots. Firstly, the modelled flow rates in and out of the sample quite quickly reach a state in which they are close to the eventual steady state and there is a prolonged period during which the flow out of the sample slightly exceeds that of the flow in. Secondly, the estimated volumetric strain rapidly attains a maximum value of about 0.02% and then relaxes gradually back towards zero. This model does not predict any long term volumetric swelling of the sample. In contrast, the solution to equations (25) and (26), using the same set of parameter values, is shown in Figure 5.2, together with the data from Stage 2 of the tests on sample NS01. It can be seen that the modelled transient approach to the steady state is of a more protracted duration and at all times the flow rate into the sample exceeds that out of it. Although the data are very noisy, it does appear that the new model provides a more realistic representation of the system response. The predictions of the new model for the volumetric strain are much more clearly reflecting the data from the experiment since they show the development of a long term volumetric strain of 0.8% on a timescale similar to that measured.

It was concluded that the pilot study provided good support for the suggested application of the effective head defined in equation (23) to the definition of compressibility as given in equation (24) since it both provides an improved representation of the transient flows and an explanation for the observed swelling of the shale samples in response to a change of pore fluid chemistry. Equations (25) and (26) were therefore used for all remaining model calculations.

5.2 Borehole experiment

As indicated above in Section 4, the *in situ* borehole test was carried out in three phases with extended periods in between to allow the borehole fluid and formation pore-water to return to their *in situ* composition. For the second phase the fluid in the borehole test section was replaced with de-ionised water and for the third phase the test section fluid was replaced with a hypersaline brine. By making use of the laboratory results it was possible for the interpretation of each phase to proceed by means of an initial predictive calculation based on previous data followed by parameter estimation calculations in which a good fit to the data was sought.
The compositions of the test fluids are shown in Table 4.1 and it is found that the total dissolved solids (TDS) in the three fluids amount to about 19.0 $g \cdot dm^{-3}$, 17.4 $g \cdot dm^{-3}$ and 87.5 $g \cdot dm^{-3}$ respectively. In each case the dominant component is the dissolved NaCl, although the *in situ* pore-water is clearly somewhat more complex, as would be expected, with significant concentrations of calcium, magnesium, sulphate, and bicarbonate. For the purposes of the model calculations, the TDS values were converted to NaCl concentrations of 0.324 $mol.dm^{-3}$ and 0.298 $mol.dm^{-3}$ for the pore-waters and 1.497 $mol.dm^{-3}$ for the brine.

Parameter	Laboratory study interpretation	Borehole experiment		
		Phase 2 prediction	Phase 2 interpretation †	Phase 3 interpretation
Borehole solute concentration ($mol.dm^{-3}$)	0(*)	0	0	1.497
Formation solute concentration ($mol.dm^{-3}$)	0.245(*)	0.298	0.298	0.298
Hydraulic conductivity ($m.s^{-1}$)	7.5×10^{-14}	1.9×10^{-13}	1.9×10^{-13}	1.9×10^{-13}
Diffusion coefficient ($m2.s^{-1}$)	1.0×10^{-10}	1.0×10^{-10}	1.4×10^{-10}	3.3×10^{-11}
Solid phase compressibility (Pa^{-1})	3.2×10^{-7}	3.4×10^{-9}	3.4×10^{-9}	3.4×10^{-9}
Osmotic coupling coefficient ($m^5 \cdot mol^{-1} \cdot s^{-1}$)	-1.73×10^{-15}	-4.38×10^{-15}	-7.72×10^{-15}	-3.45×10^{-15}
Osmotic efficiency	0.046	0.046	0.081	0.036
Borehole storage (m^2)	N/A	9.22×10^{-7}	2.80×10^{-7}	4.25×10^{-7}

Table 5.1: Summary of parameters used in numerical modelling. Porosity was taken as 0.13 in all computer simulations and (*) refers to concentrations on either side of the laboratory sample NS01. (†) Phase 3 prediction was carried out using all the parameters from the Phase 2 interpretation except that the borehole solute concentration was set to 1.497 $mol.dm^{-3}$.

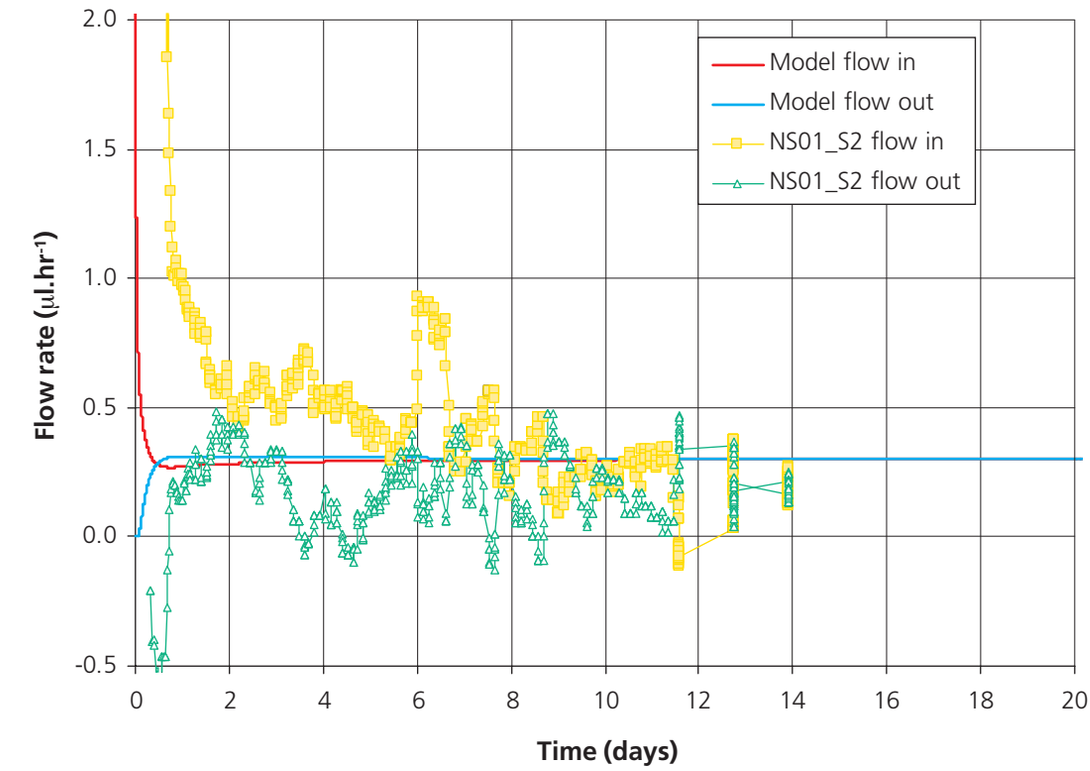

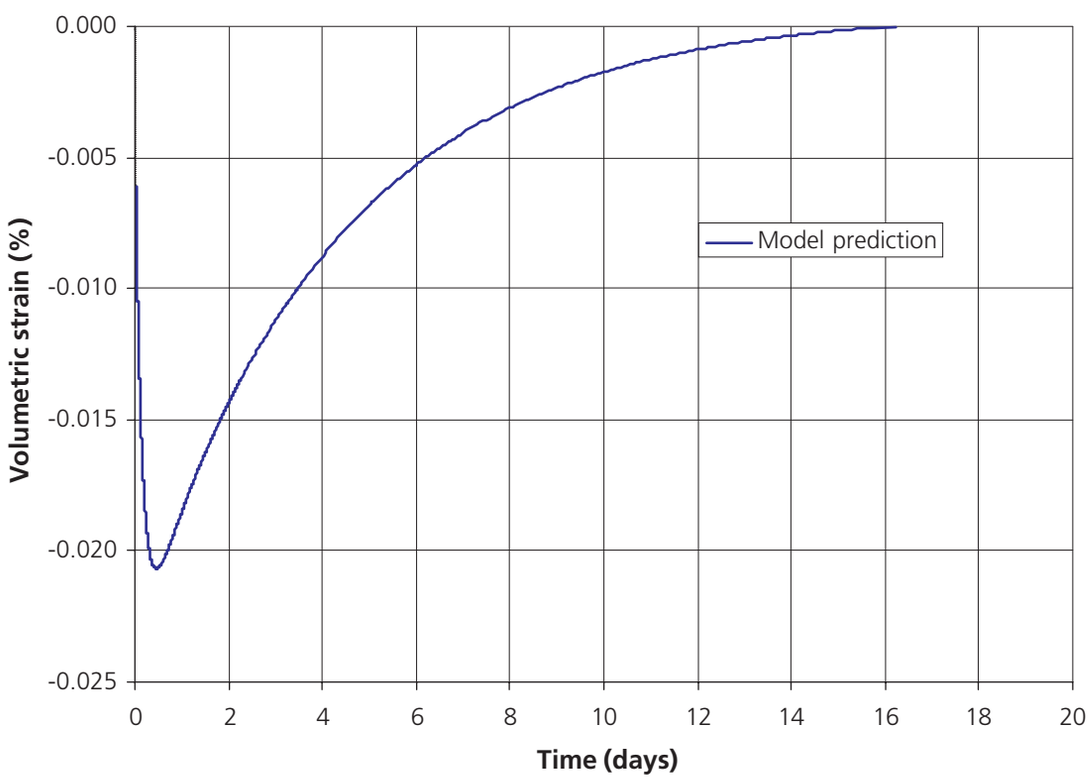

Figure 5.1: Model predictions of flows and volumetric strain as a function of time using equations (15) and (21) compared to the data from laboratory pilot study NS01 Stage 2. Negative volumetric strain indicates swelling of the sample (the data for volumetric strain are off scale in this plot, c.f. Figure 5.2).

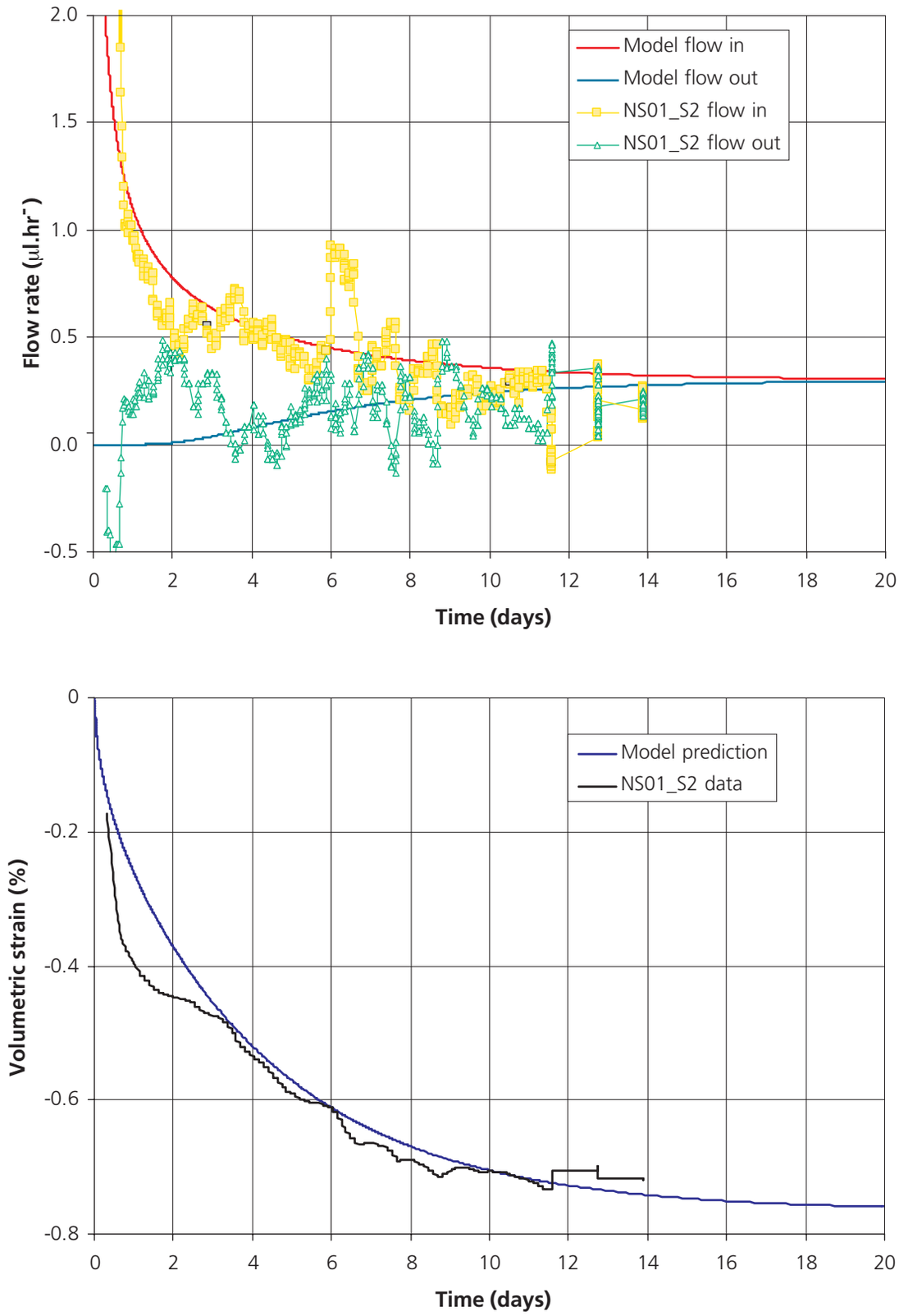

Figure 5.2: Model predictions of flows and volumetric strain as a function of time using equations (25) and (26) compared to the data from laboratory pilot study NS01 Stage 2. Negative volumetric strain indicates swelling of the sample.

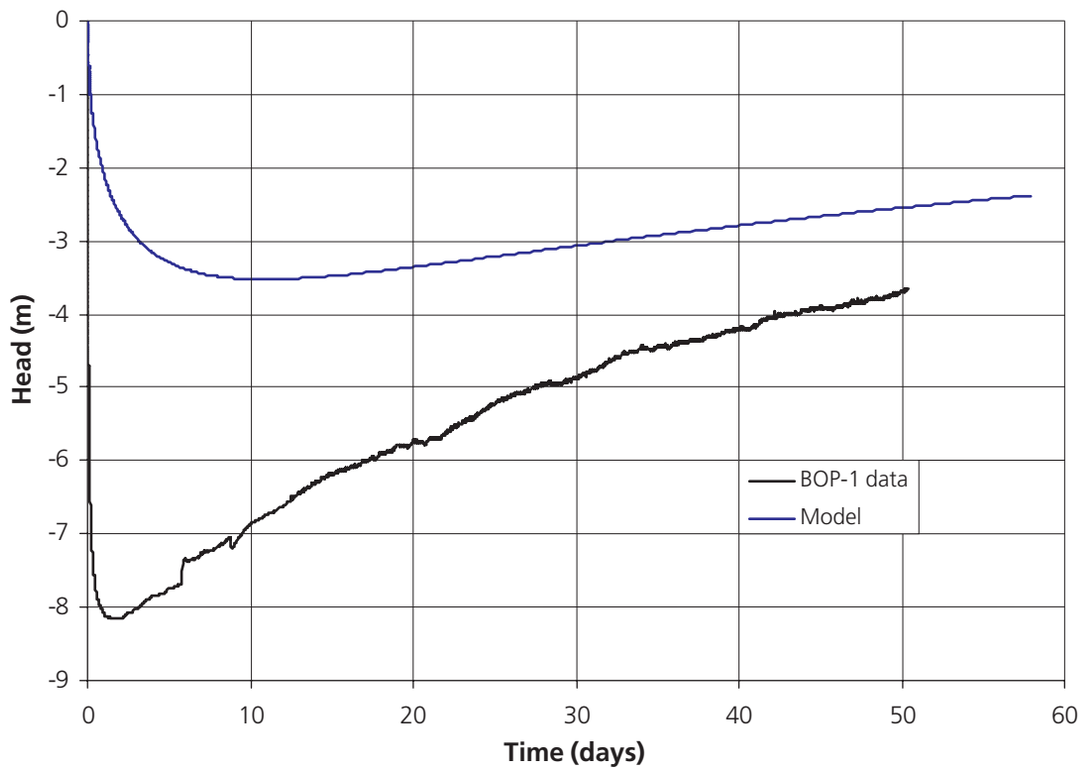

Figure 5.3: Field data from Phase 2 of the BOP-1 borehole experiment compared to the model prediction using an osmotic efficiency derived from the laboratory study (see Table 5.1 - Phase 2 prediction).

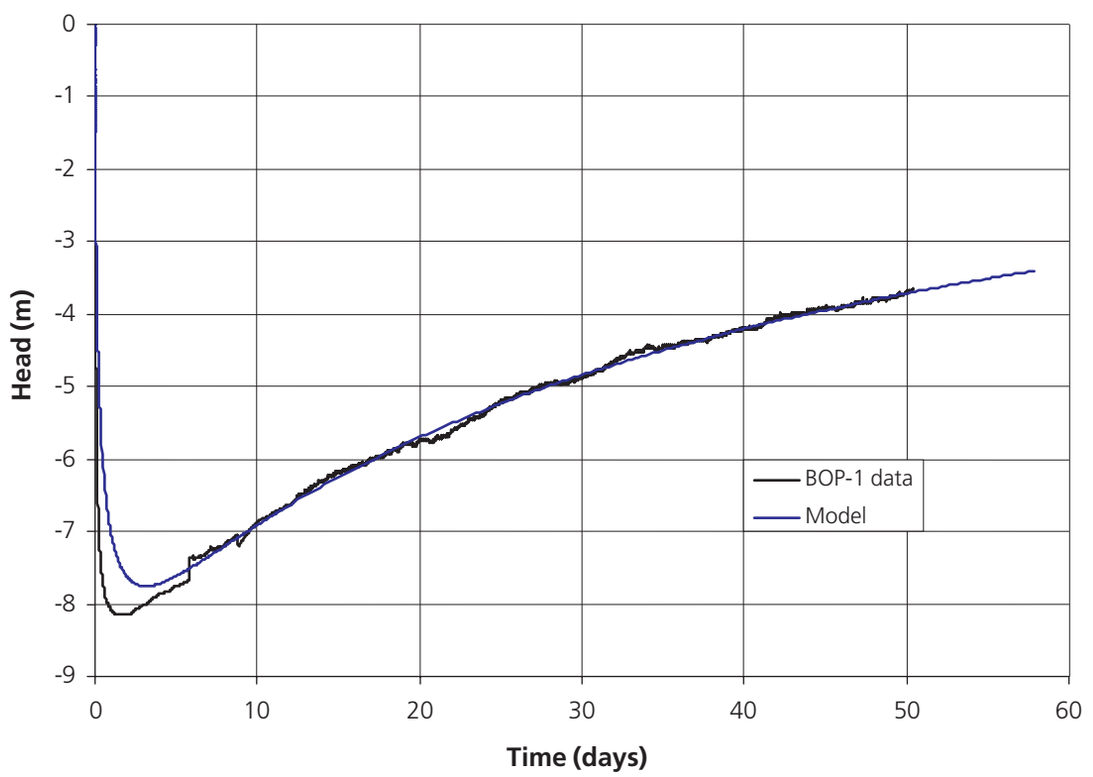

Figure 5.4: Data from Phase 2 of the BOP-1 borehole experiment compared to the model prediction based on optimised parameters (see Table 5.1).

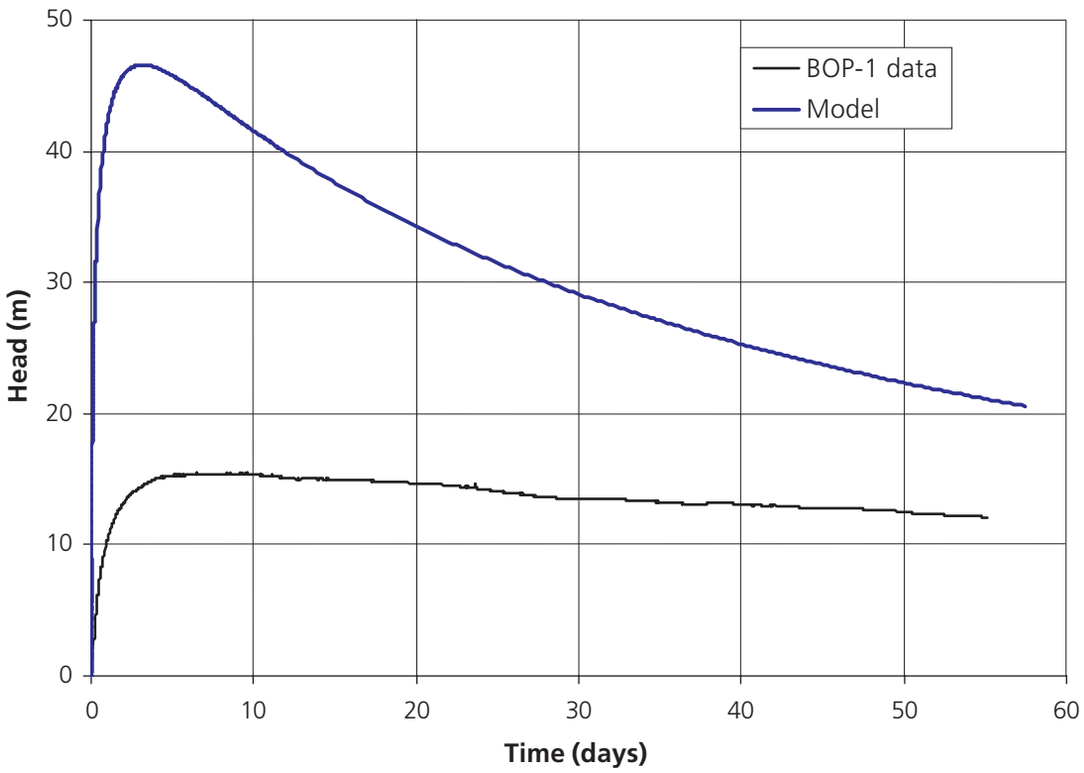

Figure 5.5: Field data from Phase 3 of the BOP-1 borehole experiment compared to the model prediction using optimised parameters derived from the Phase 2 interpretation (see Table 5.1).

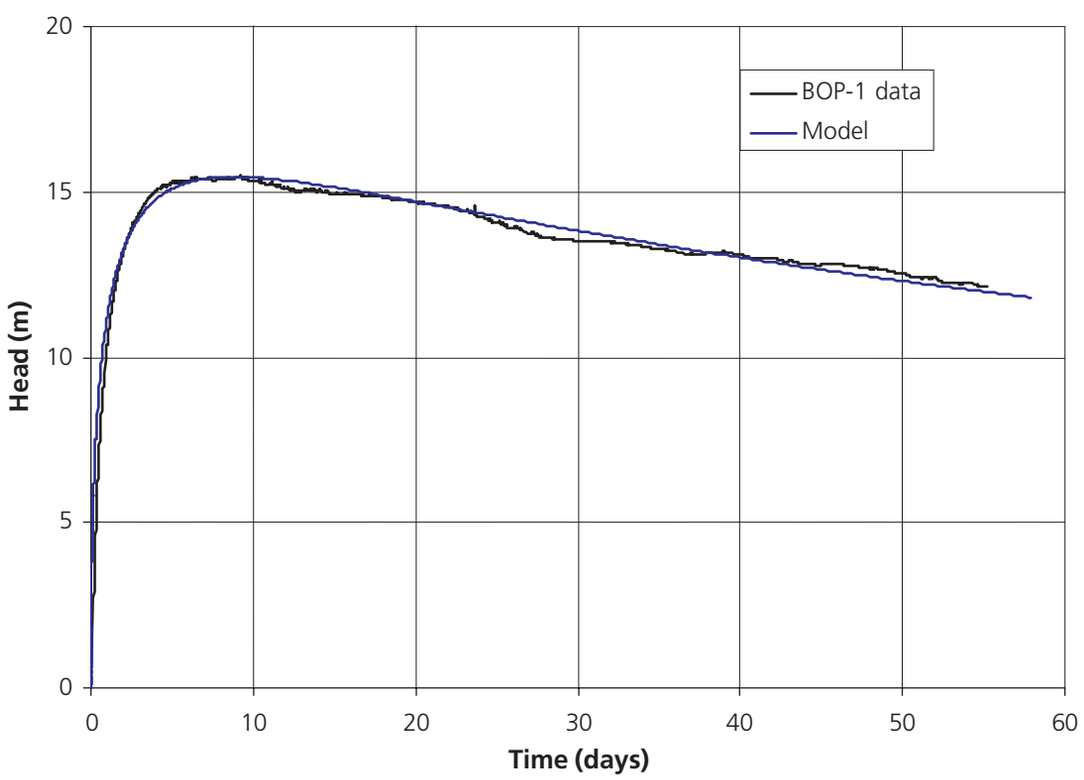

Figure 5.6: Field data from Phase 3 of the BOP-1 borehole experiment compared to the model prediction based on optimised parameters (see Table 5.1).

The initial predictive model of the first phase of the experiment was calculated using parameter values partly derived from the interpretation of the laboratory experiment described in Section 5.1. In addition, estimates of hydraulic conductivity, specific storage and borehole storage were available from independent tests of the formation (Wyss et al., 1999). The hydraulic conductivity of the formation was substantially higher than that of the laboratory sample, so is was assumed that the osmotic efficiency should be held constant. The full set of parameters used in the calculation is given in Table 5.1 (Phase 2 prediction) and the results are shown in Figure 5.3. It can be seen that the model response differs from the data in three important aspects: (a) the magnitude of the response seen in the data is much greater than was obtained from the model, (b) the data shows a much faster approach to maximum drawdown than is seen in the model, (c) the rate of recovery seen in the data is greater than predicted by the model. The sensitivity of the model to changes in the various parameters was explored by making changes to each in turn. The following responses were observed:

i) Increasing the hydraulic conductivity reduces the magnitude of the osmotic response but has little effect on the timescale of the return to equilibrium.
ii) Increasing the diffusion coefficient causes the osmotic drawdown to recover more quickly whilst at the same time slightly reducing the magnitude of the maximum response.
iii) Reducing the borehole storage has no effect on the long term recovery of the system, but does increase the rate at which the initial drawdown is expressed. The net effect is thus to slightly increase the magnitude of the maximum drawdown and sharpen the trough about the maximum response.
iv) Increasing the magnitude of the osmotic permeability, or increasing the osmotic efficiency, increases the magnitude of the overall response but has little effect on the timescale of the return to equilibrium.

Using these responses as a guide it was possible to obtain the fit to the data shown in Figure 5.4 using the parameter values listed in Table 5.1 (Phase 2 interpretation). It can be seen that an excellent fit to the data has been obtained. Comparing the new parameter values to those in Table 5.1 (Phase 2 prediction) shows that the osmotic efficiency of the formation had to be raised by a factor of about 1.8 and the borehole storage reduced by a factor of 3.3. In addition, the diffusion coefficient was increased slightly. It seems reasonable to suppose that the reduced osmotic efficiency of the laboratory sample relative to the *in situ* formation may be in part be due to the disruption caused by the sampling process.

A predictive calculation for Phase 3 was made using the same parameter values as for the Phase 2 interpretation but with the initial solute concentration in the borehole set to the 1.497 $mol.dm^{-3}$ of the brine that was exchanged into the packered borehole test interval. The result is shown in Figure 5.5, together with the data obtained from this phase of the experiment. It can be seen that the time to peak response in the data was greater than that predicted and the magnitude of the response was much smaller, peaking at about 15.4 m after 8 days, compared to the predicted peak of about 46.6 m after 3 days. Also, the rate of decline of the pressure was much slower than predicted, with the data showing only a 20% reduction from peak value after 50 days, whereas the model predicts a decline of about 50% in that time.

Using the sensitivities of the model to the parameter values noted above as a guide once more it was possible to obtain a good fit to the data, as shown in Figure 5.6, using the revised parameter values listed in Table 5.1 (Phase 3). Comparing these values with those in Table 5.1 (Phase 2 interpretation) it will be seen that the osmotic efficiency of the formation is a factor of 2.3 lower under the hypersaline conditions than under the freshwater conditions. Also, the diffusion coefficient is a factor of 4.2 lower. The borehole storage is a factor of 1.5 higher than was found before, but this is still much lower than the initial estimates.

Thus, it would seem that the osmotic permeability, and hence the osmotic efficiency, is greater at low solute concentrations than at high values. This would be consistent with the experimental findings of Fritz and Marine (1983) on osmotic flow in bentonite. The variation of the osmotic permeability with solute concentration is likely to arise from interactions between the ions in solution and the fabric of the clay minerals at the microscopic scale. One possibility would be that the high ionic strength fluid causes the separation between clay platelets to decrease in line with Double Layer Theory predictions, leading to widening of the interconnected flow channels through the clay fabric. The electrical restrictions on the passage of ions along these flow channels would decrease as their aperture increases, leading to a reduction in osmotic efficiency. These hypothesized changes in clay fabric do not explain why the diffusion coefficient should be lower in the presence of the hypersaline solution.

6 Conclusions

The programme of work on osmotic flow in Opalinus Clay comprised three main activities, a laboratory pilot study on samples, an *in situ* experiment in a borehole at the Mt Terri Rock Laboratory and a theoretical study supported by mathematical modelling.

The pilot study demonstrated that the shale behaves as a leaky semi-permeable membrane with an osmotic efficiency in the range 1.5 to 6%. It is thus possible to generate a measurable flow of water when a sample is exposed to a solute concentration gradient in the absence of a pressure gradient. When pore-water was replaced by distilled water, the sample swelled by up to 0.9%. Clearly, a simple change in pore-water salinity can lead to a change in shale volume.

The results of the laboratory study were initially analysed using equations for chemico-osmotically coupled flow and solute transport developed by Greenberg et. al. (1973). Some aspects of the transient flows and the long term swelling behaviour seen in the data could not be explained by the original equations and a modification to the definition of compressibility was proposed which improves the representation of these transient effects.

The *in situ* borehole experiment in the Mt Terri Rock Laboratory lasted nearly five years and utilized a specially-designed packer system in which the chemistry of the sealed test interval could be controlled and changed without disturbing the pressure regime. After filling the test interval with an aqueous solution matched to the natural formation water, the pressure evolution was monitored for approximately two years. The test interval pressure at the end of this phase was 900 ± 20 kPa.

In the second phase, the original test fluid was sampled and replaced with de-ionised water and the fluid was allowed to equilibrate with formation water for another two years. Immediately after shut-in pressure began to fall, reaching a minimum of 812 kPa after 52 hours. Interval pressure then began to slowly increase. The magnitude of the *in situ* response obtained was significantly greater than that predicted on the basis of the parameters from the laboratory pilot study. It was found that both the osmotic efficiency and the diffusion coefficient were larger in the *in situ* formation than in the laboratory sample.

In the third and last phase, the test fluid was replaced with hypersaline solution. In contrast to the previous response, pressure then began to rise after shut-in, reaching a maximum of 1082 kPa after 221 hours. After reaching the maximum, interval pressure slowly began to decrease. The initial predictive model calculation for this phase was based on the interpretation and parameters of the previous phase. The observed response was smaller than the predicted. Parameters were adjusted and the model re-calculated to fit the data. This demonstrated that both the osmotic efficiency and the diffusion coefficient were lower under the high salinity pore-water conditions of the last phase.

The osmotic efficiency of the Opalinus Clay was generally lower than might be anticipated for this well-compacted argillaceous rock. A possible explanation for low osmotic efficiency and the unusually large compressibility seen in laboratory testing is that the test material contained a network of microcracks which opened up during de-stressing, sample preparation and testing. The aperture of such cracks (typically μm-scale) would be sufficiently large to allow the solutes to diffuse through the rock virtually unimpeded by the relatively short-range (typically nm-scale) electrostatic interactions with the clay mineral surfaces.

It is possible that the shale around the borehole wall was also damaged by unloading and deformation. It is entirely feasible that undisturbed rock remote from the excavations could display a lower compressibility and a significantly higher osmotic efficiency.

7 References

Abd-el-Aziz, M. & Taylor, S.A. (1964): Simultaneous flow of water and salt through unsaturated porous media, 1: Rate equations. Soil Sci. Soc. America Proc. 29, 141.

Banin, A. and Low, P.F. (1971): Simultaneous transport of water and salt through clays, 2: Steady-state distribution of pressure and applicability of irreversibility of thermodynamics. Soil Sci. America Proc. 112, 69-88.

Bear J. (1972): Dynamics of fluids in porous media. Elsevier, New York.

Berry F.A.F. (1960): Geologic evidence suggesting membrane properties of shales. Bull. Amer. Assoc. Petroleum Geol. 44(6), 953-954.

Bolt, G.H. & de Haan, F.A.M. (1962): Anion exclusion in soils. In: Soil Chemistry, Developments in Soil Science, Elsevier, Amsterdam.

Cave, M.R., Reeder, S., Entwisle, D.C., Blackwell, P.A., Trick, J.K., Wragg, J. & Vickers, B. (1998): Chemical characterisation of squeezed pore-waters and aqueous leachates from Opalinus Marl core material from the Mont Terri tunnel, Switzerland. In: Bossart, P. (ed.): Basic geochemical data from water sampling (WS) experiments, Phases 1 and 2. Mont Terri Project Technical Report 97-02, Swiss National Hydrological and Geological Survey, Bern.

Chenevert, M.E. (1970): Shale alteration by water adsorption. J. Petroleum Tech., 1141-1148.

Coplen, TB. and Hanshaw, B.B. (1973): Ultrafiltration by a compacted clay membrane. I. Oxygen and hydrogen isotopic fractionation. Geochim. Cosmochim. Acta 37, 2295-2310.

Everett, D.H. (1988): Basic Principles of Colloid Science. Royal Society of Chemistry Publications.

Fargue, D., Goblet, P. & Jamet, Ph. (1989): Étude sous l'angle theromodynamique des processus de transfert potentials non-dominants des radionucléides dans les géosphère. Final Rapport LHM/RD/89/52, Centre D'Informatique Géologique, École Nationale Supérieure des Mines de Paris.

Fritz, S.J. (1986): Ideality of clay membranes in osmotic processes: A review. Clays & Clay Minerals 34/2, 214-223.

Fritz, S.J. & Marine, I.W., 1983. Experimental support for predictive osmotic model of clay membranes. Geochim. Cosmochim. Acta 47, 1515-1522.

Graf, D.L. (1982): Chemical osmosis, reverse chemical osmosis and the origins of subsurface brines. Geochim. Cosmochim. Acta 46, 1431-1448.

Greenberg J.A. (1971): Diffusional flow of salt and water in soils. Ph.D. thesis, University of California, Berkeley, USA.

Greenberg, J.A., Mitchell, J.K. and Witherspoon, P.A. (1973): Coupled salt and water flows in a groundwater basin. J. Geophys. Res. 78, 6341 - 6353.

Hanshaw, B.B. (1962): Membrane properties of compacted clays. Ph.D. thesis, Harvard University, USA.

Hindmarsh, A.C. (1982): ODEPACK, a systematized collection of ODE solvers. Lawrence Livermore National Laboratory Report, UCRL-88007.

Horseman, S.T. (1996):. Guidelines for chemico-osmotic experiments in Opalinus Clay. Unpublished Technical Note TN96-21, Mont Terri Project, Switzerland.

ISRM (1981): Rock Characterization, Testing and Monitoring. In: Brown E.T. (ed.): International Society of Rock Mechanics, Commission on Testing Methods. Pergamon Press, Oxford.

Kemper ,W.D. & Evans, N.A. (1963): Movements of water as affected by free energy and pressure gradients, III, Restriction of solutes by membranes. Soil Sci. Soc. America Proc. 27, 485-490.

Kemper ,W.D. & Rollins, J.B. (1966): Osmotic efficiency coefficients across compacted clays. Soil Sci. Soc. America Proc. 30, 529-534.

Kharaka, Y.K. & Berry F.A.F. (1973): Simultaneous flow of water and solutes through geological membranes - I. Experimental investigation. Geochim. Cosmochim. Acta 37, 2577-2603.

Kirkwood, J.G. (1954): Transport of ions through biological membranes from the standpoint of irreversible thermodynamics. In: Clarke, H. (ed.): Ion Transport Across Membranes. Academic Press, New York.

Letey J, and Kemper, W.D. (1969): Movement of water and salt through a clay-water system: Experimental verification of Onsager reciprocal relation. Soil Sci. Soc. America Proc. 33, 25-29.

Marine, W.I. and Fritz, S.J. (1981): Osmotic model to explain anomalous hydraulic heads. Water Resources Research 17, 73-82.

Neuzil, C.E. (1994): How permeable are clays and shales? Water Resources Research 30, 145-150.

Neuzil C.E. (2000): Osmotic generation of "anomalous" fluid pressures in geological environments. Nature 403, 182-184.

Noy D.J. (1998): A user guide for OSMO1R: a program for solution of radial groundwater flow and solute transport with chemico-osmotic coupling. British Geological Survey Technical Report WE/98/37, Keyworth, Nottingham.

Olsen H.W. (1969): Simultaneous fluxes of liquid and charge in saturated kaolinite. Soil Sci. Soc. America Proc. 33, 338-344.

Pearson, F.J., Scholtis, A., Gautschi, A., Baeyens, A., Bradbury, M. and Degueldre, C. (1999): Chemistry of porewater. In: Thury M. and Bossart P. (eds): Mont Terri Rock Laboratory: results of the hydrogeological, geochemical and geotechnical experiments per-

formed in 1996 and 1997. Swiss National Hydrological and Geological Survey, Geological Reports No. 23, Bern.
PETZOLD, L.R. (1982): A description of DASSL: a differential/algebraic system solver. Sandia National Laboratories report SAND82-8637.
SCHLEMMER, R., FRIEDHEIM, J.E., GROWCOCK, F.B., BLOYS, J.B., HEADLEY, J.A. & POLNASZEK, S.C. (2002): Membrane efficiency in shale: an empirical evaluation of drilling fluid chemistries and implications for fluid design. Presented at IADC/SPE Drilling Conference, Dallas, Texas, Feb. 2002, Paper 74557.
SHERWOOD J.D. (1993): Biot poroelasticity of a chemically active shale. Proc. Royal Soc. London A 440, 365-377.
SOLER, J.M. (1999): Coupled transport phenomena in the Opalinus Clay: implications for radionuclide transport. Paul Scherrer Institut Report 99-07. Also published as Nagra Technical Report NTB 99-09.
Soler, J.M. (2001): The effect of coupled transport phenomena in the Opalinus Clay and implications for radionuclide transport. J. Contaminant Hydrology 53, 63-84.
THURY, M. (1999): Extended summary. In: Thury, M. and Bossart, P. (eds): Mont Terri Rock Laboratory: results of the hydrogeological, geochemical and geotechnical experiments performed in 1996 and 1997. Swiss National Hydrological and Geological Survey, Geological Reports No. 23, Bern.
THURY, M. AND BOSSART P. (1999): The Mont Terri Rock Laboratory, a new international research project in a Mesozoic shale formation in Switzerland. Engineering Geol. 52, 347-359.
VAN OORT, E. (1994): A novel technique for the introduction of drilling fluid induced borehole instability in shales. In: Eurock '94, Balkema, Rotterdam, 293-308.
WONG, S.W. AND HEIDUG, W.K. (1994): Borehole stability in shales: A constitutive model for the mechanical and chemical effects of drilling fluid invasion. In: Eurock '94, Balkema, Rotterdam, 251-257.
WYSS, E., MARSCHALL, P. & ADAMS, J. (1999): Hydraulic parameters and formation pressures in matrix and faults. In: Thury, M. and Bossart, P. (eds): Mont Terri Rock Laboratory: results of the hydrogeological, geochemical and geotechnical experiments performed in 1996 and 1997. Swiss National Hydrological and Geological Survey, Geological Reports No. 23, Bern.
YOUNG, A. & LOW, P.F. (1965): Osmosis in argillaceous rocks. Bull. Amer. Assoc. Petroleum Geol. 49/7, 1004-1008.

Mont Terri Technical Notes

TN 96-21: S.T. Horseman: Guidelines for chemico-osmotic experiments in OPA. British Geological Survey; Mont Terri internal, unpublished report.

TN 97-39: J.F. Harrington and S.T. Horseman: Laboratory experiments on hydraulic and osmotic flow in Opalinus Clay. British Geological Survey; Mont Terri internal, unpublished report.

TN 98-48: D.J. Noy: Parameter estimates from 1D modelling of osmotic experiments. British Geological Survey; Mont Terri internal, unpublished report.

TN 99-81: D.J. Noy and S.T. Horseman: OP Experiment: Design calculation. Determination of the osmotic pressure response of borehole BOP-1 to a change of borehole fluid. British Geological Survey; Mont Terri internal, unpublished report.

TN 2000-44: D.J. Noy: OP Experiment: Simulation of fluid exchange carried out in borehole BOP-1. British Geological Survey; Mont Terri internal, unpublished report.

TN 2002-19: D.J. Noy: Osmotic Pressure Experiment: Fluid exchange with a high saline solution. British Geological Survey; Mont Terri internal, unpublished report.

TN 2002-21: H.R. Fisch and P. Bossart: Experiment OP: Fluid exchange in borehole BOP-1 with a 100 g dm-3 NaCl fluid. The field data set. Solexperts & Geotechichal Institute; Mont Terri internal, unpublished report.